“Elucidating the Structural Basis of Substrate Recognition by the Proteasomes: A Global Approach”

By
Nikhil Sangith
[LIFE09200804013]

Tata Memorial Centre
Mumbai

A thesis submitted to the
Board of Studies in Life Sciences
In partial fulfillment of requirements
for the Degree of

DOCTOR OF PHILOSOPHY
of
HOMI BHABHA NATIONAL INSTITUTE

June, 2015

Homi Bhabha National Institute

Recommendations of the Viva Voce Committee

As members of the Viva Voce Committee, we certify that we have read the dissertation prepared by **Nikhil Sangith** entitled **"Elucidating the Structural Basis of Substrate Recognition by the Proteasomes: A Global Approach"** and recommend that it may be accepted as fulfilling the thesis requirement for the award of Degree of Doctor of Philosophy.

S.V. Chiplunkar — **Date:** 22/5/15

Chairperson- Dr. S.V. Chiplunkar

V. Prasanna — **Date:** 22/5/15

Guide / Convener – Dr. Prasanna Venkatraman

Kakoli Bose — **Date:** 22/5/15

Member – Dr. Kakoli Bose

Ashok Varma — **Date:** 22/5/15

Member- Dr. Ashok Varma

Sanjeev Galande — **Date:** 22/05/2015

Invitee- Dr. Sanjeev Galande

R. Sowdhamini — **Date:** 22/5/'15

External Examiner- Dr. R. Sowdhamini

Final approval and acceptance of this thesis is contingent upon the candidate's submission of the final copies of the thesis to HBNI.

I hereby certify that I have read this thesis prepared under my direction and recommend that it may be accepted as fulfilling the thesis requirement.

Date: 22 May, 2015

Place: Navi Mumbai

V. Prasanna 22/5/15

<Signature>

Guide

STATEMENT BY AUTHOR

This dissertation has been submitted in partial fulfillment of requirements for an advanced degree at Homi Bhabha National Institute (HBNI) and is deposited in the Library to be made available to borrowers under rules of the HBNI. Brief quotations from this dissertation are allowable without special permission, provided that accurate acknowledgement of source is made. Requests for permission for extended quotation from or reproduction of this manuscript in whole or in part may be granted by the Competent Authority of HBNI when in his or her judgment the proposed use of the material is in the interests of scholarship. In all other instances, however, permission must be obtained from the author.

Nikhil Sangith

DECLARATION

I, hereby declare that the investigation presented in the thesis has been carried out by me. The work is original and has not been submitted earlier as a whole or in part for a degree /diploma at this or any other Institution / University.

Nikhil Sangith

List of Publications arising from the thesis

Journal

1. **Nikhil Sangith**, Kannan Srinivasaraghavan, Indrajit Sahu, Ankita Desai, Spandana Medipally, Arun Kumar Somavarappu, Chandra Verma, Prasanna Venkatraman. Discovery of Novel Interacting Partners of PSMD9 a Proteasomal Chaperone –Role of the PDZ-Domain Motif Interaction and Putative Function in Quality Control. **FEBS Open Bio**, 2014. doi:10.1016/j.fob.2014.05.005

2. Indrajit Sahu, **Nikhil Sangith**, Manoj Ramteke, Rucha Gadre, PrasannaVenkatraman. A novel role for the Proteasomal Chaperone PSMD9 and hnRNPA1 in enhancing IκBα degradation and NF-κB activation - Functional Relevance of predicted PDZ domain-motif interaction, **FEBS Journal**, 2014. doi: 10.1111/febs.12814.

3. Vinita Wadhawan, Yogesh A. Kolhe, **Nikhil Sangith**, Amit Kumar Singh Gautam, Prasanna Venkatraman. From prediction to experimental validation: desmoglein 2 is a functionally relevant substrate of matriptase in epithelial cells and their reciprocal relationship is important for cell adhesion, **Biochemical Journal**, 2012. doi:10.1042/BJ20111432.

Conferences

1. Best Poster award , 79th Society of Biological Chemists (SBCI) Meet/ 2010, Indian Institute of Science, Bangalore (Poster presentation)

2. INDO-US Workshop/ Symposium, Modern Trends in Macromolecular Structures, 2011, Indian Institute of Technology Bombay, Mumbai, India (Participation).

3. 1st Global Cancer Genomics Consortium, 2011, TMC Symposium, ACTREC-TMC, Navi Mumbai, India (Participation).

4. ATW Satellite Meeting, "The DNA damage response and cell cycle control in cancer cells", 2012, ACTREC-TMC, Navi Mumbai, India (Participation).

5. International Symposium on Stem Cell Biology, 2012, ACTREC-TMC, Navi Mumbai, India (Participation).

6. Ninth National Research Scholars Meet (NRSM), 2013, ACTREC-TMC, Navi Mumbai, India (Oral presentation).

ACKNOWLEDGEMENT

The submission of this thesis will be the end of the journey of obtaining PhD. There is great joy in remembering this journey and the people who have helped and supported me along this long, but fulfilling road. I would like to express my heartfelt gratitude to my mentor Dr. Prasanna Venkatraman who was supportive, patient and inspirational throughout this journey. I joined this lab as a short term trainee for my MSc. dissertation after which I was enrolled as a PhD student in this lab. I am grateful to madam for having faith in me in this venture and also helping me grow as a researcher and a better human being.

I take this opportunity to thank Dr. S.V. Chiplunkar (Director, ACTREC), Dr. Rajiv Sarin (Former Director, ACTREC) and Dr. Surekha M. Zingde (Former Deputy Director) for their providing sound research infrastructure.

I would like to thank my doctoral committee members Dr. S.V. Chiplunkar (present Chairperson, ACTREC), Dr. M.V. Hosur (former Chairperson, ACTREC), Dr. Kakoli Bose (ACTREC) and Dr. Sanjeev Galande (IISER, Pune) for their valuable comments and suggestions during my regular progress report presentations.

I would like to sincerely thank Dr. Lawrence J.Stern (Professor, Department of Pathology, University of Massachusetts Medical School, Worcester, MA) for providing me an opportunity to work in his laboratory for a period of six months and learn many techniques related to purification and crystallization of proteins. Dr. Stern was kind enough to provide me fellowship from the Global Health grant during my stay in Worcester.

I would like to thank Department of Biotechnology (DBT), Government of India, for providing fellowship during my PhD tenure. I express my sincere gratitude to the former

coordinator of DBT, Prof. J.K. Pal for being extremely supportive whenever I had problems regarding fellowship.

Working in a lab for six years will be memorable only if there is a good working environment provided by friends and colleagues. I joined this lab as a trainee under Dr. Amit Kumar Singh Gautam. I thank Amit as well as another beloved senior, Dr. Manoj Ramteke, who were excellent human beings and great mentors. I have learnt many things from them and both of them have looked after me like a younger brother throughout this venture. Things would not have been so easy if both of you would not have been in the lab. I also thank one of my very good friend and batchmate Dr, Padma P. Nanaware, who has been extremely supportive and helpful in these six years. She has been extremely helpful during tough times. I thank Mr. Vinay Ludbe and Kamlesh Israni who have been extremely helpful on many occasions. Mr. Ludbe has been father-like figure and has helped me in many of the cell culture experiments. I also thank Indrajit, who has worked with me in many experiments and writing manuscripts. I thank my juniors Mahalakshmi, Burhan and Siam and post doctoral fellows Dr. Vinita Wadhawan and Dr. Priya Sundararajan for providing a wonderful environment in the lab.

I would like to thank my trainees Ankita Desai, Jinu Mathew and Shreya Bharghava, who were extremely helpful in carrying out many of the experiments reported in this thesis. Their sincerity and hard work has contributed a lot in this piece of work.

I thank all the members of JRF batch 2008- Padma, Manohar, Anjana, Rashmi, Lumbini, Surya, Vikrant, Nitu, Peeyush, Zahid, Lalit, Monica for their encouragement and support.

Life outside the lab and institute is equally important. I thank my room-mates Kaushal, Bhavik, Gopal and Sujath for being such wonderful friends. They have been the best companions and have been of great help in tough times.

I take this opportunity to thank many friends who were extremely helpful during my visit to UMass Medical School, Worcester. I would like to thank Peter Trenh, who helped me out of the way in the lab and also helped me in sorting out many problems I had before settling down. Thank you very much Peter, you were such a great source of help. I also thank Zachary and Zu, who were great colleagues in the lab and helped me in many experiments. I also thank Mr. Richard Madison and Mrs. Kathy Bateman (UMass Medical School), who helped me out of the way in the administrative work in UMass Medical School. I am very grateful to Dr. Mei Xu, who provided a great home to stay in Worcester. She helped me in such a tough time by providing me a home when I was homeless in Worcester. She took great care of me like a mother. Thank you very much Mei. I also thank Bindu, Kishan and Harsha Patel who were extremely supportive during my stay in the US.

Lastly, I would like to thank my family for all their love and encouragement. For my parents, who raised me with all love and supported me in all my pursuits. Without them nothing would have been possible. And for my loving, supportive, encouraging, and patient wife Navya whose faithful support during the final stages of this Ph.D. is so appreciated. Thank you.

Nikhil Sangith

CONTENTS **Page No.**

Synopsis **1**

List of figures **15**

List of tables **16**

List of abbreviations **17**

Chapter 1: Introduction **19**

Chapter 2: Review Of Literature

2.1 Protein turnover: from a vague idea to present understanding **26**
2.2 The 26S Proteasome **27**
2.2.1 The 20S Core Particle **27**
2.2.2 Assembly of 20S Core **29**
2.2.3 The 19S Regulatory Particle (RP) **30**
2.2.4 Assembly of 19S Regulatory Particle **35**
2.3 Accessory machinery for degradation- The Ubiquitination Machinery **36**
2.3.1 The Ubiquitin-Activating Enzyme, E1 **37**
2.3.2 Ubiquitin-activating enzymes, E2 (Ubiquitin-carrier enzymes) **38**
2.3.3 Ubiquitin-protein Ligases, E3 **38**
2.4 Substrate Recognition by the Proteasome **39**
2.4.1 Role of adapter or ancillary proteins in protein degradation **40**
2.4.2 'Cis-acting elements' within the substrate contribute to degradation **41**
2.5 PSMD9: a non-ATPase of the 19S Regulatory particle **41**
2.5.1 PSMD9 harbors a PDZ-like domain **42**
2.5.2 Bridge-1: A coactivator of insulin gene transcription **42**
2.5.3 PSMD9 regulates melanin synthesis in melanoma cells **43**
2.5.4 PSMD9 regulates activin signaling in human ovarian granulosa cells **43**
2.6 The PDZ domain **43**
2.6.1 PDZ-PDZ interactions **46**
2.6.2 Internal Motif Recognition **46**
2.6.3 Other ligands of the PDZ **47**
2.7 Protein-Protein Interactions: The Premise of Protein Structure and Function **48**
2.8 Library-based methods to detect protein-protein interactions **50**

Chapter 3: Material And Methods

3.1 Buffers and Reagents **53**
3.1.1 Luria-Bertani (LB) *Medium* (for 1 L) **53**
3.1.2 LB-Ampicillin Agar Plates (for 1 L) **53**
3.1.3 Tris-EDTA (TE) Buffer (for 50 ml) **53**
3.1.4 Ampicillin Stock **54**
3.1.5 50X TAE Buffer (for 1 L) **54**
3.1.6 6X Gel Loading Buffer for DNA (for 100 ml) **54**
3.1.7 Ethidium Bromide (EtBr) **54**
3.1.8 Buffers for Ni NTA Column Purification and Gel Filtration **54**

3.1.8.1 Ni-NTA Lysis Buffer (for 1 L) **54**
3.1.8.2 Ni-NTA Binding/Washing Buffer (for 1 L) **55**
3.1.8.3 Ni-NTA Elution Buffer (for 1 L) **55**
3.1.8.4 Transport buffer (for 50 ml) **55**
3.1.8.5 1X Phosphate buffer saline pH 7.5 (1 L) for GST-fusion protein purification **56**
3.1.10. 1X Transfer buffer **56**
3.1.8.6 Elution buffer for GST-fusion protein purification (for 50 ml) **56**
3.1.8.7 Binding and washing buffer for MBP- fusion protein purification (for 1L) **56**
3.1.9 NP40 lysis buffer (for 50ml) **56**
3.1.10 10mM Phosphate buffer pH 7.5 (for 1L) **56**
3.1.11 10mM Sodium bicarbonate buffer pH 9.3 (50 ml) **57**
3.1.12 Tris Base Saline Tween 20 (TBST) (for 1L) **57**
3.1.13 1X Transfer buffer (For 1L) **57**
3.1.14 Tissue Culture Reagents **57**
3.1.14.1 10X Phosphate buffered saline (PBS) (for 1L) **58**
3.1.14.2 10X Trypsin (0.25%) **58**
3.1.14.3 2X BBS (BES Buffered Saline) (for 50 ml) **58**
3.1.14.4 0.5M $CaCl_2$ (for 50 ml) **58**
3.1.15 Other reagents **59**
3.2 Experimental protocol **59**
3.2.1 Primer reconstitution **59**
3.2.2 Determination of nucleic acid concentration **59**
3.2.3 Polymerase Chain Reaction (PCR) **59**
3.2.4 Site directed mutagenesis **60**
3.2.5 Restriction digestion reaction **61**
3.2.6 Agarose gel electrophoresis of DNA **61**
3.2.7 Recovery of DNA from low melting agarose gel **61**
3.2.8 Ligation/Cloning **62**
3.2.9 Transformation **62**
3.2.10 Plasmid mini preparation **62**
3.2.11 Plasmid construction **63**
3.2.12 Protein Expression **66**
3.2.13 Ni-NTA Agarose Affinity Chromatography **66**
3.2.14 Glutatione-S-Transferase purification affinity Chromatography **67**
3.2.15 Ion exchange chromatography **67**
3.2.16 Gel Filtration Chromatography **67**
3.2.17 Protein Estimation using Bradford Assay **68**
3.2.18 SDS PAGE **68**
3.2.19 Preparation of Glycerol Stocks **68**
3.2.20 Enzyme Linked Immuno Sorbent Assay **69**
a) Peptide screening **69**
b) Protein-protein interaction **69**
3.2.21 GST pull down assay **70**
3.2.22 MBP pull down assay **70**
3.2.23 Western blotting **70**
3.2.24 Homology modeling of PSMD9, its PDZ domain and peptide docking **71**
a) Homology modeling of PDZ domain of PSMD9 **71**

b) Peptide docking **72**
c) Modeling of full length PSMD9 and D157P mutant **72**
3.2.25 Molecular Dynamic simulations **73**
3.2.26 Routine Maintenance of Cell Lines **74**
3.2.27 Freezing and Revival of Cell cultures **75**
3.2.28 Transfection of plasmid DNA in HEK 293 cells **75**
3.2.29 Generation of over expressing stable HEK 293 cells **76**
3.2.30 NF-κB activation- Luciferase assay **76**
3.2.31 Soft agar assay **76**
3.2.32 Affinity pull down assay **77**
3.2.33 RNA extraction and cDNA synthesis **77**

Chapter 4. A Distinctive Approach to Identify Interacting Partners of PSMD9

4.1 Introduction **80**
4.2 Results and Discussion **81**

Chapter 5. Role of PDZ domain in interaction in interaction of PSMD9
5.1 Introduction **89**
5.2 Results and Discussion **89**

Chapter 6. Fuctional Modules Regulated by PSMD9

6.1 Introduction **102**
6.2 Results and Discussion **102**

Chapter 7. Specificity of PDZ domain of PSMD9 and Possible Modes of Binding

7.1 Introduction **111**
7.2 Results and Discussion **111**

Chapter 8. Validation of Interaction in Mammalian Cells and Role in NF-κB Signaling

8.1 Introduction **120**
8.2 Results and Discussion **120**

Chapter 9. Crystallization of PSMD9
9.1 Introduction **128**
9.2 Results and Discussion **129**

Chapter 10. Conclusions and Significance of Study **139**

References **144**

Reprints of Published Articles **163**

Homi Bhabha National Institute

Ph. D. PROGRAMME

1. **Name of the Student:** Nikhil Sangith
2. **Name of the Constituent Institution:** Tata Memorial Centre (TMC), Advanced Centre for Treatment, Research and Education in Cancer (ACTREC)
3. **Enrolment No. :** LIFE09200804013
4. **Title of the Thesis:** Elucidating the Structural Basis of Substrate Recognition by the Proteasomes: A Global Approach.
5. **Board of Studies:** Life Sciences (LS)

SYNOPSIS

Elucidating the Structural Basis of Substrate Recognition by the Proteasomes- A Global Approach

Introduction:

Protein degradation plays a significant role in maintaining cellular homeostasis and survival (Glickman and Ciechanover, 2002). In eukaryotic cells, two major pathways mediate protein turnover- the lysosomal pathway and the ubiquitin proteasome pathway. The lysosomal machinery comprises of acidic proteases which remove bulk of the extracellular proteins, whereas the ubiquitin-proteasome system (UPS) aids in removing intracellular proteins (Ciechanover, 2005). The proteasome also plays a crucial role in removing abnormal or damaged proteins and in antigen processing and presentation (Saberi et al., 2006). Proteins destined for degradation by the proteasome are conjugated by a conserved 76 amino acid protein called ubiquitin and subsequently degraded by the proteasome (Pickart, 2001). Proteins like Thymidylate synthase and ornithine decarboxylase are degraded independent of ubiquitin manner (Forsthoefel et al., 2004; Hoyt et al., 2003). In the case of thymidylate synthase, it has been shown that the cooperation of a structurally disordered region and a helical segment of these proteins is sufficient for ubiquitin-independent degradation (Melo et al., 2011). Our lab has demonstrated that the disordered F-helix of apomyoglobin initiates the ubiquitin-independent degradation by the eukaryotic proteasome *in vitro* (Singh Gautam et al., 2012). Therefore, ubiquitin may not be the exclusive signal that is required for the substrates to be degraded by the proteasome.

The 26S proteasome can be topologically divided two modules- the 19S regulatory particle and the 20S proteolytic core. The 20S core particle is responsible for hydrolysis of the protein into its constituent amino acids, while the 19S regulatory particle plays an important role in substrate recognition and unfolding. The 19S regulatory particle is made up of 13 non identical subunits, 6 of which belong to the AAA ATPase family. (Goldberg, 2003; Lander et al., 2012). The ATPases at the base of the regulatory particle aid in substrate unfolding, gate opening and translocation of substrates to the 20S proteolytic chamber. The functions of some of the non-ATPase subunits are known. Subunits like PSMD4 and Ubp 6 deubiquitinate the substrate during degradation, and those like PSMD5, PSMD9 and PSMD10 act as chaperones enabling the assembly of an intact 19S regulatory complex (Kaneko et al., 2009).

It is interesting to note that some of the 19S subunits are reportedly involved in transcriptional activation of various genes in eukaryotic cells. Sug1 or PSMC5 acts as helicase and regulates transcription along with RNA polymerase II. S6a ATPase or PSMC3 acts as a coactivator of Class II MHC gene (Fraser et al., 1997; Truax et al., 2010). Recently, it has been reported that Sug1, S7, and S6a form transcriptional activation complex along with RNA polymerase II, for the expression of the inflammatory gene CIITApIV (Maganti et al., 2014). Despite growing understanding of the importance of few subunits of the proteasome in degradation and transcription, the role of majority of 19S subunits in carrying out diverse functions of the proteasome is still unclear.

In an attempt to explore the role of non-ATPases in protein degradation and in other physiological processes, we came across a non-ATPase subunit called PSMD9 (Nas2 in yeast, Bridge-1 in rat). It drew our attention because this subunit possessed a PDZ-like domain, a well conserved domain known for protein-protein interaction (Thomas et al., 1999). PDZ domains [post synaptic density protein (PSD95), Drosophila disc large tumor suppressor (Dlg1), and zonula occludens-1 protein (zo-1)] are well known for protein-protein interactions and play a major role in various physiological processes like signaling (Jelen et al., 2003). PDZ domains generally interact with the C-terminus of the interacting partner. The domain has characteristic canonical α-turn-β fold that forms a hydrophobic docking site for the C-terminal residues, which is generally hydrophobic (Jelen et al., 2003). PSMD9 forms a stable sub-complex with PSMC3 and 6, two of the AAA ATPases of the proteasome (Watanabe et al., 1998). Bridge1 interacts with transcription factors E12 and PDX-1, and histone acetyl transferase, p300 via its PDZ-like domain to activate insulin gene transcription (Lee et al., 2005; Thomas et al., 1999). Overexpression of Bridge 1 in β pancreatic islets causes diabetes mellitus in rats (Volinic et al., 2006). PSMD9 regulates the degradation of the enzyme tyrosinase, which is known to play a crucial part in synthesis of melanin (Godbole et al., 2006).Activin A, a member of the transforming growth factor beta (TGF- β) superfamily, was found to up-regulate the production of Bridge-1 in human ovary (granulosa) cells, which in turn increases the production of Smads 2, 3 and 4, implying that Bridge1 may play a role in granulosa cell proliferation and differentiation (Banz et al., 2010). With this background, we defined the following objectives for the thesis.

1. To elucidate the structural basis of substrate recognition by the 19S subunits (PSMD9) of the proteasome and map the interaction sites.

2. To explore if any isolated functions of the subunits exist apart from their role in substrate recognition and degradation.

Results and Discussion:

1. Genome wide analysis of C-terminal sequences and validation of interacting partners of PSMD9.

Many non-homologous proteins share identical C-terminus and by virtue of conservation of typically three, four or eight amino acid residues. They also seem to share similar properties and functions (Chung et al., 2003). Chung et al., had classified proteome from drosophila/yeast/human by recognizing conserved C-terminal residues in some of these proteins and listed out 30 tetra-peptide sequences which have more than 10 members in their group (Chung et al., 2003). The concept of C-terminal conservation may be useful in identifying proteins that interact with PDZ-like domain of PSMD9. We hypothesized that if any conserved C-terminus were to interact, it is possible that PSMD9 may regulate the functions of these proteins. PDZ domains require a minimum of only four residues for interaction (Sheng and Sala, 2001). We chose 12 tetra-peptide sequences from Chung's list, where we included peptides with acidic, basic and polar residues apart from hydrophobic ones which PDZ domains generally prefer. We also included a peptide, AGHM, which is the C-terminus of human E12 transcription factor, mouse homolog of which is known to interact with the PDZ-like domain of PSMD9. We cloned, expressed and purified recombinant His-tagged PSMD9 and checked its interaction with N-terminal biotinylated tetra-peptides by ELISA. Results show that apart from AGHM, two other peptides interacted significantly with PSMD9. They were GRRF and SCGF, which were the C-termini of heterogeneous ribonucleoprotein A1 (hnRNPA1) and growth hormone (GH), respectively. GRRF had a lower affinity (K_d 651.7±76 μM), compared to SCGF (K_d 8.6±1.2 μM). *In vitro* pull down results show that recombinant His-PSMD9 interact with hnRNPA1, GH and E12. Mutations at the C-termini of hnRNPA1 (hnRNPA1 F372G and hnRNPA1 CΔ7) and E12 (M651G and E12 CΔ7) abrogated the interaction, implying that the terminal residue plays a major role in the interaction. However, GH F217G still interacted with His-PSMD9, whereas deletion mutant GH CΔ7 failed to interact with His-PSMD9. The dissociation constants (K_d) for hnRNPA1-PSMD9 and GH-PSMD9 interactions were found to be 1.33 ±0.04 μM and 0.84±0.07 μM, respectively by ELISA. Peptide competition experiments clearly show that peptide GRRF, but not GRRG could inhibit PSMD9-hnRNPA1 interaction (K_i 326.5±0.25 μM). Both SCGF and

SCGG could inhibit PSMD9-GH interaction (K*i* 36.7±0.29 and 35.6±0.24, respectively), which justifies the GH F217G-PSMD9 interaction.

To test the role of each residue in SCGF motif in the interaction with PSMD9, the last two and three residues (ΔGF and ΔCGF, respectively) of GH were deleted. ΔCGF mutant failed to interact with PSMD9. Also, SGGF peptide, were only the cysteine is mutated to glycine, failed to interact with PSMD9, showing the importance of cysteine in the interaction. Binding assays of PSMD9-SCGF in the presence of 1mM DTT did not show any abrogation in binding, implying that mode of interaction is non-covalent and not through disulphide linkage.

To test whether hnRNPA1 and GH interact in mammalian cells, we co-expressed FLAG-PSMD9 and HA tagged- hnRNPA1 or GH respectively, along with C-terminal deletion mutants. Immunoprecipitation experiments clearly show that both hnRNPA1 and GH interact with PSMD9, where the C-terminal deletion mutants failed to do so.

2. Computational modeling of PDZ-like domain of PSMD9, docking with peptide ligands and validation of residues important for interaction.

Since the crystal structure of PSMD9 is unknown, we decided to model the PDZ-like domain of PSMD9 (collaboration with Dr. Chandra Verma, Bioinformatics Institute, Singapore). Model was constructed by comparative homology modeling using Modeler, where PDZ2 domain of harmonin bound with C-terminal peptide of Cadherin 23 (PDB code 2KBS) (Pan et al., 2009) was used as a template. BLAST search showed that the PDZ shares 42% sequence similarity with PDZ2 domain of harmonin. Peptide docking was carried out with two different docking programs, HADDOCK (Dominguez et al., 2003), which is a defined docking program and ATTRACT (Zacharias, 2003), a blind docking program. Both programs revealed that GRRF peptide binds to the classical canonical α-turn-β structure in the PDZ domain. The peptide binds in an extended, antiparallel manner through canonical interactions that extend the beta sheet by an additional strand. The hydrophobic side chain of Phe4 of the peptide is deeply buried in the hydrophobic pocket formed by Leu124, Val139, Leu153, Ile159 and Phe 162 from the β sheet. The peptide further interacts with the beta sheet mainly through backbone/side chain hydrogen bonds with residues Leu124, Gly125, Gln126, Glu128 of β sheet of the PDZ domain. In addition the side chain of Arg2 of the peptide forms a salt bridge with the side chain of Glu128. To validate the modeling and docking studies, we mutated the following residues in the PDZ-like domain of PSMD9- F162G, L153G and a triple mutation comprising of L124G/Q126G/E128G,

respectively from the β sheet, Q181G, which is in close proximity to the ligand and L173G, which is outside the binding pocket. *In vitro* pull down assays and ELISA, showed that L173G consistently interacted with hnRNPA1 and GH like WT PSMD9 (K_d 1.33±0.16 and 1.2±0.09, respectively), whereas Q181G and triple mutant had a lower affinity (K_d 27.42±4.8 and 13.26±2.1), respectively. Mutants L153G and F162G also failed to bind to PSMD9 in pull down assays. Circular dichroism studies revealed that PSMD9 WT protein had 49% helicity, L173G mutant showed 43% helical structure and Q181G mutant contributed to 39% helicity. The hydrophobic residue mutants L153G and F162 contribute to 45% and 42% helicity, respectively indicating a local secondary structure change in the mutants. There was no change in tryptophan fluorescence in the PSMD9 mutants when compared to wild type confirming that there is no tertiary structure distortion due to the mutation.

3. Molecular Dynamic (MD) Simulation of PSMD9 and its mutants with peptide ligands.

The PDZ domain of PSMD9 docked with GRRF, subjected to MD simulation for 100 ns clearly revealed that Phe of GRRF peptide is buried in the hydrophobic pocket with charge-charge interactions between Arg2 and Glu128 on β sheet are preserved during the 100 ns simulation. The bound conformation of the peptide was further stabilized via backbone hydrogen bond interactions with residues Leu124, Gly125, Gln126 and Glu128 from β sheet of the canonical pocket. When GRRG was docked to PSMD9 WT, we observed that the peptide was displaced within 5 ns of simulation. It undergoes translation and rotations that prevent it from rebinding in the canonical interaction mode. Thus our simulations suggest that the burial of Phe in the hydrophobic pocket is crucial for the stabilization of this peptide in its bound conformation.

4. Probable functional modules regulated by PSMD9

To enhance our understanding about the role of PSMD9 in regulating other functions in mammalian cells, we screened peptides harbouring GRRX and SCGX (where X is any residue) sequences which are a part of C-terminus of proteins in the human proteome. , There are six variants of GRRX where X is C, E, I, L, N, Q or R. Peptide binding by ELISA showed that GRRC, GRRL, GRRI, GRRR and SCGL interacted with PSMD9, whereas GRRE and GRRN failed to interact. GRRC is the C-terminus of endothelial protein C receptor, GRRL is the C-terminus of S14 ribosomal protein, GRRR and SCGL are harbored by UPF2 transcription factor and interleukin 6 (IL6) receptor, respectively. We cloned and expressed S14 and FN3 domain of IL6 receptor since they had a hydrophobic residue at the C-termini. PSMD9 interacts with S14

ribosomal protein and FN3 domain of IL6 receptor. Like hnRNAP1, C-terminal mutation, S14 L151G and S14 CΔ7 failed to interact with PSMD9 *in vitro* and *ex vivo*, respectively. FN3 F365G, like F217G mutant of GH still interacted with PSMD9 like FN3 WT, whereas FN3 CΔ7 failed to interact *in vitro* and *ex vivo*, respectively.

5. Degradation dependent and independent functions of PSMD9.

It is known that hnRNPA1- I*κ*Bα interaction is important for I*κ*Bα degradation by the 26S proteasome (Hay et al., 2001). Work from our lab has shown that residues in the PDZ domain of PSMD9 are important for recruiting I*κ*Bα for degradation, thereby causing NF-*κ*B activation (Sahu et al., 2014). S14 ribosomal protein plays a major role in regulating the stability of p53 by interacting with MDM2 and prevents the ubiquitination of p53 (Zhou et al., 2013a). PSMD9 may thus play a role in regulating p53 stability. Though secretory proteins and membrane proteins are transported directly through vesicles, misfolded proteins are transported to the cytosol and degraded by the proteasome. Evidences show that certain hereditary mutations in helix 2 of the human GH leads to formation of aggregates, which are degraded by the proteasome in neuroendocrine cells (Kannenberg et al., 2007). Many proteins like T cell receptor and HMG-CoA reductase, when misfolded in the ER, is transported to the cytosol for proteasomal degradation (Fra and Sitia, 1993; Lord, 1996). Membrane proteins like growth hormone receptor (GHR) and epithelial sodium channel (ENaC) are ubiquitinated for vesicular internalization and are degraded by the proteasomes (Schild et al., 1996; Shimkets et al., 1997; Strous and Govers, 1999). Similarly PSMD9 may recruit IL6- receptor to the proteasome for degradation.

It is still unclear whether proteasome subunits perform degradation independent functions. Bridge-1 (rat homolog of PSMD9) PDZ domain interacts with C-terminus of PSMD9 and activates insulin gene transcription (Thomas et al., 1999). PDZ domains are well known to regulate signaling in mammalian cells (Jelen et al., 2003). It is also known that PDX-1 transcription factor, which interacts with Bridge-1ensures cell survival by an unknown mechanism in pancreatic cells under low doses of insulin. The Akt pathway, which is stimulated by insulin, is not important under these conditions (Johnson et al., 2006). Under these conditions, the levels of Bridge-1 are shown to increase, and therefore it may be possible that Bridge-1 can regulate cell survival through a non-classical pathway, which is yet to be explored. PSMD9 may regulate the transport and splicing of mRNA, through its association with hnRNPA1. hnRNPA1

is well known in regulating splicing of pyruvate kinase mRNA, where it generates M2 isoform in dividing cells like cancer, but M1 isoform in differentiated cells (Clower et al., 2010). Similarly PSMD9 may regulate the functions of S14 in regulating the turnover of c-myc mRNA through Argonaute 2, thereby regulating cell survival (Zhou et al., 2013b). S14 binds to the 5' UTR of mRNA and forms a platform for translation initiation (Marzi et al., 2007). PSMD9 may regulate translation initiation through its interaction with S14.

6. Crystallization of full length PSMD9 using fluorescence based thermofluor assay.

The structure of human PSMD9 is not solved. However, the structure of Nas2 PDZ domain is solved (Singh et al., 2014). In an attempt to understand the structure of PSMD9, we collaborated with Dr. Lawrence J. Stern, University of Massachussets Medical School, Worcester, MA, USA. Recombinant his-tagged PSMD9 was purified from E, coli BL21 DE (3) cells and was subjected to ion exchange and gel filtration chromatography. His tag was also cleaved using thrombin. To screen for optimal conditions for crystallization, we decided to adopt the thermofluor method for determining the conditions where the protein is most stable (Santos et al., 2012). Thermofluor determines the protein melting temperature (Tm), and is based on the interaction between the dye (SYPRO orange) and the hydrophobic regions of the protein, which are exposed upon protein thermal denaturation. We initially used different pH conditions (pH 2-11) from Hampton screen and found that PSMD9 was most stable in pH 6.2, 6.4, 6.8, 7.2, 7.4, 8.2 and 8.6. Further under these conditions various salts and solvents were added ranging from 20mM to 100mM to find out conditions where PSMD9 is most stable. Small crystals were found in the condition comprising 0.1M Tris pH 8.5, 1.5M ammonium sulphate and 12% glycerol. Fine tuning of this condition by varying the concentration of ammonium sulphate and glycerol independently did not yield better results. The small crystals did not diffract. Further optimization and standardization is still required to obtain fine quality crystals of reasonable size for diffraction.

7. Summary.

To understand the role of PDZ domain of PSMD9 in regulating many physiological processes, we chanced upon the observation of Chung et. al, where many proteins may have identical C-termini, which may serve as signatures for common biochemical functions in the cell. Keeping this in mind, we screened 12 tetra peptides which are representative C-termini of

proteins in the human proteome. We found that peptides- AGHM, GRRF and SCGF which are the C-termini of E12, hnRNPA1 and growth hormone (GH) interacted with PSMD9 in ELISA. We further prove that C-terminal residues of the above mentioned proteins interact with PSMD9. With the help of modeling and docking studies, we have characterized the key residues in the PDZ domain of PSMD9 that are important for interaction. Because the peptides were derived from the human proteome we were able to identify hnRNPA1 as a valid interacting partner despite the fact that the peptide GRRF bound with very low afffninity. , Such low affinity interactions may be neglected in other peptide screens like phage display. Alhough this low throughput approach allowed us to quickly identify novel interacting partners of PSMD9, it had limitations. Chung et al., had classified proteome from drosophila/yeast/human by recognizing conserved C-terminal residues in some of these proteins and listed out 30 tetra-peptide sequences which have more than 10 members in their group (Chung et al., 2003). Upon further investigation, we found that most of the members of the group were isoforms of the same proteins or some were predicted or hypothetical proteins. Independent analysis of these 30 tetra-peptide sequences and their constituent members and further curation using Uniprot database (ftp://ftp.uniprot.org/pub/databases/uniprot/current_release/knowledgebase/) also revealed that most of the members were isoforms and rarely more than 2 unique protein members.

In order to expand the utility of the C-terminal short motifs for the identification of functional modules, we screened the variants of GRRF (GRRX) and SCGF (SCGX) for binding to PSMD9. Peptides GRRL, GRRI, GRRR, GRRC and SCGL bound and the corresponding proteins S14 ribosomal protein (GRRL) and FN3 domain of IL 6 receptor isoform 2 (SCGL) interact through the PDZ domain of PSMD9, We also established that the C-terminal residues were important for interaction. We were successful in elucidating the role of PSMD9-hnRNPA1 interaction in IκB α degradation and NF-κB activation. PSMD9 similarly may regulate functions of S14, GH and IL6 receptor in mammalian cells which may be dependent or independent of proteasomal degradation.

8. References

Banz, C., Munchow, B., and Diedrich, K. (2010). Bridge-1 is expressed in human granulosa cells and is involved in the activin A signaling cascade. Fertil Steril *93*, 1349-1352.

Chung, J.J., Yang, H., and Li, M. (2003). Genome-wide analyses of carboxyl-terminal sequences. Mol Cell Proteomics *2*, 173-181.

Ciechanover, A. (2005). Proteolysis: from the lysosome to ubiquitin and the proteasome. Nat Rev Mol Cell Biol *6*, 79-87.

Clower, C.V., Chatterjee, D., Wang, Z., Cantley, L.C., Vander Heiden, M.G., and Krainer, A.R. (2010). The alternative splicing repressors hnRNP A1/A2 and PTB influence pyruvate kinase isoform expression and cell metabolism. Proc Natl Acad Sci U S A *107*, 1894-1899.

Dominguez, C., Boelens, R., and Bonvin, A.M. (2003). HADDOCK: a protein-protein docking approach based on biochemical or biophysical information. J Am Chem Soc *125*, 1731-1737.

Forsthoefel, A.M., Pena, M.M., Xing, Y.Y., Rafique, Z., and Berger, F.G. (2004). Structural determinants for the intracellular degradation of human thymidylate synthase. Biochemistry *43*, 1972-1979.

Fra, A., and Sitia, R. (1993). The endoplasmic reticulum as a site of protein degradation. Subcell Biochem *21*, 143-168.

Fraser, R.A., Rossignol, M., Heard, D.J., Egly, J.M., and Chambon, P. (1997). SUG1, a putative transcriptional mediator and subunit of the PA700 proteasome regulatory complex, is a DNA helicase. J Biol Chem *272*, 7122-7126.

Glickman, M.H., and Ciechanover, A. (2002). The ubiquitin-proteasome proteolytic pathway: destruction for the sake of construction. Physiol Rev *82*, 373-428.

Godbole, D., Mojamdar, M., and Pal, J.K. (2006). Increased level of p27 subunit of proteasomes and its co-localization with tyrosinase in amelanotic melanoma cells indicate its direct role in the regulation of melanin biosynthesis. Cell Biol Int *30*, 895-902.

Goldberg, A.L. (2003). Protein degradation and protection against misfolded or damaged proteins. Nature *426*, 895-899.

Hay, D.C., Kemp, G.D., Dargemont, C., and Hay, R.T. (2001). Interaction between hnRNPA1 and IkappaBalpha is required for maximal activation of NF-kappaB-dependent transcription. Mol Cell Biol *21*, 3482-3490.

Hoyt, M.A., Zhang, M., and Coffino, P. (2003). Ubiquitin-independent mechanisms of mouse ornithine decarboxylase degradation are conserved between mammalian and fungal cells. J Biol Chem *278*, 12135-12143.

Jelen, F., Oleksy, A., Smietana, K., and Otlewski, J. (2003). PDZ domains - common players in the cell signaling. Acta Biochim Pol *50*, 985-1017.

Johnson, J.D., Bernal-Mizrachi, E., Alejandro, E.U., Han, Z., Kalynyak, T.B., Li, H., Beith, J.L., Gross, J., Warnock, G.L., Townsend, R.R., *et al.* (2006). Insulin protects islets from apoptosis via Pdx1 and specific changes in the human islet proteome. Proc Natl Acad Sci U S A *103*, 19575-19580.

Kaneko, T., Hamazaki, J., Iemura, S., Sasaki, K., Furuyama, K., Natsume, T., Tanaka, K., and Murata, S. (2009). Assembly pathway of the Mammalian proteasome base subcomplex is mediated by multiple specific chaperones. Cell *137*, 914-925.

Kannenberg, K., Wittekindt, N.E., Tippmann, S., Wolburg, H., Ranke, M.B., and Binder, G. (2007). Mutant and misfolded human growth hormone is rapidly degraded through the proteasomal degradation pathway in a cellular model for isolated growth hormone deficiency type II. J Neuroendocrinol *19*, 882-890.

Lander, G.C., Estrin, E., Matyskiela, M.E., Bashore, C., Nogales, E., and Martin, A. (2012). Complete subunit architecture of the proteasome regulatory particle. Nature *482*, 186-191.

Lee, J.H., Volinic, J.L., Banz, C., Yao, K.M., and Thomas, M.K. (2005). Interactions with p300 enhance transcriptional activation by the PDZ-domain coactivator Bridge-1. J Endocrinol *187*, 283-292.

Lord, J.M. (1996). Go outside and see the proteasome. Protein degradation. Curr Biol *6*, 1067-1069.

Maganti, N., Moody, T.D., Truax, A.D., Thakkar, M., Spring, A.M., Germann, M.W., and Greer, S.F. (2014). Nonproteolytic roles of 19S ATPases in transcription of CIITApIV genes. PLoS One *9*, e91200.

Marzi, S., Myasnikov, A.G., Serganov, A., Ehresmann, C., Romby, P., Yusupov, M., and Klaholz, B.P. (2007). Structured mRNAs regulate translation initiation by binding to the platform of the ribosome. Cell *130*, 1019-1031.

Melo, S.P., Barbour, K.W., and Berger, F.G. (2011). Cooperation between an intrinsically disordered region and a helical segment is required for ubiquitin-independent degradation by the proteasome. J Biol Chem *286*, 36559-36567.

Pan, L., Yan, J., Wu, L., and Zhang, M. (2009). Assembling stable hair cell tip link complex via multidentate interactions between harmonin and cadherin 23. Proc Natl Acad Sci U S A *106*, 5575-5580.

Pickart, C.M. (2001). Mechanisms underlying ubiquitination. Annu Rev Biochem *70*, 503-533.

Saberi, M.T., Stewart, S.A., Annette, M., Knowles, A.L., Attaix, D., and Samuels, S.E. (2006). Effect of energy substrates on protein degradation in isolated small intestinal enterocytes from rats. JPEN J Parenter Enteral Nutr *30*, 497-502.

Sahu, I., Sangith, N., Ramteke, M., Gadre, R., and Venkatraman, P. (2014). A novel role for the proteasomal chaperone PSMD9 and hnRNPA1 in enhancing IkappaBalpha degradation and NF-kappaB activation - functional relevance of predicted PDZ domain-motif interaction. FEBS J *281*, 2688-2709.

Santos, S.P., Bandeiras, T.M., Pinto, A.F., Teixeira, M., Carrondo, M.A., and Romao, C.V. (2012). Thermofluor-based optimization strategy for the stabilization and crystallization of Campylobacter jejuni desulforubrerythrin. Protein Expr Purif *81*, 193-200.

Schild, L., Lu, Y., Gautschi, I., Schneeberger, E., Lifton, R.P., and Rossier, B.C. (1996). Identification of a PY motif in the epithelial Na channel subunits as a target sequence for mutations causing channel activation found in Liddle syndrome. EMBO J *15*, 2381-2387.

Sheng, M., and Sala, C. (2001). PDZ domains and the organization of supramolecular complexes. Annu Rev Neurosci *24*, 1-29.

Shimkets, R.A., Lifton, R.P., and Canessa, C.M. (1997). The activity of the epithelial sodium channel is regulated by clathrin-mediated endocytosis. J Biol Chem *272*, 25537-25541.

Singh, C.R., Lovell, S., Mehzabeen, N., Chowdhury, W.Q., Geanes, E.S., Battaile, K.P., and Roelofs, J. (2014). 1.15 A resolution structure of the proteasome-assembly chaperone Nas2 PDZ domain. Acta Crystallogr F Struct Biol Commun *70*, 418-423.

Singh Gautam, A.K., Balakrishnan, S., and Venkatraman, P. (2012). Direct ubiquitin independent recognition and degradation of a folded protein by the eukaryotic proteasomes-origin of intrinsic degradation signals. PLoS One *7*, e34864.

Strous, G.J., and Govers, R. (1999). The ubiquitin-proteasome system and endocytosis. J Cell Sci *112 (Pt 10)*, 1417-1423.

Thomas, M.K., Yao, K.M., Tenser, M.S., Wong, G.G., and Habener, J.F. (1999). Bridge-1, a novel PDZ-domain coactivator of E2A-mediated regulation of insulin gene transcription. Mol Cell Biol *19*, 8492-8504.

Truax, A.D., Koues, O.I., Mentel, M.K., and Greer, S.F. (2010). The 19S ATPase S6a (S6'/TBP1) regulates the transcription initiation of class II transactivator. J Mol Biol *395*, 254-269.

Volinic, J.L., Lee, J.H., Eto, K., Kaur, V., and Thomas, M.K. (2006). Overexpression of the coactivator bridge-1 results in insulin deficiency and diabetes. Mol Endocrinol *20*, 167-182.

Watanabe, T.K., Saito, A., Suzuki, M., Fujiwara, T., Takahashi, E., Slaughter, C.A., DeMartino, G.N., Hendil, K.B., Chung, C.H., Tanahashi, N., *et al.* (1998). cDNA cloning and characterization of a human proteasomal modulator subunit, p27 (PSMD9). Genomics *50*, 241-250.

Zacharias, M. (2003). Protein-protein docking with a reduced protein model accounting for side-chain flexibility. Protein Sci *12*, 1271-1282.

Zhou, X., Hao, Q., Liao, J., Zhang, Q., and Lu, H. (2013a). Ribosomal protein S14 unties the MDM2-p53 loop upon ribosomal stress. Oncogene *32*, 388-396.

Zhou, X., Hao, Q., Liao, J.M., Liao, P., and Lu, H. (2013b). Ribosomal protein S14 negatively regulates c-Myc activity. J Biol Chem *288*, 21793-21801.

Publications:

1. Nikhil Sangith, Kannan Srinivasaraghavan, Indrajit Sahu, Ankita Desai, Spandana Medipally, Arun Kumar Somavarappu, Chandra Verma, Prasanna Venkatraman. Discovery of Novel Interacting Partners of PSMD9 a Proteasomal Chaperone –Role of the PDZ-Domain Motif Interaction and Putative Function in Quality Control. FEBS Open Bio, 2014.
2. Sahu I, Sangith N, Ramteke M, Gadre R, Venkatraman P. A novel role for the Proteasomal Chaperone PSMD9 and hnRNPA1 in enhancing IκBα degradation and NF-κB activation - Functional Relevance of predicted PDZ domain-motif interaction, FEBS Journal, 2014.
3. Wadhawan V, Kolhe YA, Sangith N, Gautam AK, Venkatraman P From prediction to experimental validation: desmoglein 2 is a functionally relevant substrate of matriptase in epithelial cells and their reciprocal relationship is important for cell adhesion, Biochemical Journal, 2012.

Signature of the Student

Date: 30/07/14

Doctoral Committee:

S. No.	Name	Designation	Signature	Date
1.	Dr. S. Chiplunkar	Chairman		22/8/14
2.	Dr. Prasanna Venkatraman	Convener		05/08/14
3.	Dr. Kakoli Bose	Member		05/08/14
4.	Dr. Ashok K. Varma	Member		05/08/14
5.	Dr. Sanjeev Galande	Invitee		31/07/14

Forwarded through:

Dr. S. Chiplunkar
(Director, ACTREC
Chairperson, Academic and
Training programme, ACTREC)

Dr. K.S. Sharma
(Director, Academics, TMC)

Prof. K.S. Sharma
DIRECTOR - ACADEMICS, TMC
Mumbai - 400 012

List of figures

S.No.	Figure	Page No.
1.	Figure 2.1 Subunits of the 26S proteasome as illustrated by Murata and colleagues.	**31**
2	Figure 2.2 Assembly of the 19S regulatory particle.	**36**
3	Figure 2.3 The Ubiquitin Conjugation System.	**37**
4.	Figure 2.4 PDZ domain of GRASP55.	**44**
5.	Figure 2.5 PDZ-peptide interaction in the carboxylate binding loop	**45**
6	Figure 2.6 Internal motif recognition by Par6 PDZ domain.	**47**
7	Figure 4.1 Purification of recombinant his-PSMD9.	**82**
8	Figure 4.2 Preliminary screen for identification of putative C-terminal motifs which interact with PSMD9.	**83**
9	Figure 4.3 Validation of putative interacting partners of PSMD9 and the importance of C-terminal Residues in interaction.	**85**
10	Figure 4.4 C-terminal peptides inhibit protein-protein interaction *in vitro*.	**86**
11	Figure 5.1 Identification and validation of important residues in the PDZ domain of PSMD9 with the aid of computational modelling and docking.	**91**
12	Figure 5.2 Molecular dynamic simulation of docked structures of modelled PDZ domain of PSMD9.	**94**
13	Figure 5.3 Modeling of full length PSMD9 and importance of D157 residue.	**97**
14	Figure 5.4 Effect of mutations on secondary and tertiary structure of PSMD9.	**99**
15	Figure 6.1 Interaction of PSMD9 with C-terminal variants of hnRNPA1 and GH from the human proteome.	**105**
16	Figure 6.2 Funcional Modules of PSMD9 and its probable role in quality control by the proteasome.	**108**
17	Figure 7.1 Different specificity of PSMD9 towards GRRF and SCGF motifs.	**112**
18	Figure 7.2 SCGF peptide interacts non-covalently with PSMD9.	**115**
19	Figure 7.3 Probable modes of bind of C-terminal peptides to PSMD9.	**117**
20	Figure 8.1 PSMD9 interacts with hnRNPA1 and increases IκBα degradation and NF-κB activation.	**123**
21	Figure 9.1 Purification of PSMD9 for crystallization.	**130**
22	Figure 9.2 Thermal stability of PSMD9 under different pH conditions.	**133**
23	Figure 9.3Thermal stability of PSMD9 with different additives at pH 7.4.	**134**
24	Figure 9.4 Thermal stability of PSMD9 with different conditions of Morpheus screen.	**135**
25	Figure 10 Model representing the approach used in our study.	**143**

List of Tables

S. No.	Table	Page No.
1	Table 2.1 Subunits of the Proteasome.	**31**
2	Table 3.1 List of primers for cloning and site directed mutagenesis.	**64**
3	Table 4.1 Proteins of the human proteome harboring the C-terminal tetrapeptide sequences as reported by Chung *et. al* in 2003	**81**
4	Table 5.1 Interaction of hnRNPA1 with PSMD9 and its mutants.	**92**
5	Table 5.2 Fraction of helicity of PSMD9 WT and mutants analyzed by circular dichroism.	**99**
6	Table 6.1 Proteins in the human proteome harboring GRRX sequence at their C-terminus.	**104**
7	Table 6.2 Binding of GRRX peptides to PSMD9 by ELISA (X is any amino acid).	**106**
8	Table 7.1 Quantitative analysis of interaction of PSMD9 with hnRNPA1 and growth hormone and their C-terminal mutants.	**113**
9	Table 9.1 List of additives used to increase the thermal stability of PSMD9.	**131**
10	Table 9.2 Conditions of Morpheus screen which gave a proper thermal transition curve in the thermofluor assay.	**136**
11	Table 9.3 Conditions of Morpheus screen used for crystallization trials shortlisted from the thermofluor assay.	**137**

List of Abbreviations

BME	ß- Mercaptoethanol
BSA	Bovine Serum Albumin
cDNA	complimentary Deoxyribonucleic acid
Dlg2	Disc Large Homolog 2
DNA	Deoxyribonucleic acid
DTT	Dithiothreitol
kDa	Kilodalton
ELISA	Enzyme Linked Immunosorbent Assay
M	Molar
mM	Millimolar
MQ	Milli Q (water)
NCBI	National Centre for Biotechnology Information
Ni-NTA	Nickel-nitriloacetic acid
GH	Growth Hormone
GST	Glutathione S-transferase
hnRNPA1	Heterogenous Ribonucleoprotein A1
IL6	Interleukin 6
PAGE	Polyacrylamide gel electrophoresis
PCR	Polymerase chain reaction
PDB	Protein Data Bank
PDZ	**P**SD95, **D**lg2 and **Z**O1
PSD95	Post Synaptic Density 95

PSMD9 Proteasome Macropain non-ATPase subunit 9

SDS Sodium dodecyl sulphate

TBST Tris buffered saline with 0.1% Tween-20

TEMED N,N,N‟,N‟ Tetramethyl ethylene diamine

WISE Whole interactome scanning experiment

WT Wild-type

ZO1 Zonula Occludens1

CHAPTER 1

INTRODUCTION

It is the balance between protein degradation and its synthesis that determines the concentration of proteins in the cell, which in turn regulates cellular homeostasis and survival (Glickman and Ciechanover, 2002). Compartmentalization is central to regulating proteolysis. In eukaryotic cells, a special membrane bound structure called the lysosome degrades extracellular and membrane proteins by vesicle sorting. Another form of compartmentalization is self-compartmentalization, where different polypeptides assemble into a barrel shaped structure which harbors active sites in its inner compartment. A classic example of such a structure is the 26S proteasome. It consists of a 20S catalytic core, which forms the cylindrical structure comprising four heptametrical rings of different subunits stacked one over the other with active sites in the inner compartment. Since the access to these proteolytic nano-compartments are restricted to unfolded proteins or peptides, the 20S catalytic core is coupled to two 19S regulatory complexes which are capable of recognizing, binding and unfolding proteins that are targeted for proteasome degradation. The 19S regulatory particle is made up of 13 non identical subunits, 6 of which belong to the AAA ATPase family. (Goldberg, 2003; Lander et al., 2012). The ATPases at the base of the regulatory particle aid in substrate unfolding, gate opening and translocation of substrates into the 20S proteolytic chamber. Functions of many of the individual subunits are unknown. However few of the non-ATPase subunits have been assigned specific functions. For example, PSMD4 and Ubp 6 deubiquitinate the substrate during degradation, and those like PSMD5, PSMD9 and PSMD10 act as chaperones enabling the assembly of an intact 19S regulatory complex (Kaneko et al., 2009). Sug1 or PSMC5 acts as a helicase and Sug1, along with RNA polymerase II, S6a (PSMC3) and S7 (PSMC2) of the 19S ATPase subunits form a transcriptional activation complex, resulting in the expression of the inflammatory gene CIITApIV (Maganti et al., 2014).

Generally, proteins are conjugated to ubiquitin and subsequently degraded by the proteasome (Pickart, 2001). However, some substrates like Thymidylate synthase and ornithine decarboxylase are degraded in an ubiquitin independent manner (Forsthoefel et al., 2004; Hoyt et al., 2003). Our lab has demonstrated that the disordered F-helix of apomyoglobin initiates the ubiquitin-independent degradation of apomyoglobin by the eukaryotic proteasome *in vitro* (Singh Gautam et al., 2012). Since ubiquitin is removed prior to degradation, to prevent premature release, 19S subunits of the proteasome must engage in interaction with sequences on the substrate. Again using apomyoglobin as a model substrate, we showed that A-helix of the substrate interacts with the 19S regulatory particle and the peptide derived from the region inhibits binding of apomyoglobin to the proteasome. The details of molecular mechanism of substrate recognition by the 19S regulatory particle, the requirement for a specific sequence or structure and the domains of the 19S subunits involved in protein-protein interaction is an active area of investigation.

We were interested in exploring the role of 19S subunits in protein degradation and degradation independent functions. PSMD9, one of the non-ATPase subunits has a PDZ-like domain, responsible for protein-protein interaction. The PDZ domains are well conserved from drosophila to mammals, and generally interact with the C-terminus of the interacting partner (Jelen et al., 2003).The rat homolog of PSMD9, Bridge1, plays an important role in regulating insulin gene transcription by interacting with the C-terminus of helix-loop-helix transcription factor E12, N-terminus of PDX-1 and internal regions of histone acetyl transferase p300. The PDZ domain plays a crucial role in this process. PSMD9 is seems to play an important role in tyrosinase degradation which in turn regulates melanin biosynthesis. It also regulates the transcription of Smad transcription factors during activin signaling. The human PSMD9 and its

PDZ-like domain are not characterized. The specificity of the PDZ domain of PSMD9, its homologs and orthologs is yet to be studied in detail. Here, we presume that

a) the PDZ-like domain of PSMD9 may interact with C-termini of substrates,
b) By recognizing specific but degenerate motifs on substrates, PSMD9 may help in substrate recognition and binding prior to degradation of the substrate by the 20S catalytic core.
c) PDZ domains are known to interact with multiple proteins both acting as a scaffold and as a regulatory protein in processes such as cell signaling. Therefore, it is possible that PSMD9 may interact with multiple proteins and regulate different physiological processes.

In order to explore the potential interacting partners of PSMD9, we took advantage of the specificity that PDZ domains exhibit towards C-termini of its interacting partners. We chanced upon the observation of Chung et. al, who reported that many non-homologous proteins share identical C-terminus by virtue of conservation of typically three, four or eight amino acid residues. Such a group or family of proteins, seem to share similar properties and functions. Chung et al., classified proteome from drosophila/yeast/human by recognizing conserved C-terminal residues in proteins and listed 30 tetra-peptide sequences which have more than 10 members in their group. We chose 12 tetra-peptide sequences from this list. We included peptides with hydrophobic, acidic, basic and polar residues. We also included a peptide, AGHM, which is the C-terminus of human E12 transcription factor, mouse homolog of which is known to interact with the PDZ-like domain of PSMD9. We found that apart from AGHM, two peptides GRRF and SCGF interacted with purified, recombinant PSMD9 by Enzyme Linked Immunosorbent Assay (ELISA). Proteins harboring GRRF motif– heterogenous

ribonucleoprotein A1 (hnRNPA1) and SCGF motif- human somatotrophin (growth hormone, GH) interact with PSMD9. Mutations at the C-termini of these proteins showed that the majority of binding energy came from the C-terminus. We also found that the specificity of the PDZ domain of PSMD9 is different towards GRRF and SCGF. While the terminal residue (P_0) phenylalanine is crucial for interaction in GRRF, cysteine (P_{-2}) is important in the SCGF motif. By homology modeling of the PDZ domain of PSMD9 and docking studies we found putative residues that may be important for protein-protein interaction. By site directed mutagenesis we confirmed that the residues predicted by the docking studies were indeed located in the binding pocket.

Our aim was to find a method that will allow us to quickly move from prediction to validation and functional significance. hnRNPA1 with carries GRRF at the C-terminus is an RNA binding protein. Surprisingly hnRNPA1 was shown to interact with IκBα and this interaction resulted in the activation of NF-κB by an unknown mechanism. Taking cue from this study and based on our observation that C-terminus of hnRNPA1 interacts with PDZ domain of PSMD9, we show that hnRNPA1 recruits IκBα for proteasomal degradation during which PSMD9 acts as a subunit acceptor that binds hnRNPA1 thus facilitating degradation by the protesome resulting in NF-κB activation (Indrajit Sahu thesis and publication). In this thesis we report that this mechanism is probably responsible for increased anchorage independent growth in HeLa cells.

To expand our knowledge on the repertoire of interacting partners of PSMD9, we decided to screen peptides GRRX and SCGX (where X is any amino acid) which are variants of GRRF and SCGF within the human proteome. We found that GRRL, GRRI, GRRQ, GRRR GRRC and SCGL interact with PSMD9, whereas peptides like GRRN, GRRE and GRRG do not interact.

Proteins harboring hydrophobic residues at the terminal residue in the motif – S14 ribosomal protein (GRRL at the C-terminus) and IL6 receptor isoform 2 (SCGL at the C-terminus) interact with PDZ domain of PSMD9. Site directed mutagenesis also confirmed that the C-termini of these proteins are important for interaction both *in vitro* and *ex vivo*. Taking strength from literature, we propose possible physiological relevance of these interactions. .

We also attempted to crystallize recombinant human PSMD9. We standardized a thermoflour assay to determine conditions for crystallization by virtue of protein stability. Crystals were obtained, but they did not diffract. Further standardizations are required to obtain crystals of good quality to elucidate the structure of PSMD9.

We hereby report that using a novel structural bioinformatic principle, and a low throughput cost effective method, we have identified several novel interacting partners of PSMD9, an uncharacterized proteasomal assembly chaperone. We provide a first look at the probable structure of its PDZ domain through computational approaches and identify the important residues that are relevant for interaction and the physiological function of PSMD9 in mammalian cells.

CHAPTER 2

REVIEW OF LITERATURE

2.1 Protein turnover: from a vague idea to present understanding

About six decades ago, proteins were understood as a source of fuel which provide structural and functional support to the body. Later Schoenheimer and Rittenberg used radio labeled tyrosine and leucine to track the amount of proteins that were incorporated into tissues of rat and the amount that was excreted. They found that, only a minute amount of radiolabeled proteins were found in the tissues, of which only a fraction was attached to the original carbon chain, while the bulk was distributed over other nitrogenous groups of the proteins (M.V., 1953; Ratner S, 1940). These experiments clearly showed that proteins were in a dynamic state of synthesis and degradation in an organism. Later in 1949, Christian de Duve discovered membrane bound structures that contain acid proteases. Independent experiments later proved that these hydrolytic enzymes were responsible for protein degradation (M.V., 1953). Under more extreme conditions, cell organelles are engulfed by a process called autophagy by the lysosomes (Ashford and Porter, 1962). It took the world by surprise when ATP was found to be required for degradation of majority of the intracellular proteins and this degradation was independent of the lysosomes (Etlinger and Goldberg, 1977; Hayashi et al., 1973). These experiments paved the way for the discovery of the Ubiquitin Proteasome System (UPS) which degrades intracellular proteins, conjugated to a polymer of a small protein now called ubiquitin, in an ATP dependent manner. Ciecanhover and his colleagues were successful in demonstrating protein degradation in reticulocyte lysates. With the help of biochemical reconstitution experiments, this group was able to identify some of the additional requirements that seemed necessary for protein degradation in these lysates. For example a factor called APF-1, now known as ubiquitin, was identified, and was found conjugated with protein substrates in the presence of ATP which seemed important for

protein degradation (Ciechanover et al., 1980; Ciehanover et al., 1978; Hershko et al., 1980). Later from the experiments on monoubiquitinated H2A, ubiquitin linkage was characterized and it was found to be linked via an isopeptide bond formed between the glycine residue of ubiquitin and lysine of the substrate H2A (Matsumoto et al., 1983). Waxman and his group identified a 1.5 MDa protease, which was later termed as the 26S proteasome (Hough et al., 1987; Waxman et al., 1987). It is now very well known that proteasomes play a vital role in maintaining homeostasis and cellular survival, regulating processes like transcription, translation, DNA repair, regulation of immune and inflammatory responses, amalgamation and development of major networks involving the nervous system, etc. Proteins like cyclins and cyclin-dependent inhibitors, tumor-suppressors, along with transcriptional activators and inhibitors form, as well as misfolded and dysfunctional proteins form the usual substrates of proteasome, going on to highlight its prima facie role in key cellular events (Glickman and Ciechanover, 2002). and any defects in the UPS may lead to various disorders and diseases (Glickman and Ciechanover, 2002).

2.2 The 26S Proteasome

To gain a clear understanding about the functions of the proteasome, it is necessary to understand the structure of the proteasome. The proteolytic mediator which degrades proteins in the absence of lysosome was correlated with a multisubunit 26S assembly by Wilk and Orlowski (Wilk and Orlowski, 1983). Coux, *et al*. later termed this complex as the proteasome(Coux et al., 1996). The 26S proteasome is topologically divided into 20S core particle (CP) and a 19S regulatory particle (RP) (Glickman and Ciechanover, 2002).

2.2.1 The 20S Core Particle

The 20S core particle is largely implicated in the proteolytic activity of the proteasome. Electron microscopy studies on the 700kDa 20S core particle from different tissues and species demonstrated it to be composed of four stacked rings assembled in a cylinder-shape. The diameter of the cavity formed by the cylinder is 12nm and overall length is 17nm (Baumeister et al., 1988; Kopp et al., 1986). X-ray crystallography studies have confirmed that 20S core has 14 alpha and beta subunits with the orientation of $\alpha_7\beta_7\beta_7\alpha_7$ (Lowe et al., 1995).

In higher eukaryotes the subunit composition depends on the cellular environment. For example, on γ-interferon treatment three of the β subunits are replaced in the newly synthesized proteasome by the distinct low-molecular-weight-proteins, called the LMP subunits (LMP2, LMP7 and MECL-1) which convert the activity niche of the proteasome to favor antigen presentation. Under such circumstances, the proteasome is known as the 'immunoproteasome'(Coux et al., 1996)'(Yewdell, 2005).

Depending on the type of tissue or developmental stage of an organism, the composition of the alpha and beta subunits vary (Van Kaer et al., 1994) (Coux et al., 1996). When we compare the sequence of all the subunits of the 20S core, there is very little similarity between individual subunits. The similarity in the primary sequence among the α subunits ranges from 47-56%, whereas the identity varies from 32-39%. In the case β subunits, the similarity ranges from 31-45%, whereas identity varies from 18-33%. A characteristic motif called the GXXXD motif is present in all subunits. The relevance of this motif is still unclear.(Coux et al., 1996)' (Coux et al., 1994), (Lupas et al., 1993), (Kopp et al., 1995).

The β subunits are known for the proteolytic (peptidase) activity required for the hydrolysis of the proteins marked for degradation. They carry active sites that are of chymotrypsin,

trypsin and caspase-like specificities. The α subunits possess a highly conserved N-terminal motif, an RPXG motif of unknown function as well as a nuclear localization signal (NLS). This NLS also has a putative complementary motif that allows for shuttling between the cytoplasm and the nucleus (Coux et al., 1994). By virtue of a molecular gate formed by the loops of the subunits, the α rings unless activated, prevent the entry of cytosolic proteins into β subunits (Coux et al., 1996; Kopp et al., 1986) . Assembly with the 19 S or the 11S regulatory particles results in activation via gate opening.

2.2.2 Assembly of 20S Core

The α-subunits play a crucial role in the initial stages of assembly. There are two chaperone complexes, the Poc1-Poc2 complex and the Poc3-Poc4 complex which associate with seven α subunits to form the ring. This forms the template for another chaperone Ump 1 which brings β subunits sequentially- β2, β3 and β4, followed by β5, β6 and β1 after which β7 is added to the ring. The chaperone complexes- Poc1-Poc2, Poc3-Poc4 and Ump1 are degraded (20S Proteasome Assembly Is Orchestrated by Two Distinct Pairs of Chaperones in Yeast and in Mammals). It is only after the α rings are formed that the β subunits, harboring the pro-sequence, are brought together. (Voges et al., 1999), (Lecker et al., 2006). The protease activity of the β subunits is activated only when there is a cleavage of a N-terminal pro-sequence that exposes a threonine residue for catalysis (Coux et al., 1996).Therefore, the unfolded protein is inserted into the α compartments, which further direct them to the inner β rings that degrade them to short oligopeptides. These are further hydrolyzed by the cytosolic peptidases to amino acids.

2.2.3 The 19S Regulatory Particle (RP)

As is evident from the functions of the 20S CP, the α and β subunits are largely involved in the hydrolysis and breakdown of the unfolded polypeptide (Voges et al., 1999). It was also observed that the 20S core particlces were not capable of degrading substrates in the presence of ATP indicating substrate unfolding must be performed by other subunits. . Glickman, *et al*. biochemically characterized the 19S regulatory particle (RP), earlier termed as PA700 (due to its molecular weight speculated to be 700kDa) and found it to be composed of 18 subunits, of which 6 possessed ATPase activities (Glickman et al., 1998). This 19S RP is a 1 MDa multi-subunit complex that may assemble at one or both ends of the 20S CP (Coux et al., 1996; Glickman and Ciechanover, 2002).

The subunits of the 19S RP can be divided into the `base' and the `lid' (Glickman et al., 1998)' (Zwickl et al., 1999). The base consists of all the ATPases which form the ring like structure along with a few non-ATPases. The lid comprises of non-ATPases only. There is a great deal of sequence similarity between most of the subunits of the lid with that of a large signaling complex called the COP9 signalosome complex, which is involved in many functions[1] (Glickman et al., 1998).

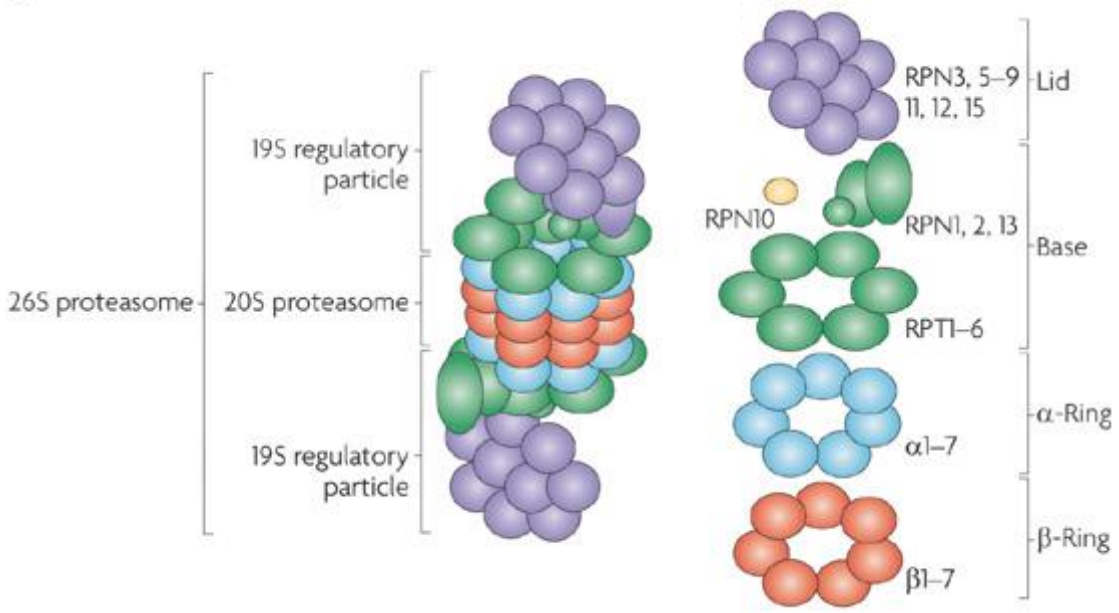

Figure 2.1 Subunits of the 26S proteasome as illustrated by Murata and colleagues (Murata et al., 2009).

Table 2.1 Subunits of the Proteasome

Standard	Alternative	UniProt	Gene*	Miscellaneous	Accession no.*	Length (a.a.)	MW (Da)
20S Proteasome							
α-type subunits							
α1	iota	α6	PSMA6	Pros27, p27k, C7, Prs2, Y8, Prc2, Scl1	P60900	246	27399
α2	C3	α2	PSMA2	Hc3, Psc3, Pre8, Prs4, Y7, Lmpc3	P25787	233	25767
α3	C9	α4	PSMA4	Hc9, Psc9, Pre9, Prs5, Y13	P25789	261	29484

α4	C6	α7	PSMA7	RC6-1, XAPC7, Hspc, Pre6	O14818	248	27887
α5	zeta	α5	PSMA5	Pup2, Doa5	P28066	241	26411
α6	C2	α1	PSMA1	Hc2, Nu, Pros30, Psc2, Pre5	P25786	263	29556
α7	C8	α3	PSMA3	Hc8, Psc8, Pre10, Prs1, C1, Prc1	P25788	254	28302
β-type subunits							
β1	Y	β6	PSMB6	delta, Lmpy, Pre3, Lmp19	P28072	239/205**	25358/21904**
β1i	Lmp2	β9	PSMB9	Psmb6i, Ring12	P28065	219/199**	23264/21276**
β2	Z	β7	PSMB7	alpha, Pup1, Mmc14	Q99436	277/234**	29965/25295**
β2i	MECL-1	β10	PSMB10	Lmp10	P40306	273/234**	28936/24648**
β3	C10	β3	PSMB3	theta, Pup3, C10-II	P49720	205	22818
β4	C7	β2	PSMB2	Pre1, C11, C7-I	P49721	201	22836
β5	X	β5	PSMB5	epsilon, LmpX, MB1, Pre2, Doa3, Prg1	P28074	263/204**	28480/22458**
β5i	Lmp7	β8	PSMB8	Psmb5i, Ring10, Y2, C13, Mc13	P28062	276/204**	30354/22660**
β5t	-	β11	PSMB11	beta5i-like	A5LHX3	300/251**	32530/27232**
β6	C5	β1	PSMB1	gamma, Psc5, Pre7, Prs3, Pts1	P20618	241	26489

β7	N3	β4	PSMB4	beta, Pros26, HsN3, Pre4, Rn3, Lmp3	P28070	264/219**	29204/24392**
19S Proteasome (PA700) Regulator							
ATPase subunits							
Rpt1	S7	Subunit 7	PSMC2	Mss1, Yta3, Cim5	P35998	432	48503
Rpt2	S4	Subunit 4	PSMC1	Yhs4, Yta5, P26s4	P62191	440	49185
Rpt3	S6b	Subunit 6b	PSMC4	S6, Mip224, Tbp7, Yta2, Ynt1, Cip21	P43686	418	47336
Rpt4	S10b	Subunit 10b	PSMC6	p42, Sug2, Prs10, Pcs1, Crl13	P62333	389	44173
Rpt5	S6a	Subunit 6a	PSMC3	S6', p50, Tbp1, Yta1, Sata	P17980	439	49204
Rpt6	S8	Subunit 8	PSMC5	p45, Trip1, Sug1, Cim3, Crl3, Tbpy, Tby1	P62195	406	45626
Non-ATPase subunits							
Rpn1	S2	Subunit 2	PSMD2	p97, Trap2, Hrd2, Nas1, Rpd1	Q13200	908	100200
Rpn2	S1	Subunit 1	PSMD1	p112, Sen3	Q99460	953	105836
Rpn3	S3	Subunit 3	PSMD3	p58, Sun2, P91a, Tstap91a	O43242	534	60978
Rpn4	-	-	RPN4	Son1, Ufd5	Q03465 (S.c.)	531	60153

			(S.c.)				
Rpn5	-	Subunit 12	PSMD12	p55, Nas5	O00232	455	52773
Rpn6	S9	Subunit 11	PSMD11	p44.5, Nas4	O00231	421	47333
Rpn7	S10a	Subunit 6	PSMD6	SGA-113M, p44S10, p42A, PFAAP4	Q15008	389	45531
Rpn8	S12	Subunit 7	PSMD7	p40, Mov34L	P51665	324	37025
Rpn9	S11	Subunt 13	PSMD13	p40.5, Les1, Nas7	Q9UNM6	376	42945
Rpn10	S5a	Subunit 4	PSMD4	ASF1, Mcb1, Sun1	P55036	377	40737
Rpn11	S13	Subunit 14	PSMD14	Poh1, Mpr1, Mad1, Pad1	O00487	310	34577
Rpn12	S14	Subunit 8	PSMD8	p31, Nin1	P48556	350	39612
Rpn13			RPN13 (S.c.)	DAQ1	O13563 (S.c.)	156	17902
-	S5b	Subunit 5	PSMD5		Q16401	503	56065
-	S15	Subunit 9	PSMD9	p27	O00233	223	24682
Gankyrin	-	Subunit 10	PSMD10	p28, p28(GANK)	O75832	226	24428

*Human gene/accession number. **Pro/mature form. Source: (Baumeister et al., 1998; Dubiel et al., 1995; Dubiel et al., 1992b; Finley et al., 1998; Ma et al., 1992)

The ATPase posses a conserved AAA domain (implying ATPases associated with multiple activities) (Dubiel et al., 1992a). They facilitate unfolding of the target proteins and have therefore been termed ‘reverse chaperones’ or ‘unfoldases’ (Lupas et al., 1993). Structural features such as the N-terminal coiled coil region has been shown to be accountable for interaction with the α subunits, and may also be involved, in the association between the individual ATPases (Zwickl et al., 1999). Besides unfolding, these ATPases are presumably

involved in the insertion of the target proteins into the gate of the core (Coux et al., 1996),(Zwickl et al., 1999). Few ATPases like CIM3 and CIM5 in yeast also recognize substrates such as CLB2 and CLB3 cyclins, as well as the fusion protein Ub-Pro-P-galactosidase (Ghislain et al., 1993). Some of these ATPase subunits are responsible for regulating transcriptional activities (Coux et al., 1996). Sug1 or PSMC5 acts as helicase and regulates transcription along with RNA polymerase II. S6a ATPase or PSMC3 acts as a coactivator of Class II MHC gene (Fraser et al., 1997; Truax et al., 2010). Recently, it has been reported that Sug1, S7, and S6a form transcriptional activation complex along with RNA polymerase II, for the expression of the inflammatory gene CIITApIV (Maganti et al., 2014).

The functions of most of the non-ATPases however are unclear and poorly studied. p31, a human homolog of Nin1p, a non-ATPase subunit in yeast, is associated with G1 to S, and from G2 to M transition in cell cycle (Schwob et al., 1994). Subunits such as p112, p97 and p40 contain KEKE motif known to regulate key functions of cell cycle proteins (Coux et al., 1996) (Pentz et al., 1986), (Gridley et al., 1990). Some non-ATPase subunits have also been associated with the isopeptidase activity involved in removal and recycling of the re-utilizable ubiquitin. For example, PSMD4 and Ubp 6 are known to deubiquitinate the substrate during degradation (Kaneko et al., 2009).

2.2.4 Assembly of 19S Regulatory Particle

p27 (PSMD9), p28 (PMD10) and S5b (PSMD5) act as chaperones and aid in the assembly of the 19S regulatory particle. Each subunit binds to specific set of ATPases and non-ATPases to initially form the base of the 19S RP, which provides the foundation for the lid formation (Figure 2.2). p27 (PSMD9) interacts with two ATPases Rpt4 (PSMC6) and Rpt5 (PSMC3) to form one

of the modules which aid in the assembly of the base of the 19S regulatory particle. p27 interacts with Rpt5 via its C-terminal residues (Kaneko et al., 2009; Lee et al., 2011).

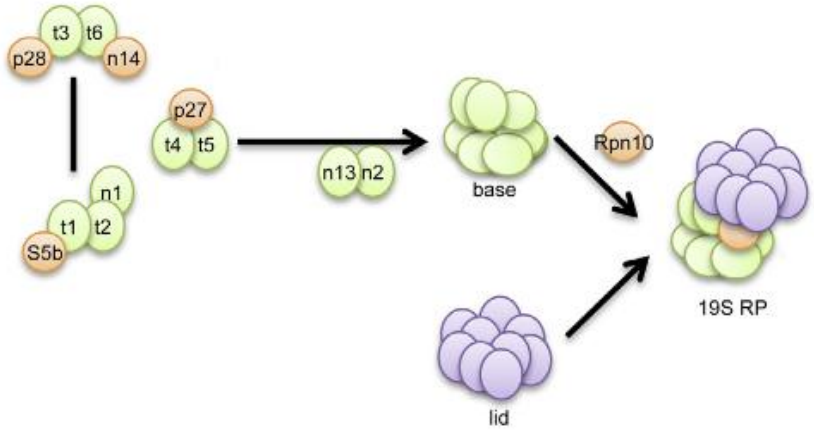

Figure 2.2 Assembly of the 19S regulatory particle. Role of chaperones- p27, p28 and S5b in the assembly of 19S regulatory particle.

2.3 Accessory machinery for degradation- The Ubiquitination Machinery

The key steps which are required for successful degradation of proteins by the 26S proteasome are covalent tagging of polyubiquitin chains to the substrate protein and recognition of these ubiquitinated proteins by the 26S proteasome followed by release of free ubiquitin by deubiquitinating enzymes, unfolding of the polypeptide and hydrolysis of the protein.

A three-step cascade mechanism is implicated in ubiquitin conjugation to the target protein.

The presence of a C-terminal glycine in ubiquitin facilitates its conjugation to ubiquitin molecules and other substrates, while internal lysine residues assist creation of polyubiquitin chains. The enzymatic cascade is initiated by ubiquitin activating enzymes called E1. This enzyme activates ubiquitin by formation of an ubiquitin thiolester in an ATP-dependent reaction. Following its activation, Ub is transferred to sulphydryl group of E2-also referred to as Ub-conjugating enzyme (Glickman and Ciechanover, 2002). The reactive cysteine of E2 is part of a

16kDa conserved region in the 30-40 E2 molecules present in mammalian cells (Lecker et al., 2006). The fully activated Ub is then transferred to a cysteine within a Ub ligase enzyme or E3 causing formation of a third high-energy thiol ester. It is the E3 enzyme that catalyses transfer of the Ub to an internal lysine or terminal group of the substrate protein marked for destruction. Assembly of the multiple Ub chains occurs after this step, via the lysine residues present internal to the Ub (Glickman and Ciechanover, 2002; Lecker et al., 2006) (Seufert and Jentsch, 1991).

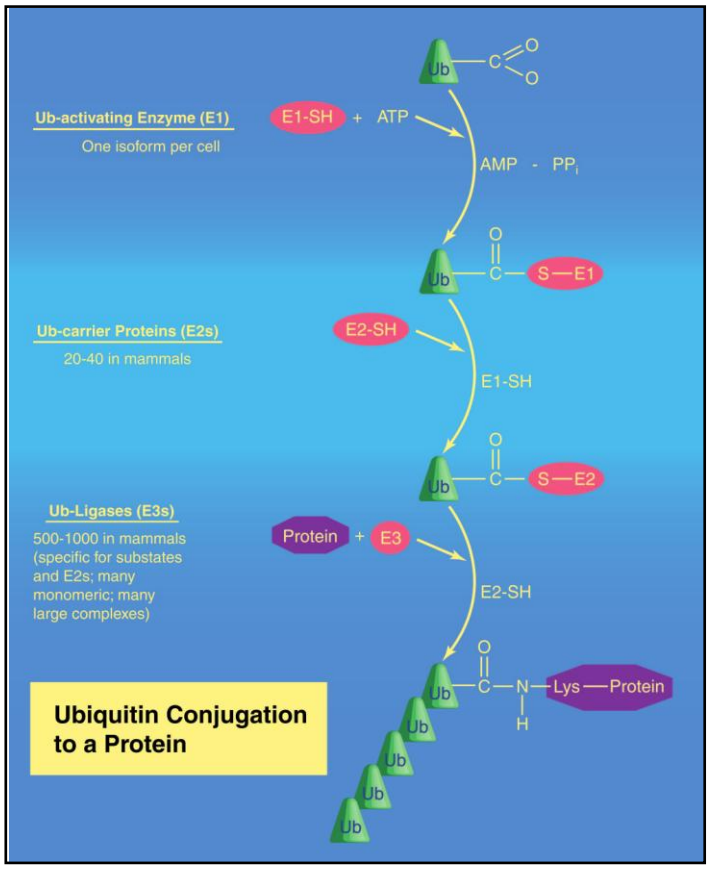

Figure 2.3 The Ubiquitin Conjugation System (Lecker et al., 2006)

2.3.1 The Ubiquitin-Activating Enzyme, E1

The ubiquitin activating enzyme (UBA1), coded by a single gene in yeast and mammalian cells was found to be very important as disruption of this gene was lethal to the cell. (Glickman and

Ciechanover, 2002; Lecker et al., 2006) (Hochstrasser, 1996). This enzyme utilizes energy in the form of ATP to yield a high-energy thiolester-ubiquitin intermediate before it transfers ubiquitin to ubiquitin activating enzyme, E2 (Lecker et al., 2006).

2.3.2 Ubiquitin-activating enzymes, E2 (Ubiquitin-carrier enzymes)

These enzymes represent the first selective step in the ubiquitin-dependent proteasomal pathway. All the E2 isoforms are known to share a 16kDa C-terminal region that harbors the reactive cysteine implicated as the primary residue through which it mediates its action. The substrate specificity is attributable to the vast variety of substrates this enzyme's isoforms are able to recognize. Mammalian cells have a more diverse set of these enzymes and some of the mammalian isoforms of these enzymes are shown to mediate rare activities. For example BRUCE (BIR-repeat containing ubiquitin-conjugating enzyme) is an E2 enzyme found in mice. It is shown to bear a baculovirus inhibitor of apoptosis repeat (BIR) motif, which is found in exclusively in apoptosis inhibitors (Glickman and Ciechanover, 2002; Haas et al., 1982; Hochstrasser, 1996).

2.3.3 Ubiquitin-protein Ligases, E3

The vast repertoire of substrates recognized by ubiquitin can be largely accredited to this family of proteins that have the most number of isoforms compared to the other two. On the basis of the mechanism of ubiquitin addition to the substrate, two types of E3 ligases have been identified- the HECT and the RING ligases (Hershko et al., 1983; Hochstrasser, 1996). HECT ligases are large and monomeric E3s harboring a 350 amino acid residue sequence homologous to the COOH-terminal domain of E6-AP (E6 associated protein) that forms a thiolester bond with ubiquitin at a conserved cysteine residue, which delinks it from E2, and then allows for substrate linkage of ubiquitin. Thus these HECT domain E3s are distinguishable from the RING domain

E3s that function as scaffolds to bring together E2-ubiquitin and the protein substrate. The RING domains are 40-60 residue zinc-binding motifs that contain core amino acids cysteine and histidine. These domains may be a part of monomeric proteins or multiple subunits, both having equal capacity to mediate their specific function. Monomeric RING domain E3s include Mdm2, which functions as an efficient physiological regulator p53 in normal cells (Elenbaas et al., 1996). Ring-finger E3s containing multiple subunits are comprised of certain key proteins such as anaphase promoting complex that is involved in ubiquitin-mediated degradation of cell-cycle control proteins, like cyclins and other associated proteins (Lecker et al., 2006). The largest group of E3 is comprised of Cullin-RING ligases, which have the characteristic cullin subunit that binds RING domain and the E2 at one end, and the substrate-interacting protein at the other, often via other adaptor proteins. An additional subset of the E3 ligases containing the U-Box domain have been identified to function as scaffolds adding transfer of ubiquitin from E2 to a pre-assembled ubiquitin moiety, most likely in poly-ubiquitin chain assemble (Glickman and Ciechanover, 2002).

2.4 Substrate Recognition by the Proteasome

The discriminatory ability of the proteasome in protein degradation is remarkable. This is achieved with the help of various factors. Substrate degradation is subject to spatial and temporal regulation aided by factors like intrinsic signals within the protein, or post translational modification on the protein (Glickman and Ciechanover, 2002). For example, phosphorylation of the target acts like functional stimuli for ubiquitination. Most proteins undergo phosphorylation for recognition by E3 ligases eg., Iκβα, the inhibitor of the nuclear transcription factor NF-κB, and β-catenin. Phosphorylation of serine residues at positions 32 and 36 are compelling signals

for degradation of IκBα. This is a physiologically essential event crucial for various activities of the cell, specifically in immune responses mediated by expression of certain cytokines and inflammatory factors (Glickman and Ciechanover, 2002). β-Catenin interacts with cadherin to participate in cell-cell adhesion and regulates gene expression by acting as a transcriptional co-activator(Radz and Nash, 1998; Willert and Nusse, 1998). In the absence of extracellular stimuli, cytosolic β-catenin is phosphorylated by glycogen synthase kinase-3β, leading to its ubiquitination and subsequent degradation by the 26 S proteasome. However, extracellular stimuli, such as Wnt signaling, lead to the inhibition of glycogen synthase kinase-3β, escape of β-catenin from ubiquitin-dependent proteolytic degradation, and subsequent cytosolic accumulation of β-catenin (Aberle et al., 1997). The accumulated β-catenin translocates into the nucleus in association with members of the T cell-factor (Tcf)1/lymphoid-enhancer-factor (Lef) family of transcription factors, leading to stimulation or suppression of target gene transcription.

2.4.1 Role of adapter or ancillary proteins in protein degradation

The ubiquitin-mediated proteolytic pathway is also regulated by ancillary proteins that may include molecular chaperones which function as *trans*-acting elements, permitting association with a select number of ligases. An example of such a *trans*-acting ancillary protein is the viral protein E6. It forms a ternary complex with the HECT-domain E3 E6-AP and the tumour-suppressor protein p53, which results in the ubiquitination and subsequent degradation of p53. (Glickman and Ciechanover, 2002). Experiments in Schizosaccharomyces pombe have clearly shown that the degradation of the metabolic enzyme ornithine decarboxylase (ODC) requires the binding of an adapter protein called antizyme. Proteasome degradation of ODC was significantly affected in mutants lacking antizyme (Chattopadhyay et al., 2001).

2.4.2 'Cis-acting elements' within the substrate contribute to degradation

The contribution of the substrate protein to the specificity of the ubiquitin-proteasome pathway is attributable to the N-end rule, as explained by Varshavsky. This correlates the metabolic instability of a protein to the presence of certain key sequences in the N-terminus of the protein, termed as N-degron. In eukaryotes, these sequences include the N-terminal residues along with an internal lysine on which the ubiquitin chains are transferred) (Varshavsky, 1995). In the case of thymidylate synthase, the N-terminal residues acted as degrons, where degradation was found to be independent of ubiquitin. DHFR could be degraded by the proteasome by artificially fusing an unstructured tag and a proteasome subunit (Henderson et al., 2011). The destabilization of F-helix of apomyoglobin due to the removal of heme makes it susceptible for degradation by the proteasome in an ubiquitin independent manner. The residues of the A-helix of apomyoglobin were shown to be important for the interaction with the 19S RP of the 26S proteasome (Singh Gautam et al., 2012). This shows that there are intrinsic signals within the protein that are responsible for degradation by the 26S proteasome and the 19S RP subunits may play a major role in binding and recruitment of substrate prior to degradation.

2.5 PSMD9: a non-ATPase of the 19S Regulatory particle

Studies on the regulatory particle (PA700) revealed the presence of a trimer modulator that enhanced the association of the regulatory particle complex with 20S and increased the protease activity by about 8 fold (DeMartino et al., 1996). Further characterization revealed that this trimeric complex composed of three subunits two of which were ATPases- p42 (Rpt4 or PSMC6) and p50 (Rpt5 or PSMC3) and a non-ATPase subunit p27 (human: PSMD9, rat: Bridge-1 and yeast: Nas2). The non-ATPase subunit p27 was later found to be a chaperone that binds selectively to these subunits for the assembly of the 19S regulatory particle (Kaneko et al.,

2009). The gene encoding p27 was mapped to the region q24.2-q24.3 of chromosome 12 (Watanabe et al., 1998).

2.5.1 PSMD9 harbors a PDZ-like domain

PSMD9 is a 24 KD protein with 223 amino acids. Thomas et. al in 1999 reported that the residues 138-178 of the rat homolog of PSMD9, Bridge-1 are conserved with well-known PDZ domain containing proteins. Rat Bridge-1 and human PSMD9 are highly homologous, with 70% identity (156 of 222 amino acids) and 82% similarity at the protein level. The two sequences diverge at the carboxy termini of the proteins. Comparison of the first 184 amino acids of rat Bridge-1 and p27 proteins yields 84% identity and 98% similarity. Homologies with other proteins having PDZ domains ranged from 27 to 54% identity and 46 to 77% similarity (Thomas et al., 1999).

2.5.2 Bridge-1: A coactivator of insulin gene transcription

In an attempt to deduce the proteins involved in insulin gene transcription in rat insulinoma cells, Thomas et. al found that rat Bridge-1 interacted with E12, which is a member of the basic helix-loop-helix transcription factors. The PDZ domain of Bridge-1 interacted with C-terminus of E12 and activated the insulin gene transcription. Later, it was discovered that Bridge-1 also interacted with the N-terminus of another transcription factor PDX-1 and internal C2H2 regions of a histone acetyl transferase p300 to activate the insulin gene (Lee et al., 2005; Thomas et al., 1999). This was surprising because PDZ domains are well known to interact with C-terminal residues of the interacting partner. Here it seemed that Bridge-1 had a unique PDZ domain of a different specificity that could interact with the N-terminus of PDX-1 and internal regions of p300. Another interesting observation was that overexpression of Bridge-1 in rat pancreatic β-cells resulted in apoptosis, thereby causing type II diabetes in rats. It is assumed that a particular

concentration of Bridge-1 is required in the cells so that the stoichiometry of Bridge-1 and its interacting partners are maintained to form an active transcription activation complex to activate insulin gene transcription (Volinic et al., 2006).

2.5.3 PSMD9 regulates melanin synthesis in melanoma cells

Studies on melanin biosynthesis in mouse melanoma cells by Godbole *et al*., have outlined the role of p27 in degradation of the enzyme tyrosinase, which is known to play a crucial part in synthesis of melanin (Godbole et al., 2006). Therefore a specific and selective interaction of this non-ATPase subunit with a regulatory enzyme has also been established.

2.5.4 PSMD9 regulates activin signaling in human ovarian granulosa cells

Activin A, is a member of the transforming growth factor beta (TGF- β) superfamily, and is involved in regulation of various cellular processes such as growth and differentiation. This protein was found to upregulate the production of Bridge-1 in human ovary (granulosa) cells. This activation in synthesis of Bridge-1 was found to be the positive regulator in the production of Smads 2, 3 and 4, thereby implying a role that Bridge1 could play in granulosa cell proliferation and differentiation (Banz et al., 2010).

Given all these roles mentioned above it is clear that PSMD9 has a greater role to play in regulating many physiological processes in the cell, and the importance of the PDZ domain in regulating these processes cannot be ruled out.

2.6 The PDZ domain

The PDZ domains are well conserved, most widespread protein-protein interaction modules. The name PDZ is derived from the first letter of three proteins- postsynaptic density protein-95

(PDZ-95), disks large tumor suppressor (DLG) and zonula occludens-1 (ZO-1), which were discovered about two decades ago (Cho et al., 1992; Kim et al., 1995; Woods and Bryant, 1993) The abundance of PDZ domains in unicellular organisms is very less compared to multicellular organisms. This indicates that PDZ domains evolved with multicellularity (Harris and Lim, 2001). The PDZ domains have approximately 80-90 amino acids having 2 α helices and 6 β strands with β1–β2–β3–α1–β4–β5–α2–β6 secondary structure arrangements (Figure 2.3).

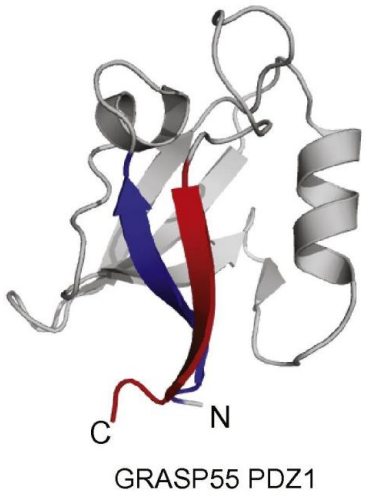

Figure 2.4 PDZ domain of GRASP55. PDZ domain of GRASP55(PDB code 3RLE) with N and C- terminus in blue and red respectively, having 2 α helices and 6 β strands.

PDZ domains recognize C-terminal sequences of the interacting partner. Based on the nature of the C-terminus they interact, PDZ domains are classified into three classes- class 1 (*X*-[T/S]*X*-Φ-$_{OOH}$) and class 2 (*X*-Φ-*X*-Φ$_{COOH}$), where *X* is any residue and Φ is a hydrophobe. Less

common classes of PDZ domains, such as class 3 recognizing the motif _*X*-[E/D]-*X*ϕ_{COOH} (Nourry et al., 2003; Songyang et al., 1997; Stricker et al., 1997). The PDZ binding groove is also termed as the carboxylate- binding loop which consists of a well conserved motif R/K-X-X-X-G-LG-F where the residues C-terminal peptide sequence form a network of hydrogen bonds with the main chain amide groups of the loop (Figure 2.4). In addition to this, the β-strand-β-strand interactions between the peptide and strand βB enables better positioning of the peptide, where we can find the P_0 and P_{-2} ligand residues point directly into the base of the peptide-binding groove (Harris and Lim, 2001).

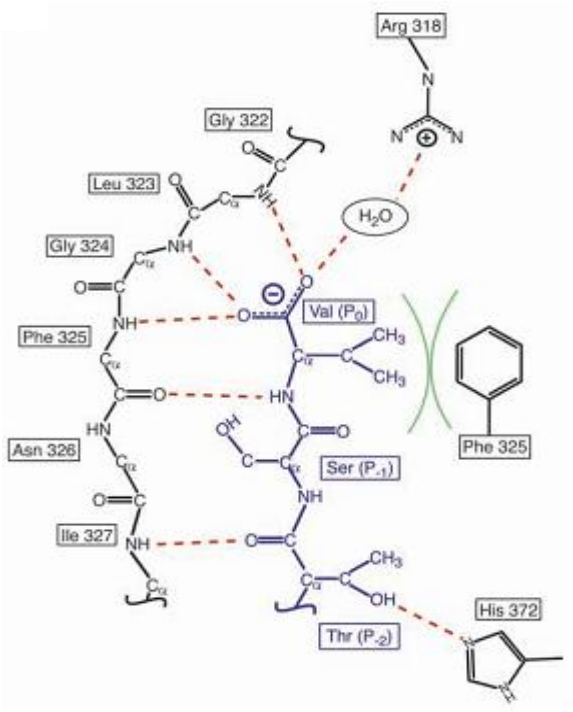

Figure 2.5 PDZ-peptide interaction in the carboxylate binding loop (Harris and Lim, 2001).

PDZ-peptide interactions lack salt bridges, which make these interactions indirect. This property may help in prevent nonspecific recognition of free C-termini of amino acids or

carboxylates. These interactions are also of much low affinity (low-to-mid micro molar) range aiding its regulatory functions (Haq et al., 2012)

2.6.1 PDZ-PDZ interactions

Approximately 30% of PDZ domains are involved in PDZ-PDZ interactions, which are mostly with low micromolar affinity. The dimerization or oligomerization of these domains enables these proteins in engaging in processes like cell signaling or signal transduction (Lau and Hall, 2001; Xu et al., 1998). The peptide binding sites are also available in these multimeric complexes. For example, the PDZ domain of ZO-1 dimerizes and swaps its β1 with β2 of the other domain retaining its overall fold and peptide binding site. This increases the avidity of binding (Chen et al., 2008; Fanning et al., 2007).

2.6.2 Internal Motif Recognition

PDZ domains are well known for recognizing C-terminal motifs, but there are many evidences which show that they interact with internal motifs (Ellencrona et al., 2009; Hillier et al., 1999; Hurd et al., 2003; London et al., 2004; Sengupta and Linstedt, 2010; Uemura et al., 2004; Wong et al., 2003; Zhang et al., 2007). In this kind of interaction, there is always a chance of steric hindrance caused by amino acids in the internal segment and the hydrophobic groove. This hindrance is avoided by generally adopting a β structure in place of the C-terminal motif, which perfectly enters the hydrophobic pocket. The classical example of internal motif binding to the PDZ domain is the interaction of α-1-syntrophin (SNTA1) with 30 amino acid residue extension of the nitric oxide synthase (nNOS) PDZ domain (Figure 2.5) (Hillier et al., 1999). In some interactions which involve internal motifs with the PDZ domain, the PDZ domain undergoes conformational changes to accommodate the motif within the pocket (Peterson et al., 2004). The ability to interact with the internal motifs enables formation

of multimeric protein complexes which may be necessary in regulating many functions in the cell. For example, the PDZ domain of PSD-95 interacts with the N-terminal regions and C-terminus of shaker-type K^+ channels regulating potassium currents across the membrane (Eldstrom et al., 2002).

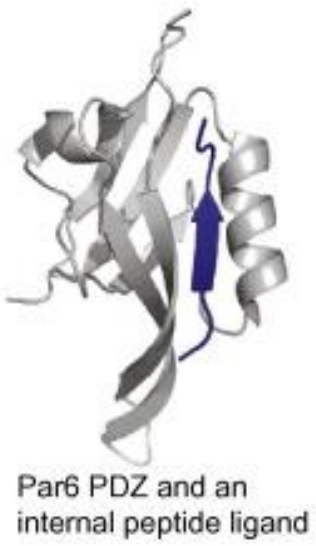

Figure 2.6 Internal motif recognition by Par6 PDZ domain. Internal motif of the interacting partner (PALS1) complexed with Par6 PDZ domain (PDB code (1X8S) (Penkert et al., 2004).

2.6.3 Other ligands of the PDZ

It was about a decade ago that researchers discovered that PDZ domains could interact with small molecules in the cell, apart from peptides and proteins (Zimmermann et al., 2002). Phosphoinositide (PIP) are phosphorylated molecules of inositol, which serve as regulators of cell signaling and polarization. They are well secondary messengers in different signaling cascades within the cell. It was found that the PDZ domain of syntenin interacts with phosphotidyl inositol 4,5- bisphosphate and this complex was found to play a crucial role in cell spreading and directional movements in zebra fish (Lambaerts et al., 2012; Zimmermann et al.,

2005). There are various examples which show that PDZ domains interact with phosphoinositides on the membrane and thus enable clustering of its interacting partners or recruiting important kinases or phosphatases which regulate various signaling cascades. For example, the second PDZ domain of Par3 interacts with PIPs in the membrane so that the third PDZ domain of Par3 can recruit PTEN for signaling (Feng et al., 2008). The region of the PDZ domain that binds to PIPs is the same as the peptide's. The PTP-BAS PDZ domain binds to PIP2 at the α2 β2 region and competes with peptide binding (Kachel et al., 2003). Based on the ability of PDZ domains interacting with lipids they are classified into Class A and Class B, respectively. Class A lipid-binding PDZ domains have topologically distinct peptide and lipid binding sites and acting as coincidence detectors of lipid and peptide signaling. Class B PDZ domains have basic clusters in or near the α2 helix that makes part of the peptide binding site (Chen et al., 2012). Exhaustive studies are still required for understanding the mechanism and function of PDZ- lipid interaction.

2.7 Protein-Protein Interactions: The Premise of Protein Structure and Function

Protein-protein interactions (PPI) are the basis of major physiological processes in the cell. Any gain or loss of functions of these interactions may lead to disorders or diseases. Most features of PPIs are characterized by the interface, the structural and chemical aspect of which is important and decisive in the interaction (Chen et al., 2013). Most interactions are reversible, where the interface of proteins which interact comprise of hydrophobic residues. The major forces involved are weak forces such as hydrogen bonds and electrostatic interactions, which exercise their effect to yield a reversible association between interacting partners. The exclusive implication of secondary structural motifs in particular reactions is not yet demonstrated, however, their presence on the interface in case of a few interactions is known (Stites, 1997).

The secondary structural elements that occupy the interface are classified as α, β, α/β, and coil (Jones and Thornton, 1995). Depending on the stability and physiological duration of the interaction, PPIs may be stable, transient, obligate or non-obligate (Nooren and Thornton, 2003). The area of the complex formed that gets buried away from the solvent is referred to as the buried surface area and plays an important role in affinity of the interaction (Kastritis and Bonvin, 2013). Chen, *et al*., have proved that as the buried surface area increases, the binding affinity and the binding energy increase; whereas the hydrophobicity of the interfacial or surrounding amino acids does not qualify as the prominent driving force of the interaction (Chen et al., 2013). Crucial to the thermodynamic favourability (energetics) of the reaction are certain residues, known as 'hot-spot residues'. These are defined as residues whose mutation to alanine results in a decrease in binding energy by at least 2 kcal/mol (Chen et al., 2013). They are significantly different from the null-spots, whose presence does not perturb the binding energy. The effect of 'hot-spot residues' on the binding energy can be studied using alanine-scanning mutagenesis (Kastritis and Bonvin, 2013). Mutagenesis is generally used to investigate the disruption of interfaces, or abrogation of interactions (Stites, 1997).

Certain PPI that are detrimental to cellular functioning can be specifically targeted using intricately designed small molecule inhibitors (Chen et al., 2013). The existence of this therapeutic aspect warrants the in-depth and thorough study of PPIs.

There are multiple ways of studying PPIs, quantitatively or qualitatively, most of which have been well defined by Phizicky, et al. (Phizicky and Fields, 1995). The strength of the interaction been probed can be well understood by the study of an important parameter, viz. binding constant K_d. Multiple experiments such as ELISA, fluorescence anisotropy, gel-filtration columns, and surface plasmon resonance are employed (Phizicky and Fields, 1995).

2.8 Library-based methods to detect protein-protein interactions

An *in vitro* strategy to explore protein-protein interactions in a high throughput fashion is to screen for binding of peptide motifs which can potentially interact with the protein of interest. Many domains like PDZ, WW, SH2, SH3 etc. accommodate short peptides in their binding pockets (Pawson and Nash, 2003; Pawson and Scott, 1997). To understand the repertoire of interacting partners of proteins containing these domains various peptide screening techniques have been used. Phage display has been widely used to identify peptide ligands to a number of proteins (Sidhu et al., 2000). Phage recovery and library titer depend on a number of factors such as peptide-target affinity, bacterial toxicity of encoded peptides, viability of phage after panning and particle recovery, as well as inherent infection and replication properties of targeted phage clones (Sidhu et al., 2000). SPOT synthesis is a new technology to synthesize large number of addressable peptides in small amounts, and can be coupled on to a cellulose background in short time and cost effective manner. Whenever necessary peptides can be cleaved for performing binding assays (Hilpert et al., 2007).

WISE (Whole Interactome Scanning Experiments) is a combination of the techniques mentioned above. Using phage display experiment as the foundation, Landgarf et. al have used SPOT synthesis to synthesize peptides, after which there is rapid and reliable identification of the partners of any peptide recognition module by peptide scanning of a proteome. WISE addresses the problem of identifying natural peptides with the potential for binding to any given recognition domain. Although we can use this information to infer the formation of protein complexes *in vivo,* there are a number of reasons where such inferences can turn out to be incorrect (Landgraf et al., 2004). A peptide could be unavailable for interaction in the native protein structural context or the localization of the two proteins may be in different

compartments, which makes it obvious that they will not interact. In such techniques mentioned above, one may miss out important low affinity ligands that may be very important in the context of cellular function.

Apart from the screening peptide libraries, there are number of techniques that are used to identify protein interacting partners like yeast two hybrid, chemical crosslinking and tandem affinity purification which enable researchers to find weak interactors. Mass spectrometry based SILAC techniques also help in identifying interacting partners and avoid non-specific identification. In this thesis, we report the use of a simple, cost effective, low throughput peptide screen using ELISA to identify interacting partners of a PDZ domain containing protein PSMD9. Weak interacting peptides were identified, which were C-terminal motifs of proteins that interacted in mammalian cells and were of physiological significance.

CHAPTER 3

MATERIALS AND METHODS

MATERIALS

3.1 Buffers and Reagents:

3.1.1 Luria-Bertani (LB) medium (for 1 L)

NaCl 10 g

Tryptone 10 g

Yeast extract 5 g

The components mentioned above were added to deionized water (milliQ). The pH was adjusted to 7 with 1M NaOH and autoclaved.

Or

25 g of LB powder (Merck) was dissolved in 1 L of MQ water and autoclaved.

3.1.2 LB-Ampicillin Agar Plates (for 1 L)

NaCl 10 g

Tryptone 10 g

Yeast extract 5 g

Agar 20 g

The components mentioned above were added to deionized water and pH was adjusted to 7.0 with 10 N NaOH and autoclaved. The media was cooled to about 60 °C and 1 ml of 100 mg/ml ampicillin was added. The media was poured into petri dishes (~25 ml/100 mm plate).

3.1.3 Tris-EDTA (TE) Buffer (for 50 ml)

Tris 60.66 mg (10 mM)

EDTA 14.62 (1 mM)

pH was adjusted to 7.5 with 10 N NaOH and autoclaved.

3.1.4 Ampicillin Stock

Stock concentration : 100 mg/ml (Filter sterilized using 0.2 □m membrane)

Working concentration: 100 µg/ml

3.1.5 50X TAE Buffer (for 1 L)

Tris base 242 g

Glacial acetic acid 57.1 ml

0.5 M EDTA (pH 8.0) 100 ml

Prepare 1X TAE buffer for agarose gel electrophoresis.

3.1.6 6X Gel Loading Buffer for DNA (for 100 ml)

Xylene Cyanol FF 0.25 g (migrates at 4160 bp with TAE)

Bromophenol blue 0.25 g (migrates at 370 bp with TAE)

Glycerol 30 ml

3.1.7 Ethidium Bromide (EtBr)

Stock concentration 10 mg/ml (20000X)

Working concentration 0.5 µg/ml

3.1.8 Buffers for Protein Purification and Gel Filtration:

3.1.8.1 Ni-NTA Lysis Buffer (for 1 L)

Tris 6.06 g (50 mM, pH 8.0)

NaCl 29.22 g (500 mM)

Imidazole 0.6 g (10 mM, reduces non-specific binding of proteins)

Glycerol 100 ml (10%)

TritonX-100 1 g (0.1%)

Protease inhibitor (10X) 1X

BME (14.3 M) 3.5 ml (50 mM)

Lysozyme 1 g (1 mg/ml)

3.1.8.2 Ni-NTA Binding/Washing Buffer (for 1 L)

Tris 6.06 g (50 mM, pH 8.0)

NaCl 29.22 g (500 mM)

Imidazole 0.6 g (10 mM, reduces non-specific binding of proteins)

Glycerol 100 ml (10%)

TritonX-100 1 g (0.1%)

Protease inhibitor (10X) 1X (in lysis buffer only)

BME (14.3 M) 3.5 ml (50 mM)

3.1.8.3 Ni-NTA Elution Buffer (for 1 L)

Tris 6.06 g (50 mM, pH 8.0)

NaCl 29.22 g (500 mM)

Imidazole 30.04 g (500 mM, for elution)

Glycerol 500 ml (10%)

TritonX-100 1 g (0.1%)

Protease inhibitor (10X) 1X

BME (14.3 M) 3.5 ml (50 mM)

3.1.8.4 Transport Buffer (TB) (for 50 ml)

HEPES 0.238 g (20mM, pH 7.9)

Potassium acetate 0.54 g (110mM)

Sodium acetate 0.02 g (5mM)

EGTA 0.009 g (0.5mM)

DTT 0.0077 g (1mM DTT) or 50 µl of 1M DTT solution

3.1.8.5 1X Phosphate buffer saline pH 7.5 (1 L) for GST-fusion protein purification

NaCl 8 g (137 mM)

KCl 0.2 g (2.7 mM)

Na_2HPO_4. $2H_2O$ 1.44 g (10 mM)

KH2PO4 0.24 g (2 mM)

Protease inhibitor (10X) 1X (during lysis only)

3.1.8.6 Elution buffer for GST-fusion protein purification (for 50ml)

Tris 0.3 g (50 mM, pH 8.0)

L- Glutathione reduced 0.15 g (10mM)

3.1.8.7 Binding and washing buffer for MBP- fusion protein purification (for 1L)

Tris 6.06 g (50 mM, pH 8.0)

NaCl 29.22 g (500 mM)

Protease inhibitor (10X) 1X (during lysis only)

BME (14.3 M) 3.5 ml (50 mM)

3.1.9 NP-40 Lysis Buffer (for 50 ml)

Tris 0.121 g (20 mM, pH 7.5) or 0.5 ml of 2 M Tris pH 7.5

NaCl 0.4383 g (150 mM) or 1.5 ml of 5M NaCl

NP-40 250µl of absolute solution

DTT 0.0077 g (1mM DTT) or 50 µl of 1M DTT solution

3.1.10 10 mM Phosphate Buffer pH 7.5 (1 L)

Monosodium phosphate 0.2596 g

Disodium phosphate 2.1758 g

3.1.11 10mM Sodium bicarbonate buffer pH 9.3 (50 ml)

Sodium bicarbonate 0.42 g

Sodium carbonate 0.17 g

3.1.12 Tris Base Saline Tween 20 buffer (TBST) (for 1L)

Tris 6.06 g (50 mM, pH 7.5)

NaCl 8 g (137 mM)

Tween 20 0.5 ml (0.05%)

3.1.13 1X Transfer Buffer (for 1 L)

Glycine 14.4 g

Tris Base 3.02 g

Milli-Q 0.8 L

Methanol 200 ml

3.1.14 Tissue Culture Media and Reagents

Tissue Culture Medium: Dulbecco's Modified Eagle Medium (DMEM), which contains pyridoxine hydrochloride, sodium pyruvate and high glucose (Gibco) was prepared according to the manufacturer's directions. DMEM powder was dissolved in 800 ml of sterile deionized water. To this 3.5 g sodium carbonate was added and pH was adjusted to 7.2 using 1 N HCl. The volume was made up to 1 L. The volume was made up to 1 L and the medium was filter sterilized through a 0.22 µm pore size membrane which was fitted in the sterile filter assembly. The filtered medium was stored at 4 °C as 500 ml aliquots. 10% FBS was added to DMEM to make complete medium.

3.1.14.1 10X phosphate buffered saline (PBS) (for 1 litre)

NaCl 80.8 g (137 mM)

KCl 2.0 g (2.7 mM)

Na_2HPO_4. $2H_2O$ 12.6 g (21.6 mM)

KH_2PO_4 2.0 g (293.3 mM)

Glucose 10.0 g (55.5 mM)

The components were dissolved in autoclaved deionized water and the volume made up to 1 L. The solution was filter sterilized through a 0.22 µm pore size membrane and stored at 4 °C.

3.1.14.2 10X Trypsin (0.25%)

2.75 g of trypsin was added to 110 ml of autoclaved Milli-Q water and allowed to dissolve. The solution was sterilized by filtering through a 0.22 µm pore size filter.

The solution was stored as 10 ml aliquots at -20 °C. 10X stocks were diluted to 1X working solution with 1X PBS. Working solution was stored at 4 °C.

3.1.14.3 2X BBS (BES Buffered Saline) (for 50 ml)

BES 0.533 g (50 mM)

NaCl 0.818 g (280 mM)

$Na_2HPO4.2H2O$ 0.0134 g (1.5 mM)

All the reagents were dissolved in 45 ml of Milli-Q water. The volume was made up to 50 ml and filter sterilized using 0.22 µm filter (Millipore) and stored as 0.5 ml aliquots at -20^0C.

3.1.14.4 0.5M $CaCl_2$ (for 50 ml)

CaCl2.2H2O 3.675 g

CaCl2.2H2O was dissolved in 45 ml of Milli-Q water. The volume was made up to 50 ml and filter sterilized using 0.22 µm filter (Millipore) and stored as 0.5 ml aliquots at -20^0C.

3.1.15 Other Reagents (for 100 ml)

2 M Tris 24.22 g (pH 7.5, adjust pH with concentrated HCl)

1 M $MgCl_2$ 9.52 g

1 M DTT 15.42 g

5 M NaCl 29.22 g

10 M NaOH 58.44 g

All the reagents were filtered with 0.22 µm filter membrane (Millipore).

3.2 Experimental Protocol:

3.2.1 Primer Reconstitution

Primers were obtained from Sigma Aldrich. The vials containing lyophilized primers were given a short spin after which autoclaved 10mM Tris pH 7.5 was added to the lyophilized primers to final concentration of 100 µM (volume of 10mM Tris added according to manufacturer's instructions) and kept on ice for 1 hour with intermittent vortexing. The primers were then diluted to 10 µM and used for polymerase chain reaction (PCR).

3.2.2 Determination of Nucleic Acid Concentration

The concentration of the nucleic acid in solution was estimated using NanoDrop, Model - ND 1000 spectrophotometer. The absorbance of the solution was measured at 260 nm and concentration was calculated using the following formula:1 OD260 = 50 µg/ml for double stranded DNA1 OD260 = 40 µg/ml for RNA.

3.2.3 Polymerase Chain Reaction (PCR)

PCR amplification was done using Phusion enzyme (Thermo Fischer), 25 mM dNTPs, DMSO, DpnI (Fermentas). The proofreading activity of pfu enzyme provided error free

amplification. A 50 µl PCR reaction containing 50-60 ng template plasmid and control reaction (without Phusion) was set-up.

5X – reaction Buffer 10 µl

Template DNA 50 -100 ng

25 mM dNTP Mix 1 µl

MQ Water Variable

Primer (Forward 10 µM) 1 µl

Primer (Reverse 10 µM) 1 µl

Phusion 1 U

Reaction volume 50 µl

The cycling steps used were initial denaturation- 95 °C for 5 min, denaturation- 95 ºC for 1 min, annealing - 55-65 °C for primer annealing for 1 min, extension- 72 °C for 1-3 min (depending upon PCR product size, 1 minute for 1000 bp) and final extension for 10 min at 72 °C.

3.2.4 Site Directed Mutagenesis

For site directed mutagenesis total 18 cycles were repeated without any final extension. The extension time of 30 sec per Kb of PCR product amplification was used for high fidelity fusion DNA polymerase (Thermo Scientific). The following PCR condition was used: initial denaturation – 95 ºC for 5 min, denaturation- 95 ºC for 1 min, annealing – 50 ºC for 1 min, extension- 72 ºC for 1min/kbp and number of cycle 19. The 10 µl PCR product and control reaction (every component except Pfu enzyme) were resolved on 0.8% agarose gel. After confirming amplification, DpnI digestion was setup in a 25 µl reaction using 20 µl of PCR product, 2 µl of 10X Tango buffer and 10 units of DpnI for at least 8 h at 37 ºC. DpnI would digest the parental plasmid (cleave adenomethylated dam sites). The digested

product was then transformed in XL1 blue cells. The colonies were screened, plasmids isolated and finally verified by sequencing.

3.2.5 Restriction Digestion Reaction

10X buffer (Tango/FD/FD Green) 2X

DNA template 250-300 ng

Restriction enzyme 1 unit/ 1µl for FD enzymes

Autoclaved MQ water variable

Final Reaction Volume 20 µl

Restriction reaction was carried out at 37° C for 1-4 hours.

3.2.6 Agarose Gel Electrophoresis of DNA

Agarose of 0.8 – 1 % was prepared in 1X TAE and heated to boil using microwave oven (MS-2342-AE, GE). Agarose solution was allowed to cool to 50-60 ^{0}C (5 min) and ethidium bromide (EtBr) was added to a final concentration of 0.5 µg/ml. The solution was mixed thoroughly and poured in a gel casting tray with comb. The gel was allowed to polymerize for 20-30 min. The samples were loaded along with the 1X DNA loading buffer. The samples were resolved at 120 mA for 30-50 min. The gel was then documented (UVP, Bioimaging Systems) and viewed using Launch Vision Works LS software.

3.2.7 Recovery of DNA from Low Melting Agarose Gel

Low melting agarose gel of 0.8% with ethidium bromide (0.5 µg/ml) was casted using 1X TAE buffer. The samples were loaded with DNA gel loading buffer and allowed to resolve at 120 mA for 30-50 min. The gel was then viewed under trans-illuminator and the band of interest was excised using a clean scalpel blade. The agarose gel piece containing DNA was allowed to

melt at 65°C and DNA was extracted using gel elution columns (Sigma). In final step DNA was eluted in 20 µl of elution buffer.

3.2.8 Ligation/Cloning

Ligation was set up using Fermentas rapid ligation kit. For cloning pJET cloning kit (Fermentas) was used. 20 µl of ligation reaction was set up with 80 ng of vector DNA, 30-40 ng of insert, 1U of T4 DNA ligase and 10 µl of 2X rapid ligation buffer. The ligation reaction was incubated at 22 °C for 4-5 hours.

3.2.9 Transformation

The ultra-competent cells were thawed on ice [E. coli DH5α or E. coli XL1 for mutagenesis and cloning and E. coli Bl 21 (DE3), Origami DE3 for protein expression]. 10 µl of the Ligation mixture or 100 ng of plasmid DNA was added to an aliquot of 100 µl ultra-competent cells. It was tapped gently and incubated in ice for 30 min. The cells were heat shocked at 42°C for 90 sec and incubated in ice for 2 min. 500 µl of LB medium was added to the tube and kept for outgrowth at 37 °C for 45 min with vigorous shaking (200-250 rpm). The cells were centrifuged at 5000 rpm for 3 min. The cells were suspended in 50 µl of the medium and plated on LB ampicillin (100 µg/ml) plates and incubated overnight (16 hours) at 37 ^{0}C.

3.2.10 Plasmid Mini Preparation

Colonies on the LB agar plate were picked using a sterile toothpick and inoculated in 10 ml of LB medium containing 100 µg/ml of ampicillin. The culture was allowed to grow overnight at 37 ^{0}C shaker incubator (Lab companion, Model–SIF6000R). The cells were pelleted down by centrifugation at 5000 rpm (Plasto Craft, Model - Rota 4R). Plasmid miniprep was done using plasmid extraction kit (Sigma).

3.2.11 Plasmid Construction

PSMD9 cDNA (Origene Technologies) was amplified and ligated into pRSETA TEV (Invitrogen, Life Technologies) vector between BamHI and EcoRI sites. hnRNPA1 and S14 ribosomal protein cDNA was generated by RT-PCR from RNA extracted from HEK-293 cells. E12, Growth hormone and FN3 domain of IL6 receptor were amplified from the cDNA obtained from Harvard Institute of Proteomics. hnRNPA1 was ligated in pGEX4T1 (GE Amersham). FN3 domain was cloned in pGEX4T1 between BamHI and XhoI. S14ribosomal protein and their C-terminal mutants (S14 L151G and S14 CΔ7), Growth hormone and its C-terminal mutants (GH F217G and GH CΔ7), E12 and its C-terminal mutants (E12 M651G and E12 CΔ7) were cloned in pMALC5X between BamHI and EcoRI. PSMD9 mutants (D157P, Q181G, L173G, L153G, F162G and triple mutant L124G/ Q126G/ E128G), hnRNPA1 mutants (hnRNPA1 F372G and hnRNPA1 CΔ7), Growth hormone mutants (GHΔGF and GHΔCGF) were generated by site directed mutagenesis were confirmed by sequencing (3500 Genetic Analyzer, Applied Biosystem).PSMD9 was cloned in pCMV10 3X FLAG between HindIII and EcoRI and in pTRIPZ between AgeI and XhoI (Indrajit Sahu, Prasanna lab). hnRNPA1, Growth hormone, S14 and FN3 domain of IL6 receptor and their C-terminal mutants were cloned in HA-pcDNA3 (gift from Dr. Sorab Dalal, ACTREC) between BamHI and XhoI. The list of primers are listed in Table 3.1. For NF-κB luciferase assays, 3X κB ConA Luc and ConA control vectors were used, which were kind gifts from Dr. Neil D. Perkins, Newcastle University, UK. The pCMV- IκB SR construct was a kind gift from Dr. Neelam Shirsat, ACTREC.

Table 3.1 List of primers used for cloning and site directed mutagenesis.

Gene and name of the vectors	Primers [Forward (F) and Reverse (R)] for cloning
PSMD9 in pRSETA-TEV pCMV10-3X-FLAG	F: GGATCCATGTCCGACGAGGAAGCGAG R: GAATTCGACAATCATCTTTGCAGAGG
PSMD9 in pCMV10-3X-FLAG	F: AAGCTTATGTCCGACGAGGAAGCGAG R: GAATTCGACAATCATCTTTGCAGAGG
FLAG-PSMD9 in pTRIPZ vector	F: ACCGGTCGCCACCATGGACTACAAAGACCATG R: GAATTCGACAATCATCTTTGCAGAGG
hnRNPA1 in pGEX4T1 and HA-pcDNA3	F: GGATCCATGTCTAAGTCAGAGTCT R: GAATTCTTAAAATCTTCTGCCAC
Growth hormone and its mutants in pMALC5X	F:GGATCCATGGCTACAGGCTCCCGGACGT R:GAATTCCTAGAAGCCACAGCTGCCCTCCAC R:GAATTCCTAGGGGCCACAGCTGCCCTCCAC R:GAATTCCTACTAAGAGCGGCACTGCACGAT
S14 ribosomal protein and its mutants in pMALC5X and HA-pcDNA3	F: GGATCCATGGCACCTCGAAAGGGGAAGGAA R: GAATTCTCACAGACGGCGACCACGGCGA R:GAATTCTCACCCACGGCGACCACGGCGACC R:GAATTCCTACCTGCGAGTGCTGTCAGAGGGGAT R:CTCGAGTCACCCACGGCGACCACGGCGACC R:CTCGAGCTACCTGCGAGTGCTGTCAGAGGGGAT
FN3 domain and its mutants in pGEX4T1 and HA-pcDNA3	F: CCGCGTGGATCCATGCCGGATCCGCCGGCGAACATTA R: CGGCGGCTCGAGTTACAGGCCGCAGCTGCCGCGGCGG R:CGGCGGCTGGAGTTACCCGCCGCAGCTGCCGCGGCGG R: CGGCGGCTCGAGTCAGCGGCTGCCCGGCAGGCTGGT
E12 transcription	F:GGATCCATGAACCAGCCGCAGAGGATGGCGCCT R:GAATTCTCACATGTGCCCGGCGGGGTT

factor and its mutants in pMALC5X	R: GAATTCTCACCCGTGCCCGGCGGGGTT R: GAATTCGTGCCCGGCGGGGTTGTGTCATCAGGCTTCGC
Site directed mutagenesis	**Primers[Forward (F) and Reverse (R)] for site directed mutagenesis**
PSMD9 L173G	F: CTTCCAGTCAGGGCATAACATTG R: CAATGTTATGCCCTGACTGGAAG
PSMD9 Q181G	F: GCAGTGTGGTGGGGCACAGTGAGGG R: CCCTCACTGTGCCCCACCACACTGC
PSMD9 Triple mutant (L124G/ Q126G/ E128G)	F: ATGAGCCGCAAAGGGGGTGGGAGTGGGAGCCAGGGCCCTCCACG R:CGTGGAGGGCCCTGCCCGCTCCCACTCCCACCCCCTTTGCGGCTCAT
PSMD9 F162G	F: ATTGTGGAGGCGGGCTCTGTGAA R: TTCACAGAGCCCGCCTCCACAAT
PSMD9 L153G	F: ATCGCGGGTGGGCAAGTGGATGAT R: ATCATCCACTTGCCCACCCGCGAT
PSMD9 D157P	F: CTGCAA GTG GAT CCT GAG ATT GTG GAG R: CTCCACAATCTCAGGATCCACTTGCAG
hnRNPA1 F372G in pGEX4T1	F: AGTGGCAGAAGAGGGTAAGAATTCCCGG R: CCGGGAATTCTTACCCTCTTCTGCCACT
hnRNPA1ΔC in pGEX4T1	F: CAGCAGCAGTTAATAATATGGCAGTGGC R: GCCACTGCCATATTATTAACTGCTGCTG
GHΔGF	F: AGGGCAGCTGTTAATAAGGCTTCTAGGAA R: TTCCTAGAAGCCTTATTAACAGCTGCCCT
GHΔCGF	F: TGGAGGGCAGCTAATAATGTGGCTTCT R: AGAAGCCACATTATTAGCTGCCCTCCA

3.2.12 Protein Expression

All recombinant proteins (His-PSMD9 and mutants, GST-hnRNPA1 and mutants, MBP-S14 and mutants, MBP-GH and mutants, GST and MBP) were expressed and purified by using Escherichia coli BL21 (DE3) strain. A single, transformed, isolated colony of E. coli BL 21 (DE3) was inoculated in 10 ml LB medium and grown overnight at 37° C with vigorous shaking (200-250 rpm). Inoculum of 10 ml was made in 1 litre LB broth and allowed to reach 0.8- 0.9 O.D.600 (Biophotometer, Eppendorf). Protein was induced with 100 µM isopropyl-D-thiogalactoside (IPTG) and growth was continued at 20 °C for 16 hours. Cells were lysed by sonication in lysis buffer (50 mM Tris (pH 7.5), 50 mM β-mercaptoethanol (BME), 500 mM NaCl, 10% glycerol, 0.1% Triton X-100) with protease inhibitor cocktail (Sigma). The culture was transferred into HS50 tubes (Tarson) and centrifuged at 15000 rpm for 30 min at 4 °C using SS-34 rotor in Sorvall RC5C Plus centrifuge. The supernatant containing soluble protein was used for further purification. Individual protein was purified by nickel-nitriloacetic acid (NiNTA) agarose affinity chromatography (Invitrogen).

Cell Density Measurement

The O.D. was measured at 600 nm with LB medium as blank using with the help of Biophotometer (Eppendorf).

3.2.13 Ni-NTA Agarose Affinity Chromatography

Ni–NTA agarose beads of 1-2 ml from Invitrogen were liquated in 1X 30 cm econo column (Bio-Rad). Beads were washed with 1X washing/equilibration buffer with at least two column volumes under native conditions. Equilibrated Ni-NTA beads were incubated with protein lysate at 4 °C for about 30 min. After incubation unbound lysate (flow through) were

collected separately. Beads were washed with washing buffer with 2-3 column volume. 6X His tagged protein were eluted with elution buffer containing imidazole (250 mM).

3.2.14 Glutatione-S-Transferase purification affinity Chromatography

For purification of GST fusion proteins, glutathione beads (GE, Healthcare) were used. 200 µl of beads were used for purification for 250 ml induced culture. Beads were equilibrated with 1X PBS buffer containing 10 mM DTT. Equilibrated beads were incubated with protein lysate at 4 °C for about 30 min. After incubation unbound lysate (flow through) were collected separately. Beads were washed thoroughly 6 -7 times with 1X PBS. Bound protein was eluted using 10mM Glutathione in 50mM Tris, pH 8.0. The proteins were dialyzed in 50mM Tris, pH 7.5.

3.2.15 Ion exchange chromatography

Recombinant PSMD9 was subject to ion exchange chromatography (anion exchange chromatography) with the help of monoQ column (GE Amersham) connected to AKTA FPLC (GE Amersham). After binding PSMD9 to the column, a wash with a gradient of NaCl (1M) is given at a flow rate of 0.5 ml/min to elute the protein.

3.2.16 Gel Filtration Chromatography

For further purification of protein, it was subjected for gel filtration chromatography using sephadex G-200 or (for crystallization) G-75 beads (GE Healthcare Life Sciences). Initially the gel filtration column was equilibrated with gel filtration running buffer with the flow rate of 0.5 ml/min using HPLC system (Bio-Rad) or AKTA (for crystallization). Molecular weight markers (GE Amersham) were loaded to the column before loading our protein of interest. 2 ml (3-4 mg) of total protein volume injected in the gel filtration column and eluted under native conditions.

Peak fraction were collected either separately or pulled together, dialyzed against Tris buffer pH 7.5 and used for further experiments.

3.2.17 Protein Estimation using Bradford Assay

BSA standards (1, 0.5, 0.25, and 0.125 mg/ml) were prepared from 30 mg/ml of BSA stock. Unknowns (protein samples) were taken in various dilutions. 5 µl of the standards and the unknowns were taken in duplicates in a 96-well plate and 200 µl of Bradford reagent (1:4 diluted, Bio-Rad) was added to each well. Readings were taken with ELISA plate reader (Spectra Max 790) at 595 nm using SoftMaxPro 4.6 software. Protein concentration for unknown was determined with the help of standard graph generated with BSA.

3.2.18 SDS PAGE

Protein samples were boiled using digital dry bath (JENCON-PLS) at 100 °C with 1X Laemmli buffer for 10 min before loading. The samples were loaded to the gel placed in the tank containing 1X SDS-PAGE running buffer. The gel was resolved at 150 V for 1:30 hours. The gel was stained with 0.25% coomassie brilliant blue R (Sigma) for 15-30 min. The gel was then destained overnight in the destainer (50% Methanol, 10% Acetic acid) with 2-3 changes at regular interval. The gel was finally preserved in 10% acetic acid and documented.

3.2.19 Preparation of Glycerol Stocks

100 µl of the overnight culture was transferred into autoclaved 1.7 ml microfuge tube (Axygen). To it 100 µl of 30% glycerol (autoclaved) was added to the tube and gently mixed. When the solution was homogenous glycerol stocks were stored at -80^{0}C.

3.2.20 Enzyme Linked Immuno Sorbent Assay

a) Peptide screening

N-terminal biotinylated tetra-peptides were procured from GenPro Biotech, India, (Biotin-KGG-XXXX, where XXXX represents the tetra-peptide sequence) and reconstituted to 25mM with 100% DMSO and further diluted to 5mM with distilled water. Anti-PSMD9 (Abcam) antibody in 0.1M sodium carbonate buffer, pH 9.5 was coated on Nunc-Immuno™ MicroWell™ 96 well solid plates and incubated for 16 hours at 4°C. Wells were blocked with 2% BSA in TBST (10mM Tris pH 8, 138mM NaCl and 0.5% Tween 20) for 1 hour at 37°C. His-tagged PSMD9 or its mutant proteins (5µg/ml), diluted in TBST (containing 0.1% BSA) were added and incubated at 37°C for 1 hour. Plates were washed, and biotinylated peptides (in TBST with 0.1% BSA) were added to the wells and incubated for 1 hour at 37°C. The plates were washed with TBST vigorously after each incubation step. Finally, streptavidin alkaline phosphatase (Sigma), at 1:2000 dilution in TBST (with 0.1% BSA) was added to all wells. After incubation 1 hour at 37°C, binding was detected by the addition of para-Nitro phenyl phosphate (PNPP) (Bangalore Genei, India), the substrate of alkaline phosphatase and color developed was read at 405nm (Spectramax 190, Molecular Devices). Wells that lack PSMD9 and wells that lack anti-PSMD9 antibody were taken as negative controls.

b) Protein-protein interaction

GST-hnRNPA1, its mutants and GST (5µg/ml) or MBP-growth hormone and MBP (control) were coated as described for the PSMD9 antibody (section 3.2). All incubations were performed as described for the peptide ELISA (section 3.2). His-tagged PSMD9 and its mutant proteins were titrated at different concentrations (in TBST containing 0.1% BSA) and added to the coated plates. After incubation, anti-his antibody (Cell Signalling) was added at a dilution of 1:2000,

incubated and washed. HRP conjugated anti-mouse antibody (GE Amersham) (at 1:3000 dilution) was then added. After incubation and washes, HRP substrate TMB (1X) was added to all the wells. Reaction was stopped using 2M sulfuric acid before recording the readings at 450nm. Wells not coated with GST-hnRNPA1 and wells in which PSMD9 or the mutants were not added served as negative controls. For the competition assays, recombinant his-PSMD9 was incubated with different concentrations of GRRF/GRRG or SCGF/SCGG/SGGF peptides for 1 hour at 37°C and then added to wells containing GST-hnRNPA1 or MBP-GH respectively.

3.2.21 GST pull down assay

GST-fusion proteins or their mutants diluted in Transport buffer (TB) were allowed to immobilize on GST beads for 1 hour at 4ºC. Beads were washed 2-3 times with the same buffer. His-PSMD9 or its mutants were allowed to bind for 2 hours at 4ºC. Beads were washed thoroughly (5-6 times) and boiled in the presence of Laemmli buffer. Proteins were resolved on a 12% SDS PAGE and western blotting was performed using anti-his antibody.

3.2.22 MBP pull down assay

MBP-fusion proteins or their mutants diluted in Transport buffer (TB) were allowed to immobilize on amylose beads for 1 hour at 4ºC. Beads were washed 2-3 times with the same buffer. His-PSMD9 or its mutants were allowed to bind for 2 hours at 4ºC. Beads were washed thoroughly (5-6 times) and boiled in the presence of Laemmli buffer. Proteins were resolved on a 12% SDS PAGE and western blotting was performed using anti-his antibody.

3.2.23 Western blotting

For western blotting samples were resolved on 12% SDS PAGE. Proteins were transferred on polyvinylidene difluoride (PVDF) membrane (Hybond, GE Healthcare). PVDF membrane was blocked with 3% BSA in TBST at room temperature for 1 hour on rocker. PVDF

membrane was incubated with 1:1000 dilution of anti-his antibody (abcam) or 1:1000 dilution of anti-FLAG (Sigma) or 1:1000 dilution of anti-HA (Abcam) or for 1 hour at room temperature on rocker. Antibodies were diluted in TBST (TBST - 50 mM Tris, 150 mM NaCl, 0.1% Tween 20) containing 1% BSA. After 1 hour, primary antibody was removed and membrane was washed with TBST at least four times, 15 min each time at room temperature on rocker. Membrane was incubated with corresponding secondary antibody (1:5000 dilution; Sigma) at room temperature for 1 hour on rocker. Secondary antibody was removed and membrane was washed with TBST at least four times, 15 min each time on rocker at room temperature. Membrane was incubated with ECL plus reagent (GE Healthcare) was exposed to X-ray film (Kodak) and was developed using automated developer machine (Optimax 2010, Protec GmBH & Co.). Developed X-rays was analyzed for the corresponding western blotting.

3.2.24 Homology modeling of PSMD9, its PDZ domain and peptide docking

a) Homology modeling of PDZ domain of PSMD9

There is currently no crystal structure available for PSMD9 protein. A homology model of PDZ domain of PSMD9 was thus constructed using comparative modeling method, by comparing the sequence of this target protein with sequence of other related proteins (template) for which experimental structures are available. BLAST search showed that the PDZ shares 42% sequence similarity with PDZ2 domain of harmonin and sequence alignment between the two reveals that this sequence similarity is distributed throughout the sequence. Solution structure of PDZ2 domain of harmonin bound with C-terminal peptide of cadherin23 (pdb code 2KBS) (Pan et al., 2009) was chosen as a template for the homology modeling. Modeller, a program for comparative protein structure modeling by satisfaction of spatial restraints (Sali and Blundell,

1993) was used for generation of the homology model. Several homology models were built based on structural information from the template, and model that showed good stereochemical property was selected for further use.

b) Peptide Docking

3D structure of Peptide GRRF and SCGF was generated using Xleap module in Amber11(Case, 2010) . Peptide in its extended conformation was docked with the generated model of PDZ domain of PSMD9 protein. Peptide docking was carried out with two different docking programs, HADDOCK (Dominguez et al., 2003) and ATTRACT (Zacharias, 2003). For HADDOCK, a binding site was defined using residues Leu124, Gly125, Gln126, Glu128 and Gln181 within the canonical pocket. No information regarding the binding site was given while using ATTRACT and a complete blind docking was performed using this program. Both the docking programs were validated earlier, by docking a set of co-crystalized peptides into the canonical pocket of the corresponding PDZ domains and the docked conformations of each peptide had RMSD values 1.5 to 2.5 Å with the corresponding experimental structures.

c) Modeling of full length PSMD9 and D157P mutant

As the experimental or 3D structure of full length PSMD9 protein is not available, a homology model was generated using Modeller9v2 [64]. While in the model described above, the structure of only the PDZ domain (residues 105-193) was constructed, here we build the structure of the full length protein (223 residues long) to study the effect of mutation of residue D157. The crystal structure of the harmonin NPDZ1 (pdb id 3K1R) [65] bound with sterile α motif - PDZ-binding motif (SAM-PBM) of Usher syndrome type-1G protein (Sans – Scaffold protein containing ankyrin repeats and SAM domain) was used as the template. PSMD9 shares ~30% sequence identity with the template harmonin NPDZ1.

3.2.25 Molecular Dynamics Simulations

Generated homology model of PDZ domain and full length, peptide GRRF (derived from C-terminus of hnRNPA1) - PDZ complex (PDZ-GRRF) (both the canonical and non-canonical binding mode) were used as the starting structure for MD simulations. Mutated structures of the protein Q181G, the triple β-sheet mutant L124G/Q126G/E128G and D157P, were also generated by replacing (mutating) the respective residues in Pymol. Hydrogen atoms were added to the WT and mutant experimental structures using the Xleap module of the Amber11 package. N-terminus of the GRRF and SCGF peptide was capped by acetylaion (ACE). Simulation systems were neutralized by the addition of counter ions. The neutralized system was solvated with TIP3P (Jorgensen, 1983) water molecules to form a truncated octahedral box with at least 10 Å separating the solute atoms and the edges of the box. MD simulations were carried out with the Sander module of the AMBER11 package in combination with the parm03 force field (Duan et al., 2003). All systems were first subjected to 100 steps of energy minimization. The protein was initially harmonically restrained (25 kcal mol^{-1} $Å^2$) to the energy minimized coordinates, and MD simulations were initiated by heating the system to 300 K in steps of 100 K followed by gradual removal of the positional restraints and a 1ns unrestrained equilibration at 300 K. The resulting system was used as starting structure for production MD run. For each case, three independent (using different initial random velocities) MD simulations were carried out starting from the well equilibrated structure. Each MD simulation was carried out for 100ns and conformations were recorded every 10ps. All MD simulations were carried out in explicit solvent at 300K. During all the simulations the long-range electrostatic interactions were treated with the particle mesh Ewald(Darden, 1993)method using a real space distance cutoff of 9 Å. The settle (Miyamoto, 1992) algorithm was used to constrain bond vibrations involving hydrogen atoms, which allowed

a time step of 2 fs during the simulations. Simulation trajectories were visualized using VMD (Humphrey et al., 1996) and figures were generated using PyMol.

3.2.26 Routine Maintenance of Cell Lines

All glassware and plastic-ware used for tissue culture work were sterile. For maintenance and experimental use, all adherent cells (HEK 293, PSMD9 overexpressing stable clones, HeLa) were trypsinized and passaged as follows. Spent medium was aspirated out using a pasteur pipette and the cells in the plate were washed twice with 1X PBS. 1X trypsin was added to the cells, and was removed after the cells rounded up but just before cells start detaching. To inhibit the trypsin activity 1ml of complete medium was added to the cells. The cells were collected in 1X PBS and the cell suspension was transferred to the centrifuge tube and tightly corked. The cell suspension was centrifuged for approx imately 3-4 min at 1000rpm in REMI bench top centrifuge. The supernatant was discarded and the cell pellet was loosened by tapping the tube gently. The cells were suspended in an appropriate volume of complete medium, cell count was taken using a haemocytometer, and the required cell number was seeded in tissue culture dishes, and incubated at 37 °C in a humidified 5% CO_2 incubator. The cultures were passaged at around 70-80% confluency or were frozen using 90% FBS in 10% DMSO when required. The cells were cultured up to 5-6 passages and fresh vial of frozen cells was revived at regular time intervals. PSMD9 over expressing stable HEK 293 cells and the vector control cells were maintained in 800 µg/ml of G418 (Sigma) for pCMV10 3X FLAG constructs and 800 ng/ml puromycin for pTRIPZ constructs.

3.2.27 Freezing and Revival of Cell cultures

Freezing: For freezing of cells, 80-90% confluent cultures were trypsinized as described above. The cell pellet was loosened by tapping the tube gently and the centrifuge tube was placed on ice for 1-2 min. Pre-chilled freezing medium (90% FBS+ 10% DMSO) was added drop wise to the cell pellet (~1 x 10^6cells/ml of freezing mixture) on ice, with constant shaking to ensure even cell suspension and transferred to pre-chilled vials. These vials were cooled gradually at 4 °C, -20 °C, -80 °C and then stored in liquid nitrogen.

Revival: To revive the frozen cells, a vial containing frozen cells was removed from liquid nitrogen and immediately thawed in a water-bath at 37 °C. As soon as the cell suspension thawed, it was transferred to a centrifuge tube containing 5 ml complete medium and centrifuged at 1000 rpm for 2 min. The supernatant was discarded, cell pellet was loosened by tapping the tube gently and re-suspended in an appropriate volume of complete medium and added to the 55 mm of tissue culture plate. The medium was replaced after the cells had adhered to the tissue culture dish on next day of revival.

3.2.28 Transfection of plasmid DNA in HEK 293 cells

HEK 293 cells were transfected with pCMV10 3X FLAG-PSMD9 or pCDNA3.1(+)-interacting partner gene or vector alone using calcium phosphate method. One day prior to transfection, the cells were trypsinized and 5x 10^5cells were seeded in a 55 mm plate. The plate should be around 60% confluent at the time of transfection. Next day, 4 hr before transfection, medium was replaced with fresh complete medium. The cells were transfected using 12 µg plasmid DNA (55 mm plate) using BBS. A total of 12 µg plasmid was diluted to 100 µl in autoclaved MilliQ in a sterile tube. 100 µl of $CaCl_2$ was added drop wise to the DNA in an autoclaved eppendorf. Then, 200 µl of 2X BBS was added drop wise and mixed gently by pipetting 3-4 times. The mix

was incubated at RT for 20 min. After 20 min, the DNA complexes were mixed gently again and added drop wise over the cells, mixed gently by swirling the medium in the plate and incubated at 37 °C in CO_2 incubator for 16 hrs. After 16 hrs, the transfection medium was replaced with fresh complete medium.

3.2.29 Generation of PSMD9 over expressing stable HEK 293 cells

HEK 293 cells were transfected with pCMV10 3X FLAG PSMD9 or vector alone using calcium phosphate method. Clonal transformants were selected in presence of 800 µg/ml G418 (Sigma). HEK293 cells were transfected with pTRIPZ FLAG PSMD9 or vector alone using calcium phosphate method. Clonal transformants were selected in presence of 800 ng/ml puromycin (Sigma) (Indrajit Sahu, Prasanna lab).

3.2.30 NF-*κ*B activation- Luciferase assay

HEK 293 cells were cotransfected with 6 µg pCMV10 3X FLAG or pCMV 10 3X FLAG PSMD9 or Q181G mutant and 6 µg of ConA control or 3 *κ*b enhancer ConA luciferase construct (a kind gift from Dr. Neil D. Perkins, UK). After 48 hours, cells were treated with 10ng/ml TNF-α (Invitrogen), lysed and luciferase assay was performed using Promega Luciferase Assay System in triplicates.

3.2.31 Soft agar assay

HeLa cells overexpressing PSMD9 or vector alone were compared for their ability to exhibit anchorage independent growth using soft agar colony formation assay. 2 x 10^3 cells in each case were overlaid on a thin layer of agar (0.4% over 1% agarose) in complete medium. Colonies formed were counted after 8 days.

3.2.32 Affinity pull down assay

Cells were harvested in NP-40 lysis buffer [20 mM Tris pH 7.5, 150 mM NaCl, 0.5% NP-40 and 1mM dithiothreitol (DTT) containing 1X protease inhibitor cocktail (Sigma)]. 1mg of total cell lysate was incubated with 10µl of M2 agarose anti -flag beads (Sigma) for 4 hours at 4ºC. Beads were washed extensively with the NP-40 lysis buffer after which western blot was performed.

3.2.33 RNA extraction and cDNA synthesis

Cell contains three types of RNA, Trizol based method extracts total RNA from the lysed cells, followed by amplification using only mRNA to synthesize cDNA using an enzyme- reverse transcriptase. $1x10^6$ HEK293 cells were suspended in 1 ml of Trizol and the sample was either processed immediately or stored at -80°C till further use. For RNA extraction the cells were thawed at RT and the cell pellet was dissolved completely by vortex mixing and repeated pipetting. 200 µl of chloroform was added and the mixture was vortex mixed for 5 min, the mixture was kept on the bench top till two phases could be distinguished and then centrifuged for 10 min at 12000xg/ 4°C. The aqueous phase was carefully transferred to a fresh tube without disturbing the interphase and the RNA was precipitated using 500 µl isopropanol at RT/10 min and spun 20 min at 12000xg/ 4°C. The isopropanol was gently removed and pellet was washed with 500 µl 75% ethanol; pellet was semi dried and dissolved in DEPC treated D/W (DEPC D/W) at 55°C; quality and quantity of RNA was assessed by measuring O.D. 260/280. First strand cDNA synthesis was carried out using FirstStrand cDNA synthesis kit (Invitrogen).

Components

RNA 2 µg

10mM dNTP Mix 1 µl (1 mM)

50 µM oligo(dT) 1 µl (5 mM)

DEPC-treated water to 10 µl

Incubate the tube at 65 °C for 5 min, then place on ice for at least 1 min. Prepare the following cDNA synthesis mix, by adding each component in the indicated order.

Components

10X RT buffer 2 µl

25 mM $MgCl_2$ 4 µl

0.1 M DTT 2 µl

RNaseOUT (40 U/µl) 1 µl

SuperScript III RT (200U/µL) 1 µl

Add 10 µl of cDNA Synthesis Mix to each RNA/primer mixture, mix gently, and collect by brief centrifugation. Incubate for 50 min at 50°C and terminate the reactions at 85°C for 5 min. Chill on ice and collect the reactions by brief centrifugation. Add 1 µl of RNase H to each tube and incubate the tubes for 20 min at 37°C. cDNA synthesis reaction can be stored at −20°C to −10°C or used for PCR immediately.

CHAPTER 4

A DISTINCTIVE APPROACH TO IDENTIFY INTERACTING PARTNERS OF PSMD9

Introduction

PSMD9, a non-ATPase subunit of the 19S regulatory particle, is known to play a role as a chaperone in the assembly of the 19S regulatory complex in yeast (Kaneko et al., 2009). Recent studies have shown that the rat homolog of PSMD9, Bridge1 acts as a transcriptional coactivator of insulin gene transcription and plays an important role in melanin biosynthesis and activin signaling (Banz et al., 2010; Thomas et al., 1999). Thomas et. al observed that a part of the primary sequence in Bridge1 was well conserved and shared sequence homology with a well conserved domain called the PDZ domain. Homologies with the aligned proteins consisting classical PDZ domains within this segment range from 27 to 54% identity and 46 to 77% similarity. The high degree of sequence similarity in this region suggests that Bridge-1 contains a PDZ-like domain. PDZ domains are well known for protein-protein interactions and it is now very well known that these domains interact with the C-terminal residues of the interacting partner.

Various approaches have been used to identify interacting partners or C-terminal ligands that interact with PDZ domains of various proteins. Peptide libraries have been created, and peptides derived from the C-terminus of the human proteome have been used by various investigators (Fuh et al., 2000; Rodi et al., 2002; Sharma et al., 2009; Tonikian et al., 2008). Phage display was one of the most widely used approaches to identify C-terminal ligands for PDZ domains. Presently, a large number of ligands can be screened using SPOT synthesis of peptides on cellulose membranes, followed by Whole Interactome Sequencing Experiments (WISE) (Landgraf et al., 2004). Here we report a simple, cost-effective method to identify C-terminal ligands which are part of the C-termini of proteins in the human proteome that interact

with the PDZ domain of PSMD9. This method was effective in identifying several novel interacting partners that are physiologically relevant in mammalian cells.

Results and Discussion

Genome wide conservation of C-termini of proteins of different proteomes

Chung et. al in 2003, reported that non-homologous proteins share identical C-terminus and by virtue of conservation of typically three, four or eight amino acid residues, they seem to share common biochemical functions. This group had classified proteome from drosophila/yeast/human by recognizing conserved C-terminal residues in some of these proteins and listed out 30 tetra-peptide sequences which have more than 10 members in their group (Table 4.1). We decided to test the binding of some of these peptides to recombinant PSMD9. We presumed that proteins harboring the C-terminal peptide sequences which interact with PSMD9 in the preliminary screen may also interact with PSMD9 *in vitro* and in mammalian cells.

Table 4.1 Proteins of the human proteome harboring the C-terminal tetrapeptide sequences as reported by Chung *et. al* in 2003.

Peptide	No. of Proteins	Peptide	No. of Proteins
KEKK	28	RKCF	15
EFMA	25	SCGF	13
TSSK	23	RRRR	13
VLRH	22	SDSD	13
GERA	20	LVCQ	13
EEVD	20	HDEL	13
SLKF	19	KDEL	13
CWNK	19	ASKE	13
GFGG	19	CGQL	12
AKGK	18	EDTM	12
NSDK	18	GEKP	12
QKAK	17	GRRF	12
TKLG	16	KEEL	12
EEEE	15	SSSS	12

IGII	11	CNKI	11

Cloning, expression and purification of PSMD9

Human PSMD9 was cloned in pRSETA-TEV vector and expressed as a his-tagged protein in BL21 DE (3) cells. The protein was purified by Ni-NTA affinity chromatography followed by size exclusion chromatography (Figure 4.1).

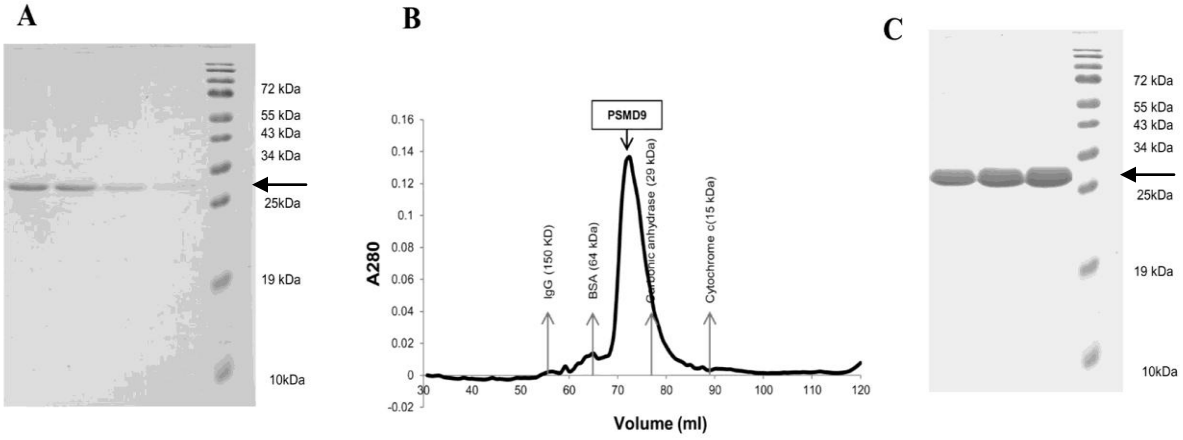

Figure 4.1 Purification of recombinant his-PSMD9. A) Recombinant His-PSMD9 (indicated by arrow) purified by Ni-NTA affinity chromatography. B) Chromatogram of size exclusion chromatography of recombinant his-PSMD9 Superdex 75 column (GE Amersham). IgG (150 kDa), Bovine Serum Albumin (BSA) (64 kDa), carbonic anhydrase (29 kDa) and cytochrome C (15 kDa) were used as molecular weight standards. C) Recombinant his-PSMD9 (indicated by arrow) purified by size exclusion chromatography.

Screening of C-terminal peptides by Enzyme Linked Immunosorbent assay (ELISA)

PDZ domains are well known to interact with hydrophobic residues at the C-terminus. Since the PDZ domain of PSMD9 is not well characterized and we do not know the specificity of

the PDZ domain of PSMD9, we decided to incorporate C-terminal peptides which harbored residues of all properties (hydrophobicity, charge and size). We included peptide AGHM, which is the C-terminus of human transcription factor E12. It is well known that rat E12 C-terminus is known to interact with Bridge1, the rat homolog of PSMD9. We found that apart from peptide AGHM, peptides GRRF and SCGF interacted with PSMD9 to appreciable extent (Figure 4.2a). Further experiments revealed that GRRF interacted with PSMD9 with a low affinity (K_d 651.7±76 μM) and SCGF (K_d 8.6±1.2 μM) interacted with a very high affinity (Figure 4.2b and c).

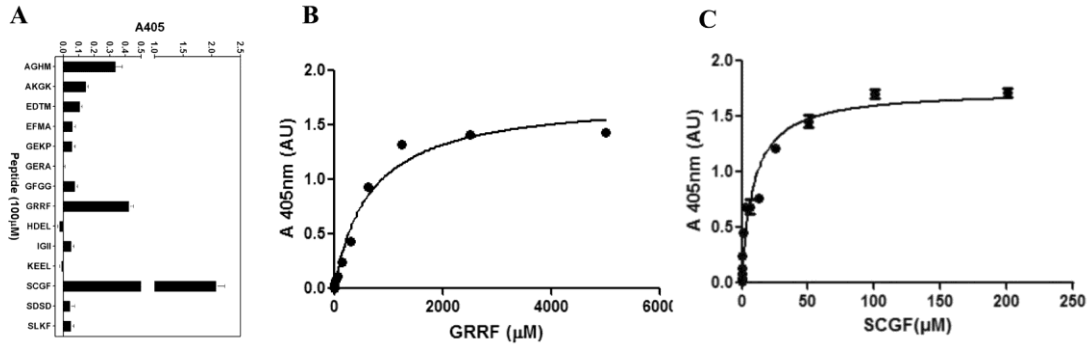

Figure 4.2 Preliminary screen for identification of putative C-terminal motifs which interact with PSMD9. A) Conserved C-terminal motifs in the form of tetra peptides were tested for binding to PSMD9 using ELISA (see methods for details). Apart from AGHM, peptides GRRF and SCGF interacted with PSMD9. Values represent mean ± SEM (Standard Error of Mean) from three different experiments performed in duplicates. B and C) ELISA was used to monitor interaction between PSMD9 and GRRF and SCGF peptides. Data were fit to one site specific binding using PRISM. The dissociation constant (K_d) for the interaction of GRRF and SCGF with PSMD9 was found to be 651.7±76 μM and 8.6±1.2 μM, respectively. Measurements were done in duplicates and data is represented as mean±SD (SD- standard deviation) for two independent experiments.

SCGF and GRRF resemble class III PDZ peptides with the sequence motif -X-[D/E/K/R]-X-Φ where Φ is hydrophobic, and X is any residue. GRRF forms the C-terminus of hnRNPA1 isoforms while SCGF belongs to human growth hormone (GH).

Validation of protein-protein interaction *in vitro*

Since peptides GRRF, SCGF and AGHM interacted with PSMD9, we presumed that the proteins harboring these sequences- hnRNPA1, growth hormone (GH) and E12 will also interact with PSMD9. Recombinant hnRNPA1 was expressed as a GST-fusion protein. C-terminal mutants hnRNPA1 F372G mutation (terminal residue mutation) and hnRNPA1 CΔ7 (deletion of seven amino acids at the C-terminus) were also expressed. Similarly recombinant GH and E12, and its C-terminal mutants (GH F217G, CΔ7, E12 M651G and E12 CΔ7) were expressed as MBP fusion proteins. Affinity pull down experiments using glutathione (GST pull down) and amylose resins (MBP pull down) clearly showed that the three full length proteins interact with PSMD9. While hnRNPA1 and E12 binding were clearly affected by simple C-terminal substitution (Phe to Gly), GH binding to PSMD9 was not affected to any measurable extent. Residual interaction of hnRNPA1 F372G with PSMD9 may be due to other regions of the protein interacting with PSMD9. But the majority of the binding energy does come from the Phe residue at the C-terminus of hnRNPA1. Deletion of C-terminal seven residues compromised binding of GH severely (Figure 4.3a, b and c). These interactions were further confirmed by ELISA and the dissociation constants of the interactions of hnRNPA1 and GH to PSMD9 were found to be 1.36±0.10 μM and 0.74±0.04 μM, respectively (Figure 4.3d and e).

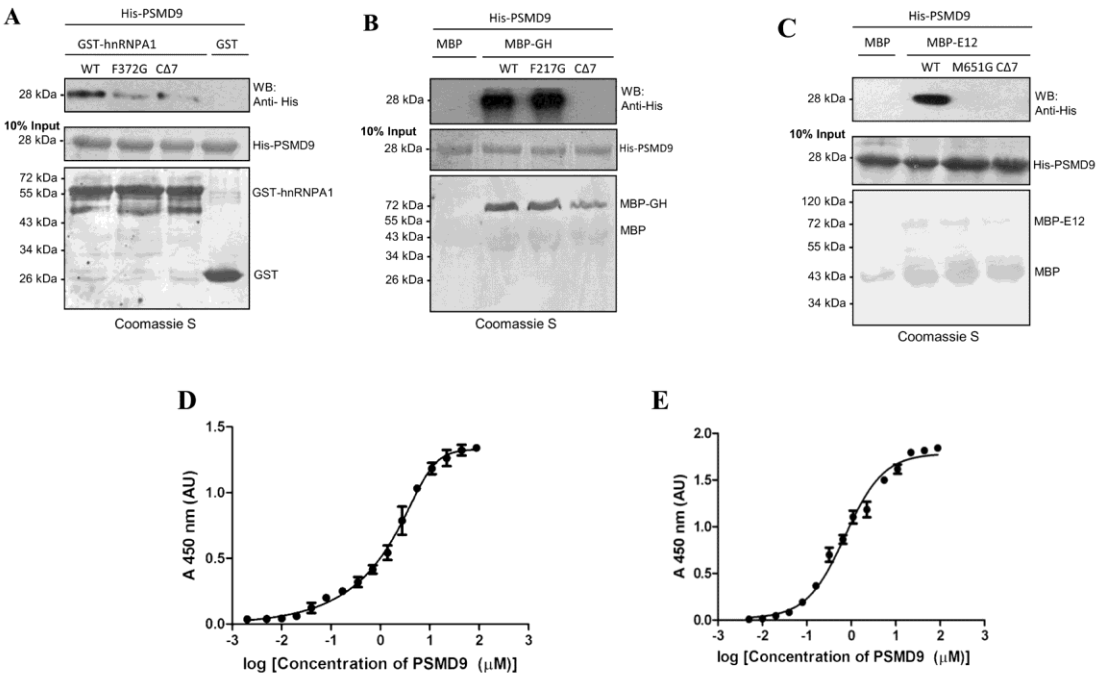

Figure 4.3 Validation of putative interacting partners of PSMD9 and the importance of C-terminal Residues in interaction. A) Recombinant WT hnRNPA1 or hnRNPA1 C-terminal mutant (F372G or CΔ7) bound to GST served as baits to pull down PSMD9. (B) Interaction of recombinant GH and its C-terminal mutants (MBP fusions) with PSMD9 was tested by in vitro affinity pull-down using MBP-agarose. C) Interaction of recombinant E12 and its C-terminal mutants (MBP-fusions) with PSMD9 (His-tag) was tested by *in vitro* affinity pull-down using MBP-agarose. D) Interaction of PSMD9 with hnRNPA1 was monitored by ELISA (see methods for details). Data were best fit to one site specific binding using GraphPad Prism (commercial software, www.graphpad.com). The dissociation constant (K_d) for the interaction was found to be 1.33 ±0.04 μM for hnRNPA1. Data from two independent experiments each done in duplicates is represented as mean ± SD (SD-standard deviation). E) Interaction of PSMD9 with Growth hormone. Data were fit to one site specific binding using PRISM. The dissociation constant (K_d) for the interaction was found to be 0.84±0.07μM for growth hormone.

Measurements were done in duplicates and data is represented as mean±SD (SD- standard deviation) for two independent experiments.

C-terminal peptides inhibit protein-protein interaction *in vitro*:

To test the importance of the C-terminal motif for interaction with PSMD9, we checked if C-terminal peptides could inhibit the interaction *in vitro*. We found that peptide GRRF could inhibit hnRNPA1-PSMD9 interaction (Ki of 326.5±0.25 μM), whereas peptide GRRG could not (Figure 4.4a). This confirms the importance of the terminal Phe residue for the interaction. Peptides SCGF and SCGG could effectively inhibit GH-PSMD9 interaction (36.7±0.29 and 35.6±0.24 μM, respectively) (Figure 4.4b). This clearly shows that terminal Phe residue of GH is not important for the interaction, and that other residues in the C-terminus may be involved in binding to PSMD9. These results confirm the results of the affinity pull down mentioned earlier, where C-terminal residues mainly contribute to the interaction, and PSMD9 shows different modes of specificities towards motifs GRRF and SCGF.

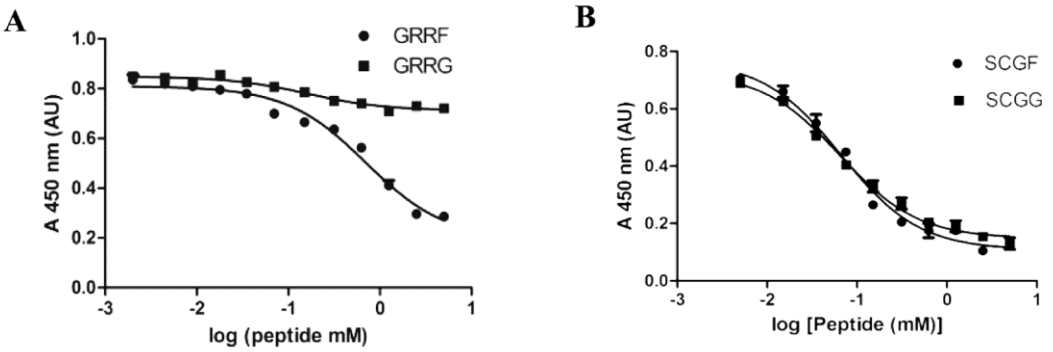

Figure 4.4 C-terminal peptides inhibit protein-protein interaction *in vitro*. A) C-terminal peptide GRRF inhibits hnRNPA1-PSMD9 interaction. Prior to its incubation with hnRNPA1 coated plates, PSMD9 (0.65 μM) was incubated with GRRF or GRRG peptides. B) C-terminal peptide SCGF and SCGG inhibit interaction of Growth hormone with PSMD9. Prior to incubation with Growth hormone, PSMD9 (0.65 μM) was incubated with SCGF or SCGG

peptides. Ki for SCGF was calculated to be 36.7±0.29 μM and for SCGG, it was 35.6±0.24 μM. Data from two independent experiments each done in duplicates is represented as mean ± SD.

These results clearly suggest that our novel structural bioinformatic strategy, combined with a simple, low throughput, cost-effective ELISA technique enabled us to find out novel interacting partners of an uncharacterized protein like PSMD9. One must note that peptides like GRRF have very low affinity and proteins harboring this motif also interacted with PSMD9. Low affinity interactions are very significant in regulating physiological processes, where associations need to be transient and quickly reversible. Most high-throughput studies are optimized for selecting peptides with high affinity, therefore interactions of low affinity, are likely to be missed. Our technique has the ability to pick weak interacting ligands which are important motifs for interaction at the protein level. Since the PDZ domain is well known to regulate many processes, it is possible that PSMD9 may regulate a wide range of physiological processes in the cell. Our approach will indeed help in easy and effective identification of interacting partners of PSMD9 which may regulate a variety of physiological processes in mammalian cells.

CHAPTER 5

ROLE OF PDZ DOMAIN

IN INTERACTION OF

PSMD9

Introduction

Our initial experiments clearly demonstrate that the C-terminal residues of hnRNPA1 and GH are involved in interaction with PSMD9. Therefore, the probability of the role of the PDZ domain of PSMD9 in the interaction is very high. In the case of interaction with rat E12, deletion of the PDZ domain of Bridge1 clearly abrogated the interaction with the C-terminal residues of E12 (Thomas et al., 1999). Such deletions could have adversely affected the conformation of Bridge1, thereby causing abrogation in the interaction. PDZ domains are very well conserved and have a characteristic GLGF motif in the hydrophobic pocket that forms hydrogen bonds with the amino acids of the C-terminal ligand. PSMD9 has a GLQV sequence, instead of the GLGF motif. The structural basis of the interaction at residue level remains to be elucidated. The crystal structure of human PSMD9 is not known. Here we predict the structure of the PDZ domain of PSMD9 using homology modeling. Using computational docking studies, followed by site directed mutagenesis, we report the important residues in the PDZ domain of PSMD9 that are crucial for the interaction with the C-terminal motifs of hnRNPA1 and GH.

Results and Discussion

Residues important for interaction in the PDZ domain of PSMD9

To better understand the role of the C-terminal residues and PDZ domain in binding and recognition, we modeled the structure of PDZ and carried out extensive molecular dynamic simulations and peptide docking studies. Modeling studies were done in collaboration with Dr. Chandra Verma, Bioinformatics Institute, where the PDZ domain of harmonin was used as a template (Figure 5.1A). There were different docking poses created, of which a complex which was similar to co-crystals of PDZ-peptide complex which have Phe at the fourth position was selected. Here, the peptide binds in an extended, antiparallel manner through canonical

interactions that extend the beta sheet by an additional strand. The hydrophobic side chain of Phe4 of the peptide is deeply buried in the hydrophobic pocket formed by Leu124 from β_2, Val139, from β_3, Leu153 from β_4, Ile159, Phe 162, from β_4. The peptide further interacts with the beta sheet mainly through backbone/side chain hydrogen bonds with residues Leu124, Gly125, Gln126, and Glu128 of β_2 of the PDZ domain. In addition, the side chain of Arg2 of the peptide forms a salt bridge with the side chain of Glu128 from β_2 (Figure 5.1B and C). We mutated residues in this hydrophobic pocket. Three single amino acid mutations F162G, L153G, Q181G and a triple mutation, L124G/Q126G/E128G were generated. Peptide binding was affected drastically when hydrophobic residues in the pocket L153 and F162 in the pocket were mutated (Figure 5.1D and E). *In vitro* pull-down shows that these mutations affect GH and hnRNPA1 binding to PSMD9. Mutation of residue L173, part of the α2 helix, that is relatively outside the pocket, did not affect the binding of hnRNPA1 and GH (Figure 5.1F and G). To confirm the role of these residues, ELISA was performed to monitor interaction of PSMD9 WT, L173G, Q181G and triple mutant (L124G/Q126G/E128G) with hnRNPA1. PSMD9 WT and L173G interacted with the same affinity, whereas the affinity of the mutants were reduced (Table 5.1 and Figure 5.1H). Thus, the hydrophobic pocket mutations predicted by the docking studies were specific for interaction with the C-terminal peptides.

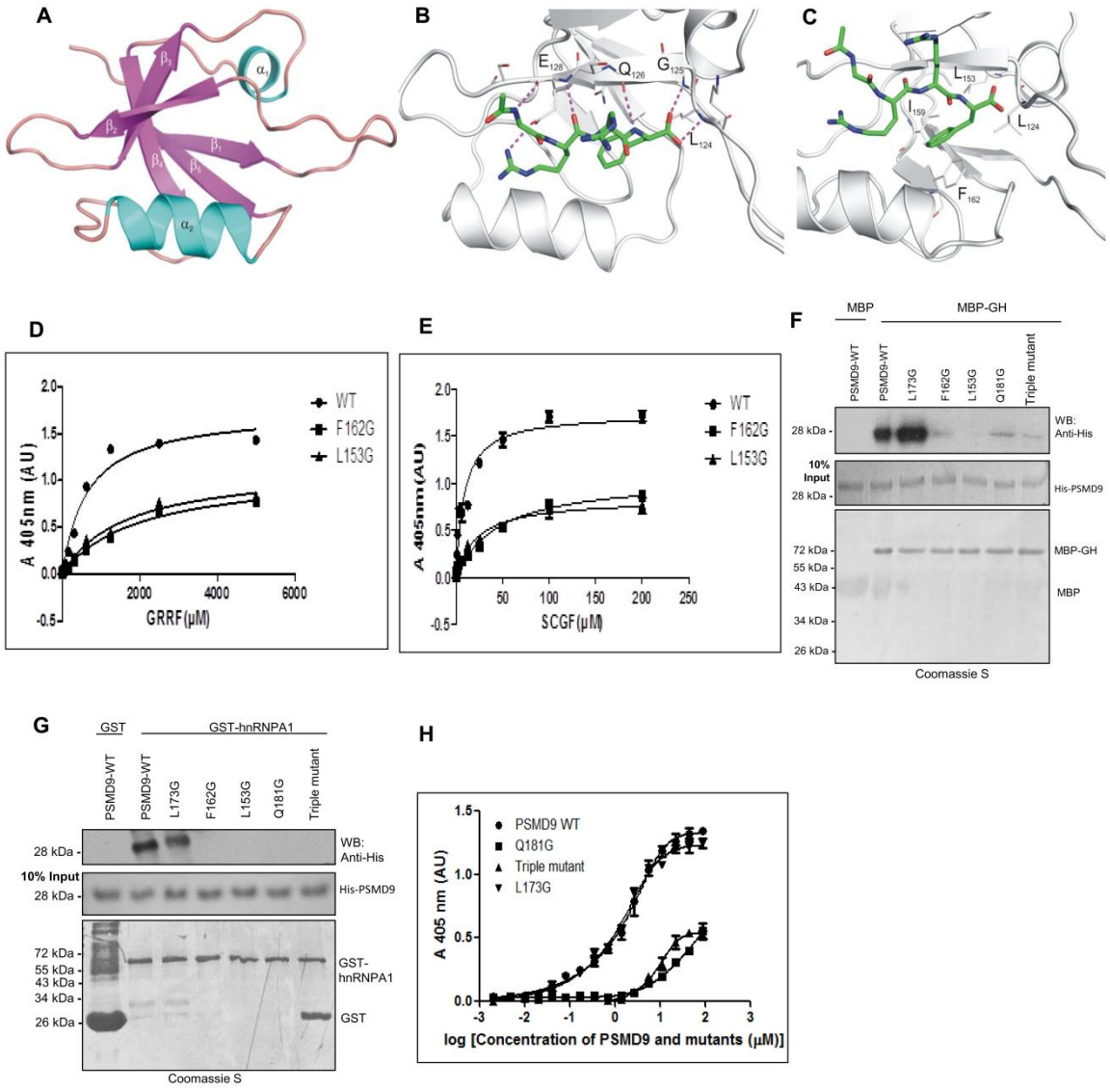

Figure 5.1 Identification and validation of important residues in the PDZ domain of PSMD9 with the aid of computational modeling and docking. A) Cartoon representation of PDZ domain of PSMD9 built using PDZ2 domain of harmonin as the template. B) And C) Structure of PDZ domain bound to GRRF. A clear cleft that is bordered by α-helix and a β-strand can be seen in the PDZ domain similar to ligand bound PDZ structures. D) ELISA was used to monitor interaction between PSMD9 or its mutants L153G or F162G with GRRF peptide. Data

were fit to one site specific binding using PRISM. The dissociation constants (K_d) for the interaction of GRRF and SCGF with PSMD9, L153G and F162G were found to be 651.7±76 μM, 1634±194 μM and 1959±197.2 μM, respectively. E) ELISA was used to monitor interaction between PSMD9 or its mutants L153G or F162G with SCGF peptide as described in (A) The dissociation constants (K_d) for the interaction of SCGF with PSMD9, L153G and F162G were found to be 8.6±1.2 μM, 44.4±5.7 μM and 21.6±2.49 μM , respectively. Measurements were done in duplicates and data is represented as mean±SD (SD- standard deviation) for two independent experiments. F) Mutation of residues in the canonical pocket of PDZ domain [Q181G, Triple mutant (L124G/Q126G/E128G), L153G and F162G] abrogate binding to GH *in vitro*. G)Mutation of residues in the canonical pocket of PDZ domain [Q181G, Triple mutant (L124G/Q126G/E128G), L153G and F162G] abrogate binding to hnRNPA1. H) WT hnRNPA1 interaction with recombinant WT PSMD9 or its mutant proteins was detected by ELISA. Three independent experiments each in duplicates were performed and data is represented as mean ± SD (SD- standard deviation).

Table 5.1 Interaction of hnRNPA1 with PSMD9 and its mutants.

	K_d (μM) (Interaction with hnRNPA1)
PSMD9 WT	1.33±0.16
L173G	1.2±0.09
Q181G	27.42±4.8
Triple Mutant (L124G/Q126G/E128G)	13.26±2.1

Dissociation constants (K_d) of hnRNPA1 interaction with PSMD9 and its mutants obtained by ELISA experiments. Data represented as mean±SD from three independent experiments.

Molecular Dynamic Simulation (MD Simulation) (In collaboration with the A*Star group in Singapore)

During MD simulation, in the PDZ domain without the peptide (apo PDZ), alpha/beta binding groove (canonical binding site) showed increased flexibility (Figure 5.2). The α_2/β_2 binding pocket was found to be partially deformed. This structure was stabilized upon peptide binding. Increased flexibility of PDZ domains in their apo form have been reported by others (Munz et al., 2012). The intrinsic flexibility of PDZ domains is probable the key reason that allows them to recognize a wide repertoire of peptide ligands. Throughout the protein-peptide simulation, Phe4 remains deeply buried in the hydrophobic pocket (Movie1: http://web.bii.a-star.edu.sg/bmad/PDZ/PDZ-PEP-WT-Top.mpg). Charge-charge interactions between Arg2 and Glu128 on β_2 are preserved during the 100ns simulation. The bound conformation of the peptide was further stabilized via backbone hydrogen bond interactions with residues Leu124, Gly125, Gln126 and Glu128 from β_2 in the canonical binding site. In the complex where Phe4 was mutated to Gly, the peptide unbinds from the canonical binding site within ~5-10 ns and doesn't bind again (Movie 2: http://web.bii.a-star.edu.sg/bmad/PDZ/PDZ-PEP_GRRG-Top.mpg). Although the peptide stays close to the canonical site due to charge-charge interactions with the protein residues, it undergoes translation and rotations that prevent it from rebinding in the canonical interaction mode. Thus, our MD simulations suggest that the burial of Phe in the hydrophobic pocket is crucial for the stabilization of this peptide in its bound conformation. MD simulations (Movie 3: http://web.bii.a-star.edu.sg/bmad/PDZ/PDZPEP_L124G_Q126G_E128G-Top.mpg and Movie 4: http://web.bii.a-star.edu.sg/bmad/PDZ/PDZ-PEP_Q181G-Top.mpg), also clearly showed that these sites were important for interaction. MD Simulation experiments clearly support the docking and mutagenesis studies. Our interaction experiments earlier with

GRRF and GRRG peptides, as well as F372G mutation in hnRNPA1 clearly showed the importance of the terminal Phe residue in the interaction with PSMD9. MD simulation experiments confirm this observation.

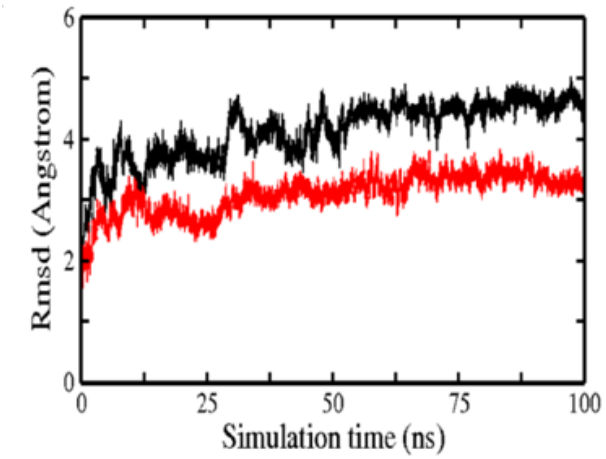

Figure 5.2 Molecular dynamic simulation of docked structures of modelled PDZ domain of PSMD9. RMSD of the conformations of PDZ domain of PSMD9 in its apo state (black lines) and in complex with the GRRF peptide (red lines).

The GLQV pocket of the PDZ domain of PSMD9

Studies on Bridge1-p300 interaction revealed that internal regions of p300 interacted with PSMD9. Since the GLGF motif is very important for interaction with C-terminal regions in most PDZ domains (Jelen et al., 2003). Human PSMD9 and its rat homolog Bridge1 have a GLQV sequence instead of GLGF motif. Lee et. al mutated D156 residue, which is downstream of the GLQV motif, to a proline and showed Bridge1-p300 interaction was abrogated. In our model, GLQV region does not fall in the canonical binding pocket, but is a part of a loop region close to the pocket. Some PDZ domains carry additional structural elements that are located outside of the canonical PDZ fold, and are reported to influence affinity and specificity (Doyle et al., 1996; Nomme et al., 2011; Pan et al., 2011). For example the third PDZ domain of PSD-95 (PDZ3)

contains an alpha helix located at the C-terminus outside of the canonical PDZ fold (Doyle et al., 1996). Although this helix (termed alpha3) is located far from the binding groove (~6A), either deletion or mutation of residues in this helix alpha3 has a profound effect on the affinity between PDZ3 and peptide ligands, and is hypothesized to originate in allosteric regulation (Petit et al., 2009; Saro et al., 2007; Wang et al., 2010). There are several example of allosteric regulation of canonical PDZ domains (Diehl et al., 2010; Fuentes et al., 2004; Gerek and Ozkan, 2011; Gianni et al., 2011; Ho and Agard, 2010). PDZ domains have been popular model systems for the study of single-domain allostery. Several computational and experimental studies have suggested that network of connected residues can be used to evolve allosteric switches and thus peptide binding can be regulated allosterically (Basdevant et al., 2006; Chi et al., 2012; Dhulesia et al., 2008; Mostarda et al., 2012). Residues that are located far from the canonical site can affect the peptide binding at the canonical site through allosteric communication. Hence we decided to model the full length PSMD9 protein.

The homology model of PSMD9 was constructed using crystal structure of the harmonin NPDZ1 (PDB 3K1R) (Yan et al., 2010) bound with sterile α motif - PDZ-binding motif (SAM-PBM) of Usher syndrome type-1G protein (Sans – Scaffold protein containing ankyrin repeats and SAM domain) as the template. This model reveals that the PSMD9 protein carries a coil-coil domain at the N-terminal ranging from residues1 to 104, followed by a PDZ domain ranging from residues 105 to 193 and an extra structural element at the C-terminus of PDZ domain ranging from residue 194 to 223 (Figure 5.3A). It is clear that the wild type structure is stable while the D157P mutant undergoes perturbations as revealed by the root mean squared deviation with time relative to a starting structure (Figure 5.3B). Peptide GRRF could not be docked stably at this site.

The MD simulations suggest that in the wild type, a network of interactions including hydrogen bonds, salt bridges between Q154, D156, D157 and R194 acts as a node across which the extra C-terminal structural element oscillates between two states, one of which brings the region of R202 into hydrogen bonding proximity of Q126/S172 which lie at the end of the binding groove which accommodates the N-terminus of the peptide GRRF. The binding groove remains well formed in wild type PSMD9 protein (Figure 5.3C and D). In contrast, the replacement of D157 by P perturbs the node of interactions and a new salt bridge is formed between D156 and K211. The latter lies in the extra C-terminal structural element and brings the Q200-R202 region into interacting distance with one side of the binding groove (the L124-S127 region), destabilizing the binding groove integrity (Figure 5.3E and F Movie 5: http://web.bii.a-star.edu.sg/bmad/PDZ/PSMD9-APO-D157P-Top.mpg). Mutation D157P abrogated the interaction with hnRNPA1 (Figure 5.3G) proving that this residue is indeed important for interaction, which may act as an allosteric site on the PDZ domain of PSMD9.

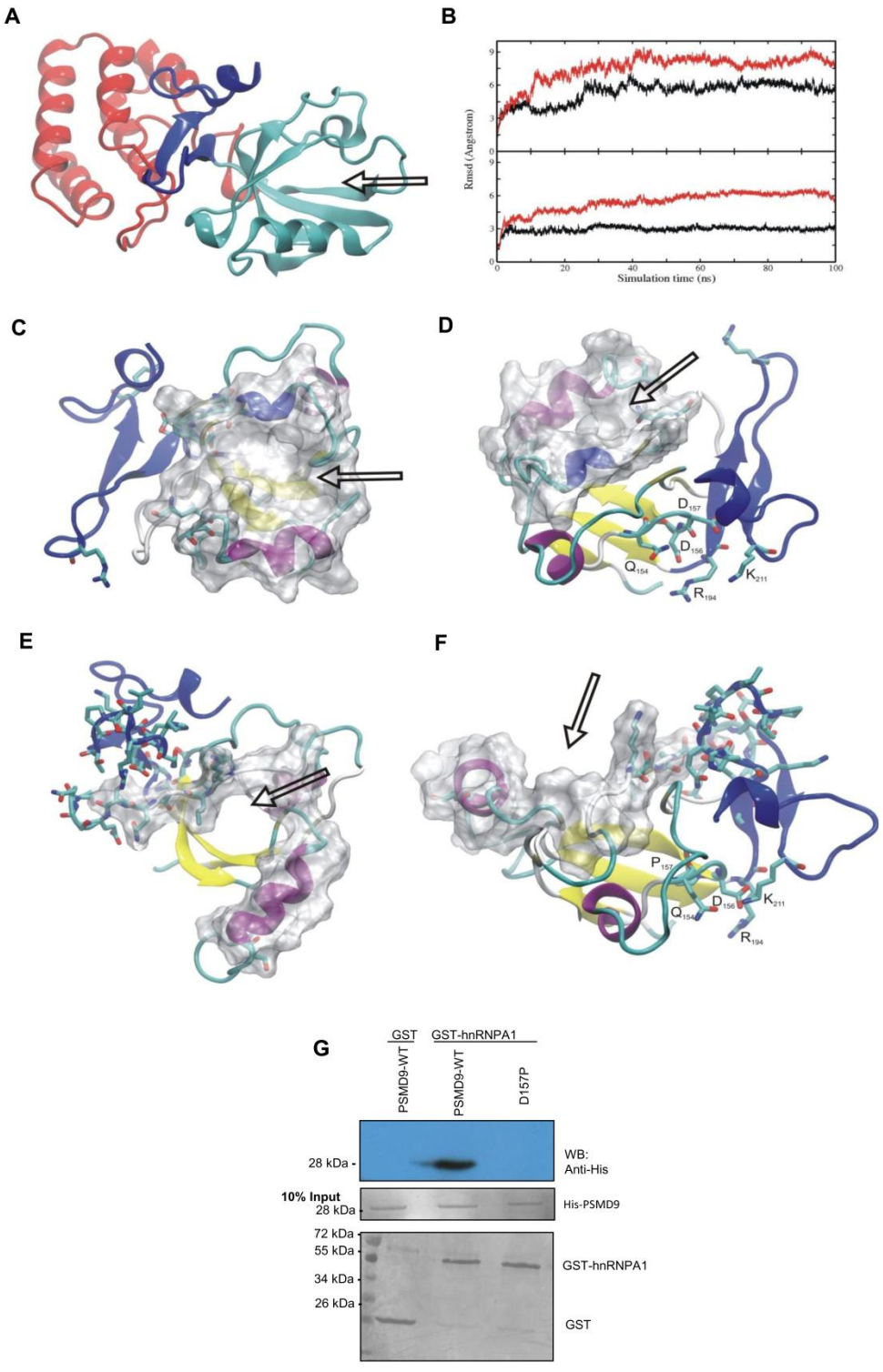

Figure 5.3 Modeling of full length PSMD9 and importance of D157 residue. A) Cartoon representation of full length model of human PSMD9 protein (Red: coiled coil domain, Cyan:

PDZ domain, Blue: Additional structural element at the C-terminal of PDZ domain). B) RMSD of the sampled conformations of full length PSMD9 (top) and rmsd of only PDZ domain (bottom) (full length protein was simulated, but the RMSD calculated for only the PDZ domain) in its apo state. Full length PSMD9 wild type in black lines and D157P mutant in red lines. MD simulation snapshot of wild type PSMD9 protein (C) top view (D) side view. MD simulation snapshot of D157P mutant PSMD9 protein (E) top view (F) side view. (For clarity purpose only, the PDZ domain as a cartoon representation, colored according to the secondary structure and the additional structural element at the C-terminus of PDZ domain in blue color). The peptide binding groove is indicated with an arrow. G) D157P mutation abrogates interaction with hnRNPA1 *in vitro*.

Effect of mutations on secondary and tertiary structure of PSMD9

To understand the effect of mutations on the secondary and tertiary structure of PSMD9, circular dichroism and fluorescence studies, respectively were performed. Circular dichroism studies clearly showed that helicity of PSMD9 was affected due to mutation (Figure 5.4A Table 5.2). WT PSMD9 records 49% helicity, while the L173G mutant shows 43% helical structure, Q181G mutant contributes to 39% helicity, L153G and F162G contribute to 45% and 42% helicity, respectively. The secondary structure of the mutant L173G which still has the ability to interact with the interacting partners is also affected. D157P recorded 37% helicity. Thus, there is a local secondary structure change in all the PSMD9 mutants. To find whether there is change in the tryptophan environment on mutation, which is sign of tertiary structure alteration, fluorescence experiments were conducted with WT PSMD9 and mutants. There was no shift in the emission maxima, clearly showing the absence of any alteration in the tertiary structure (Figure 5.4B).

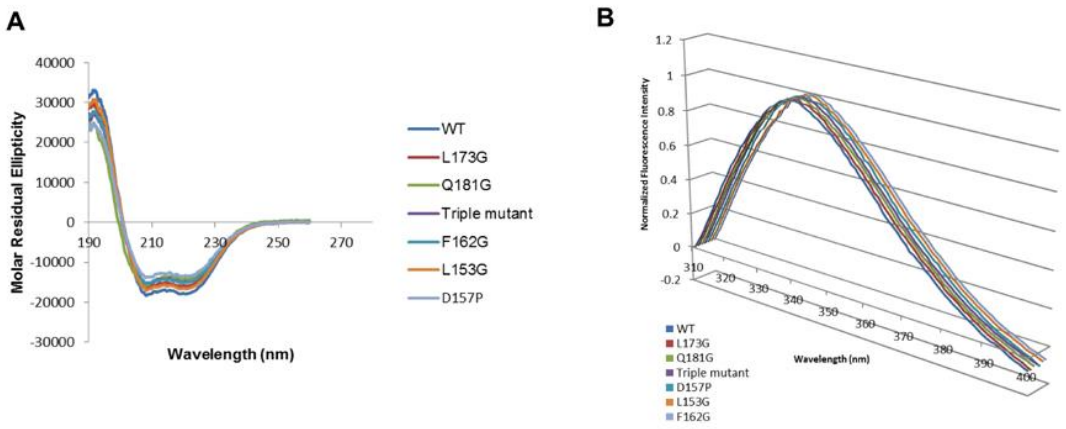

Figure 5.4 Effect of mutations on secondary and tertiary structure of PSMD9. A) Circular dichroism of PSMD9 WT and the PDZ mutants were recorded at 2μM concentration between 260 nm and 195 nm. Molar residual ellipticity is plotted against wavelength. B) Fluorescence spectra of PSMD9 WT and its mutants were recorded between 310 nm and 410 nm (Excitation wavelength 295nm). Data are represented as normalized fluorescence intensity against wavelength of emission.

Table 5.2. Fraction of helicity of PSMD9 WT and mutants analyzed by circular dichroism.

Protein	$[\theta]_{222}$ (deg.cm^2.dmol^{-1})	Helicity predicted by CONTIN(%)	Helicity predicted by formula*(%)
PSMD9 WT	-17281.7± 368.34	47.5±0.96	52±0.94
L173G	-15377.4± 327.75	41.93±0.77	47.1±0.8
Q181G	-13734.7± 292.14	38±0.72	42.9±0.7
Triple mutant L124G/Q126G/E128G	-14485.3± 308.74	40.13±0.77	44.8±0.7
D157P	-13348.2± 208.24	37.3±0.52	41.9±0.67

*The fraction of α-helix present in PSMD9 and mutants were calculated using the CONTIN software available in DICHROWEB server and the helicity is also predicted by the formula $fH = ([\theta]_{222}$-3000)/(-36000-3000) (appendix Eq. 1) (Morrisett et al., 1973), where [θ]222 is mean molar residual ellipticity at 222 nm.

We have successfully deduced the binding pocket of PSMD9 and the residues important for the interaction. The hydrophobic environment created by these residues creates an apt niche for the peptides like GRRF to bury its Phe residue in the pocket and stabilize the PDZ domain.

Modelling of full length PSMD9 enabled understanding the role of D157 residue in the interaction. Though D157 is not part of the canonical hydrophobic pocket of the PDZ domain, may act as an allosteric site for C-terminal motifs and influence the interaction of these ligands in the canonical hydrophobic pocket.

CHAPTER 6

FUNCTIONAL MODULES REGULATED BY PSMD9

Introduction

Our peptide screening was based on the observation of Chung et. al, that many proteins share a common C-terminus, which may be significant in contributing to cellular and biochemical functions (Chung et al., 2003). We presumed that since PSMD9 has a PDZ domain, and being a part of the 19S regulatory particle of the proteasome, it can potentially interact with many proteins in the cell via their C-termini for degradation or for other physiological functions. From our preliminary screening experiments, we found that, of the 12 C-terminal tetra-peptide sequences we screened, GRRF and SCGF interacted with the PDZ domain of PSMD9, and the proteins harbouring the motifs interacted as well. In order to find out more interacting partners of PSMD9, we decided to screen more peptides which were reported by Chung et. al. In this chapter, we describe the shortcomings of this approach and report the discovery of two more interacting partners of PSMD9- S14 ribosomal protein and the FN3 domain of the IL6 receptor isoform 2.

Results and Discussion

Though our low throughput approach gave us clues about the interacting partners of PSMD9, it had a few drawbacks. Chung et al., had classified proteome from drosophila/yeast/human by recognizing conserved C-terminal residues in some of these proteins and listed out 30 tetra-peptide sequences which have more than 10 members in their group (Chung et al., 2003). When we further investigated, we found that most of the members of the group were isoforms of the same proteins or some were predicted or hypothetical proteins. Independent analysis of these 30 tetra-peptide sequences and their constituent members and further curation using Uniprot database (ftp://ftp.uniprot.org/pub/databases/uniprot/current_release/knowledgebase/) also revealed that

most of the members were isoforms and rarely more than 2 unique protein members. To better define the role of C-terminus in functional grouping beyond isoforms, and predict the modules that may be regulated by PSMD9, we analyzed C-terminal variants of GRRF and SCGF from the human proteome. There are ten variants of GRRX where X is C, E, G I, K, L, N, P, Q or R (Table 6.1). SCGL at the C-terminus was a single variant of SCGF. We screened seven variants of GRRF (GRRG was already tested as a control) i.e., GRRC, GRRE, GRRI, GRRL, GRRN, GRRQ and GRRR as well as the SCGL peptide for binding to PSMD9 by ELISA (Figure 6.1A). GRRL, GRRI and GRRQ interacted with PSMD9 with almost the same affinity as GRRF. GRRC and GRRR had 14 fold higher affinities than GRRF. SCGL had a similar affinity as SCGF (Table 6.2). We can thus group these peptides into three different groups. Group I peptides, hydrophobic residues such as F, L, I at P_0 provide specificity, group II peptides, Cys or Arg at P_0 increases affinity by 10 fold as compared to that of group I peptides and group III peptides, SCG variants SCGF and SCGL bind with the highest affinity. It is surprising that peptides like GRRC and GRRR which have Cys and Arg at the P0 position have relatively higher affinity. We were interested in proteins harbouring GRRL and SCGL motifs since they have a hydrophobic residue at the P_0 position. We cloned and expressed S14 ribosomal protein and the FN3 domain of IL6 receptor isoform 2 and found that both these proteins interacted with PSMD9. The C-temini of these proteins and the PDZ domain of PSMD9 are important for the interaction (Figure 6.2B, C, D and E) further confirming that our C-terminal peptide screening technique indeed gives the right directions to find out interacting partners of PSMD9.

Table 6.1 Proteins in the human proteome harboring GRRX sequence at their C-terminus.

C-terminus	Name of the protein	Swissprot/NCBI ID
GRRC	FGFR2_HUMAN Isoform 19 of Fibroblast growth factor receptor 2	>sp|P21802-19|
GRRC	EPCR_HUMAN Endothelial protein C receptor	>sp|Q9UNN8|
GRRE	HUMAN Isoform 4 of Dynein heavy chain 17	>sp|Q9UFH2-4|
GRRF	HUMAN Isoform A1-A of Heterogeneous nuclear ribonucleoprotein A1	>sp|P09651-2|
GRRF	HUMAN Isoform 2 of Heterogeneous nuclear ribonucleoprotein A1	>sp|P09651-3|
GRRF	HUMAN Heterogeneous nuclear ribonucleoprotein A1	>sp|P09651|
GRRF	HUMAN Heterogeneous nuclear ribonucleoprotein A1	>sp|Q32P51|
GRRG	HUMAN Isoform 2 of Serine/threonine-protein kinase 11-interacting protein	>sp|Q8N1F8-2|
GRRG	HUMAN Isoform 3 of Abhydrolase domain-containing protein 11	>sp|Q8NFV4-3|
GRRG	HUMAN Isoform 2 of Protein FAM115C	>sp|A6NFQ2-2|
GRRG	HUMAN Protein phosphatase 1 regulatory subunit 15A	>sp|O75807|
GRRI	Hypothetical protein	
GRRK	HUMAN Isoform 3 of Spectrin beta chain	>sp|Q9H254-3|
GRRK	|HUMAN Spectrin beta chain	>sp|Q9H254
GRRK	HUMAN Isoform 3 of UPF0378 protein	>sp|Q14667-3|
GRRK	HUMAN Isoform 2 of UPF0378 protein	>sp|Q14667-2|
GRRK	HUMAN UPF0378 protein	>sp|Q14667|
GRRL	HUMAN 40S ribosomal protein S14	>sp|P62263|
GRRP	VAPB_HUMAN Isoform 2 of Vesicle-associated membrane protein-associated protein B/C	>sp|O95292-2|
GRRQ	HUMAN Isoform 3 of Solute carrier family 45 member 4	>sp|Q5BKX6-3|
GRRR	HUMAN Regulator of nonsense transcripts 2	>sp|Q9HAU5|
GRRS	HUMAN Neuroblastoma breakpoint family member 10	>sp|Q6P3W6|

List of proteins from Uniprot possessing GRRX sequence at their C-termini.

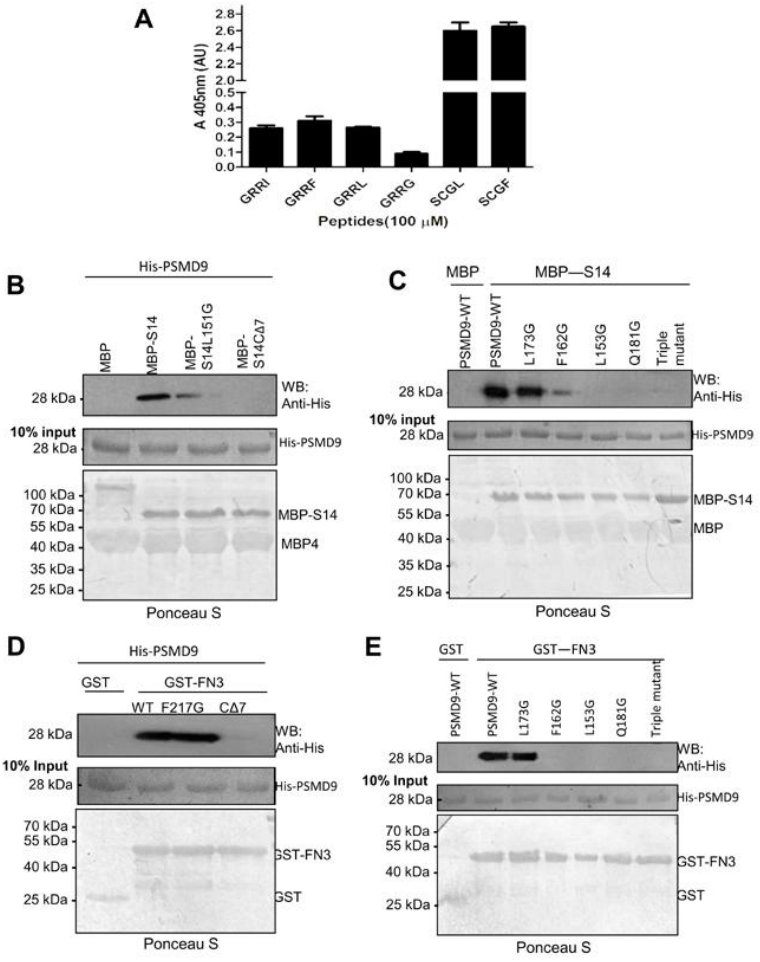

Figure 6.1 Interaction of PSMD9 with C-terminal variants of hnRNPA1 and GH from the human proteome (A) Binding of peptide variants GRRX to recombinant PSMD9. GRRX peptide (X= any residue) binding to PSMD9 was detected and measured by ELISA. Values from three experiments done in duplicates are represented as means ± SEM. (B) S14 ribosomal protein interacts with PSMD9 via its C- terminal residues. Complex formed between S14 wild type (MBP fusion), S14 L151G or C-terminal deletion mutant S14 CΔ7 was isolated as described in methods. Any bound PSMD9 (His tagged) was detected using anti-His antibody (C) PDZ domain of PSMD9 is important for interaction with S14 ribosomal protein *in vitro*. *For* the *in*

vitro pull-down, MBP-S14 fusion and his-PSMD9 or its mutant proteins were processed as described previously. (D) FN3 domain of IL6 receptor interacts with PSMD9 *in vitro*. GST-WTFN3, FN3 F365G mutant or C-terminal deletion mutant (FN3C Δ7) were used to pull down PSMD9 (His-tag) and probed for the presence PSMD9 using anti–His antibody. (E) PDZ domain of PSMD9 is important for interaction with the FN3 domain *in vitro*.

Table 6.2. Binding of GRRX peptides to PSMD9 by ELISA (X is any amino acid).

Peptide	**Dissociation constant (K_d) (μM)**
GRRL	668 ± 82.2
GRRI	638 ± 65.6
GRRQ	447.5 ± 53
GRRC	44.12 ± 5.2
GRRR	53.43 ± 7.2

PSMD9 may regulate the functions of the four interacting partners hnRNPA1, GH, S14 ribosomal protein and IL6 receptor isoform 2. Since hnRNPA1- I*κ*Bα interaction is important for I*κ*Bα degradation by the 26S proteasome, PSMD9 may be important in degradation of I*κ*Bα and NF-*κ*B activation (Figure 6.2A). S14 ribosomal protein plays a major role in regulating the stability of p53 by interacting with MDM2 and prevents the ubiquitination of p53 (Zhou et al., 2013). S14 may behave like hnRNPA1 interacting with PSMD9 and regulate the degradation of substrates like p53 (Figure 6.2B). Bridge1, the rat homolog of PSMD9 activates transcription through its interaction with E12 (Thomas et al., 1999). E12 may also be a substrate of the proteasome, where PSMD9 may regulate the degradation process (Figure 6.2C). The role of proteasome in regulating the degradation of endosomal proteins is well known. Many proteins like T cell receptor and HMG-CoA reductase, when misfolded in the ER, is transported to the cytosol for proteasomal degradation (Fra and Sitia, 1993; Lord, 1996). A mutant of growth hormone is responsible for Isolated Growth Hormone Deficiency (IGHD II). Upon proteasome inhibition the mutant accumulates as a misfolded protein in the cytoplasm of neuroendocrine

cells (Kannenberg et al., 2007). One may speculate that degradation of this misfolded protein (and the WT) is probably mediated by PSMD9 through interaction with the C-terminal motif (Figure 6.2D). Membrane proteins like growth hormone receptor (GHR) and epithelial sodium channel (ENaC) are ubiquitinated for vesicular internalization and are degraded by the proteasomes (Schild et al., 1996; Shimkets et al., 1997; Strous and Govers, 1999). Membrane associated proteasomes have been reported where proteins like Sec62 in yeast are degraded with the help of ubiquitin conjugating enzymes UBC6 and UBC7 (Mayer et al., 1998). Similarly, PSMD9 may play an important role in the degradation of IL6 receptor (Figure 6.2D). Thus, PSMD9 may regulate multiple functions within the cell. It remains to be explored the unifying role of PSMD9 in regulating these functions to ensure quality control and regulate signalling or transcriptional programs.

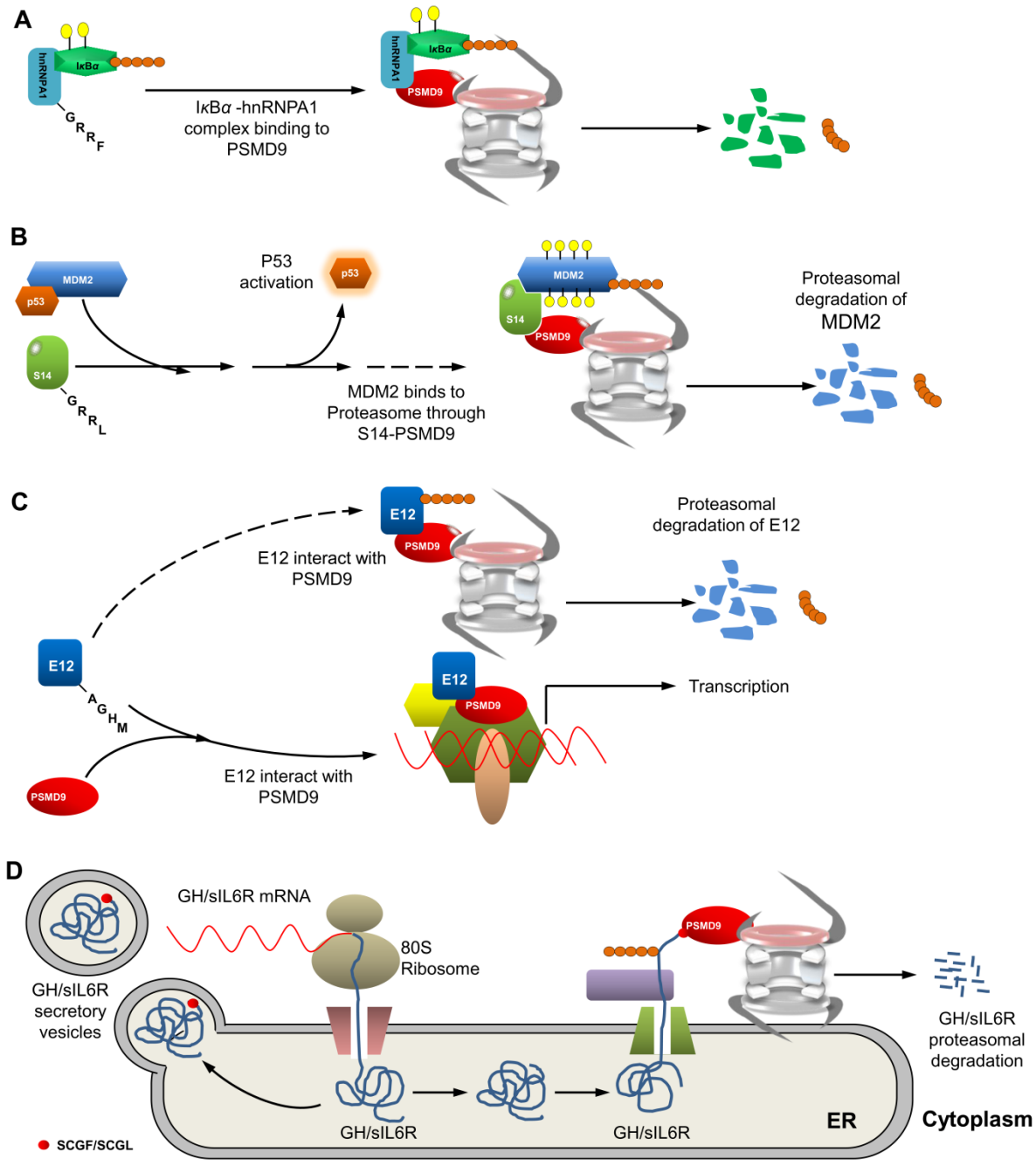

Figure 6.2 Funcional Modules of PSMD9 and its probable role in quality control by the proteasome. (A) Role of PSMD9 in I*κ*Bα degradation. hnRNPA1 is assumed to be an adaptor protein or a shuttle receptor that recruits ubquitinated I*κ*Bα to the proteasome by interacting with PDZ-PSMD9 via its C-terminus. PSMD9 acts as the subunit acceptor that helps to anchor I*κ*Bα via hnRNPA1 (B) Probable role of PSMD9 in regulating the stability of p53. S14 interacts with

MDM2 and regulates the stability of p53. PSMD9 may modulate the ability of MDM2 to regulate p53 activity in two different ways (please see the discussion for details). (C) PSMD9-E12 interaction may be relevant for transcriptional coactivation/repression of many genes. PSMD9 may also play a regulatory role in proteasomal degradation of E12 to terminate transcription. (D) Model showing the probable role of PSMD9 in ER associated proteasomal degradation. Misfolded or aggregated secretory proteins like IL6 receptor and growth hormone are retro-translocated from ER and to ER associated proteasome for degradation. PSMD9 may help in anchoring the translocated substrate by grabbing the C-terminal residues.

CHAPTER 7

SPECIFICITY OF PDZ DOMAIN OF PSMD9

AND

POSSIBLE MODES OF BINDING

Introduction

PDZ domains possess αB and βB structural elements to form a hydrophobic pocket which allows the binding of the C-terminal peptide. It is well known that based on the nature of the C-terminal sequence the PDZ domain interacts, they are classified into three classes- class I domains prefer

-X-[S/T]-X-Φ motifs and class II domains prefer –X-Φ-X-Φ motifs and class III domains prefer -X-[D/E/R/K]-X-Φ (where Φ is a hydrophobic residue) (Jelen et al., 2003). This classification cannot be generalized because there are many peptide ligands that bind to the PDZ that do not fall into any of the categories mentioned above. The PDZ domain of PSMD9 cannot be categorized under any of the classes of PDZ domains mentioned above because it can recognize ligands like GRRF and GRRL which are class III ligands, but also recognize other ligands like SCGF, SCGL, GRRC, GRRR and AGHM. It is already reported that the PDZ domain of the rat homolog of PSMD9, Bridge1 can interact with the N-terminus of PDX-1 transcription factor and internal regions of histone acetyl transferase p300 to activate insulin gene transcription (Lee et al., 2005; Thomas et al., 1999). These results show that PDZ domain of PSMD9 may be quite different from the classical PDZ domains. Results from *in vitro* experiments mentioned in the previous chapter clearly showed that the terminal Phe residue was important in the GRRF for interaction, but not in the case of the SCGF motif. Here we attempt to try and understand the different specificities of the PDZ domain of PSMD9 towards GRRF and SCGF motifs.

Results and Discussion

C-terminal mutant of hnRNPA1, hnRNPA1 F372G mutation clearly failed to interact with PSMD9 in vitro, whereas the interaction between PSMD9 and GH F217G of the growth hormone remained unaffected. This clearly showed that other residues in the C-terminus of GH

were involved in the interaction. To elucidate the important residues that are important in the SCGF motif, we generated deletion of mutants of GH- GH ΔGF and GH ΔCGF, which had two and three residues deleted from the GH C-terminus, respectively. *In vitro* pull down experiments and ELISA experiments clearly showed that GH ΔCGF mutant but not GH ΔGF failed to interact with PSMD9, whereas terminal residue mutation hnRNPA1 F372G was sufficient to inhibit the interaction, clearly showing the role of cysteine in the SCGF motif (Figure 7.1 and Table 7.1). We also performed peptide inhibition experiments using peptides SCGF and SGGF. Peptide SCGF could inhibit the PSMD9-GH interaction, whereas SGGF could not, further confirming the role of cysteine in the interaction (Figure 7.1D).

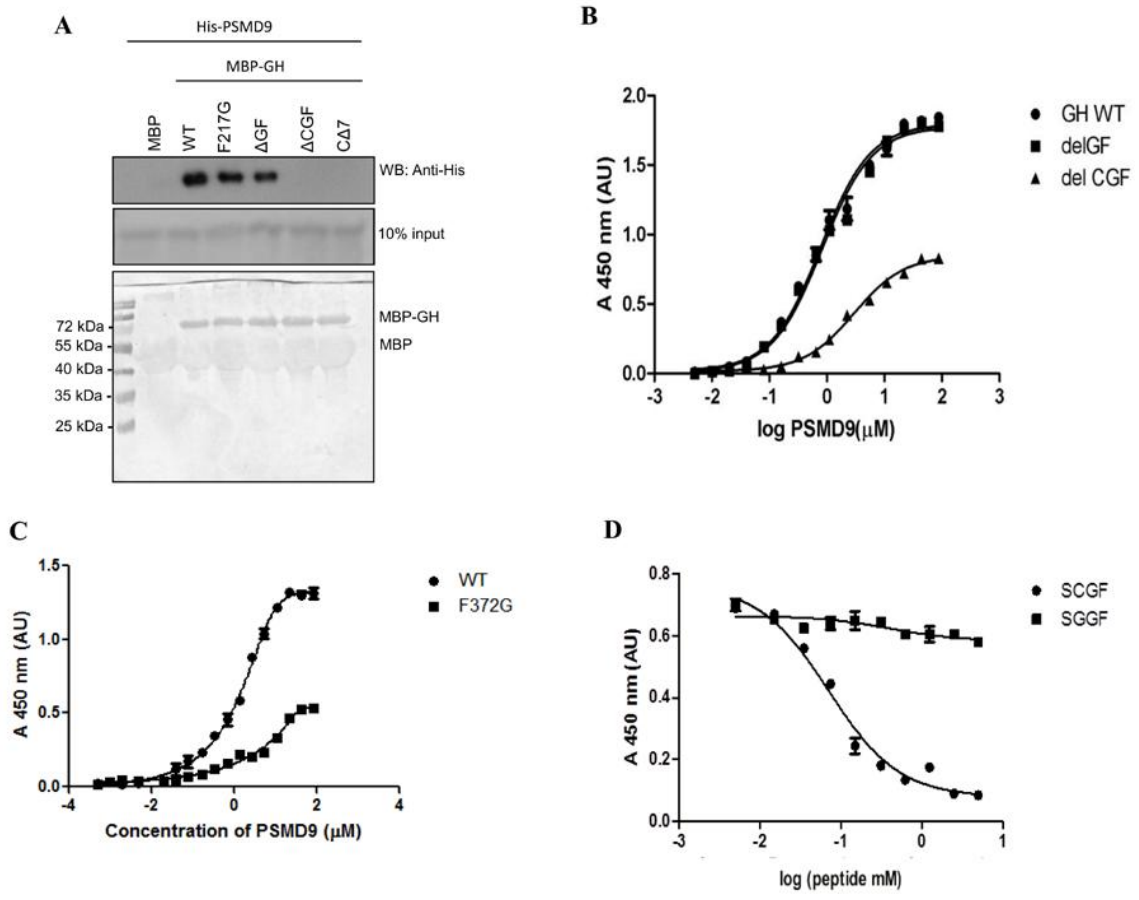

Figure 7.1 Different specificity of PSMD9 towards GRRF and SCGF motifs. A) Interaction of recombinant GH and its C-terminal mutants F217G, ΔGF, ΔCGF and CΔ7 (MBP fusions) with PSMD9 was tested by in vitro affinity pull-down using MBP-agarose. B) ELISA was used to monitor interaction between PSMD9 and WT GH or its C-terminal mutants. Data were fit to one site specific binding using PRISM. The dissociation constant (K_d) for the interaction of WT Growth hormone, ΔGF and ΔGF with PSMD9 was found to be 0.74±0.04μM, 0.8±0.03 and 2.64±0.02 μM, respectively. Measurements were done in duplicates and data is represented as mean±SD (SD- standard deviation) for three independent experiments. C) ELISA was used to monitor interaction between PSMD9 and WT hnRNPA1 or its C-terminal mutant hnRNPA1 F372G. Data were fit to one site specific binding using PRISM. The dissociation constant (K_d) for the interaction of WT hnRNPA1 and hnRNPA1 F372G with PSMD9 was found to be 1.36±0.10 and 3.47±0.57 μM, respectively. Measurements were done in duplicates and data is represented as mean±SD (SD- standard deviation) for three independent experiments. D) C-terminal peptide SCGF, and not SGGF, inhibit interaction of Growth hormone with PSMD9. Prior to incubation with Growth hormone, PSMD9 (0.65 μM) was incubated with SCGF or SCGG peptides. Ki for SCGF was calculated to be 36.7±0.29 μM. Data from two independent experiments each done in duplicates is represented as mean ± SD.

Table 7.1 Quantitative analysis of interaction of PSMD9 with hnRNPA1 and Growth hormone and their C-terminal mutants by ELISA.

Protein interacting with PSMD9	**Dissociation constant (K_d)(μM)**	**Bmax (AU)**
WT hnRNPA1	1.36±0.10	1.34±0.026
hnRNPA1F372G	3.47±0.57	0.52±0.048

WT Growth hormone	0.74±0.04	1.79±0.024
GHΔGF	0.8±0.03	1.77±0.05
GHΔCGF	2.64±0.02	0.84±0.15

Dissociation constants (K_d) of interaction of WT hnRNPA1 and WT growth hormone and their mutants with PSMD9 obtained by ELISA experiments. Data represented as mean±SD from three independent experiments.

PSMD9 possesses three cysteine residues. Therefore, there is a possibility of a disulfide linkage between any one of these cysteine residues and the cysteine of the SCGF motif. We performed peptide binding experiments with PSMD9 in the presence of reducing agents like dithiothreitol (DTT) and β- mercaptoethanol (BME). Addition of reducing agents did not affect the interaction (Figure 7.2A). We also incubated recombinant PSMD9 with biotinylated SCGF peptide at 37^{o}C for an hour in the presence or absence of reducing agents. The complexes were then probed for presence of the biotinylated peptide using streptavidin-HRP. Biotinylated L-Phytohaemagglutinin was loaded as a positive control for detection of biotin. If the interaction between SCGF and PSMD9 was a covalent disulfide linkage, detection of the protein-peptide complex should be possible when probed with streptavidin-HRP. We could not detect PSMD9-SCGF complexes in the absence of reducing agents (Figure 7.2B). This clearly shows that the interaction between SCGF and PSMD9 is clearly non-covalent and that there are no disulfide linkages involved.

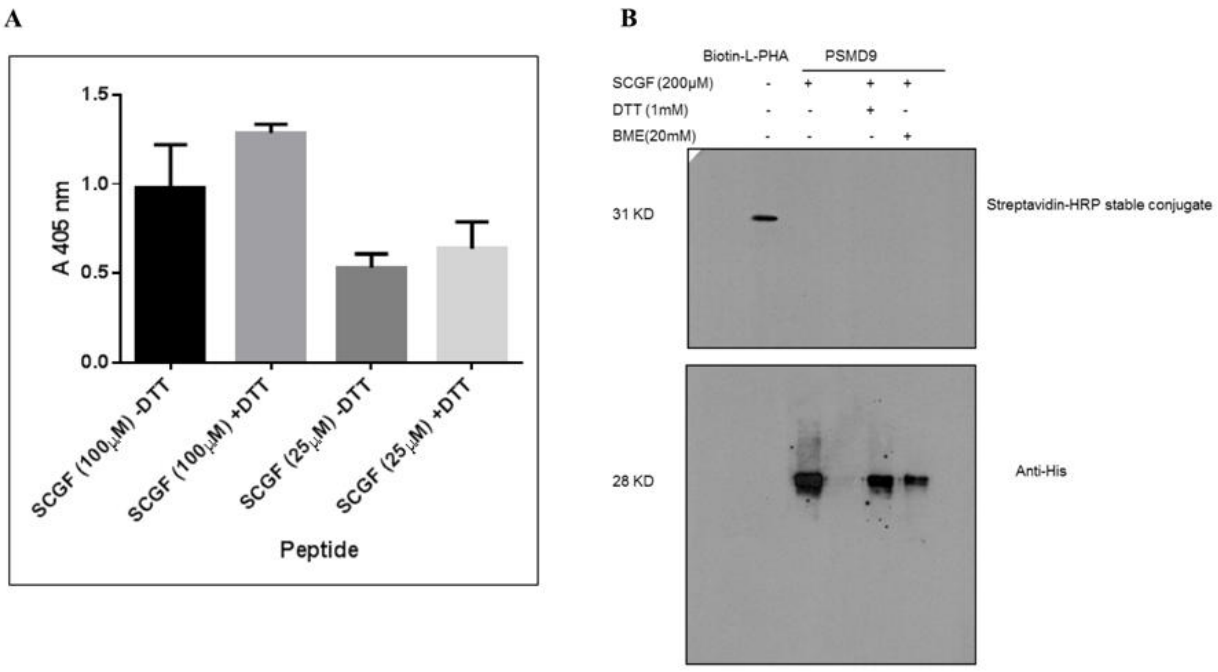

Figure 7.2 SCGF peptide interacts non-covalently with PSMD9. A) ELISA experiments showing binding of SCGF peptide (100 μM and 25 μM) to recombinant his- PSMD9 under non-reducing and reducing (1mM DTT) conditions. B) In vitro binding experiment of biotinylated SCGF peptide (200 μM) with recombinant his- PSMD9 in the presence or absence of reducing agents (1Mm DTT or 20mM BME). Presence of the peptide-protein complex was detected by Streptavidin-HRP conjugate (1:1000). Biotinylated-L-PHA was used as a positive control for biotin detection.

Specificity and modes of binding of C-terminal peptides

It is now very clear that PSMD9 interacts with GRRF and SCGF motifs with distinct specificities. Another observation is that the affinity of SCGF is 50 times higher than that of GRRF. Though peptide GRRF interacts with low affinity (657 μM), the protein hnRNPA1 interacts with a higher affinity (1 μM). This may due to different reasons. C-terminal residues may be the primary recognition motif for PSMD9 but stabilization by the extended structure of

the N-terminal residues of the protein increases the affinity. There is also a possibility of a two step binding mechanism which involves an initial C-terminal binding phase followed by binding of other residues of the protein to some other site, other than the hydrophobic pocket. Further studies are required to understand the precise and detailed mechanism of interaction.

It is very clear that the P_0 position of peptide GRRF is very important for interaction with PSMD9, whereas the P_{-2} position is important in the SCGF peptide. Presence of cysteine is not very common in PDZ ligands. Studies have shown that cysteine has a hydrophobicity index close to that of phenylalanine (Janin, 1979; Kyte and Doolittle, 1982; Wolfenden et al., 1981). Therefore, cysteine can probably behave like a hydrophobic residue in a hydrophobic environment. P_0 position has no specific conformational preference in the Ramachandran plot. In contrast the P_{-1}, P_{-2} and P_{-3} residues show a strong preference and occupy either a strand or an extended conformation (Lee and Zheng, 2010). Such a conformational preference, especially of the P_{-2} residue may explain the high affinity interaction seen with SCGX peptides.

Three modes of peptide binding to PDZ domains in proteins GRASP, PDLIM and MAST4 have been identified. In the structures of GRASP-peptide complexes, two chains of the protein bind to the same peptide in two different binding modes- the intermediate mode and the perpendicular mode, which may be kinetic intermediates. The other mode is the stable, well known canonical mode. In the perpendicular mode, the terminal P_0 residue is very important, whereas in the canonical mode, the peptide lies in an antiparallel orientation where the P_{-2} residue stabilizes the interaction (Figure 7.3). We can draw a parallel from these observations, where GRRF may frequent the perpendicular orientation, whereas the SCGF may frequent the canonical orientation. We had already mentioned in the previous chapter about the grouping of C-terminal peptides in our study. Group I peptides have hydrophobic residues such as F, L, I at

P_0 which provide specificity, group II peptides possess Cys or Arg at P_0 which increases affinity by 10 fold as compared to that of group I peptides and group III peptides, SCG variants - SCGF and SCGL bind with the highest affinity. The group I peptides, probably bind in the non-canonical or perpendicular orientation as seen with other PDZ binding peptides. This orientation will depend exclusively on the burial of the terminal residue for affinity. The group II peptides, GRRC and GRRR peptides probably favor the intermediate orientation, wherein the P_0 residue is anchored. Our experiments clearly suggest that P-2 of the group III peptides SCGF and SCGL is important. Therefore, these peptides may bind with the classical canonical or antiparallel mode.

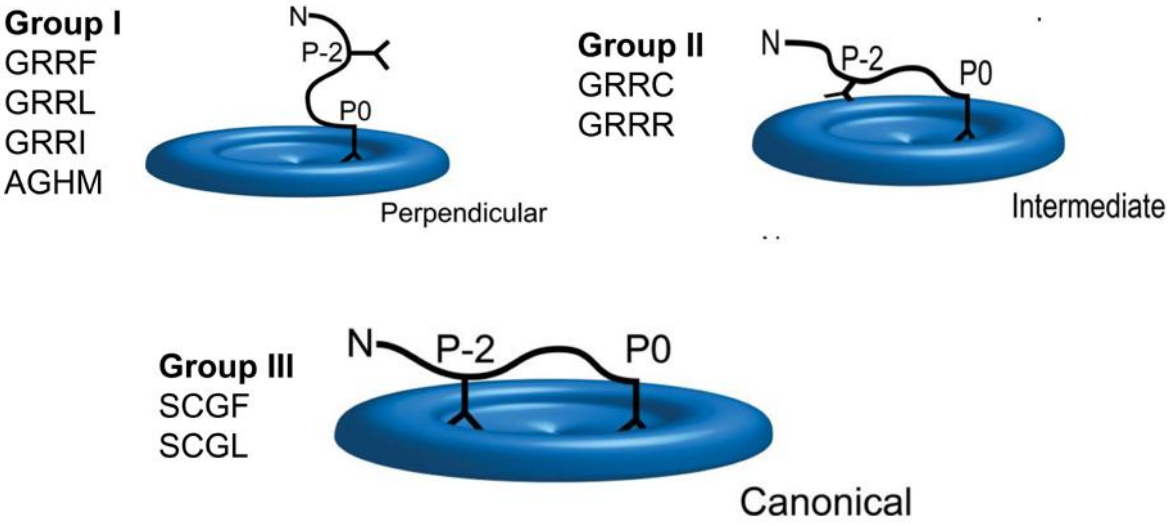

Figure 7.3 Probable modes of bind of C-terminal peptides to PSMD9. Figure shows the probable modes of binding of peptides used in our study to the PDZ of PSMD9. Modes of binding of three groups of peptides (classified based on affinity and specificity towards P_0 or P_{-2}) are speculated based on the crystal structures of the PDZ domain ligand complexes of GRASP and PDLIM proteins reported by Elkins et. al, in 2009). Do u want to make ur own figure/

Through our binding experiments, involving site directed mutagenesis and affinity measurements, we can clearly understand the structural basis of interaction, especially about the important residues involved in the interaction. We can nearly speculate the probable binding mechanisms by correlating our observations with available literature. Solving the crystal structure of PSMD9 complexed with the C-terminal peptides will surely help in understanding the binding mode and specificity of interaction in greater detail.

CHAPTER 8

VALIDATION OF INTERACTION IN MAMMALIAN CELLS AND ROLE OF PSMD9 IN NF-κB SIGNALING

Introduction

Protein-protein interactions are operative at almost every level of cell function, in the structure of sub-cellular organelles, the transport machinery across the various biological membranes, packaging of chromatin, the network of sub-membrane filaments, muscle contraction, and signal transduction, regulation of gene expression, to name a few. Aberrant protein-protein interactions have implicated in a number of neurological disorders such as Creutzfeld-Jacob and Alzheimer's disease. The role of Bridge1, rat homolog of PSMD9, in regulating the transcription of insulin gene is well established (Thomas et al., 1999). Though we have proved that the PDZ domain of PSMD9 interacts with the C-termini of proteins like hnRNPA1, GH, S14 ribosomal protein and the FN3 domain of IL6 receptor isoform 2, it is important to confirm if they interact in mammalian cells. Using affinity pull down studies, we report that all the interacting partners interact with PSMD9 via their C-termini.

Since hnRNPA1 is well known to act as an adaptor protein to subject IκBα for degradation by the proteasome, we decided to check the role of PSMD9 in this process, as it interacts with hnRNPA1 (part of Indrajit Sahu thesis). In this chapter, we also report the role of PSMD9 in NF-κB signaling and its effects on anchorage independent growth in HeLa cells.

Results and Discussion

Validation of interacting partners

To validate the interactions mediated by PSMD9 in mammalian cells, we cloned PSMD9 and its interacting partners in mammalian expression vectors. PSMD9 was expressed as a FLAG tagged protein, whereas all the interacting partners and their C-terminal mutants were expressed as HA tagged proteins. Affinity pull down experiments showed that hnRNPA1, GH, S14 ribosomal protein and FN3 domain interacted with PSMD9 in HEK 293 cells. C-terminal

mutants GH F217G and FN3 L365G failed to abrogate the interaction with PSMD9 (Figure 8.1). Similar results were observed in our *in vitro* pull down assays. It is now very clear that there are distinct modes of binding to different C-termini by the PDZ domain of PSMD9.

Role of PSMD9 in NF-κB signaling

Hay et. al reported that hnRNPA1 regulated the proteasome mediated degradation of IκBα, where the N-terminus of hnRNPA1 interacts with the C-terminus of IκBα, leading to NF-κB activation (Hay et al., 2001). Our lab was interested in this observation, since PSMD9 interacted with C-terminal residues of hnRNPA1. We conducted experiments in HEK 293 cells, where on PSMD9 overexpression, along with TNF α treatment increased the degradation of IκBα, leading to NF-κB activation (Figure 8.1A and B). Overexpression of hnRNPA1 also caused the same phenomenon, but deleting the C-terminal residues caused stabilization of IκBα, abrogating NF-κB activation (Figure 8.1C and D). Similarly, mutating the PDZ domain also resulted in the stabilization of IκBα, and therefore, abrogating NF-κB activation (Figure 8.1D and E) (Indrajit Sahu thesis). These experiments demonstrate that PSMD9-hnRNPA1 interaction plays a key role in the degradation of IκBα, and therefore NF-κB activation. PSMD9 is a well-known chaperone for chaperone for 19S regulatory particle assembly. It is known to be a transient subunit on the 19S regulatory complex. Therefore, it is possible that PSMD9 may act as an acceptor for substrates like IκBα, for their degradation by the 26S proteasome.

It is a well-known fact that increased NF-κB activation increases tumorogenic properties of cells. By increasing transcription of genes like Cox 2, it promotes anchorage independent growth in mammalian cells (Activation of the Nuclear Factor κB Pathway by Astrocyte). To test the role of PSMD9 in this phenomenon, we overexpressed PSMD9 and its PDZ mutants in HeLa cells and checked its effect on anchorage independent growth. We found that PSMD9

overexpression clearly promoted anchorage independent growth, whereas the mutant Q181G failed to do so (Figure 8.1F). It is possible that such a phenomenon can occur due to increased NF-κB activation. To confirm this, we overexpressed a non-degradable form of IκBα, called the IκBα super repressor (Ser 32 is mutated to Ala), which can suppress NF-κB activation, along with PSMD9. We found that on overexpression of the IκBα super repressor, anchorage independent growth was similar as that of vector control, and significantly less than cells overexpressing PSMD9 (Figure 8.1G). All these results clearly suggest that PSMD9-hnRNPA1 interaction plays a crucial role in NF-κB signaling. Therefore, PSMD9 may affect other properties of mammalian cells due to this phenomenon like proliferation, migration and invasion which may depend on the cell /tissue type.

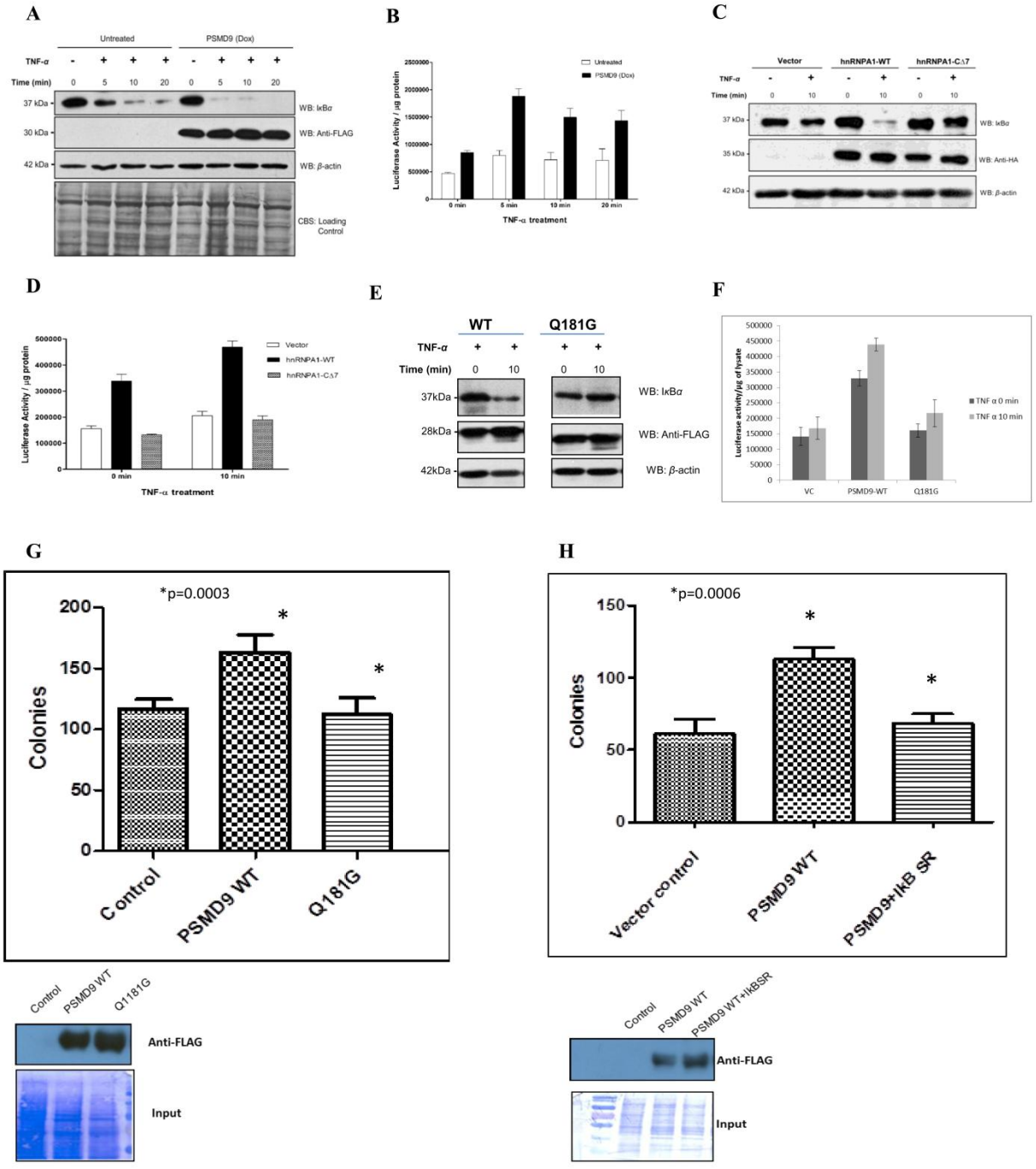

Figure 8.1 PSMD9 interacts with hnRNPA1 and increases IκBα degradation and NF-κB activation. A) Levels of IκBα from inducible FLAG-PSMD9 HEK293stable clones treated with doxycycline (1µg/ml) and TNFα (20 ng/ml) for different time intervals (0-20 minutes) B)

HEK293 cells inducibly expressing FLAG-PSMD9 were transfected with 3x κB ConA luc vector or ConA luc control vector. Transfected cells were treated with doxycycline (1μg/ml) and TNFα (20 ng/ml) for different time intervals (0-20 minutes). After 48 h of induction NF-κB activity was checked by measuring luciferase activity using dual luciferase substrate. Luciferase activity from firefly luciferase was normalized with renilla luciferase used as a transfection control. Data represent mean luciferase activity per microgram of protein ± SEM of two independent experiments done in triplicate. C) Levels of IκBα from HEK 293 cells overexpressing HA-hnRNPA1 or HA-hnRNPA1ΔC mutant treated with TNFα (20 ng/ml) for different time intervals (0 and10 minutes). D) NF-κB activity was checked in the cells overexpressing HA-hnRNPA1 or or HA-hnRNPA1ΔC mutant treated with TNFα (20 ng/ml) for different time intervals (0 and10 minutes) by measuring luciferase activity using dual luciferase substrate as described in B). Data represent mean luciferase activity per microgram of protein ± SEM of two independent experiments done in triplicate. E)) Levels of IκBα from HEK 293 cells overexpressing FLAG-PSMD9 or FLAG-Q181G mutant treated with TNFα (20 ng/ml) for different time intervals (0 and10 minutes). F) NF-κB activity was checked in the cells overexpressing FLAG-PSMD9 or FLAG-Q181G mutant treated with TNFα (20 ng/ml) for different time intervals (0 and10 minutes) by measuring luciferase activity using dual luciferase substrate as described in B). Data represent mean luciferase activity per microgram of protein ± SEM of two independent experiments done in triplicate. F) PSMD9 overexpression induces anchorage independent growth. FLAG-PSMD9 or FLAG-Q181G was overexpressed in HeLa cells by transient transfection after which they were grown on soft agar plates in triplicate. Data represent number of colonies ± SD. One way ANOVA indicated a p value of 0.0003 ($p<0.05$) showing that results are significant. Western blot (below) shows overexpression of FLAG-PSMD9 and FLAG-Q181G mutant. G)

Anchorage independent growth is due to NF-κB activation. HeLa cells were transfected with FLAG-PSMD9 or FLAG-PSMD9 and IκBα SR (super repressor) after which they were grown on soft agar plates in triplicate. Data represent number of colonies ± SD. One way ANOVA indicated a p value of 0.0006 ($p<0.05$) showing that results are significant. Western blot (below) shows overexpression of FLAG-PSMD9.

It is well known that NF-κB regulates such properties that are crucial in cancer (Dhruv et al., 2013; Singel et al., 2014). Gankyrin or PSMD10, a non-ATPase of the 19S regulatory particle acts as an oncogene and is overexpressed in a variety of cancers like hepatocellular carcinoma (Fu et al., 2002; Li et al., 2011). In such cancers, PSMD10 is shown to inhibit NF-κB by interacting with it and recruiting it to the cytoplasm (Higashitsuji et al., 2007). Therefore, in these cell types, we find that suppression of NF-κB, still leads to tumorigenesis. NF-κB is well known to promote apoptosis in some cells (Khandelwal et al., 2011). Therefore, one may speculate that overexpression of PSMD9 may induce apoptosis in such cells. Since NF-κB is a well-known player in tumorigenesis, it is reported as a drug target (Zingarelli et al., 2003). We know that the residue of the PDZ of PSMD9 are important for NF-κB activation and we believe that it may be possible to develop small molecule inhibitors to shut down the activity of NF-κB by blocking IKba degradation.

To understand the role of PSMD9 in regulation of NF-κB signaling, understanding PSMD9-hnRNPA1 interaction is very important. Our screening technique therefore has the potential to identify functions regulated by PSMD9 in the cell. We must remember that GRRF peptide has very low affinity to PSMD9. Such weak interacting motifs also play a key role in regulating functions in the cell. Here, we have demonstrated the role of hnRNPA1, one of the new interacting partners of PSMD9 which we have discovered. As discussed in the previous

chapter, it is possible that PSMD9 may also regulate other functions in mammalian cells by interacting with proteins like GH, S14 ribosomal protein and IL6 receptor isoform 2.

CHAPTER 9

CRYSTALLIZATION

OF

PSMD9

Introduction

The crystal structure of human PSMD9 is not known. Though our computational modeling, docking and molecular dynamic simulation studies provide a relatively clear picture about the probable structure of the PDZ domain of PSMD9 and the important residues involved in the interaction with C-terminal motifs, solving the crystal structure of the protein would definitely help in greater understanding on the structural basis of the domain-motif interaction. In this chapter, we describe our attempts to crystallize full length recombinant human PSMD9.

One of the basic requirements for crystallization of the proteins, is it stability which can be measured by heating the protein and simultaneously monitoring its structural integrity to thermal denaturation (Kopec and Schneider, 2011). Proteins tend to unfold in a cooperative manner in a short range of temperature on exposure to increasing temperatures. The midpoint of this thermal transition is called melting temperature (Tm). Different methods are currently available to obtain the Tm of a protein like circular dichroism, fluorescence spectroscopy and differential scanning calorimetry (Brandts and Lin, 1990; Eftink, 1994; Pantoliano et al., 2001). Differential scanning fluorimetry (DSF) also known as thermofluor or thermal stability assay, is used to screen a number of parallel reaction conditions, and it requires only microgram quantities of protein. A common fluoroprobe is used for all proteins. The thermofluor method can be performed on nearly all qPCR machines and can be used to validate the quality of protein preparations, screen for ligands or cofactors, and discover buffers and additives which maximize protein stability. Thermofluor determines the protein melting temperature (T_m) which is based on the interaction between the dye and the hydrophobic regions of the protein that are exposed during thermal denaturation. The dye (e.g., SYPRO Orange) should have low fluorescence quantum yield in aqueous environment, but must be highly fluorescent in non-

polar environments (Thermofluor-based high-throughput stability optimization of proteins for structural studies, Thermodynamic stability of carbonic anhydrase: measurements of binding affinity and stoichiometry using thermofluor, Methods for protein characterization by mass spectrometry, thermal shift (thermofluor) assay, and multiangle or static light scattering). As the temperature increases, the protein unfolds and exposes its hydrophobic regions which cause increase in the fluorescence signal due to the strong interaction of the dye with those regions. Here we use this assay to screen for conditions that give maximum stability to PSMD9, which may assist in crystallization of the protein. This work was done in collaboration with Dr. Lawrence J. Stern, Department of Pathology, University of Massachusetts Medical School (UMass Medical School), Worcester, MA, USA.

Results and Discussion

Recombinant His-tagged PSMD9 using metal affinity chromatography. After cleavage of the his tag using thrombin, the protein was further purified by anion exchange chromatography and size exclusion chromatography (Figure 9.1). Since there is no report yet on biophysical or crystallization studies about PSMD9, we wanted to find out conditions that could keep the protein thermally stable, which is one of the major criteria for crystallization. Thermofluor assay was used for this purpose as we can screen multiple conditions for the stability of PSMD9, in a short time with a small amount of protein. We used SYPRO orange as the fluorescence probe. We started with the pH screen (pH 2-11), to check the pH at which PSMD9 is most stable. We found that PSMD9 is stable in a range of pH 6.2 to 8.6 (Figure 9.2). There are many salts that are added into buffers that stabilize the proteins. Solvents and other additives are also incorporated to increase the thermal stability of the protein, thereby increasing the chances of crystallization. We added salts at different concentrations (0-100mM at 5mM intervals) to

buffers of pH 6.2 to 8.6 and other solvent additives before checking the Tm of PSMD9 (Table 9.1). The conditions which show a higher Tm for PSMD9 are shown in the Figure 9.3. Apart from salts, we also included a number of solvents, which could increase the Tm of PSMD9 further (Table 9.1 and Figure 9.3).

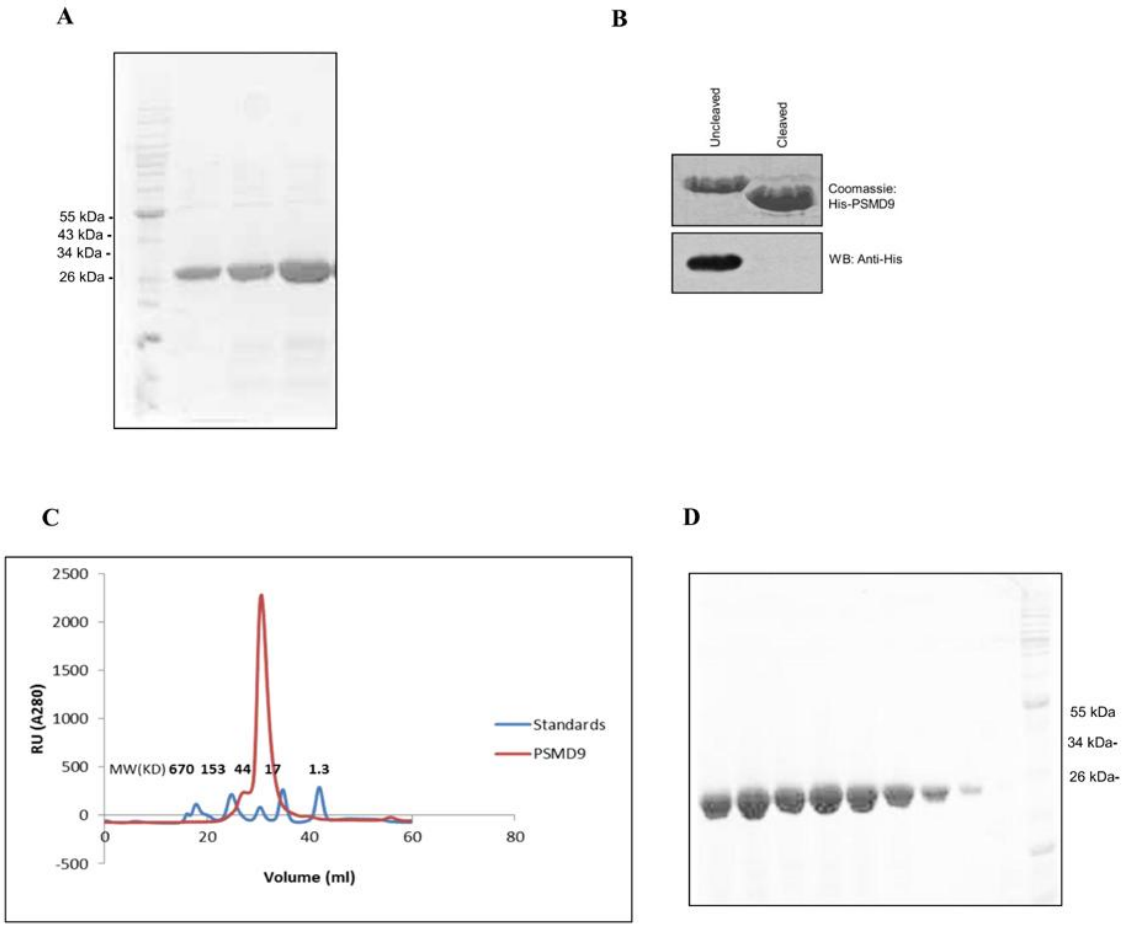

Figure 9.1 Purification of PSMD9 for crystallization. A) Recombinant his PSMD9 purified by Ni-NTA chromatography. B) Cleavage of his tag of PSMD9. Recombinant his PSMD9 was incubated with thrombin (1U for 1mg protein) for 2 hours at room temperature. Western blot with anti-his antibody confirms the absence of his tag. C) Size exclusion chromatography to

purify recombinant PSMD9 using Superdex 75 column. Molecular weight marker mix (GE Amersham) was loaded prior to loading of recombinant PSMD9. D) Pure fractions of recombinant PSMD9 after size exclusion chromatography.

Table 9.1 List of additives used to increase the thermal stability of PSMD9

Additive	**Concentration (with an interval of 5mM for salts and 1% for solvents)**
CaCl2	20mM to 100Mm
CdCl2	20mM to 100mM
ZnSO4	20mM to 100mM
CuSO4	20mM to 100mM
MgCl2	20mM to 100mM
NaCl	20mM to 100mM
KCl	20mM to 100mM
LiCl2	20mM to 100mM
CsCl2	20mM to 100mM
Glycine	20mM to 100mM
LiSO4	20mM to 100mM
CaSO4	20mM to 100mM
Sarcosine	20mM to 100mM
CoCl2	20mM to 100mM

Taurine	20mM to 100mM
FeCl3	20mM to 100mM
Urea	10mM
DMSO	5-10%
Isopropanol	5-10%
1,6- hexanediol	5-10%
Methanol	5-10%
Acetone	5-10%
PEG 400	5-10%
Ethylene glycol	5-10%
Jeffamine	2-5%

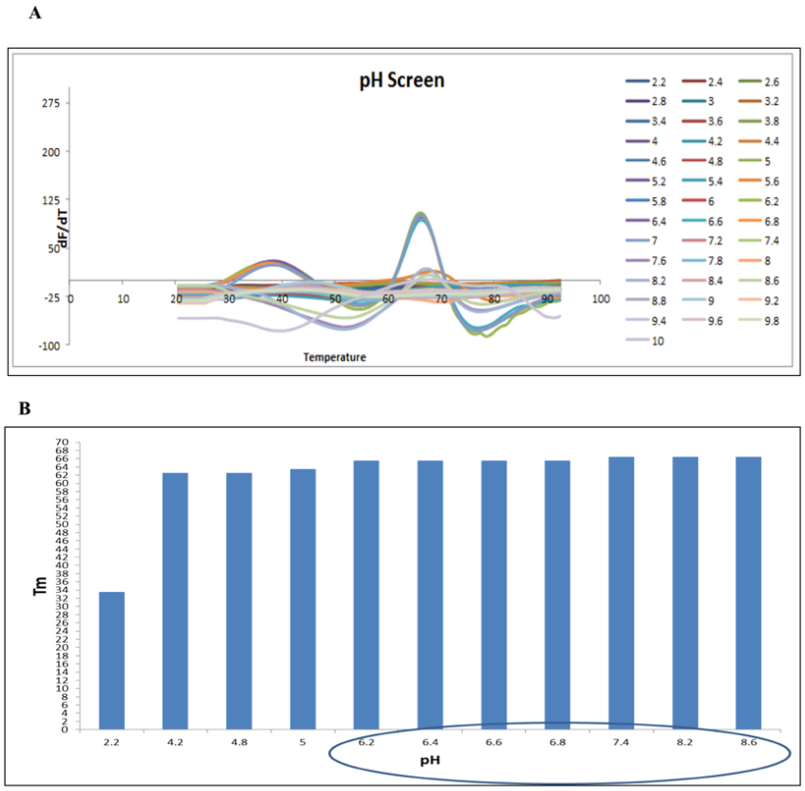

Figure 9.2 Thermal stability of PSMD9 under different pH conditions. A) Thermal stability of PSMD9 under different pH conditions using thermofluor assay. Graph represents the first derivative of fluorescence of PSMD9 incubated at different temperatures (20^0 to 95^0C). B) Plot showing the Tm values of PSMD9 at different pH conditions.

A

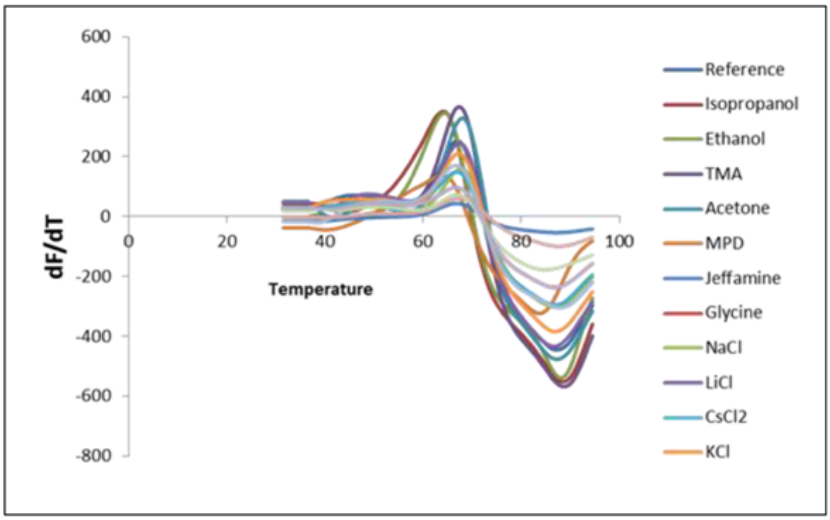

B

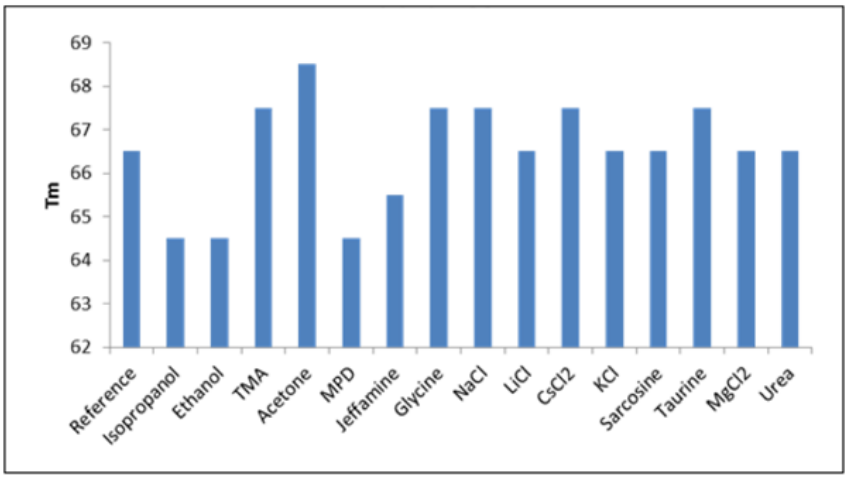

Figure 9.3Thermal stability of PSMD9 with different additives at pH 7.4. A) Representative figure of the thermofluor assay of PSMD9 at pH 7.4 with different additives (100mM for salts and 10% for solvents except Jeffamine which was used at 5%). B) Graph representing the Tm of PSMD9 at pH 7.4 with or without (reference) additives.

We found that 10% acetone, 0.1M TMA, 0.1M NaCl and 0.1M Glycine increased the thermal stability of PSMD9. We could not find any crystals under this range of pH with all the additives mentioned above. We also used the Morpheous crystal screen, which has 96 different conditions for crystallization. We performed a thermofluor assay of PSMD9 with all these conditions. We found a few conditions under which there was considerable increase in the Tm of PSMD9 (Table 9.2 and Figure 9.4).

A

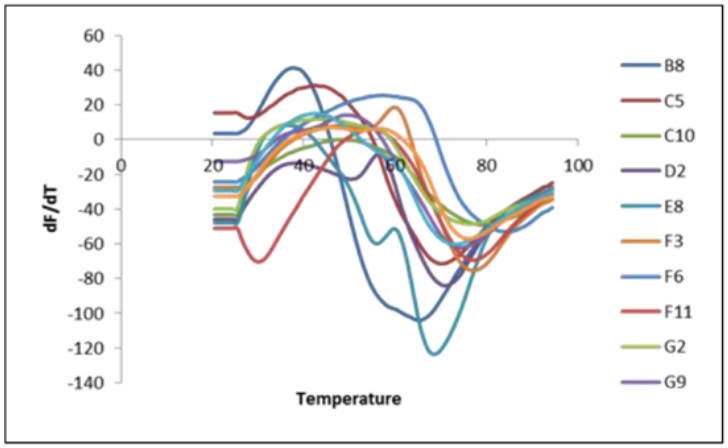

B

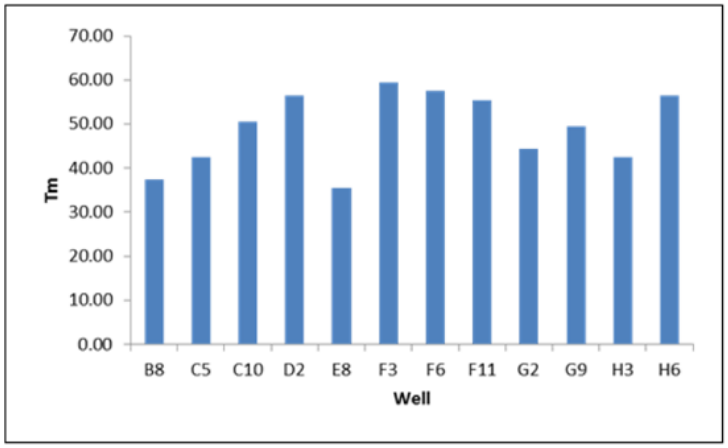

Figure 9.4 Thermal stability of PSMD9 with different conditions of Morpheus screen. A) Representative figure of the thermofluor assay of PSMD9 with different conditions of Morpheus screen (represented by their respective well number). B) Tm values of PSMD9 in few conditions of Morpheus screen.

Table 9.2 Conditions of Morpheus screen which gave a proper thermal transition curve in the thermofluor assay

Well	**Composition**
B8	0.2M ammonium sulfate, 0.1M sodium acetate pH 4.6, 25% PEG
C5	0.1M HEPES, pH7.5, 0.8M NaK Tartarate
C10	0.1M sodium acetate pH 4.6, 2M sodium formate
D2	0.1M HEPES, pH7.5, 1.4M tri sodium citrate
E8	1.5M NaCl, 10% ethanol
F3	0.1M tri sodium citrate pH 5.6, 0.5M ammonium sulfate, 1M LiSO4
F6	0.1M tri sodium citrate , 10mM FeCl3, 10% Jeffamine
F11	0.1M MES pH6.5, 1.6M ammonium sulfate, 10% dioxane
G2	0.1M MES pH6.5, 0.2M ammonium sulfate, 30% PEG MME 5000
G9	0.1M HEPES, pH7.5, 0.1M NaCl, 1.6M ammonium

	sulphate
H3	0.1M Tris pH 8.5, 0.2M MgCl2, 3.4M hexane diol
H6	0.1M Tris pH 8.5, 1.5M ammonium sulfate, 12% glycerol

When we set up crystal trials with 8 mg/ml PSMD9 under these conditions, we found tiny crystals when PSMD9 was seeded in 0.1M Tris pH 8.5, 1.5M ammonium sulfate, 12% glycerol (Table 9.3).

Table 9.3 Conditions from the Morpheus screen used for the crystallization trials shortlisted from the thermofluor assay.

Well	**Composition**	**Observation of drops**
C10	0.1M sodium acetate pH 4.6, 2M sodium formate	Clear
D2	0.1M HEPES, pH7.5, 1.4M tri sodium citrate	Clear
F3	0.1M tri sodium citrate pH 5.6, 0.5M ammonium sulfate, 1M LiSO4	Clear
F6	0.1M tri sodium citrate , 10mM FeCl3, 10% Jeffamine	Clear
F11	0.1M MES pH6.5, 1.6M ammonium sulfate, 10% dioxane	Clear
G9	0.1M HEPES, pH7.5, 0.1M NaCl, 1.6M ammonium sulphate	Clear

H6	0.1M Tris pH 8.5, 1.5M ammonium sulfate, 12% glycerol	Tiny crystal observed (6 in number)

We screened further by using different ranges of concentrations of ammonium sulfate and glycerol. The size of the crystals did not increase, whereas the number of small crystals increased. These crystals failed to diffract. Further optimization of conditions is still required for obtaining crystals of good quality. With MD simulation results, we find that the PDZ domain of PSMD9 is highly flexible and is stabilized with the C-terminal peptide GRRF. Therefore, chances of crystallization of PSMD9 may increase if we incorporate the C-terminal ligands. Also, crystallization of N-terminal region and C-terminal PDZ domains separately may increase the chances of forming crystals of great quality.

CHAPTER 10

CONCLUSION

AND

SIGNIFICANCE OF THE STUDY

Conclusion

Protein degradation plays a pivotal role in maintaining cellular homeostasis. The 26S proteasome regulates the degradation of most of the intracellular proteins in an ATP dependent process. Though a lot of information is available regarding the enzymatic machinery, we have very little understanding of the molecular basis of substrate recognition by the 26S proteasome. The substrate recognition and unfolding is performed by the 19S regulatory particle. Therefore, few, if not all, subunits of the 19S regulatory complex may be involved in protein-protein interaction which may aid in substrate recognition, or in regulating other physiological processes within the cell. Our interest in PSMD9 arose due to its PDZ-like domain, which might be involved in substrate recognition, by interacting with C-termini of various substrates in the cell. This may explain the degenerate specificity of the proteasome. We were also open to investigate the role of PSMD9 in regulating other functions in the cell, since it is a well-known transcription factor for insulin gene transcription. We chanced upon the observation of Chung et. al, where many proteins may have identical C-termini, which may serve as signatures for common biochemical functions in the cell. Keeping this in mind, we screened 12 tetra peptides which are representative C-termini of proteins in the human proteome. We found that peptides- AGHM, GRRF and SCGF which are the C-termini of E12, hnRNPA1 and growth hormone (GH) interacted with PSMD9 in ELISA. We further prove that C-terminal residues of the above mentioned proteins interact with PSMD9. With the help of modelling and docking studies, we have characterized the important residues in the PDZ domain of PSMD9 that are important for the interaction. In quest for more interacting partners, we screened the variants of GRRF and SCGF for binding to PSMD9. We report that PDZ domain of PSMD9 interacts with C-terminal residues S14 ribosomal protein and IL6 receptor. Though this low throughput approach gave us

clues about the interacting partners of PSMD9, it had a few drawbacks. Chung et al., had classified proteome from drosophila/yeast/human by recognizing conserved C-terminal residues in some of these proteins and listed out 30 tetra-peptide sequences which have more than 10 members in their group (Chung et al., 2003). When we further investigated, we found that most of the members of the group were isoforms of the same proteins or some were predicted or hypothetical proteins. Independent analysis of these 30 tetra-peptide sequences and their constituent members and further curation using Uniprot database (ftp://ftp.uniprot.org/pub/databases/uniprot/current_release/knowledgebase/) also revealed that most of the members were isoforms and rarely more than 2 unique protein members. Nevertheless, our lab was successful in elucidating the role of PSMD9-hnRNPA1 interaction in IκB α degradation and NF-κB activation. PSMD9 similarly may play other roles in regulating functions of S14, GH and IL6 receptor in mammalian cells which may be dependent or independent of proteasomal degradation. We can thus conclude that this cost effective method indeed helped us in further understanding the role of PSMD9 in regulating functions in mammalian cells.

We also tried to solve the structure of human PSMD9. With the aid of thermofluor assay, we found the conditions that could give maximum thermal stability to PSMD9, which may further increase the chances of crystallization. However, further optimization is required for obtaining crystals of good quality which will diffract.

Significance of the study

We exploited a low throughput, cost effective technique of peptide screening to identify the interacting partners of an uncharacterized protein like PSMD9. For the first time, we are providing a glimpse of the structure of PDZ domain of PSMD9 using computational modeling and docking studies. One must note that peptides like GRRF and GRRL interacted with a very low affinity with PSMD9. Such ligands are generally neglected in phage display and other high throughput approaches. Moreover, some protein-protein interactions within the cell are transient to bring about relevant functions like signaling. We successfully demonstrate that such weak interacting ligands can be physiologically relevant. The interaction of the PDZ of PSMD9 with the GRRF motif of hnRNPA1 is crucial in regulating NF-κB signaling. It is well known that NF-κB signaling regulates many processes like cell survival, tumorigenesis and inflammation. We showed that PSMD9 increases anchorage independent growth in HeLa cells. Our work has successfully elucidated the important residues that are involved in this process which has laid a platform for generation pharmacological drugs and peptide mimetics which may alter NF-κB signaling in many diseases and disorders. Apart from this, our study has revealed the potential role that PSMD9 can possibly play in regulating the functions of S14 ribosomal protein, GH and IL6 receptor. Screening of more peptides will give a bigger picture about the functions that PSMD9 may regulate in the cell. The model given below (Figure 10.1) summarizes how a prudent and simple assay led to the discovery of new function and other possible functions of PSMD9.

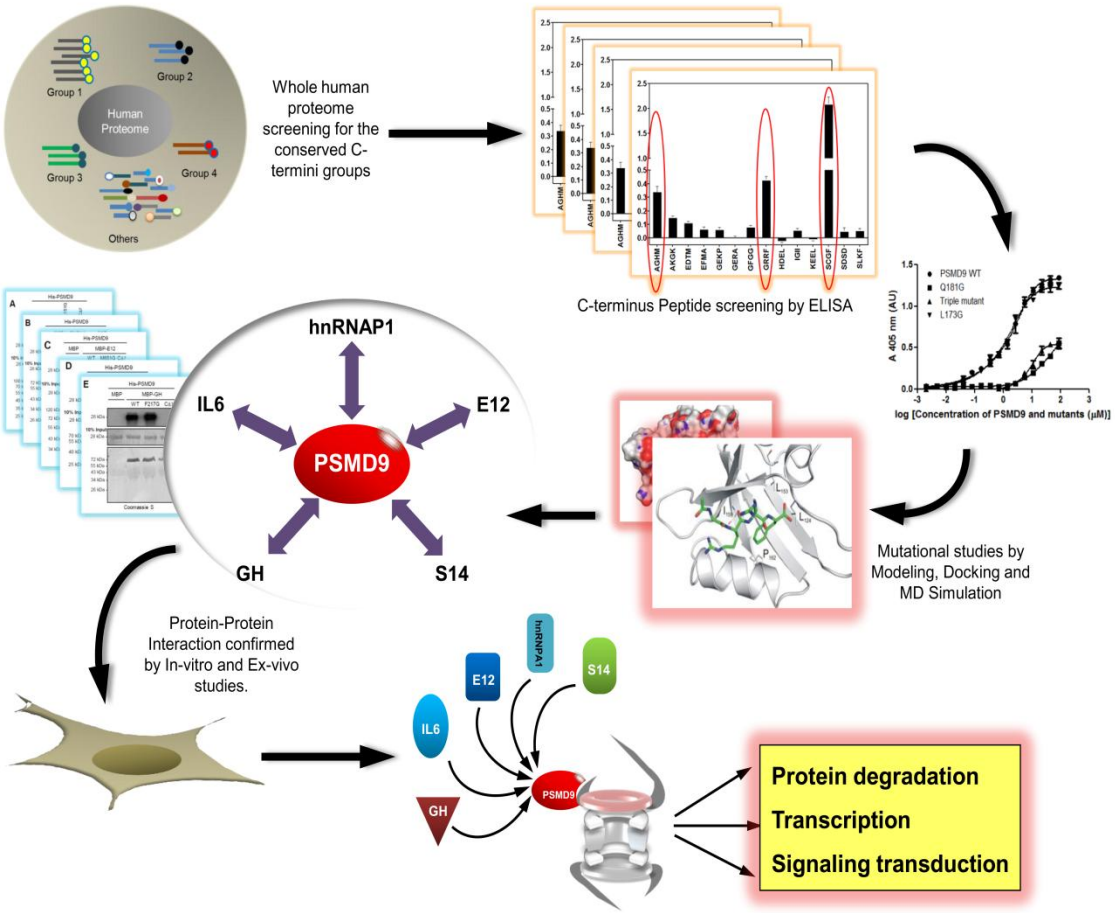

Figure 10 Model representing the approach used in our study. Approach used in our study- Grouping of proteins based on conserved C-termini, C-terminal peptide screening, validation of interacting partners of PSMD9, identification of residues involved in interaction by computational methods and validating them *in vitro* and *ex vivo* and exploring possible functions regulated by PSMD9 in mammalian cells.

References

Aberle, H., Bauer, A., Stappert, J., Kispert, A., and Kemler, R. (1997). beta-catenin is a target for the ubiquitin-proteasome pathway. EMBO J *16*, 3797-3804.

Ashford, T.P., and Porter, K.R. (1962). Cytoplasmic components in hepatic cell lysosomes. J Cell Biol *12*, 198-202.

Banz, C., Munchow, B., and Diedrich, K. (2010). Bridge-1 is expressed in human granulosa cells and is involved in the activin A signaling cascade. Fertil Steril *93*, 1349-1352.

Basdevant, N., Weinstein, H., and Ceruso, M. (2006). Thermodynamic basis for promiscuity and selectivity in protein-protein interactions: PDZ domains, a case study. J Am Chem Soc *128*, 12766-12777.

Baumeister, W., Dahlmann, B., Hegerl, R., Kopp, F., Kuehn, L., and Pfeifer, G. (1988). Electron microscopy and image analysis of the multicatalytic proteinase. FEBS Lett *241*, 239-245.

Baumeister, W., Walz, J., Zuhl, F., and Seemuller, E. (1998). The proteasome: paradigm of a self-compartmentalizing protease. Cell *92*, 367-380.

Brandts, J.F., and Lin, L.N. (1990). Study of strong to ultratight protein interactions using differential scanning calorimetry. Biochemistry *29*, 6927-6940.

Case, D. (2010). Amber 9. University of California Sanfrancisco -, -.

Chattopadhyay, M.K., Murakami, Y., and Matsufuji, S. (2001). Antizyme regulates the degradation of ornithine decarboxylase in fission yeast Schizosaccharomyces pombe. Study in the spe2 knockout strains. J Biol Chem *276*, 21235-21241.

Chen, J., Pan, L., Wei, Z., Zhao, Y., and Zhang, M. (2008). Domain-swapped dimerization of ZO-1 PDZ2 generates specific and regulatory connexin43-binding sites. EMBO J *27*, 2113-2123.

Chen, J., Sawyer, N., and Regan, L. (2013). Protein-protein interactions: general trends in the relationship between binding affinity and interfacial buried surface area. Protein Sci *22*, 510-515.

Chen, Y., Sheng, R., Kallberg, M., Silkov, A., Tun, M.P., Bhardwaj, N., Kurilova, S., Hall, R.A., Honig, B., Lu, H., *et al.* (2012). Genome-wide functional annotation of dual-specificity protein- and lipid-binding modules that regulate protein interactions. Mol Cell *46*, 226-237.

Chi, C.N., Haq, S.R., Rinaldo, S., Dogan, J., Cutruzzola, F., Engstrom, A., Gianni, S., Lundstrom, P., and Jemth, P. (2012). Interactions outside the boundaries of the canonical binding groove of a PDZ domain influence ligand binding. Biochemistry *51*, 8971-8979.

Cho, K.O., Hunt, C.A., and Kennedy, M.B. (1992). The rat brain postsynaptic density fraction contains a homolog of the Drosophila discs-large tumor suppressor protein. Neuron *9*, 929-942.

Chung, J.J., Yang, H., and Li, M. (2003). Genome-wide analyses of carboxyl-terminal sequences. Mol Cell Proteomics *2*, 173-181.

Ciechanover, A., Heller, H., Elias, S., Haas, A.L., and Hershko, A. (1980). ATP-dependent conjugation of reticulocyte proteins with the polypeptide required for protein degradation. Proc Natl Acad Sci U S A *77*, 1365-1368.

Ciehanover, A., Hod, Y., and Hershko, A. (1978). A heat-stable polypeptide component of an ATP-dependent proteolytic system from reticulocytes. Biochem Biophys Res Commun *81*, 1100-1105.

Coux, O., Nothwang, H.G., Silva Pereira, I., Recillas Targa, F., Bey, F., and Scherrer, K. (1994). Phylogenic relationships of the amino acid sequences of prosome (proteasome, MCP) subunits. Molecular & general genetics : MGG *245*, 769-780.

Coux, O., Tanaka, K., and Goldberg, A.L. (1996). Structure and functions of the 20S and 26S proteasomes. Annual review of biochemistry *65*, 801-847.

Darden, T. (1993). Particle mesh Ewald: an N•log(N) method for Ewald sums in large systems. J Chem Phys *98*, 10089-10092.

DeMartino, G.N., Proske, R.J., Moomaw, C.R., Strong, A.A., Song, X., Hisamatsu, H., Tanaka, K., and Slaughter, C.A. (1996). Identification, purification, and characterization of a PA700-dependent activator of the proteasome. The Journal of biological chemistry *271*, 3112-3118.

Dhruv, H.D., McDonough Winslow, W.S., Armstrong, B., Tuncali, S., Eschbacher, J., Kislin, K., Loftus, J.C., Tran, N.L., and Berens, M.E. (2013). Reciprocal activation of transcription factors underlies the dichotomy between proliferation and invasion of glioma cells. PLoS One *8*, e72134.

Dhulesia, A., Gsponer, J., and Vendruscolo, M. (2008). Mapping of two networks of residues that exhibit structural and dynamical changes upon binding in a PDZ domain protein. J Am Chem Soc *130*, 8931-8939.

Diehl, C., Engstrom, O., Delaine, T., Hakansson, M., Genheden, S., Modig, K., Leffler, H., Ryde, U., Nilsson, U.J., and Akke, M. (2010). Protein flexibility and conformational entropy in ligand design targeting the carbohydrate recognition domain of galectin-3. J Am Chem Soc *132*, 14577-14589.

Dominguez, C., Boelens, R., and Bonvin, A.M. (2003). HADDOCK: a protein-protein docking approach based on biochemical or biophysical information. J Am Chem Soc *125*, 1731-1737.

Doyle, D.A., Lee, A., Lewis, J., Kim, E., Sheng, M., and MacKinnon, R. (1996). Crystal structures of a complexed and peptide-free membrane protein-binding domain: molecular basis of peptide recognition by PDZ. Cell *85*, 1067-1076.

Duan, Y., Wu, C., Chowdhury, S., Lee, M.C., Xiong, G., Zhang, W., Yang, R., Cieplak, P., Luo, R., Lee, T., *et al.* (2003). A point-charge force field for molecular mechanics simulations of

proteins based on condensed-phase quantum mechanical calculations. J Comput Chem *24*, 1999-2012.

Dubiel, W., Ferrell, K., Pratt, G., and Rechsteiner, M. (1992a). Subunit 4 of the 26 S protease is a member of a novel eukaryotic ATPase family. The Journal of biological chemistry *267*, 22699-22702.

Dubiel, W., Ferrell, K., and Rechsteiner, M. (1995). Subunits of the regulatory complex of the 26S protease. Mol Biol Rep *21*, 27-34.

Dubiel, W., Pratt, G., Ferrell, K., and Rechsteiner, M. (1992b). Purification of an 11 S regulator of the multicatalytic protease. J Biol Chem *267*, 22369-22377.

Eftink, M.R. (1994). The use of fluorescence methods to monitor unfolding transitions in proteins. Biophys J *66*, 482-501.

Eldstrom, J., Doerksen, K.W., Steele, D.F., and Fedida, D. (2002). N-terminal PDZ-binding domain in Kv1 potassium channels. FEBS Lett *531*, 529-537.

Elenbaas, B., Dobbelstein, M., Roth, J., Shenk, T., and Levine, A.J. (1996). The MDM2 oncoprotein binds specifically to RNA through its RING finger domain. Mol Med *2*, 439-451.

Ellencrona, K., Syed, A., and Johansson, M. (2009). Flavivirus NS5 associates with host-cell proteins zonula occludens-1 (ZO-1) and regulating synaptic membrane exocytosis-2 (RIMS2) via an internal PDZ binding mechanism. Biol Chem *390*, 319-323.

Etlinger, J.D., and Goldberg, A.L. (1977). A soluble ATP-dependent proteolytic system responsible for the degradation of abnormal proteins in reticulocytes. Proc Natl Acad Sci U S A *74*, 54-58.

Fanning, A.S., Lye, M.F., Anderson, J.M., and Lavie, A. (2007). Domain swapping within PDZ2 is responsible for dimerization of ZO proteins. J Biol Chem *282*, 37710-37716.

Feng, W., Wu, H., Chan, L.N., and Zhang, M. (2008). Par-3-mediated junctional localization of the lipid phosphatase PTEN is required for cell polarity establishment. J Biol Chem *283*, 23440-23449.

Finley, D., Tanaka, K., Mann, C., Feldmann, H., Hochstrasser, M., Vierstra, R., Johnston, S., Hampton, R., Haber, J., McCusker, J., *et al.* (1998). Unified nomenclature for subunits of the Saccharomyces cerevisiae proteasome regulatory particle. Trends Biochem Sci *23*, 244-245.

Forsthoefel, A.M., Pena, M.M., Xing, Y.Y., Rafique, Z., and Berger, F.G. (2004). Structural determinants for the intracellular degradation of human thymidylate synthase. Biochemistry *43*, 1972-1979.

Fra, A., and Sitia, R. (1993). The endoplasmic reticulum as a site of protein degradation. Subcell Biochem *21*, 143-168.

Fraser, R.A., Rossignol, M., Heard, D.J., Egly, J.M., and Chambon, P. (1997). SUG1, a putative transcriptional mediator and subunit of the PA700 proteasome regulatory complex, is a DNA helicase. J Biol Chem *272*, 7122-7126.

Fu, X.Y., Wang, H.Y., Tan, L., Liu, S.Q., Cao, H.F., and Wu, M.C. (2002). Overexpression of p28/gankyrin in human hepatocellular carcinoma and its clinical significance. World J Gastroenterol *8*, 638-643.

Fuentes, E.J., Der, C.J., and Lee, A.L. (2004). Ligand-dependent dynamics and intramolecular signaling in a PDZ domain. J Mol Biol *335*, 1105-1115.

Fuh, G., Pisabarro, M.T., Li, Y., Quan, C., Lasky, L.A., and Sidhu, S.S. (2000). Analysis of PDZ domain-ligand interactions using carboxyl-terminal phage display. J Biol Chem *275*, 21486-21491.

Gerek, Z.N., and Ozkan, S.B. (2011). Change in allosteric network affects binding affinities of PDZ domains: analysis through perturbation response scanning. PLoS Comput Biol *7*, e1002154.

Ghislain, M., Udvardy, A., and Mann, C. (1993). S. cerevisiae 26S protease mutants arrest cell division in G2/metaphase. Nature *366*, 358-362.

Gianni, S., Haq, S.R., Montemiglio, L.C., Jurgens, M.C., Engstrom, A., Chi, C.N., Brunori, M., and Jemth, P. (2011). Sequence-specific long range networks in PSD-95/discs large/ZO-1 (PDZ) domains tune their binding selectivity. J Biol Chem *286*, 27167-27175.

Glickman, M.H., and Ciechanover, A. (2002). The ubiquitin-proteasome proteolytic pathway: destruction for the sake of construction. Physiological reviews *82*, 373-428.

Glickman, M.H., Rubin, D.M., Fried, V.A., and Finley, D. (1998). The regulatory particle of the Saccharomyces cerevisiae proteasome. Molecular and cellular biology *18*, 3149-3162.

Godbole, D., Mojamdar, M., and Pal, J.K. (2006). Increased level of p27 subunit of proteasomes and its co-localization with tyrosinase in amelanotic melanoma cells indicate its direct role in the regulation of melanin biosynthesis. Cell biology international *30*, 895-902.

Goldberg, A.L. (2003). Protein degradation and protection against misfolded or damaged proteins. Nature *426*, 895-899.

Gridley, T., Gray, D.A., Orr-Weaver, T., Soriano, P., Barton, D.E., Francke, U., and Jaenisch, R. (1990). Molecular analysis of the Mov 34 mutation: transcript disrupted by proviral integration in mice is conserved in Drosophila. Development *109*, 235-242.

Haas, A.L., Warms, J.V., Hershko, A., and Rose, I.A. (1982). Ubiquitin-activating enzyme. Mechanism and role in protein-ubiquitin conjugation. J Biol Chem *257*, 2543-2548.

Haq, S.R., Chi, C.N., Bach, A., Dogan, J., Engstrom, A., Hultqvist, G., Karlsson, O.A., Lundstrom, P., Montemiglio, L.C., Stromgaard, K., *et al.* (2012). Side-chain interactions form

late and cooperatively in the binding reaction between disordered peptides and PDZ domains. J Am Chem Soc *134*, 599-605.

Harris, B.Z., and Lim, W.A. (2001). Mechanism and role of PDZ domains in signaling complex assembly. J Cell Sci *114*, 3219-3231.

Hay, D.C., Kemp, G.D., Dargemont, C., and Hay, R.T. (2001). Interaction between hnRNPA1 and IkappaBalpha is required for maximal activation of NF-kappaB-dependent transcription. Mol Cell Biol *21*, 3482-3490.

Hayashi, M., Hiroi, Y., and Natori, Y. (1973). Effect of ATP on protein degradation in rat liver lysosomes. Nat New Biol *242*, 163-166.

Henderson, A., Erales, J., Hoyt, M.A., and Coffino, P. (2011). Dependence of proteasome processing rate on substrate unfolding. J Biol Chem *286*, 17495-17502.

Hershko, A., Ciechanover, A., Heller, H., Haas, A.L., and Rose, I.A. (1980). Proposed role of ATP in protein breakdown: conjugation of protein with multiple chains of the polypeptide of ATP-dependent proteolysis. Proc Natl Acad Sci U S A *77*, 1783-1786.

Hershko, A., Heller, H., Elias, S., and Ciechanover, A. (1983). Components of ubiquitin-protein ligase system. Resolution, affinity purification, and role in protein breakdown. J Biol Chem *258*, 8206-8214.

Higashitsuji, H., Liu, Y., Masuda, T., Fujita, T., Abdel-Aziz, H.I., Kongkham, S., Dawson, S., John Mayer, R., Itoh, Y., Sakurai, T., *et al.* (2007). The oncoprotein gankyrin interacts with RelA and suppresses NF-kappaB activity. Biochem Biophys Res Commun *363*, 879-884.

Hillier, B.J., Christopherson, K.S., Prehoda, K.E., Bredt, D.S., and Lim, W.A. (1999). Unexpected modes of PDZ domain scaffolding revealed by structure of nNOS-syntrophin complex. Science *284*, 812-815.

Hilpert, K., Winkler, D.F., and Hancock, R.E. (2007). Peptide arrays on cellulose support: SPOT synthesis, a time and cost efficient method for synthesis of large numbers of peptides in a parallel and addressable fashion. Nat Protoc *2*, 1333-1349.

Ho, B.K., and Agard, D.A. (2010). Conserved tertiary couplings stabilize elements in the PDZ fold, leading to characteristic patterns of domain conformational flexibility. Protein Sci *19*, 398-411.

Hochstrasser, M. (1996). Ubiquitin-dependent protein degradation. Annu Rev Genet *30*, 405-439.

Hough, R., Pratt, G., and Rechsteiner, M. (1987). Purification of two high molecular weight proteases from rabbit reticulocyte lysate. J Biol Chem *262*, 8303-8313.

Hoyt, M.A., Zhang, M., and Coffino, P. (2003). Ubiquitin-independent mechanisms of mouse ornithine decarboxylase degradation are conserved between mammalian and fungal cells. J Biol Chem *278*, 12135-12143.

Humphrey, W., Dalke, A., and Schulten, K. (1996). VMD: visual molecular dynamics. J Mol Graph *14*, 33-38, 27-38.

Hurd, T.W., Gao, L., Roh, M.H., Macara, I.G., and Margolis, B. (2003). Direct interaction of two polarity complexes implicated in epithelial tight junction assembly. Nat Cell Biol *5*, 137-142.

Janin, J. (1979). Surface and inside volumes in globular proteins. Nature *277*, 491-492.

Jelen, F., Oleksy, A., Smietana, K., and Otlewski, J. (2003). PDZ domains - common players in the cell signaling. Acta Biochim Pol *50*, 985-1017.

Jones, S., and Thornton, J.M. (1995). Protein-protein interactions: a review of protein dimer structures. Prog Biophys Mol Biol *63*, 31-65.

Jorgensen, W. (1983). Comparison of simple potential functions for simulating liquid water. . J Chem Phys *79*, 926-935.

Kachel, N., Erdmann, K.S., Kremer, W., Wolff, P., Gronwald, W., Heumann, R., and Kalbitzer, H.R. (2003). Structure determination and ligand interactions of the PDZ2b domain of PTP-Bas (hPTP1E): splicing-induced modulation of ligand specificity. J Mol Biol *334*, 143-155.

Kaneko, T., Hamazaki, J., Iemura, S., Sasaki, K., Furuyama, K., Natsume, T., Tanaka, K., and Murata, S. (2009). Assembly pathway of the Mammalian proteasome base subcomplex is mediated by multiple specific chaperones. Cell *137*, 914-925.

Kannenberg, K., Wittekindt, N.E., Tippmann, S., Wolburg, H., Ranke, M.B., and Binder, G. (2007). Mutant and misfolded human growth hormone is rapidly degraded through the proteasomal degradation pathway in a cellular model for isolated growth hormone deficiency type II. J Neuroendocrinol *19*, 882-890.

Kastritis, P.L., and Bonvin, A.M. (2013). Molecular origins of binding affinity: seeking the Archimedean point. Curr Opin Struct Biol *23*, 868-877.

Khandelwal, N., Simpson, J., Taylor, G., Rafique, S., Whitehouse, A., Hiscox, J., and Stark, L.A. (2011). Nucleolar NF-kappaB/RelA mediates apoptosis by causing cytoplasmic relocalization of nucleophosmin. Cell Death Differ *18*, 1889-1903.

Kim, E., Niethammer, M., Rothschild, A., Jan, Y.N., and Sheng, M. (1995). Clustering of Shaker-type K+ channels by interaction with a family of membrane-associated guanylate kinases. Nature *378*, 85-88.

Kopec, J., and Schneider, G. (2011). Comparison of fluorescence and light scattering based methods to assess formation and stability of protein-protein complexes. J Struct Biol *175*, 216-223.

Kopp, F., Kristensen, P., Hendil, K.B., Johnsen, A., Sobek, A., and Dahlmann, B. (1995). The human proteasome subunit HsN3 is located in the inner rings of the complex dimer. Journal of molecular biology *248*, 264-272.

Kopp, F., Steiner, R., Dahlmann, B., Kuehn, L., and Reinauer, H. (1986). Size and shape of the multicatalytic proteinase from rat skeletal muscle. Biochimica et biophysica acta *872*, 253-260.

Kyte, J., and Doolittle, R.F. (1982). A simple method for displaying the hydropathic character of a protein. J Mol Biol *157*, 105-132.

Lambaerts, K., Van Dyck, S., Mortier, E., Ivarsson, Y., Degeest, G., Luyten, A., Vermeiren, E., Peers, B., David, G., and Zimmermann, P. (2012). Syntenin, a syndecan adaptor and an Arf6 phosphatidylinositol 4,5-bisphosphate effector, is essential for epiboly and gastrulation cell movements in zebrafish. J Cell Sci *125*, 1129-1140.

Lander, G.C., Estrin, E., Matyskiela, M.E., Bashore, C., Nogales, E., and Martin, A. (2012). Complete subunit architecture of the proteasome regulatory particle. Nature *482*, 186-191.

Landgraf, C., Panni, S., Montecchi-Palazzi, L., Castagnoli, L., Schneider-Mergener, J., Volkmer-Engert, R., and Cesareni, G. (2004). Protein interaction networks by proteome peptide scanning. PLoS Biol *2*, E14.

Lau, A.G., and Hall, R.A. (2001). Oligomerization of NHERF-1 and NHERF-2 PDZ domains: differential regulation by association with receptor carboxyl-termini and by phosphorylation. Biochemistry *40*, 8572-8580.

Lecker, S.H., Goldberg, A.L., and Mitch, W.E. (2006). Protein degradation by the ubiquitin-proteasome pathway in normal and disease states. J Am Soc Nephrol *17*, 1807-1819.

Lee, H.J., and Zheng, J.J. (2010). PDZ domains and their binding partners: structure, specificity, and modification. Cell Commun Signal *8*, 8.

Lee, J.H., Volinic, J.L., Banz, C., Yao, K.M., and Thomas, M.K. (2005). Interactions with p300 enhance transcriptional activation by the PDZ-domain coactivator Bridge-1. J Endocrinol *187*, 283-292.

Lee, S.Y., De la Mota-Peynado, A., and Roelofs, J. (2011). Loss of Rpt5 protein interactions with the core particle and Nas2 protein causes the formation of faulty proteasomes that are inhibited by Ecm29 protein. J Biol Chem *286*, 36641-36651.

Li, J., Knobloch, T.J., Kresty, L.A., Zhang, Z., Lang, J.C., Schuller, D.E., and Weghorst, C.M. (2011). Gankyrin, a biomarker for epithelial carcinogenesis, is overexpressed in human oral cancer. Anticancer Res *31*, 2683-2692.

London, T.B., Lee, H.J., Shao, Y., and Zheng, J. (2004). Interaction between the internal motif KTXXXI of Idax and mDvl PDZ domain. Biochem Biophys Res Commun *322*, 326-332.

Lord, J.M. (1996). Go outside and see the proteasome. Protein degradation. Curr Biol *6*, 1067-1069.

Lowe, J., Stock, D., Jap, B., Zwickl, P., Baumeister, W., and Huber, R. (1995). Crystal structure of the 20S proteasome from the archaeon T. acidophilum at 3.4 A resolution. Science *268*, 533-539.

Lupas, A., Koster, A.J., and Baumeister, W. (1993). Structural features of 26S and 20S proteasomes. Enzyme & protein *47*, 252-273.

M.V., S. (1953). The release of labeled amino acids from proteins in liver slices. J Biol Chem *201*, 143-154.

Ma, C.P., Slaughter, C.A., and DeMartino, G.N. (1992). Identification, purification, and characterization of a protein activator (PA28) of the 20 S proteasome (macropain). J Biol Chem *267*, 10515-10523.

Maganti, N., Moody, T.D., Truax, A.D., Thakkar, M., Spring, A.M., Germann, M.W., and Greer, S.F. (2014). Nonproteolytic roles of 19S ATPases in transcription of CIITApIV genes. PLoS One *9*, e91200.

Matsumoto, Y., Yasuda, H., Marunouchi, T., and Yamada, M. (1983). Decrease in uH2A (protein A24) of a mouse temperature-sensitive mutant. FEBS Lett *151*, 139-142.

Mayer, T.U., Braun, T., and Jentsch, S. (1998). Role of the proteasome in membrane extraction of a short-lived ER-transmembrane protein. EMBO J *17*, 3251-3257.

Miyamoto, S. (1992). Settle: an analytical version of the SHAKE and RATTLE algorithm for rigid water models. . J Comput Chem *13*, 952-962.

Morrisett, J.D., David, J.S., Pownall, H.J., and Gotto, A.M., Jr. (1973). Interaction of an apolipoprotein (apoLP-alanine) with phosphatidylcholine. Biochemistry *12*, 1290-1299.

Mostarda, S., Gfeller, D., and Rao, F. (2012). Beyond the binding site: the role of the beta(2)-beta(3) loop and extra-domain structures in PDZ domains. PLoS Comput Biol *8*, e1002429.

Munz, M., Hein, J., and Biggin, P.C. (2012). The role of flexibility and conformational selection in the binding promiscuity of PDZ domains. PLoS Comput Biol *8*, e1002749.

Murata, S., Yashiroda, H., and Tanaka, K. (2009). Molecular mechanisms of proteasome assembly. Nat Rev Mol Cell Biol *10*, 104-115.

Nomme, J., Fanning, A.S., Caffrey, M., Lye, M.F., Anderson, J.M., and Lavie, A. (2011). The Src homology 3 domain is required for junctional adhesion molecule binding to the third PDZ domain of the scaffolding protein ZO-1. J Biol Chem *286*, 43352-43360.

Nooren, I.M., and Thornton, J.M. (2003). Diversity of protein-protein interactions. EMBO J *22*, 3486-3492.

Nourry, C., Grant, S.G., and Borg, J.P. (2003). PDZ domain proteins: plug and play! Sci STKE *2003*, RE7.

Pan, L., Chen, J., Yu, J., Yu, H., and Zhang, M. (2011). The structure of the PDZ3-SH3-GuK tandem of ZO-1 protein suggests a supramodular organization of the membrane-associated guanylate kinase (MAGUK) family scaffold protein core. J Biol Chem *286*, 40069-40074.

Pan, L., Yan, J., Wu, L., and Zhang, M. (2009). Assembling stable hair cell tip link complex via multidentate interactions between harmonin and cadherin 23. Proc Natl Acad Sci U S A *106*, 5575-5580.

Pantoliano, M.W., Petrella, E.C., Kwasnoski, J.D., Lobanov, V.S., Myslik, J., Graf, E., Carver, T., Asel, E., Springer, B.A., Lane, P., *et al.* (2001). High-density miniaturized thermal shift assays as a general strategy for drug discovery. J Biomol Screen *6*, 429-440.

Pawson, T., and Nash, P. (2003). Assembly of cell regulatory systems through protein interaction domains. Science *300*, 445-452.

Pawson, T., and Scott, J.D. (1997). Signaling through scaffold, anchoring, and adaptor proteins. Science *278*, 2075-2080.

Penkert, R.R., DiVittorio, H.M., and Prehoda, K.E. (2004). Internal recognition through PDZ domain plasticity in the Par-6-Pals1 complex. Nat Struct Mol Biol *11*, 1122-1127.

Pentz, E.S., Black, B.C., and Wright, T.R. (1986). A diphenol oxidase gene is part of a cluster of genes involved in catecholamine metabolism and sclerotization in drosophila. I. Identification of the biochemical defect in Dox-A2 [l(2)37Bf] mutants. Genetics *112*, 823-841.

Peterson, F.C., Penkert, R.R., Volkman, B.F., and Prehoda, K.E. (2004). Cdc42 regulates the Par-6 PDZ domain through an allosteric CRIB-PDZ transition. Mol Cell *13*, 665-676.

Petit, C.M., Zhang, J., Sapienza, P.J., Fuentes, E.J., and Lee, A.L. (2009). Hidden dynamic allostery in a PDZ domain. Proc Natl Acad Sci U S A *106*, 18249-18254.

Phizicky, E.M., and Fields, S. (1995). Protein-protein interactions: methods for detection and analysis. Microbiol Rev *59*, 94-123.

Pickart, C.M. (2001). Mechanisms underlying ubiquitination. Annu Rev Biochem *70*, 503-533.

Radz, G.M., and Nash, R.W. (1998). Full-arch rehabilitation utilizing pressed ceramic veneers and full-coverage crowns. Pract Periodontics Aesthet Dent *10*, 629-634; quiz 636.

Ratner S, R.D., Keston AS and Schoenheimer R. (1940). Studies in protein metabolism: XIV. The chemical interaction of dietary Glycine and body proteins in rats. . J Biol Chem *12*, 665-676.

Rodi, D.J., Makowski, L., and Kay, B.K. (2002). One from column A and two from column B: the benefits of phage display in molecular-recognition studies. Curr Opin Chem Biol *6*, 92-96.

Sali, A., and Blundell, T.L. (1993). Comparative protein modelling by satisfaction of spatial restraints. J Mol Biol *234*, 779-815.

Saro, D., Li, T., Rupasinghe, C., Paredes, A., Caspers, N., and Spaller, M.R. (2007). A thermodynamic ligand binding study of the third PDZ domain (PDZ3) from the mammalian neuronal protein PSD-95. Biochemistry *46*, 6340-6352.

Schild, L., Lu, Y., Gautschi, I., Schneeberger, E., Lifton, R.P., and Rossier, B.C. (1996). Identification of a PY motif in the epithelial Na channel subunits as a target sequence for mutations causing channel activation found in Liddle syndrome. EMBO J *15*, 2381-2387.

Schwob, E., Bohm, T., Mendenhall, M.D., and Nasmyth, K. (1994). The B-type cyclin kinase inhibitor p40SIC1 controls the G1 to S transition in S. cerevisiae. Cell *79*, 233-244.

Sengupta, D., and Linstedt, A.D. (2010). Mitotic inhibition of GRASP65 organelle tethering involves Polo-like kinase 1 (PLK1) phosphorylation proximate to an internal PDZ ligand. J Biol Chem *285*, 39994-40003.

Seufert, W., and Jentsch, S. (1991). Yeast ubiquitin-conjugating enzymes involved in selective protein degradation are essential for cell viability. Acta Biol Hung *42*, 27-37.

Sharma, S.C., Memic, A., Rupasinghe, C.N., Duc, A.C., and Spaller, M.R. (2009). T7 phage display as a method of peptide ligand discovery for PDZ domain proteins. Biopolymers *92*, 183-193.

Shimkets, R.A., Lifton, R.P., and Canessa, C.M. (1997). The activity of the epithelial sodium channel is regulated by clathrin-mediated endocytosis. J Biol Chem *272*, 25537-25541.

Sidhu, S.S., Lowman, H.B., Cunningham, B.C., and Wells, J.A. (2000). Phage display for selection of novel binding peptides. Methods Enzymol *328*, 333-363.

Singel, S.M., Batten, K., Cornelius, C., Jia, G., Fasciani, G., Barron, S.L., Wright, W.E., and Shay, J.W. (2014). Receptor-interacting protein kinase 2 promotes triple-negative breast cancer cell migration and invasion via activation of nuclear factor-kappaB and c-Jun N-terminal kinase pathways. Breast Cancer Res *16*, R28.

Singh Gautam, A.K., Balakrishnan, S., and Venkatraman, P. (2012). Direct ubiquitin independent recognition and degradation of a folded protein by the eukaryotic proteasomes-origin of intrinsic degradation signals. PLoS One *7*, e34864.

Songyang, Z., Fanning, A.S., Fu, C., Xu, J., Marfatia, S.M., Chishti, A.H., Crompton, A., Chan, A.C., Anderson, J.M., and Cantley, L.C. (1997). Recognition of unique carboxyl-terminal motifs by distinct PDZ domains. Science *275*, 73-77.

Stites, W.E. (1997). Proteinminus signProtein Interactions: Interface Structure, Binding Thermodynamics, and Mutational Analysis. Chem Rev *97*, 1233-1250.

Stricker, N.L., Christopherson, K.S., Yi, B.A., Schatz, P.J., Raab, R.W., Dawes, G., Bassett, D.E., Jr., Bredt, D.S., and Li, M. (1997). PDZ domain of neuronal nitric oxide synthase recognizes novel C-terminal peptide sequences. Nat Biotechnol *15*, 336-342.

Strous, G.J., and Govers, R. (1999). The ubiquitin-proteasome system and endocytosis. J Cell Sci *112 (Pt 10)*, 1417-1423.

Thomas, M.K., Yao, K.M., Tenser, M.S., Wong, G.G., and Habener, J.F. (1999). Bridge-1, a novel PDZ-domain coactivator of E2A-mediated regulation of insulin gene transcription. Mol Cell Biol *19*, 8492-8504.

Tonikian, R., Zhang, Y., Sazinsky, S.L., Currell, B., Yeh, J.H., Reva, B., Held, H.A., Appleton, B.A., Evangelista, M., Wu, Y., *et al.* (2008). A specificity map for the PDZ domain family. PLoS Biol *6*, e239.

Truax, A.D., Koues, O.I., Mentel, M.K., and Greer, S.F. (2010). The 19S ATPase S6a (S6'/TBP1) regulates the transcription initiation of class II transactivator. J Mol Biol *395*, 254-269.

Uemura, T., Mori, H., and Mishina, M. (2004). Direct interaction of GluRdelta2 with Shank scaffold proteins in cerebellar Purkinje cells. Mol Cell Neurosci *26*, 330-341.

Van Kaer, L., Ashton-Rickardt, P.G., Eichelberger, M., Gaczynska, M., Nagashima, K., Rock, K.L., Goldberg, A.L., Doherty, P.C., and Tonegawa, S. (1994). Altered peptidase and viral-specific T cell response in LMP2 mutant mice. Immunity *1*, 533-541.

Varshavsky, A. (1995). The N-end rule. Cold Spring Harb Symp Quant Biol *60*, 461-478.

Voges, D., Zwickl, P., and Baumeister, W. (1999). The 26S proteasome: a molecular machine designed for controlled proteolysis. Annual review of biochemistry *68*, 1015-1068.

Volinic, J.L., Lee, J.H., Eto, K., Kaur, V., and Thomas, M.K. (2006). Overexpression of the coactivator bridge-1 results in insulin deficiency and diabetes. Mol Endocrinol *20*, 167-182.

Wang, C.K., Pan, L., Chen, J., and Zhang, M. (2010). Extensions of PDZ domains as important structural and functional elements. Protein Cell *1*, 737-751.

Watanabe, T.K., Saito, A., Suzuki, M., Fujiwara, T., Takahashi, E., Slaughter, C.A., DeMartino, G.N., Hendil, K.B., Chung, C.H., Tanahashi, N., *et al.* (1998). cDNA cloning and characterization of a human proteasomal modulator subunit, p27 (PSMD9). Genomics *50*, 241-250.

Waxman, L., Fagan, J.M., and Goldberg, A.L. (1987). Demonstration of two distinct high molecular weight proteases in rabbit reticulocytes, one of which degrades ubiquitin conjugates. J Biol Chem *262*, 2451-2457.

Wilk, S., and Orlowski, M. (1983). Inhibition of rabbit brain prolyl endopeptidase by n-benzyloxycarbonyl-prolyl-prolinal, a transition state aldehyde inhibitor. J Neurochem *41*, 69-75.

Willert, K., and Nusse, R. (1998). Beta-catenin: a key mediator of Wnt signaling. Curr Opin Genet Dev *8*, 95-102.

Wolfenden, R., Andersson, L., Cullis, P.M., and Southgate, C.C. (1981). Affinities of amino acid side chains for solvent water. Biochemistry *20*, 849-855.

Wong, H.C., Bourdelas, A., Krauss, A., Lee, H.J., Shao, Y., Wu, D., Mlodzik, M., Shi, D.L., and Zheng, J. (2003). Direct binding of the PDZ domain of Dishevelled to a conserved internal sequence in the C-terminal region of Frizzled. Mol Cell *12*, 1251-1260.

Woods, D.F., and Bryant, P.J. (1993). ZO-1, DlgA and PSD-95/SAP90: homologous proteins in tight, septate and synaptic cell junctions. Mech Dev *44*, 85-89.

Xu, X.Z., Choudhury, A., Li, X., and Montell, C. (1998). Coordination of an array of signaling proteins through homo- and heteromeric interactions between PDZ domains and target proteins. J Cell Biol *142*, 545-555.

Yan, J., Pan, L., Chen, X., Wu, L., and Zhang, M. (2010). The structure of the harmonin/sans complex reveals an unexpected interaction mode of the two Usher syndrome proteins. Proc Natl Acad Sci U S A *107*, 4040-4045.

Yewdell, J.W. (2005). Immunoproteasomes: regulating the regulator. Proceedings of the National Academy of Sciences of the United States of America *102*, 9089-9090.

Zacharias, M. (2003). Protein-protein docking with a reduced protein model accounting for side-chain flexibility. Protein Sci *12*, 1271-1282.

Zhang, Y., Appleton, B.A., Wu, P., Wiesmann, C., and Sidhu, S.S. (2007). Structural and functional analysis of the ligand specificity of the HtrA2/Omi PDZ domain. Protein Sci *16*, 1738-1750.

Zhou, X., Hao, Q., Liao, J., Zhang, Q., and Lu, H. (2013). Ribosomal protein S14 unties the MDM2-p53 loop upon ribosomal stress. Oncogene *32*, 388-396.

Zimmermann, P., Meerschaert, K., Reekmans, G., Leenaerts, I., Small, J.V., Vandekerckhove, J., David, G., and Gettemans, J. (2002). PIP(2)-PDZ domain binding controls the association of syntenin with the plasma membrane. Mol Cell *9*, 1215-1225.

Zimmermann, P., Zhang, Z., Degeest, G., Mortier, E., Leenaerts, I., Coomans, C., Schulz, J., N'Kuli, F., Courtoy, P.J., and David, G. (2005). Syndecan recycling [corrected] is controlled by syntenin-PIP2 interaction and Arf6. Dev Cell *9*, 377-388.

Zingarelli, B., Sheehan, M., and Wong, H.R. (2003). Nuclear factor-kappaB as a therapeutic target in critical care medicine. Crit Care Med *31*, S105-111.

Zwickl, P., Voges, D., and Baumeister, W. (1999). The proteasome: a macromolecular assembly designed for controlled proteolysis. Philosophical transactions of the Royal Society of London Series B, Biological sciences *354*, 1501-1511.

REPRINT OF PUBLISHED ARTICLES

FEBS Open Bio 4 (2014) 571–583

ELSEVIER

FEBS openbio

journal homepage: www.elsevier.com/locate/febsopenbio

Discovery of novel interacting partners of PSMD9, a proteasomal chaperone: Role of an Atypical and versatile PDZ-domain motif interaction and identification of putative functional modules

Nikhil Sangith [a], Kannan Srinivasaraghavan [b,c], Indrajit Sahu [a], Ankita Desai [a], Spandana Medipally [a], Arun Kumar Somavarappu [a], Chandra Verma [b,d,e], Prasanna Venkatraman [a,*]

[a] Advanced Centre for Treatment, Research and Education in Cancer (ACTREC), Tata Memorial Centre (TMC), Kharghar, Navi Mumbai 410210, India
[b] Bioinformatics Institute A*STAR, 30 Biopolis Street, #07-01 Matrix, Singapore 138671, Singapore
[c] Experimental Therapeutics Centre (A*STAR), 31 Biopolis Street, #03-01 Helios, Singapore 138669, Singapore
[d] School of Biological Sciences, Nanyang Technological University, 60 Nanyang Drive, Singapore 637551, Singapore
[e] Department of Biological Sciences, National University of Singapore, 14 Science Drive 4, Singapore 117543, Singapore

ARTICLE INFO

Article history:
Received 26 February 2014
Revised 20 May 2014
Accepted 24 May 2014

Keywords:
Proteasome
C-termini
PSMD9
PDZ

ABSTRACT

PSMD9 (Proteasome Macropain non-ATPase subunit 9), a proteasomal assembly chaperone, harbors an uncharacterized PDZ-like domain. Here we report the identification of five novel interacting partners of PSMD9 and provide the first glimpse at the structure of the PDZ-domain, including the molecular details of the interaction. We based our strategy on two propositions: (a) proteins with conserved C-termini may share common functions and (b) PDZ domains interact with C-terminal residues of proteins. Screening of C-terminal peptides followed by interactions using full-length recombinant proteins, we discovered hnRNPA1 (an RNA binding protein), S14 (a ribosomal protein), CSH1 (a growth hormone), E12 (a transcription factor) and IL6 receptor as novel PSMD9-interacting partners. Through multiple techniques and structural insights, we clearly demonstrate for the first time that human PDZ domain interacts with the predicted Short Linear Sequence Motif (SLIM) at the C-termini of the client proteins. These interactions are also recapitulated in mammalian cells. Together, these results are suggestive of the role of PSMD9 in transcriptional regulation, mRNA processing and editing, hormone and receptor activity and protein translation. Our proof-of-principle experiments endorse a novel and quick method for the identification of putative interacting partners of similar PDZ-domain proteins from the proteome and for discovering novel functions.

1. Introduction

Almost every cellular pathway involved in the biology and homeostasis of a eukaryotic organism is regulated by the Ubiquitin Proteasome System (UPS) [1]. Impairment in the function of UPS components results in the accumulation of proteins leading to cellular stress and apoptosis [2]. While the role of proteasome in normal biology and disease is by and large well studied, the precise mechanism, the sequence and the structural requirements for substrate recognition, direct and indirect protein–protein interactions required for recruiting a substrate to the proteasome, remain obscure [3]. The structure and the domain functions of various 19S subunits and their role in proteasome dependent and independent functions are unclear. We recently showed that a 13 residue peptide of the A-helix from myoglobin acts as an anchor while a floppy region, the 'F-helix' acts as an initiator of proteasome mediated ubiquitin independent degradation of apomyoglobin [4]. We identified new interacting partners of gankyrin, a chaperone of the proteasome assembly and an oncoprotein by recognizing proteins that share EEVD, a conserved Short Linear Sequence Motif (SLIM) seen at the gankyrin and S6 ATPase interface [5]. Interaction between gankyrin and chloride intracellular channel protein through the conserved hot spot site enhances the migratory potential of breast carcinoma cell line. In addition, we demonstrated a role for Sug 1, an ATPase of the proteasome in transcriptional regulation of MHC

Abbreviations: ELISA, enzyme linked immunosorbent assay; GH, growth hormone; hnRNPA1, heterogeneous nuclear ribonucleoprotein A1; IL6 receptor, interleukin 6 receptor; PSMD9, Proteasome Macropain non-ATPase subunit 9

* Corresponding author. Address: Protein Interactome Lab for Structural and Functional Biology, KS-244, ACTREC, Tata Memorial Centre (TMC), Kharghar, Navi Mumbai 410210, India. Tel.:+91 022 27405091; fax: +91 022 27405085.
E-mail address: vprasanna@actrec.gov.in (P. Venkatraman).

http://dx.doi.org/10.1016/j.fob.2014.05.005

proteins [6]. We described a novel role of PSMD9–hnRNPA1 interaction in basal and signal induced NF-κB activation via enhanced proteasomal degradation of IκBα [7]. We show that in this signaling pathway, proteasome bound PSMD9 acts as a subunit acceptor and hnRNPA1 as a shuttle receptor that recruits IκBα for degradation. Here, we exploit the presence of PDZ domain in PSMD9, a non-ATPase subunit, and a chaperone, of proteasome assembly to identify novel interacting partners and suggest putative functions of this biologically important molecule.

2. Material and methods

2.1. Plasmids

PSMD9 cDNA (Origene Technologies) was amplified and ligated into pRSETA vector between BamHI and EcoRI sites. hnRNPA1 and S14 ribosomal protein cDNA was generated by RT-PCR from RNA extracted from HEK293 cells. E12, growth hormone and the FN3 domain of IL6 receptor were amplified from the cDNA obtained from Harvard Institute of Proteomics. hnRNPA1 was ligated in pGEX4T1 (GE Amersham). FN3 domain was cloned in pGEX4T1 between BamHI and XhoI. S14, ribosomal protein, growth hormone and E12 were cloned in pMALC5 between BamHI and EcoRI sites. Mutations generated by site directed mutagenesis were confirmed by sequencing. PSMD9 was cloned in pCMV10 3X FLAG between HindIII and EcoRI sites. In doxycycline inducible pTRIPZ vector, PSMD9 was cloned between AgeI and EcoRI sites. All the interacting partners of PSMD9 were cloned in HA-pcDNA3.1 (A gift from Dr. Sorab Dalal, ACTREC) between BamHI and XhoI sites. Also see primers (Table S6).

2.2. Expression and purification of recombinant proteins

All recombinant proteins were expressed in *E.coli* BL21 DE (3) using 100 μM IPTG at 20 °C for 16 h. His-PSMD9 and its mutants were purified by Ni-NTA chromatography (Qiagen); GST, GST-hnRNPA1, GST-FN3 and its mutants were purified using glutathione sepharose (GE Amersham); MBP and MBP-S14, E12 and growth hormone were purified using amylose resin (NEB), according to manufacturer's protocol.

2.3. ELISA with tetra-peptides

N-terminal biotinylated tetra-peptides were procured from GenPro Biotech, India, (Biotin-KGG-XXXX, where XXXX represents the tetra-peptide sequence) and reconstituted to 25 mM with 100% DMSO and further diluted to 5 mM with distilled water. Anti-PSMD9 (Abcam) antibody in 0.1 M sodium carbonate buffer, pH 9.5 was coated on Nunc-Immuno™ MicroWell™ 96 well solid plates and incubated for 16 h at 4 °C. Wells were blocked with 2% BSA in TBST (10 mM Tris pH8, 138 mM NaCl and 0.5% Tween-20) for 1 h at 37 °C. His-tagged PSMD9 or its mutant proteins (5 μg/ml), diluted in TBST (containing 0.1% BSA) were added and incubated at 37 °C for 1 h. Plates were washed, and biotinylated peptides (in TBST with 0.1% BSA) were added to the wells and incubated for 1 h at 37 °C. The plates were washed with TBST vigorously after each incubation step. Finally, streptavidin alkaline phosphatase (Sigma), at a dilution of 1:2000 in TBST containing 0.1% BSA was added to all wells. After incubation for 1 h at 37 °C, binding was detected by the addition of para-Nitro phenyl phosphate (PNPP) (Bangalore Genei, India), the substrate of alkaline phosphatase and color developed was read at 405 nm (Spectramax 190, Molecular Devices). Wells that lack PSMD9 and wells that lack anti-PSMD9 antibody were taken as negative controls.

2.4. ELISA for PSMD9-hnRNPA1 and PSMD9-growth hormone interaction

GST-hnRNPA1, its mutants and GST only (control; 5 μg/ml) or MBP-growth hormone and MBP only (control; 5 μg/ml) were coated as described for the PSMD9 antibody (Section3.2). All incubations were performed as described for the peptide ELISA (Section3.2). Different concentrations of His-tagged PSMD9 or its mutant proteins were (in TBST containing 0.1% BSA) added to the coated plates. After incubation, anti-his antibody (Cell Signaling) was added at a dilution of 1:2000, incubated and washed. HRP conjugated anti-mouse antibody (GE Amersham) (at 1:3000 dilution) was then added. After incubation and washes, HRP substrate TMB (1X) was added to all the wells. Reaction was stopped using 2 M sulfuric acid before recording the readings at 450 nm. Wells not coated with GST-hnRNPA1 and wells in which PSMD9 or the mutants were not added served as negative controls. For the competition assays, recombinant his-PSMD9 was incubated with different concentrations of GRRF/GRRG or SCGF/SCGG/SGGF peptides for 1 h at 37 °C and then added to wells containing GST-hnRNPA1 or MBP-GH respectively.

2.5. In vitro pull down assay

Recombinant GST, GST- hnRNPA1, and its mutants (baits) were allowed to bind with glutathione sepharose beads (GE Amersham) in Transport Buffer (TB, 20 mM HEPES pH 7.9, 110 mM potassium acetate, 5 mM sodium acetate, 0.5 mM EGTA and 1 mM DTT) for 1 h at 4 °C. Beads were washed, following which PSMD9 or its mutants (in TB 0.1% BSA) were incubated with each bait for 4 h at 4 °C. Binding was monitored by Western blot using anti-His antibody (Cell Signaling). Cell lysates of MBP, MBP-S14, growth hormone, E12 or their respective C-terminal mutants were allowed to bind with amylose resin (NEB) in Transport Buffer for 1 h at 4 °C. Further incubations with PSMD9 or mutants were performed as described above except that anti- His antibody (Cell Signaling) was used to detect bound PSMD9.

2.6. Homology modeling

There is currently no crystal structure available for PSMD9 protein. A homology model of PDZ domain of PSMD9 was thus constructed using comparative modeling method, by comparing the sequence of this target protein with sequence of other related proteins (template) for which experimental structures are available. BLAST search showed that the PDZ domain shares 42% sequence similarity with PDZ2 domain of harmonin and sequence alignment between the two reveals that this sequence similarity is distributed throughout the sequence. Solution structure of PDZ2 domain of harmonin bound with C-terminal peptide of cadherin23 (PDB code 2KBS) [8] was chosen as a template for the homology modeling. Modeller, a program for comparative protein structure modeling by satisfaction of spatial restraints [9] was used for generation of the homology model. Several homology models were built based on structural information from the template, and model that showed good stereochemical property was selected for further use.

2.7. Peptide docking

3D structure of peptides GRRF and SCGF was generated using Xleap module in Amber11 [10]. Peptide in its extended conformation was docked with the generated model of PDZ domain of PSMD9 protein. Peptide docking was carried out with two different docking programs, HADDOCK [11] and ATTRACT [12]. For HADDOCK, a binding site was defined using residues Leu124, Gly125, Gln126, Glu128 and Gln181 within the canonical pocket. No information regarding the binding site was given while using ATTRACT and a complete

blind docking was performed using this program. Both the docking programs were validated earlier, by docking a set of co-crystallized peptides into the canonical pocket of the corresponding PDZ domains, and the docked conformations of each peptide had rmsd values 1.5–2.5 A with the corresponding experimental structures.

2.8. Molecular dynamics simulations

Generated homology model of PDZ domain, peptide GRRF (derived from C-terminus of hnRNPA1) - PDZ complex (PDZ-GRRF) and peptide SCGF – PDZ complexes (PDZ-SCGF) (both the canonical and non-canonical binding mode) were used as the starting structure for MD simulations. Mutated structures of the protein Q181G and the*triple* β-sheet mutant L124G/Q126G/E128G were also generated by replacing (mutating) the respective residues in PyMol. Hydrogen atoms were added to the WT and mutant experimental structures using the Xleap module of the Amber11 package. N-terminus of the GRRF and SCGF peptide was capped by acetylation (ACE). Simulation systems were neutralized by the addition of counter ions. The neutralized system was solvated with TIP3P [13] water molecules to form a truncated octahedral box with at least 10 Å separating the solute atoms and the edges of the box. MD simulations were carried out with the Sander module of the AMBER11 package in combination with the parm03 force field [14]. All systems were first subjected to 100 steps of energy minimization. The protein was initially harmonically restrained (25 kcal mol^{-1} $Å^2$) to the energy minimized coordinates, and MD simulations were initiated by heating the system to 300 K in steps of 100 K followed by gradual removal of the positional restraints, and a 1 ns unrestrained equilibration at 300 K. The resulting system was used as starting structure for production MD run. For each case, three independent (using different initial random velocities) MD simulations were carried out starting from the well equilibrated structure. Each MD simulation was carried out for 100 ns and conformations were recorded every 10 ps. All MD simulations were carried out in explicit solvent at 300 K. During all the simulations, the long-range electrostatic interactions were treated with the particle mesh Ewald [15] method using a real space distance cutoff of 9 Å. The settle [16] algorithm was used to constrain bond vibrations involving hydrogen atoms, which allowed time step of 2 fs during the simulations. Simulation trajectories were visualized using VMD [17] and figures were generated using PyMol.

2.9. Immunoprecipitation

FLAG-PSMD9 and HA tagged interacting partners were overexpressed in HEK293 cells. Lysates were added either to M2-Agarose (Sigma) or to anti HA-agarose beads and incubated for 3 h at 4 °C to immunoprecipitate the complex. Either anti-HA antibody or anti-FLAG antibody (Sigma) was used for detection.

2.10. Circular dichroism of PSMD9 and its mutants

Far-UV CD spectrum (Jasco, J815) of PSMD9-WT and its mutant proteins were recorded between 260 nm and 190 nm in a 2 mm path length cuvette. A protein concentration of 2 μM, in a volume of 500 μl (10 mM phosphate buffer (pH 7.5)) was used for collecting data at 20 °C. Data were normalized to obtain molar ellipticity values and fitted using Dichroweb's CONTIN software.

2.11. Tryptophan fluorescence of PSMD9 and mutants

Tryptophan fluorescence of PSMD9-WT and PSMD9-PDZ-mutants was recorded at a concentration of 1.5 μM. Emission spectra between 310 and 400 nm were collected upon excitation at 295 nm with a slit width of 5 nm and scan speed of 50 nm/s using Fluorolog HORIBA fluorimeter.

2.12. Western blotting

Samples were separated on 15% SDS PAGE gels and Western blots were performed using standard protocols. Depending on the protein under study, anti-His antibody (mouse monoclonal, Cell Signaling), anti-FLAG antibody (rabbit polyclonal, Sigma) or anti-HA antibody (rabbit polyclonal, Sigma) were used.

3. Results

3.1. A screen for putative PSMD9 interacting partners and validation using full length proteins

Many methods capitalize on the ability of the PDZ domains to recognize C-terminal residues in proteins to primarily define their binding specificity [18–22]. Peptide libraries have been created, and peptides derived from the C-terminus of the human proteome have been used by various investigators [18,23–25]. We chose C-terminal peptides of the human proteome as baits to identify novel interacting partners of PSMD9. Premise for this study is that modification-independent, sequence specific recognition is central to many biological processes, and rules inherent to this recognition process can bring together proteins of very different functions under a master regulator. Chung et al., had classified proteome from drosophila/yeast/human by recognizing conserved C-terminal residues in some of these proteins [26]. These C-terminal peptides were tested here for the following reasons. (1) Most high-throughput studies are optimized for selecting peptides with high affinity while many protein–protein interactions are of low affinity and, therefore, are likely to be missed. (2) If the corresponding protein/proteins were to interact, one could quickly move to associated functions, and finally (3) such a guided approach prevents identification of those peptides that are not represented in the human proteome and, are physiologically irrelevant. Due to financial constraints, thirteen among the thirty conserved tetra peptides from the human proteome were chosen. These sequences differ in charge, hydrophobicity and size and represent some of the known sequence specificity seen with other PDZ domains. AGHM, the C-terminus of E12 transcription factor, the human homolog of rat E2, was specifically included. E12 was shown to interact with Bridge 1 (homolog of PSMD9 with a PDZ domain) during insulin signaling [27–29]. We cloned, expressed and purified human PSMD9 and used enzyme-linked immunosorbent assay (ELISA), to test for binding of the peptides. GRRF, SCGF and AGHM peptides bound to PSMD9 to an appreciable extent with SCGF demonstrating highest affinity (Fig. 1A and Fig. S1A and B). SCGF and GRRF resemble class III PDZ peptides with the sequence motif-X-[D/E/K/R]-X-Φ where Φ is hydrophobic, and X is any residue. GRRF forms the C-terminus of hnRNPA1 isoforms while SCGF belongs to growth hormone (CSH1; referred from henceforth as GH). To test if the corresponding full length proteins would interact with PSMD9, we cloned and expressed the longer isoform of hnRNPA1 as a GST fusion protein, GH and E12 as MBP fusion proteins. PSMD9 was expressed as a His-Tag protein. Affinity pull-down followed by Western blot showed that the three full length proteins interact with PSMD9 (Fig. 1B–D). While hnRNPA1 (Fig 1E andTable S4) and E12 binding (Fig 1C) were clearly affected by simple C-terminal substitution (Phe to Gly), GH binding to PSMD9 was not affected to any measurable extent (Fig. 1D). Deletion of C-terminal seven residues compromised binding of GH severely (Fig. 1D) and not surprisingly those of hnRNPA1 and E12, as well (Fig. 1B and C). These interactions were further confirmed using ELISA and the

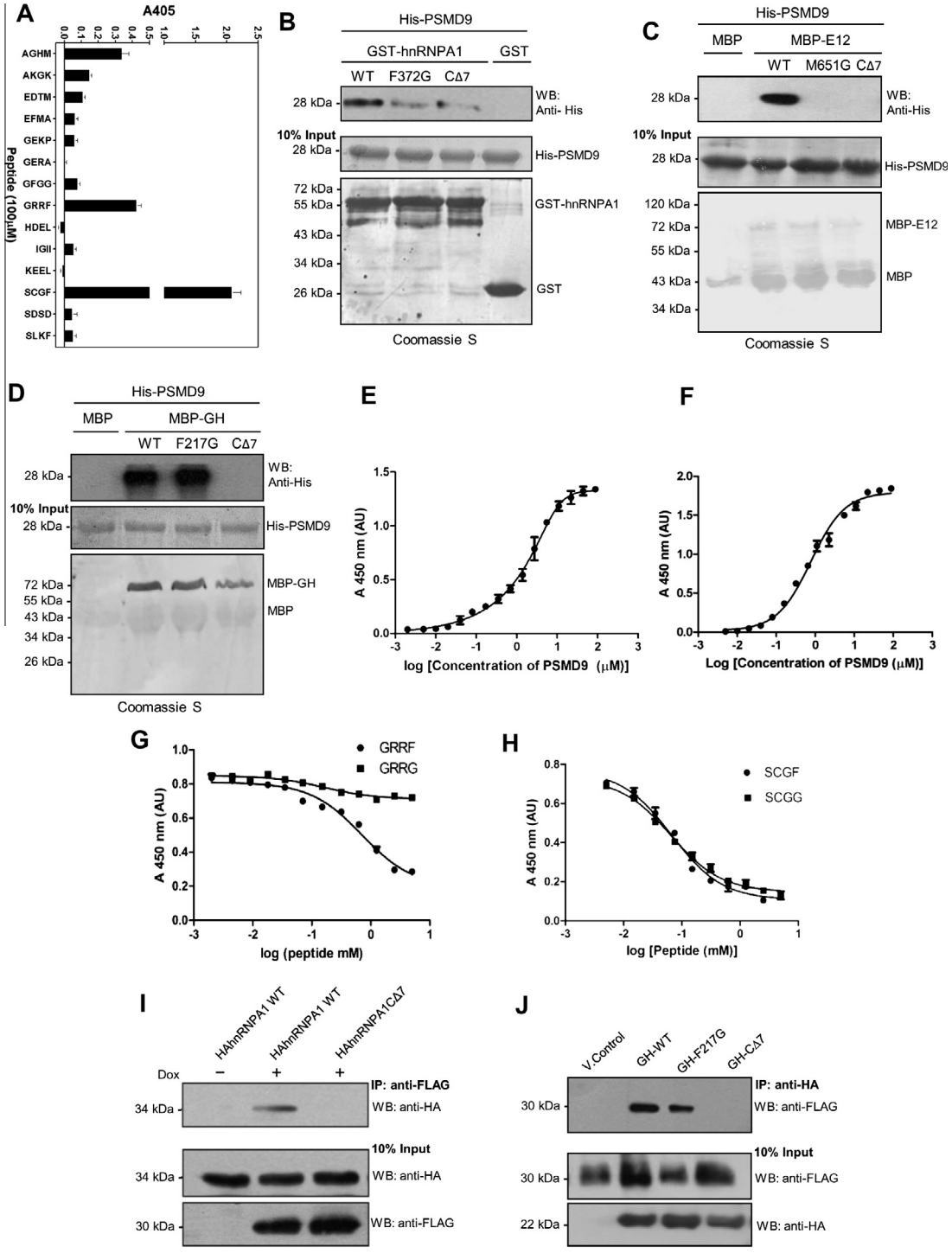

Fig. 1. Identification of putative interacting partners of PSMD9, and the importance of C-terminal residues in interaction. (A) Conserved C-terminal motifs in the form of tetra peptides were tested for binding to PSMD9 using ELISA (see Section2 for details). Values represent mean ± SEM (Standard Error of Mean) from three different experiments performed in duplicates.(B) Recombinant WT hnRNPA1 or hnRNPA1 C-terminal mutant (F372G or CΔ7) bound to GST served as baits to pull down PSMD9. (C) Interaction of recombinant E12 and its C-terminal mutants (MBP-fusions) with PSMD9 (His-tag) were tested by *in vitro* affinity pull-down using MBP-agarose (see Section2 for details). (D) Interaction of recombinant GH and its C-terminal mutants (MBP fusions) with PSMD9 was tested by *in vitro* affinity pull-down using MBP-agarose (see Section2 for details). (E) Interaction of PSMD9 with hnRNPA1 was monitored by ELISA (see Section2 for details). Data were best fit to one site specific binding using GraphPad Prism (commercial software, www.graphpad.com). The dissociation constant (K_d) for the interaction was found to be 1.33 ± 0.04 μM for hnRNPA1. Data from two independent experiments each done in duplicates is represented as mean ± SD (SD-standard deviation). (F) Interaction of PSMD9 with growth hormone. Data were fit to one site specific binding using PRISM. The dissociation constant (K_d) for the interaction was found to be 0.84 ± 0.07 μM for growth hormone. Measurements were done in duplicates and data is represented as mean ± SD (SD- standard deviation) for two independent experiments. (G) C-terminal peptide GRRF inhibits hnRNPA1-PSMD9 interaction. Prior to its incubation with hnRNPA1 coated plates, PSMD9 (0.65 μM) was incubated with GRRF or GRRG peptides. (H) C-terminal peptide SCGF and SCGG inhibit interaction of growth hormone with PSMD9. Prior to incubation with growth hormone, PSMD9 (0.65 μM) was incubated with SCGF or SCGG peptides. Ki for SCGF was calculated to be 36.7 ± 0.29 μM and for SCGG, it was 35.6 ± 0.24 μM. Data from two independent experiments each done in duplicates is represented as mean ± SD. (I) Interaction of hnRNPA1 and PSMD9 in mammalian cells. FLAG-tagged PSMD9 or its C-terminal mutant and HA- tagged hnRNPA1 were co-expressed in HEK293 cells. FLAG-PSMD9 was immunoprecipitated using M2-Agarose beads, followed by Western blot with anti-HA antibody. (J) Growth hormone and PSMD9 interact upon co-expression in mammalian cells. HA-Growth hormone or its C-terminal mutants and FLAG-PSMD9 were co-expressed in HEK293 cells and interaction was monitored by Co-IP as described in supplementary methods.

estimated dissociation constant K_d for PSMD9-hnRNPA1 interaction is 1.33 ± 0.16 μM and of PSMD9-GH interaction is 0.74 ± 0.04 μM and ΔG for the interaction between PSMD9 and WT-hnRNPA1 or GH were calculated to be 6.9 ± 0.04 and 7.1 ± 0.09 kcal/mol, respectively. Peptide GRRF and not GRRG inhibited hnRNPA1 binding (Ki of 326.5 ± 0.25 μM) confirming the importance of C-terminal residues (Fig. 1G) in this interaction. Again, as seen with the C-terminal substitutions of GH, inhibition of GH-PSMD9 interaction by SCGG was as good as SCGF and the Ki values for these peptides were 36.7 ± 0.29 and 35.6 ± 0.24 μM, respectively (Fig. 1H). These pairwise interactions and the role of C-terminal residues were confirmed in mammalian cells using co-immunoprecipitation assays (Fig. 1I and J).

3.2. The fine specificity of SCG derivatives

Unlike hnRNPA1 GRRG mutant, mutant GH with a C-terminal substituted SCGG binds to the PDZ domain of PSMD9 and interaction is inhibited only upon deletion of C-terminal residues (Δ7 mutant). To identify the minimal motif important for GH interaction, we engineered ΔGF, and ΔCGF mutants of GH and interaction with PSMD9 was tested by pull down and ELISA (Fig. 2 A and B and Table S4). While ΔGF mutant bound with PSMD9, deletion of one more residue, Cysteine, ΔGFC, impaired the interaction. By ELISA, the estimated K_d values were 0.8 ± 0.02 μM for ΔGF and 2.6 ± 0.011 μM for ΔCGF mutant. The % occupancy of GH was unaltered in the ΔGF mutant but was reduced to ~45% in the case of the ΔCGF mutant. This result emphasizes the importance of P−2 residue in interaction with PSMD9. The importance of the P−2 Cys was further confirmed by demonstrating the failure of peptide SGGF to inhibit the binding of GH to PSMD9 (Fig. 2C). As noted before both SCGF and SCGG can inhibit binding between the two proteins.

Our results help to clarify some of the observations made earlier with respect to Nas-2-Rpt5 interaction in yeast (PSMD9 homolog and the ATPase subunit of the 19S regulatory particle). Here, single C-terminal residue deletion in Rpt5 did not affect its binding to Nas-2 that made the authors conclude that the PDZ like domain of Nas2 may not confirm to the classical description [30]. Based on our results on human PSMD9 using similar pull down assays, other comparative studies and quantitative analysis, we show that the precise role of the C-terminal residues in the interaction is likely to be context dependent. In the case of hnRNPA1 (GRRF) and E12 (AGHM), bulk of the binding energy is derived from the C-terminal residue much like the classical PDZ domains. In GH with SCGF at the C-terminus, however, the terminal residue is less important. These differences are also reflected in the binding affinity of the three peptides to PSMD9. While GRRF binds weakly (K_d 651.7 ± 76 μM), peptide SCGF binds tightly to PSMD9 (K_d 8.6 ± 1.2 μM). One possible explanation is that these peptides may bind in different modes or orientations at the binding groove (discussed below). While results observed with the C-terminal peptides can be readily extrapolated to protein binding, stable binding of the full length protein may require additional interactions. It is also likely that, besides the canonical α–β groove, the protein, may bind elsewhere on PSMD9 perhaps at an allosteric site while the C-terminal sequence acts as initial recognition element that docks the protein at the canonical site.

3.3. Role of PDZ domain in interaction: modeling and site directed mutagenesis

To better understand the role of the C-terminal residues and PDZ domain in binding and recognition, we modeled the structure of PDZ and carried out extensive molecular dynamic simulations and peptide docking studies (supplementary methods). Several

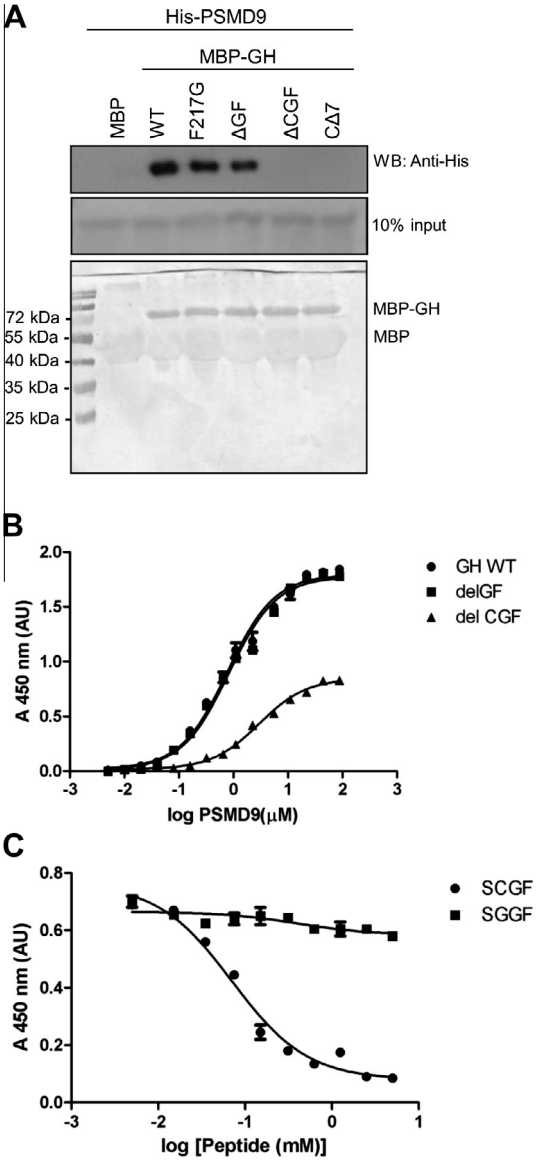

Fig. 2. Importance of Cysteine in growth hormone-PSMD9 interaction. (A) Interaction of recombinant GH and its C-terminal mutants F217G, ΔGF, ΔCGF and CΔ7 (MBP fusions) with PSMD9 was tested by *in vitro* affinity pull-down using MBP-agarose. (B) ELISA was used to monitor interaction between PSMD9 and GH or its C-terminal mutants. Data were fit to one site specific binding using PRISM. The dissociation constant (K_d) for the interaction of WT growth hormone, ΔGF and ΔGF with PSMD9 was found to be 0.74 ± 0.04 μM, 0.8 ± 0.03 and 2.64 ± 0.02 μM, respectively. Measurements were done in duplicates and data is represented as mean ± SD (SD-standard deviation) for two independent experiments (Also see Table S4). (C) C-terminal peptide SCGF and not SGGF inhibit interaction of growth hormone with PSMD9. Prior to incubation with growth hormone, PSMD9 (0.65 μM) was incubated with SCGF or SCGG peptides. Ki for SCGF was calculated to be 36.7 ± 0.29 μM. Data from two independent experiments each done in duplicates is represented as mean ± SD.

docking poses were created. Upon visual inspection of all the docked poses, a peptide-protein complex similar to that seen in the co-crystals of other PDZ-peptide complex with Phe at the fourth position was chosen. In this conformation, the peptide binds in an extended, antiparallel manner through canonical interactions that extend the beta sheet by an additional strand (Fig. 3A and B). The hydrophobic side chain of Phe4 of the peptide is deeply buried in the hydrophobic pocket formed by Leu124 from β_2, Val139, from β_3, Leu153 from β_4, Ile159, Phe 162, from β_4. The peptide further interacts with the beta sheet mainly through backbone/side chain

hydrogen bonds with residues Leu124, Gly125, Gln126, Glu128 of β_2 of the PDZ domain (Fig. 2B). In addition, the side chain of Arg2 of the peptide forms a salt bridge with the side chain of Glu128 from β_2. During MD simulation, the alpha/beta binding groove (canonical binding site) of apo PDZ showed increased flexibility (Supplementary Fig. S2). The α_2/β_2 binding pocket was partially deformed/destabilized (either collapses or widens), and is stabilized upon peptide binding. Increased flexibility of PDZ domains in their apo form have been reported by others [31]. The intrinsic flexibility of PDZ domains is a key determinant that allows them to recognize a wide repertoire of peptide ligands. Throughout the protein-peptide simulation, Phe4 remains deeply buried in the

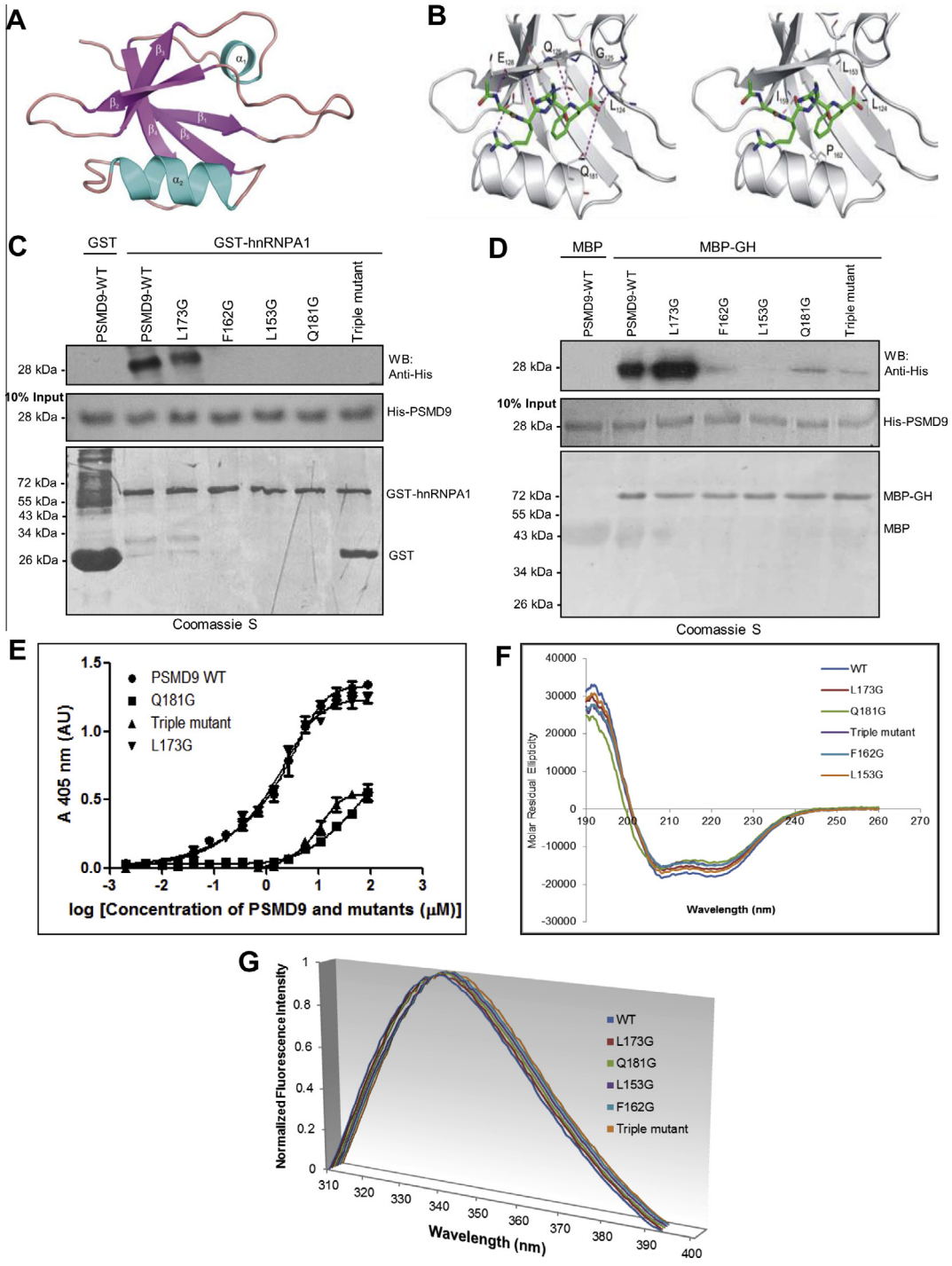

Fig. 3. Model of PDZ-domain of PSMD9 and residues important for interaction. (A) Cartoon representation of PDZ domain of PSMD9 built using PDZ2 domain of harmonin as the template. (B) Structure of PDZ domain bound to GRRF. A clear cleft that is bordered by α-helix and a β-strand can be seen in the PDZ domain similar to ligand bound PDZ structures. (C) Mutations of residues in the canonical pocket of PDZ domain [Q181G, the triple mutant (L124G/Q126G/E128G), L153G and F162G], abrogate binding to hnRNPA1 (D). Recombinant GH (expressed as MBP fusion) and PSMD9 (expressed as His-tagged) interact *in vitro*. Complex of PSMD9 or its mutants with GH was isolated using protocols described in methods. Mutations in the PDZ domain (as described in (C)) abrogate interaction. (E) WT-hnRNPA1 interaction with recombinant WT-PSMD9 or its mutant proteins was detected by ELISA. Three independent experiments each in duplicates were performed and data is represented as mean ± SD (SD- standard deviation). (F) Circular dichroism of PSMD9-WT and the PDZ mutants were recorded at 2 μM concentration between 260 nm and195 nm. Molar residual ellipticity is plotted against wavelength. (G) Fluorescence spectra of PSMD9-WT and its mutants were recorded between 310 nm and 410 nm (Excitation wavelength 295 nm). Data are represented as normalized fluorescence intensity against wavelength of emission.

hydrophobic pocket (Movie1:http://web.bii.a-star.edu.sg/bmad/PDZ/PDZ-PEP-WT-Top.mpg). Charge-charge interactions between Arg2 and Glu128 on β_2 are preserved during the 100 ns simulation. The bound conformation of the peptide was further stabilized via backbone hydrogen bond interactions with residues Leu124, Gly125, Gln126 and Glu128 from β_2 in the canonical binding site.

In the complex where Phe4 was mutated to Gly, the peptide unbinds from the canonical binding site within ~5–10 ns and doesn't bind again (Movie 2:http://web.bii.a-star.edu.sg/bmad/PDZ/PDZ-PEP_GRRG-Top.mpg). Although the peptide stays close to the canonical site due to charge-charge interactions with the protein residues, it undergoes translation and rotations that prevent it from rebinding in the canonical interaction mode. Thus, our MD simulations suggest that the burial of Phe in the hydrophobic pocket is crucial for the stabilization of this peptide in its bound conformation. Based on peptide docking and MD simulations (Movie 3:http://web.bii.a-star.edu.sg/bmad/PDZ/PDZPEP_L124G_Q126G_E128G-Top.mpg and Movie 4: http://web.bii.a-star.edu.sg/bmad/PDZ/PDZ-PEP_Q181G-Top.mpg), three single amino acid mutations F162G, L153G, Q181G and a triple mutation, L124G/Q126G/E128G were generated. *In vitro* pull-down shows that these mutations affect GH and hnRNPA1 binding to PSMD9 (Fig. 3C and D). Mutation of residue L173 (to Gly), part of the α2 helix, not involved in the interaction, did not affect the binding of peptide or the proteins (Fig. 3E and Table S1). MD simulations support this finding as the L173G PSMD9 mutant maintains the peptide in a stably bound form (not shown).

These results together, confirm the domain-motif interaction between PDZ domain of PSMD9 and the C-terminal region of the interacting proteins. The instability of the peptide-free forms is reflected in the secondary structure of these proteins determined by circular dichroism. While WT PSMD9 records 49% helicity, the L173G mutant shows 43% helical structure, Q181G mutant 39%, L153G mutant 45% and the F162G mutant shows 42% helical structure (Fig. 3F, Table 1 and Appendix Eq.(1)) [32]. Tryptophan fluorescence of these mutant proteins is less affected (Fig. 3G).

3.4. Identification of putative functional modules regulated by PSMD9

Although GRRF and SCGF were motifs under which several family members (12 and 13 respectively) were grouped by Chung et al., a detailed analysis and further curation using UniProt data (ftp://ftp.uniprot.org/pub/databases/uniprot/current_release/knowledgebase/) indicated that there was only one unique protein under each family. There are four isoforms within the GRRF family and ten isoforms within the SCGF family (Table S2). We re-analyzed other 28 families and found that, in the vast majority of the cases, the proteins grouped under each peptide family are primarily isoforms (Table S2). Although isoforms are homologous in sequence, their functions can be mutually exclusive or even counteractive [33,34]. To better define the role of C-terminus in functional grouping beyond isoforms, and predict the modules that may be regulated by PSMD9, we analyzed C-terminal variants of GRRF and SCGF from the human proteome. There are ten variants of GRRF where X is C, E, G I, K, L, N, P, Q or R (Table S3). SCGL at the C-terminus of IL6 receptor was a single variant of SCGF. We screened seven variants of GRRF (GRRG was already tested as a control) i.e., GRRC, GRRE, GRRI, GRRL, GRRN, GRRQ and GRRR as well as the SCGL peptide for binding to PSMD9 by ELISA (Fig. 4A, Table S5). Peptides GRRL, GRRI, GRRQ, GRRC, GRRR and SCGL bound to PSMD9. GRRI and GRRL binding affinity were comparable to GRRF. GRRI belongs to a hypothetical protein. GRRL belongs to S14. S14 is part of the ribosome and like hnRNPA1 is an RNA binding protein also involved in protein translation [35]. GRRC and GRRR surprisingly bound with 12–14-fold higher affinity than GRRF. GRRC belongs to endothelial receptor protein and GRRR to UPF2, a protein involved in mRNA metabolism. Like SCGF, SCGL (from IL6 receptor) bound to PSMD9 with better affinity than GRRF or its variants. We tested full length S14 and IL-6 receptor C-terminal domain for binding to PSMD9 using *in vitro* pull down assay, and both were found to interact with PSMD9. As in hnRNPA1, C-terminal substitution abrogated binding of S14 and remarkably as seen with GH, binding of IL-6 receptor was unaffected by the C-terminal Gly substitution but was inhibited upon deletion (Fig. 4B and D). Again, similar to hnRNPA1-PDZ interaction, all the PSMD9 PDZ mutants L153G, F162G, Q181G and the triple mutant L124G/Q126G/E128G, either did not recognize or bound less well to WT S14 and the FN3 domain of the IL6 receptor with intact C-terminal residues (Fig. 4C and E).

To test whether observed *in vitro* interactions can be extended to interactions within the cellular milieu, we cloned and trans-expressed S14 ribosomal protein and the FN3 domain of IL6 receptor and their respective C-terminal mutants, in HEK293 cells. Immunoprecipitation results clearly confirm all *in vitro* observations (Fig. 4F and G).

4. Discussion

Our results taken together indicate that PSMD9 carries a versatile PDZ domain and interacts with residues at the C-terminus of proteins that are non-homologous in sequence, but carry a signature Short Linear Sequence Motif. Although the number of peptides screened here is limited, substantial information can be inferred from the binding of peptides and proteins to the PDZ domain of PSMD9 and their mutant forms. Given that the information on the structure and functions of PSMD9 (and other 19S subunits) is minimal, the results reported here are highly significant. However, some amount of speculation drawing support from our own studies and those from the literature is necessary to appreciate the significance of the results.

4.1. On the origin of affinity differences

We had included 8 out of 10 C-terminal variants of GRRF, and SCGL a single variant of SCGF, from the human proteome and peptide AGHM from transcription factor E12, for their ability to

Table 1
Fraction of helicity of PSMD9 WT and mutants analyzed by circular dichroism.

Protein	$[\theta]_{222}$ (deg cm^2 d mol^{-1})	Helicity predicted by CONTIN(%)	Helicity predicted by formula*(%)
PSMD9 WT	−17281.7 ± 368.34	47.5 ± 0.96	52 ± 0.94
L173G	−15377.4 ± 327.75	41.93 ± 0.77	47.1 ± 0.8
Q181G	−13734.7 ± 292.14	38 ± 0.72	42.9 ± 0.7
Triple mutant L124G/Q126G/E128G	−14485.3 ± 308.74	40.13 ± 0.77	44.8 ± 0.7
F162G	−14863.4 ± 253.25	42.14 ± 0.65	45.8 ± 0.62
L153G	−16455.94 ± 362.63	45.3 ± 0.84	50.7 ± 0.66

* The fraction of α-helix present in PSMD9 and mutants were calculated using the CONTIN software available in DICHROWEB server and the helicity is also predicted by the formula $fH = ([\theta]_{222} - 3000)/(-36000 - 3000)$ (Appendix Eq.(1)) [21], where $[\theta]222$ is mean molar residual ellipticity at 222 nm.

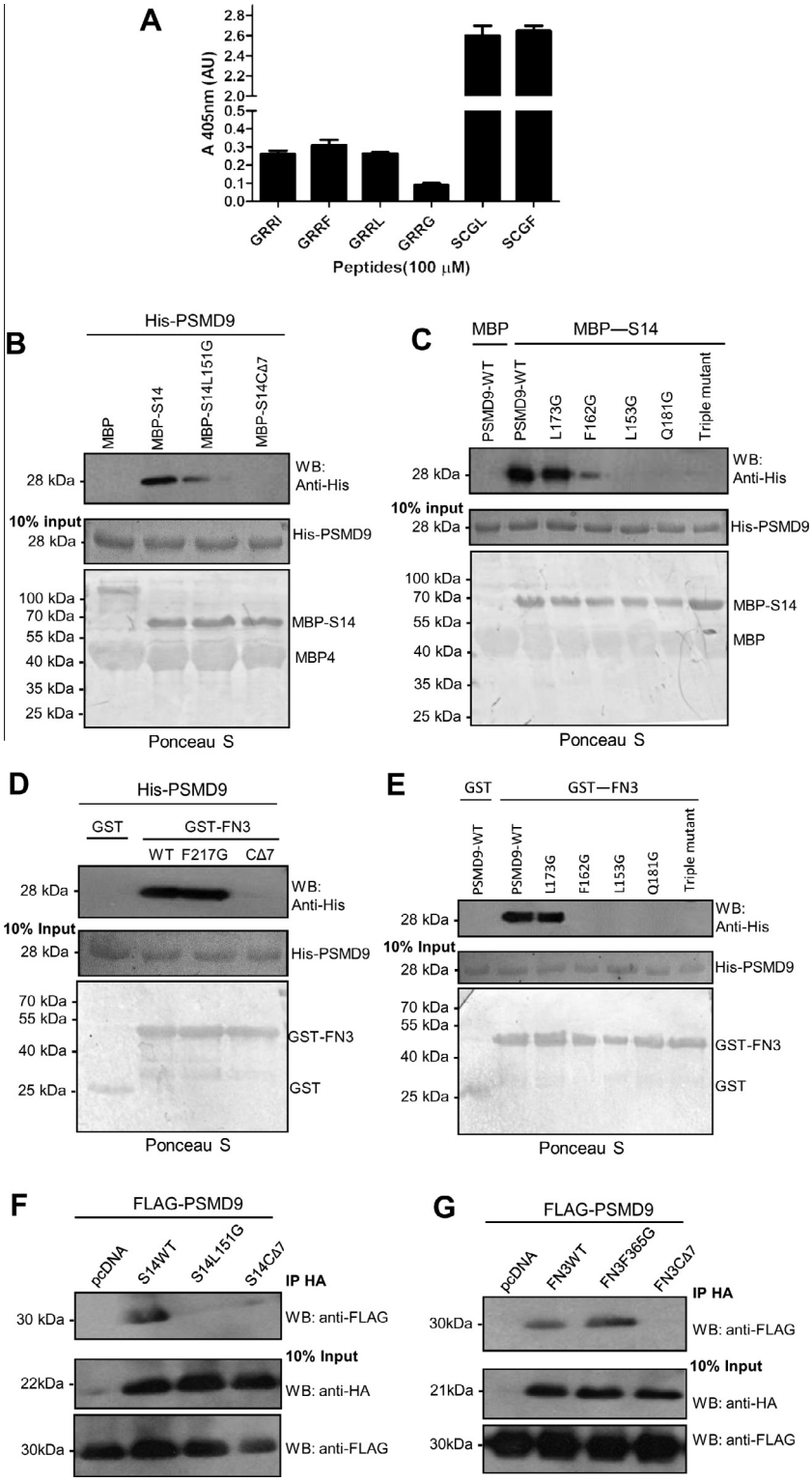

Fig. 4. Interaction of PSMD9 with C-terminal variants (from the human proteome) of hnRNPA1 and GH. (A) Binding of peptide variants GRRX to recombinant PSMD9. GRRX peptide (X = any residue) binding to PSMD9 was detected and measured by ELISA. Values from three experiments done in duplicates are represented as means ± SEM. (B) S14 ribosomal protein interacts with PSMD9 via its C-terminal residues. Complex formed between S14 wild type (MBP fusion), S14 L151G or C-terminal deletion mutant S14CΔ7 was isolated as described in methods. Any bound PSMD9 (His tagged) was detected using anti-His antibody (C) PDZ domain of PSMD9 is important for interaction with S14 ribosomal protein *in vitro*. *For* the *in vitro* pull-down, MBP-S14 fusion and his-PSMD9 or its mutant proteins were processed as described previously. (D) FN3 domain of IL6 receptor interacts with PSMD9 *in vitro*. GST-WTFN3, FN3 F365G mutant or C-terminal deletion mutant (FN3CΔ7) were used to pull down PSMD9 (His-tag) and probed for the presence PSMD9 using anti–His antibody. (E) PDZ domain of PSMD9 is important for interaction with the FN3 domain *in vitro*. (F) Interaction of S14 with PSMD9 in mammalian cells. HA-tagged WTS14 or its C-terminal mutants were co-expressed with FLAG-PSMD9, immunoprecipitated and the complexes were probed for FLAG-PSMD9. (G) Interaction of the FN3 domain of IL6 receptor with PSMD9 in mammalian cells. HA-tagged FN3 domain or its C-terminal mutants were co-expressed with Flag-PSMD9, co-immunoprecipitated and bound PSMD9 was detected using anti-Flag antibody.

interact with PSMD9. The K_d for each of these peptides is summarized in Table S3. Based on the affinity of the peptides, these variants can be classified into three groups – Group I or low affinity binders, Group II or high affinity binders and Group III tight binders or the top ranking peptides. In the Group I peptides, hydrophobic residues such as F, L, I at P0 provide specificity. In Group II peptides, Cys or Arg at P0 increases affinity by 10-fold as compared to that of Group I peptides. These two amino acids seem very different from each other and from the Group I peptides in terms of their physical properties and binding preference of the PSMD9 PDZ domain seems very intricate. The binding pocket of PSMD9 seems better adapted to bind to residues that are not bulky or highly hydrophobic explaining the high affinity binding of GRRR and GRRC. On the other hand, both Cys and Arg show characteristics of hydrophobic residues. For example, based on the hydrophobicity index Cys is classified along with Phe [36–39] and arginine, although one of the least hydrophobic amino acids, shows very interesting properties. Arginine solubilizes aggregation prone proteins helps in the elution of proteins bound to phenylsepharose column and has wide application in the purification and solubilization of inclusion bodies [40,41]. Arginine like GuHCL interacts with almost all amino acids and preferentially with aromatic residues [40], but unlike GuHCl, Arginine is not a denaturant [42]. This probably explains why these two amino acids like the hydrophobic residues occupy the P0 position. Arg substitution for a Phe in the interior of a protein will result in destabilization but less likely to do so at the protein interface.

Based on binding affinity, peptide AGHM will also fall under the Group I peptides, and methionine is known to be a hydrophobic residue. GRRE with a negatively charged C-terminus and GRRG with a small but relatively hydrophobic residue at P0 do not bind to PSMD9. These results indicate that P0 residue and not GRR is a major determinant of binding specificity in these peptides.

Compared to all peptides tested, the top ranking Group III peptides, SCG variants SCGF and SCGL bind with the highest affinity – K_d for the two peptides is four to five times less than the Group II peptides. The hydrophobicity of the C-terminal residue in SCGF and SCGL is clearly not important for binding and recognition as it can be readily replaced by a Gly. It seems that, in this set of peptides, the P−1, P−2 or P−3 residues are more important for high affinity interaction. By systematically deleting residues from the C-terminus, we identified Cys at P−2 position to be very important for interaction. In accordance with these results, peptide SGGF was unable to inhibit the interaction between GH and PSMD9.

It is clear that, in the absence of high resolution crystal structure of the complexes coupled with kinetic, thermodynamic studies using mutant peptides, it would be impossible to precisely define the molecular basis of affinity differences and positional occupancy of residues. In the absence of these details, we will have to consider different possibilities that may account for the binding preferences and affinity.

Reports from 20 complex structures of PDZ domains with C-terminal peptides of proteins indicate that the aminoacid at the P0 position has no specific conformational preference in the Ramachandran plot. In contrast the P−1, P−2 and P−3 residues show a strong preference and occupy either a strand or an extended conformation [43]. Such a conformational preference especially of the P−2 residue may explain the high affinity interaction seen with SCGX peptides. Alternatively, SCGF and SCGL peptides may mimic the internal sequences in proteins that bind PDZ domains and the Cys at P−2 may occupy the hydrophobic pocket formed by L153 and Phe 162 residues, mutations of which affect interaction. Flexibility in the binding modes is not uncommon to the peptide-PDZ domain interactions. For e.g., the P(−2) residue in some of the PDZ ligands are known to interact with αB-1 and αB-5 residues on the PDZ domain [43,44]. These residues normally interact with the P0 residues in the ligand. In the crystal structure of Dvl2 PDZ domain bound to a noncanonical C-terminal sequence, P−3 residue was seen to occupy the binding position utilized by a P−2 residue [45]. Secondary structure of the PSMD9 mutant proteins F162G (42%) and L153G (45%; very close to WT ∼48%) were not dramatically altered compared to other mutant proteins which bind the peptide (L173G 42%) or those that do not (Q181G 38%; Table 1).

Three modes of peptide binding to PDZ domains in proteins GRASP, PDLIM and MAST4 have been identified. In the structures of GRASP-peptide complexes, it is striking that the two chains of the protein bind to the same peptide in two different binding modes. Comparing these structures, a perpendicular mode, an intermediate mode – both speculated to be kinetic intermediates- and a stable canonical binding mode have been described [44]. We can draw parallels from these studies and propose the following: there exists a conformational ensemble of peptide-PSMD9 complexes. The Group I peptides, probably frequent the non-canonical or perpendicular orientation seen with other PDZ binding peptides. This orientation will rely heavily on the burial of the C-terminal residue for affinity. The Group II peptides GRRC and GRRR peptides probably frequent the intermediate population wherein the P0 residue is anchored. Peptides SCGF and SCGL populate the extended conformation in the canonical mode (although simulations propose a stable binding in the reverse orientation). The entropy cost of binding is probably paid for the SCGF and SCGL peptides as described for other protein derived C-terminal peptides bound to their cognate PDZ domain that may explain the high affinity interaction.

In our MD simulation studies, SCGF was unstable in the canonical binding mode but binds stably in a fully extended form, in the reverse orientation (Supplementary Fig. S3). Reverse binding modes of peptides have also been reported in literature, where the same peptide binds in opposite orientation i.e., N′–C′ or C′–N′ termini e.g., peptides binding to chaperone DnaK, Calmodulin and SH3 proteins [46–48]. If SCGF or SCGL peptides bind in a reverse orientation with the hydroxyl-group of the Ser residue substituting for the Phe carboxyl residue, mutation of F162 or L153 residues to Gly, will affect the binding, as seen in Supplementary Fig. S4. However, since the mutant peptide SGGF is unable to bind to PSMD9 or inhibit the binding of GH to PSMD9, the Ser residue seems unimportant for interaction. Therefore, binding of SCGF/L in the reverse orientation as a probable determinant of high affinity interaction seems less likely.

4.2. On the number of binding sites and the mechanism of binding

Mutation of the C-terminal Phe in GRRF, or Leu in GRRL or Met in AGHM, to Gly in the respective peptides or proteins inhibits interaction. Commensurate with these results, while GRRF competitively inhibits approximately 69% of the binding between hnRNPA1 and PSMD9 the mutant peptide GRRG, is unable to do so. However, substitution and even deletion of few C-terminal residues does not completely prevent binding of proteins. In all the cases, the fractional occupancy (like V_{max} in enzyme catalysis) is maximally affected by the C-terminal mutations while the affinity per se as determined by K_d (like Km for substrate binding) is less affected. In addition, the affinity differences between peptide or protein binding to PSMD9 is large. This difference is especially striking with the Group I peptides, the K_d of which are in the high μM range (∼600 μM) while the proteins bind with low micromolar affinity (1 μM). This vast discrepancy may be explained by the following: (a) C-terminal residues act primarily as signatures or bar codes that are read by the PDZ domain of PSMD9; (b) maximal affinity is contributed by a binding motif elsewhere in the protein or the binding of extended residues at the N-termini of the protein. Peptide affinity, however increases only marginally upon extension

of the N-terminal residues. For example, the nine residue C-terminal sequence of E12, with the tetrapeptide motif AGHM, interacts approximately two times more strongly than the short tetrapeptide AGHM (data not shown); and (c) the C-terminal sequences are stabilized by the structure of the full length protein. Based on these possibilities we propose a two state binding model for the interaction between PSMD9 and its client proteins – an initial weak recognition phase mediated by the C-terminal residues which act as specificity determinants followed by its consolidation via interaction of a secondary binding motif. Initial recognition of C-terminal residues in proteins by the PDZ domain may allow binding of the secondary site to an allosteric pocket on PSMD9 (Supplementary Fig. S5). These may or may not be accompanied by conformational changes in the proteins. The binding disparity between Group II peptides or the SCGF and SCGL peptides and their corresponding proteins although is much less (of the order of 8-fold), the fractional occupancy of the C-terminal deletion mutant, ΔCGF of GH is ∼45% of WT indicating that the same mechanism is probably operational. The plasticity of the PDZ domain and contribution of the overall structure to the binding is well illustrated in [31,49]. The partial loss in affinity upon mutations of residues present in different secondary structural elements of the PSMD9-PDZ domain is probably a reflection of the same paradigm.

It is also possible that the binding affinities are a reflection of the associated functions of the proteins. For example, we have demonstrated that hnRNPA1 acts as a novel shuttle receptor [7] that recruits IκBα for degradation by the proteasome. PSMD9 by interacting with hnRNPA1 and the 26S proteasome helps in anchoring IκBα and accelerating degradation. In this process, hnRNPA1 is likely to be recycled. By analogy, S14 may also act as a shuttle receptor that recruits proteins like MDM2 for degradation (Fig. 5B, see Section 4.3 for details) and must itself be released intact. Therefore, the C-terminus of these proteins may bind weakly to PSMD9. GH and IL6 receptors are the proposed direct substrates of the proteasome (Fig. 5D see Section 4.3 for details). In addition to the polyubiquitin binding, initial recognition of the C-terminal residues by PSMD9 with high affinity may be very important for the stable binding of such direct substrates to provide fatal directionality for degradation (Fig. 5D).

4.3. On the functional annotation of PSMD9 and its role in quality control by the proteasome

In this third part, we speculate on the probable regulatory role of PSMD9 by inferring on the role of its interacting partners. It is interesting that these proteins perform very different functions in the cell. At first glance, these interactions seem unusual, and the real physiological relevance may not be apparent. But detailed literature study provides substantial support for the plausible physiological role of these interactions in mammalian cells. hnRNPA1 is known to interact with IκBα in murine cells, and this interaction somehow accelerates degradation of IκBα resulting in NF-κB activation [50]. A possible functional conservation can be expected in human cells, and one may anticipate PSMD9 to regulate NF-κB signaling via IκBα degradation. In the manuscript that we published recently, we show that hnRNPA1 is a shuttle receptor that recruits IκBα for degradation and PSMD9 acts as a subunit acceptor and anchors hnRNPA1 to facilitate degradation of IκBα by the proteasome [7]. Association of proteasome with ribosome has been documented in the literature [51–53]. Whether S14 and PSMD9 interaction provides the structural scaffold for this interaction and what may be the functional consequence of this interaction in protein translation will be an interesting future investigation. In addition, S14 is known to bind to MDM2, which prevents the ability of this E3 ligase to ubiquitinate p53 thereby preventing proteasomal degradation of p53, leading to stabilization and activation of p53 [54]. Depending on whether or not the interaction between PSMD9 and S14, S14 and MDM2 are mutually exclusive, PSMD9 may influence ubiquitination, stability and functions of p53. By drawing a parallel from our studies on hnRNPA1 and PSMD9 interaction in IκBα degradation, we provide an alternate possibility for the fate of MDM2 and p53. We speculate that S14, similar to hnRNPA1 may also act as a shuttle receptor which recruits MDM2 for degradation by the proteasome (may be under similar stress conditions). Proteasome associated PSMD9 may anchor S14 (like it does hnRNPA1) to facilitate degradation of MDM2 (like IκBα) by the proteasome.

GRRR as mentioned before belongs to UPF2, yet another protein involved in RNA metabolism. UPF2 is part of a post-splicing multiprotein complex which regulate mRNA nuclear export and responsible for the detection of exported mRNAs with truncated open reading frames, resulting in nonsense-mediated mRNA decay [55].

Two other PSMD9 interacting partners GH (CHS1) and IL6 receptor are implicated in chemokine signaling [56,57]. However both GH and the IL6 receptor with SCGL at the C-termini created by alternate splicing are soluble, secreted proteins. In order to be exported out of the cell, these proteins must follow the ER-Golgi traffic [58]. Secreted proteins are inserted co-translationally into the ER lumen. Upon achieving their final folded state and post-translational modifications, these proteins are transported out of ER, through Golgi and finally out of the plasma membrane. However under stress or stimuli induced signaling, when the load on ER is more, quality control mechanisms must ensure that misfolded proteins are degraded. Misfolded and immature proteins are retro translocated by ER resident translocon and aided by ubiquitin or specialized proteins like Kar2p/BiP they are actively pulled out. These proteins are bound by the ER associated proteasomes and degraded [59–65]. Here, we speculate that while other ubiquitin binding proteins on the 19S regulatory complex of the proteasome may bind to the polyubiquitinated GH or IL6 as classically demonstrated for other proteins, PSMD9 would trap the misfolded GH or IL6R (and other such ERAD proteins) via the specific interaction of the PDZ domain with the respective C-terminal motif. Such interaction would prevent their premature release back into ER, ensure directionality and rapid clearance by the proteasome. Degradation is likely to occur at a basal rate as a routine quality control measure. The rate would be accelerated upon signal induction to truncate and attenuate the signaling process upon withdrawal of the stimuli or in response to ER stress. Therefore, PSMD9 may act as a general molecular chaperone that exerts quality control.

Soluble IL6R formed by splicing or proteolysis also bind to gp130 present on cells that lack the IL6 receptors. Soluble IL6R-IL6 complex is involved in what is called as the 'trans-signaling' an important mediator of inflammation and chemokine signaling in cancer [66]. Signaling may be attenuated by the receptor mediated endocytosis [67]. By binding to its receptor, GH may also follow receptor mediated endocytosis. The fate of such proteins engulfed by the process of endocytosis and how these may encounter the proteasome is described elegantly [60,68–71]. Some of these proteins routed by endocytosis may become shared substrates of the 'cytosolic' proteasomes and lysosomal enzymes. Different parts of the same sequence may be degraded by these degradation machineries. Our experiments designed to verify the binding of these proteins to PSMD9 in HEK293 cells upon co-expression is justified as these interactions are likely to be post endocytosis or post extraction events. Future lines of exciting studies include the characterization of the subcellular loci of these proteins and their ultimate and probably differential fate at the 'hands' of proteasome and lysosomes. GRRC belongs to endothelial receptor protein, yet another type I transmembrane protein, involved in signaling by EPCR [72].

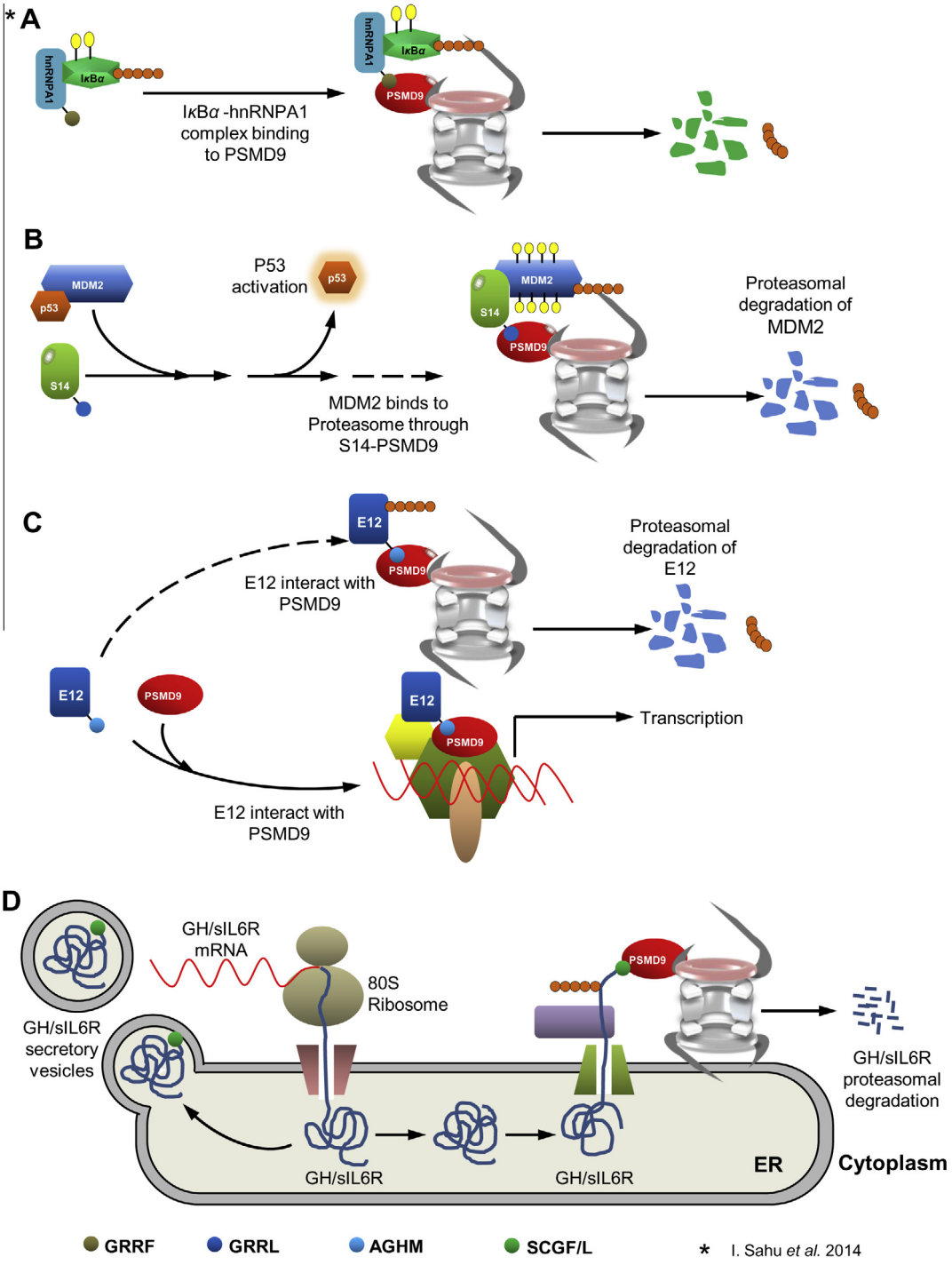

Fig. 5. Putative functional modules of PSMD9 and the probable role of PSMD9 in proteasome mediated quality control. (A) Role of PSMD9 in IκBα degradation. hnRNPA1 is assumed to be an adaptor protein or a shuttle receptor that recruits ubiquitinated IκBα to the proteasome by interacting with PDZ-PSMD9 via its C-terminus. PSMD9 acts as the subunit acceptor that helps to anchor IκBα via hnRNPA1. (B) Probable role of PSMD9 in regulating the stability of p53. S14 interacts with MDM2 and regulates the stability of p53. PSMD9 may modulate the ability of MDM2 to regulate p53 activity in two different ways (please see the Section 4 for details). (C) PSMD9-E12 interaction may be relevant for transcriptional coactivation/repression of many genes. PSMD9 may also play a regulatory role in proteasomal degradation of E12 to terminate transcription. (D) Model showing the probable role of PSMD9 in ER associated proteasomal degradation. Misfolded or aggregated secretory proteins like IL6 receptor and growth hormone are retro-translocated from ER and to ER associated proteasome for degradation. PSMD9 may help in anchoring the translocated substrate by capturing the C-terminal residues.

E12-PSMD9 interaction is likely to influence transcriptional regulation (like Bridge-1 in insulin signaling). PSMD9 may act either as a coactivator or as a repressor of many transcription events. Whether this regulatory role would involve 19S, or the entire 26S proteasome again or a proteasome independent role at the chromatin remains to be seen.

With all these examples, the grand or unifying role of PSMD9 seems to be to ensure quality control and regulate the magnitude of signaling or transcriptional programs (working model Fig. 5). The probable mechanism is likely to involve the proteasome and its proteolytic components. However, other regulatory steps involving an independent pool of PSMD9 and its interacting part-

ners within the protein–protein interaction network cannot be ruled out.

5. Conflict of interest

Authors declare that there is no conflict of interest.

Acknowledgements

The project was funded by Department of Science and Technology (DST), Government of India and Intra Mural Grant (IRG, ACTREC, TMC); N.S. acknowledges funding by the Department of Biotechnology, Government of India and A.K.S. by IRG no. 2691, ACTRC/TMC.

Appendix A.

$$f\mathrm{H} = ([\theta]_{222} - 3000)/(-36000 - 3000), \quad (1)$$

where fH is the fraction of helicity, $[\theta]_{222}$, where $[\theta]_{222}$ is the mean molar residual ellipticity at 222 nm (deg cm^2 d mol^{-1}).

Appendix B. Supplementary data

Supplementary data associated with this article can be found, in the online version, at http://dx.doi.org/10.1016/j.fob.2014.05.005.

References

[1] Glickman, M.H. and Ciechanover, A. (2002) The ubiquitin-proteasome proteolytic pathway: destruction for the sake of construction. Physiol. Rev. 82, 373–428.
[2] Groll, M. and Clausen, T. (2003) Molecular shredders: how proteasomes fulfill their role. Curr. Opin. Struct. Biol. 13, 665–673.
[3] Ravid, T. and Hochstrasser, M. (2008) Diversity of degradation signals in the ubiquitin-proteasome system. Nat. Rev. Mol. Cell Biol. 9, 679–690.
[4] Singh Gautam, A.K., Balakrishnan, S. and Venkatraman, P. (2012) Direct ubiquitin independent recognition and degradation of a folded protein by the eukaryotic proteasomes-origin of intrinsic degradation signals. PLoS One 7, e34864.
[5] Nanaware, P.P., Ramteke, M.P., Somavarapu, A.K. and Venkatraman, P. (2013) Discovery of multiple interacting partners of gankyrin, a proteasomal chaperone and an oncoprotein – evidence for a common hot spot site at the interface and its functional relevance. Proteins.
[6] Inostroza-Nieves, Y., Venkatraman, P. and Zavala-Ruiz, Z. (2012) Role of Sug1, a 19S proteasome ATPase, in the transcription of MHC I and the atypical MHC II molecules, HLA-DM and HLA-DO. Immunol. Lett. 147, 67–74.
[7] Sahu, I., Sangith, N., Ramteke, M., Gadre, R. and Venkatraman, P. (2014) A novel role for the proteasomal chaperone PSMD9 and hnRNPA1 in enhancing IkappaBalpha degradation and NF-kappaB activation – functional relevance of predicted PDZ domain-motif interaction. FEBS J..
[8] Pan, L., Yan, J., Wu, L. and Zhang, M. (2009) Assembling stable hair cell tip link complex via multidentate interactions between harmonin and cadherin 23. Proc. Natl. Acad. Sci. U.S.A. 106, 5575–5580.
[9] Sali, A. and Blundell, T.L. (1993) Comparative protein modelling by satisfaction of spatial restraints. J. Mol. Biol. 234, 779–815.
[10] Case, D. (2010). Amber 9. University of California Sanfrancisco.
[11] Dominguez, C., Boelens, R. and Bonvin, A.M. (2003) HADDOCK: a protein-protein docking approach based on biochemical or biophysical information. J. Am. Chem. Soc. 125, 1731–1737.
[12] Zacharias, M. (2003) Protein-protein docking with a reduced protein model accounting for side-chain flexibility. Protein Sci. 12, 1271–1282.
[13] Jorgensen, W. (1983) Comparison of simple potential functions for simulating liquid water. J. Chem. Phys. 79, 926–935.
[14] Duan, Y. et al. (2003) A point-charge force field for molecular mechanics simulations of proteins based on condensed-phase quantum mechanical calculations. J. Comput. Chem. 24, 1999–2012.
[15] Darden, T. (1993) Particle mesh Ewald: an N•log(N) method for Ewald sums in large systems. J. Chem. Phys. 98, 10089–10092.
[16] Miyamoto, S. (1992) Settle: an analytical version of the SHAKE and RATTLE algorithm for rigid water models. J. Comput. Chem. 13, 952–962.
[17] Humphrey, W., Dalke, A. and Schulten, K. (1996) VMD: visual molecular dynamics. J. Mol. Graph. 14 (33–8), 27–28.
[18] Fuh, G., Pisabarro, M.T., Li, Y., Quan, C., Lasky, L.A. and Sidhu, S.S. (2000) Analysis of PDZ domain-ligand interactions using carboxyl-terminal phage display. J. Biol. Chem. 275, 21486–21491.
[19] Sidhu, S.S., Fairbrother, W.J. and Deshayes, K. (2003) Exploring protein–protein interactions with phage display. ChemBioChem 4, 14–25.
[20] Sidhu, S.S. and Koide, S. (2007) Phage display for engineering and analyzing protein interaction interfaces. Curr. Opin. Struct. Biol. 17, 481–487.
[21] Stiffler, M.A., Grantcharova, V.P., Sevecka, M. and MacBeath, G. (2006) Uncovering quantitative protein interaction networks for mouse PDZ domains using protein microarrays. J. Am. Chem. Soc. 128, 5913–5922.
[22] Chen, J.R., Chang, B.H., Allen, J.E., Stiffler, M.A. and MacBeath, G. (2008) Predicting PDZ domain-peptide interactions from primary sequences. Nat. Biotechnol. 26, 1041–1045.
[23] Rodi, D.J., Makowski, L. and Kay, B.K. (2002) One from column A and two from column B: the benefits of phage display in molecular-recognition studies. Curr. Opin. Chem. Biol. 6, 92–96.
[24] Sharma, S.C., Memic, A., Rupasinghe, C.N., Duc, A.C. and Spaller, M.R. (2009) T7 phage display as a method of peptide ligand discovery for PDZ domain proteins. Biopolymers 92, 183–193.
[25] Tonikian, R. et al. (2008) A specificity map for the PDZ domain family. PLoS Biol. 6, e239.
[26] Chung, J.J., Yang, H. and Li, M. (2003) Genome-wide analyses of carboxyl-terminal sequences. Mol. Cell. Proteomics 2, 173–181.
[27] Thomas, M.K., Yao, K.M., Tenser, M.S., Wong, G.G. and Habener, J.F. (1999) Bridge-1, a novel PDZ-domain coactivator of E2A-mediated regulation of insulin gene transcription. Mol. Cell. Biol. 19, 8492–8504.
[28] Lee, J.H., Volinic, J.L., Banz, C., Yao, K.M. and Thomas, M.K. (2005) Interactions with p300 enhance transcriptional activation by the PDZ-domain coactivator Bridge-1. J. Endocrinol. 187, 283–292.
[29] Johnson, J.D. et al. (2006) Insulin protects islets from apoptosis via Pdx1 and specific changes in the human islet proteome. Proc. Natl. Acad. Sci. U.S.A. 103, 19575–19580.
[30] Lee, S.Y., De la Mota-Peynado, A. and Roelofs, J. (2011) Loss of Rpt5 protein interactions with the core particle and Nas2 protein causes the formation of faulty proteasomes that are inhibited by Ecm29 protein. J. Biol. Chem. 286, 36641–36651.
[31] Munz, M., Hein, J. and Biggin, P.C. (2012) The role of flexibility and conformational selection in the binding promiscuity of PDZ domains. PLoS Comput. Biol. 8, e1002749.
[32] Morrisett, J.D., David, J.S., Pownall, H.J. and Gotto Jr., A.M. (1973) Interaction of an apolipoprotein (apoLP-alanine) with phosphatidylcholine. Biochemistry 12, 1290–1299.
[33] Haendeler, J. et al. (2013) Two isoforms of Sister-Of-Mammalian Grainyhead have opposing functions in endothelial cells and in vivo. Arterioscler. Thromb. Vasc. Biol. 33, 1639–1646.
[34] Hakre, S., Tussie-Luna, M.I., Ashworth, T., Novina, C.D., Settleman, J., Sharp, P.A. and Roy, A.L. (2006) Opposing functions of TFII-I spliced isoforms in growth factor-induced gene expression. Mol. Cell 24, 301–308.
[35] Terada, N., Patel, H.R., Takase, K., Kohno, K., Nairn, A.C. and Gelfand, E.W. (1994) Rapamycin selectively inhibits translation of mRNAs encoding elongation factors and ribosomal proteins. Proc. Natl. Acad. Sci. U.S.A. 91, 11477–11481.
[36] Janin, J. (1979) Surface and inside volumes in globular proteins. Nature 277, 491–492.
[37] Wolfenden, R., Andersson, L., Cullis, P.M. and Southgate, C.C. (1981) Affinities of amino acid side chains for solvent water. Biochemistry 20, 849–855.
[38] Kyte, J. and Doolittle, R.F. (1982) A simple method for displaying the hydropathic character of a protein. J. Mol. Biol. 157, 105–132.
[39] Rose, G.D., Geselowitz, A.R., Lesser, G.J., Lee, R.H. and Zehfus, M.H. (1985) Hydrophobicity of amino acid residues in globular proteins. Science 229, 834–838.
[40] Das, U. et al. (2007) Inhibition of protein aggregation: supramolecular assemblies of arginine hold the key. PLoS One 2, e1176.
[41] Tsumoto, K., Ejima, D., Nagase, K. and Arakawa, T. (2007) Arginine improves protein elution in hydrophobic interaction chromatography. The cases of human interleukin-6 and activin-A. J. Chromatogr. A 1154, 81–86.
[42] Tsumoto, K., Abe, R., Ejima, D. and Arakawa, T. (2010) Non-denaturing solubilization of inclusion bodies. Curr. Pharm. Biotechnol. 11, 309–312.
[43] Lee, H.J. and Zheng, J.J. (2010) PDZ domains and their binding partners: structure, specificity, and modification. Cell Commun. Signal. 8, 8.
[44] Elkins, J.M., Gileadi, C., Shrestha, L., Phillips, C., Wang, J., Muniz, J.R. and Doyle, D.A. (2010) Unusual binding interactions in PDZ domain crystal structures help explain binding mechanisms. Protein Sci. 19, 731–741.
[45] Zhang, Y., Appleton, B.A., Wiesmann, C., Lau, T., Costa, M., Hannoush, R.N. and Sidhu, S.S. (2009) Inhibition of Wnt signaling by Dishevelled PDZ peptides. Nat. Chem. Biol. 5, 217–219.
[46] Zahn, M., Berthold, N., Kieslich, B., Knappe, D., Hoffmann, R. and Strater, N. (2013) Structural studies on the forward and reverse binding modes of peptides to the chaperone DnaK. J. Mol. Biol. 425, 2463–2479.
[47] Brokx, R.D., Lopez, M.M., Vogel, H.J. and Makhatadze, G.I. (2001) Energetics of target peptide binding by calmodulin reveals different modes of binding. J. Biol. Chem. 276, 14083–14091.
[48] Feng, S., Chen, J.K., Yu, H., Simon, J.A. and Schreiber, S.L. (1994) Two binding orientations for peptides to the Src SH3 domain: development of a general model for SH3-ligand interactions. Science 266, 1241–1247.
[49] Liu, J. et al. (2008) Conformational change upon ligand binding and dynamics of the PDZ domain from leukemia-associated Rho guanine nucleotide exchange factor. Protein Sci. 17, 1003–1014.

[50] Hay, D.C., Kemp, G.D., Dargemont, C. and Hay, R.T. (2001) Interaction between hnRNPA1 and IkappaBalpha is required for maximal activation of NF-kappaB-dependent transcription. Mol. Cell. Biol. 21, 3482–3490.
[51] Stavreva, D.A. et al. (2006) Potential roles for ubiquitin and the proteasome during ribosome biogenesis. Mol. Cell. Biol. 26, 5131–5145.
[52] Ding, Q., Dimayuga, E., Markesbery, W.R. and Keller, J.N. (2006) Proteasome inhibition induces reversible impairments in protein synthesis. FASEB J. 20, 1055–1063.
[53] Lopez, A.D., Tar, K., Krugel, U., Dange, T., Ros, I.G. and Schmidt, M. (2011) Proteasomal degradation of Sfp1 contributes to the repression of ribosome biogenesis during starvation and is mediated by the proteasome activator Blm10. Mol. Biol. Cell 22, 528–540.
[54] Zhou, X., Hao, Q., Liao, J., Zhang, Q. and Lu, H. (2013) Ribosomal protein S14 unties the MDM2-p53 loop upon ribosomal stress. Oncogene 32, 388–396.
[55] Maquat, L.E. and Serin, G. (2001) Nonsense-mediated mRNA decay: insights into mechanism from the cellular abundance of human Upf1, Upf2, Upf3, and Upf3X proteins. Cold Spring Harb. Symp. Quant. Biol. 66, 313–320.
[56] Mehrotra, S. et al. (2004) Antigen presentation by MART-1 adenovirus-transduced interleukin-10-polarized human monocyte-derived dendritic cells. Immunology 113, 472–481.
[57] Garzon, R., Soriano, S.F., Rodriguez-Frade, J.M., Gomez, L., Martin de Ana, A., Sanchez-Gomez, M., Martinez, A.C. and Mellado, M. (2004) CXCR4-mediated suppressor of cytokine signaling up-regulation inactivates growth hormone function. J. Biol. Chem. 279, 44460–44466.
[58] Corsi, A.K. and Schekman, R. (1996) Mechanism of polypeptide translocation into the endoplasmic reticulum. J. Biol. Chem. 271, 30299–30302.
[59] Bonifacino, J.S. and Weissman, A.M. (1998) Ubiquitin and the control of protein fate in the secretory and endocytic pathways. Annu. Rev. Cell Dev. Biol. 14, 19–57.
[60] Strous, G.J. and Govers, R. (1999) The ubiquitin-proteasome system and endocytosis. J. Cell Sci. 112 (Pt 10), 1417–1423.
[61] Mayer, T.U., Braun, T. and Jentsch, S. (1998) Role of the proteasome in membrane extraction of a short-lived ER-transmembrane protein. EMBO J. 17, 3251–3257.
[62] Lord, J.M. (1996) Go outside and see the proteasome. Protein Degrad. Curr. Biol. 6, 1067–1069.
[63] Christianson, J.C. and Ye, Y. (2014) Cleaning up in the endoplasmic reticulum: ubiquitin in charge. Nat. Struct. Mol. Biol. 21, 325–335.
[64] Hampton, R.Y. (2002) ER-associated degradation in protein quality control and cellular regulation. Curr. Opin. Cell Biol. 14, 476–482.
[65] Shamu, C.E., Story, C.M., Rapoport, T.A. and Ploegh, H.L. (1999) The pathway of US11-dependent degradation of MHC class I heavy chains involves a ubiquitin-conjugated intermediate. J. Cell Biol. 147, 45–58.
[66] Levine, S.J. (2004) Mechanisms of soluble cytokine receptor generation. J. Immunol. 173, 5343–5348.
[67] Jostock, T. et al. (2001) Soluble gp130 is the natural inhibitor of soluble interleukin-6 receptor transsignaling responses. Eur. J. Biochem. 268, 160–167.
[68] Ortiz-Lazareno, P.C. et al. (2008) MG132 proteasome inhibitor modulates proinflammatory cytokines production and expression of their receptors in U937 cells: involvement of nuclear factor-kappaB and activator protein-1. Immunology 124, 534–541.
[69] Peiretti, F., Canault, M., Bernot, D., Bonardo, B., Deprez-Beauclair, P., Juhan-Vague, I. and Nalbone, G. (2005) Proteasome inhibition activates the transport and the ectodomain shedding of TNF-alpha receptors in human endothelial cells. J. Cell Sci. 118, 1061–1070.
[70] Levine, S.J. et al. (2005) Proteasome inhibition induces TNFR1 shedding from human airway epithelial (NCI-H292) cells. Am. J. Physiol. Lung Cell. Mol. Physiol. 289, L233–L243.
[71] van Kerkhof, P., Alves dos Santos, C.M., Sachse, M., Klumperman, J., Bu, G. and Strous, G.J. (2001) Proteasome inhibitors block a late step in lysosomal transport of selected membrane but not soluble proteins. Mol. Biol. Cell 12, 2556–2566.
[72] Riewald, M. and Schuepbach, R.A. (2008) Protective signaling pathways of activated protein C in endothelial cells. Arterioscler. Thromb. Vasc. Biol. 28, 1–3.

the FEBS Journal

A novel role for the proteasomal chaperone PSMD9 and hnRNPA1 in enhancing IκBα degradation and NF-κB activation – functional relevance of predicted PDZ domain–motif interaction

Indrajit Sahu, Nikhil Sangith, Manoj Ramteke, Rucha Gadre and Prasanna Venkatraman

Advanced Center for Treatment, Research and Education in Cancer, Tata Memorial Centre, Kharghar, Navi Mumbai, India

Keywords
hnRNPA1; IκBα degradation; NF-κB activity; PDZ domain; PSMD9

Correspondence
P. Venkatraman, Advanced Center for Treatment, Research and Education in Cancer, Tata Memorial Centre, Kharghar, Navi Mumbai 410210, India
Fax: 022 27405085
Tel: 022 27405091
E-mail: vprasanna@actrec.gov.in

(Received 30 October 2013, revised 27 February 2014, accepted 9 April 2014)

doi:10.1111/febs.12814

PSMD9 is a PDZ domain containing chaperone of proteasome assembly. Based on the ability of PDZ-like domains to recognize C-terminal residues in their interactors, we recently predicted and identified heterogeneous nuclear ribonucleoprotein A1 (hnRNPA1) as one of the novel interacting partners of PSMD9. Contingent on the reported role of hnRNPA1 in nuclear factor κB (NF-κB) activation, we tested the role of human PSMD9 and hnRNPA1 in NF-κB signaling. We demonstrated in human embryonic kidney 293 cells that PSMD9 influences both basal and tumor necrosis factor α (TNF-α) mediated NF-κB activation through inhibitor of nuclear factor κB α (IκBα) proteasomal degradation. PSMD9 mediates IκBα degradation through a specific domain–motif interaction involving its PDZ domain and a short linear sequence motif in the C-terminus of hnRNPA1. Point mutations in the PDZ domain or deletion of C-terminal residues in hnRNPA1 disrupt interaction between the two proteins which has a direct influence on NF-κB activity. hnRNPA1 interacts with IκBα directly, whereas PSMD9 interacts only through hnRNPA1. Furthermore, hnRNPA1 shows increased association with the proteasome upon TNF-α treatment which has no such effect in the absence of PSMD9. On the other hand endogenous and trans-expressed PSMD9 are found associated with the proteasome complex. This association is unaffected by PDZ mutations or TNF-α treatment. Collectively, these interactions between IκBα, hnRNPA1 and proteasome bound PSMD9 illustrate a potential mechanism by which ubiquitinated IκBα is recruited on the proteasome for degradation. In this process, hnRNPA1 may act as a shuttle receptor and PSMD9 as a subunit acceptor. The interaction sites of PSMD9 and hnRNPA1 may emerge as a vulnerable drug target in cancer cells which require consistent NF-κB activity for survival.

Introduction

Mammalian PSMD9 is known to form a stable subcomplex with PSMC3 and PSMC6, two of the AAA-ATPases, assisting in the assembly of the 20S and 19S particles to form the holo complex [1,2]. Structurally PSMD9 contains an 88 amino acid long (108–195) PDZ-like domain [3]. Many PDZ domain containing

Abbreviations
CHX, cycloheximide; COX-2, cyclooxygenase-2; EMSA, electrophoretic mobility shift assay; HEK293 cells, human embryonic kidney 293 cells; hnRNPA1, heterogeneous nuclear ribonucleoprotein A1; ICAM-1, intercellular adhesion molecule 1; IL, interleukin; IP, immunoprecipitation; IκBα, inhibitor of nuclear factor κB α; MBP, maltose bonding protein; NF-κB, nuclear factor κB; PVDF, poly(vinylidene difluoride); shRNA, small hairpin RNA; SLIM, short linear sequence motif; TNF-α, tumor necrosis factor α; WB, western blot; wt, wild type.

proteins act as scaffolds to form supramolecular assemblies which allow them to function in signaling, mediating adhesive properties of cells, and in ion transport [4,5]. Bridge-1, the PSMD9 homolog in rats, has been shown to act as a coactivator of insulin gene transcription through interaction of its PDZ-like domain with transcription factors E12 and histone acetyl transferase, p300 [3,6]. In ovarian cells, changes in the levels of PSMD9 are known to alter activin signaling [7]. Overexpression of Bridge-1 increases pancreatic apoptosis with a reduction in the number of insulin-expressing β-cells leading to insulin deficiency and diabetes [8].

Based on the classical property of some PDZ domains to recognize 4–7 C-terminal residues or short linear sequence motifs (SLIMs) in proteins, we recently identified several novel interacting partners of PSMD9 (*FEBS Open Bio*, submitted). Such SLIMs have been identified as functionally relevant recognition motifs in SH2, SH3 domain containing proteins [9]. We recently showed that a 13 residue A-helix acts as an anchor while a floppy F-helix acts as an initiator of ubiquitin independent degradation of apomyoglobin by the proteasome [10]. We also identified novel interacting partners of gankyrin, a chaperone of the proteasome and an oncoprotein, by recognizing proteins which share EEVD, a conserved SLIM seen at the interface of gankyrin-S6 ATPase complex [11]. In addition we predicted the structure of the PDZ domain of PSMD9 and identified residues at the PDZ interface which are important for recognizing the C-terminal residues of four novel interacting partners (*FEBS Open Bio*, submitted). Heterogeneous nuclear ribonucleoprotein A1 (hnRNPA1), an RNA binding protein involved in mRNA export, splicing and protein translation, was one of the novel interacting partners. This protein in the mouse CB3 cells was reported to be responsible for inhibitor of nuclear factor κB α (IκBα) degradation by an unknown mechanism leading to transcriptional activation of nuclear factor κB (NF-κB) [12]. This observation formed the premise of this work which aims to establish the functional relevance of the newly found PSMD9–hnRNPA1 interaction.

NF-κB is a family of transcription factors that regulate expression of various genes involved in inflammatory, anti-apoptotic and immune responses [13,14]. The NF-κB family or the Rel family of proteins includes p50 (p105), p52 (p100), p65 (RelA), c-Rel and Rel-B [15,16]. If cells are not stimulated, heterodimeric NF-κB complexes remain in the cytoplasm, where they are associated with an inhibitory molecule of the IκB family [17]. In mammalian species, six structural homologs of IκB have been identified: IκBα, IκBβ, IκBε, IκBγ, Bcl-3 and IκBζ [18]. Among these, IκBα, the prototypical member of the IκB family, has been extensively studied. The canonical NF-κB p65/p50 heterodimer is largely, although not exclusively, found in complex with its inhibitor IκBα in cytoplasm. In response to stimulation by various agents such as phorbol esters (e.g. phorbol 12-myristate 13-acetate), pervanadate, tumor necrosis factor α (TNF-α), interleukin-1a (IL-1a), γ-radiation and lipopolysaccharide, IκBα undergoes phosphorylation by the IKK complex at Ser32, Ser36 and/or Tyr42 followed by polyubiquitination at Lys21 and Lys22 [19–22]. This leads to proteasomal degradation of the phosphorylated and ubiquitinated IκBα and nuclear translocation of free p50/p65, resulting in NF-κB transcription activity [13,19,23,24]. Apart from proteasomal degradation some reports suggest that in uninduced cells IκBα undergoes non-proteasomal, calcium dependent proteolysis resulting in high and consistent NF-κB activity [25–28]. Among the other IκB proteins, IκBβ, IκBε, p100 (precursors of p52) and p105 (precursors of p50) also undergo proteasomal degradation/endoproteolytic processing under induced and uninduced conditions [29–33]. Although the upstream processes of IκBα degradation are extensively deciphered, the detailed mechanism of proteasomal degradation is still not clear.

It is with this background that we were intrigued by the reports of Hay *et al*., who demonstrated interaction between ankyrin repeats of IκBα and hnRNPA1 which somehow seemed necessary for IκBα degradation and NF-κB transcriptional activity [12]. But the identity of the protease involved and the role of proteasome in this process were not established. Since the bigger and fundamental question of how IκBα is recruited to the proteasome for degradation remains largely unaddressed, it would be interesting to investigate whether hnRNPA1, well known for its role in mRNA processing and transport [34], cross-talks with the proteasomal degradation pathway in human cells. The mechanism by which ubiquitinated proteins are recruited to proteasome remains an active area of research. Based on our finding that PSMD9 interacts with hnRNPA1 *in vitro* (*FEBS Open Bio*, submitted) and the reported role of hnRNPA1 in IκBα degradation and NF-κB activity, we hypothesized that PSMD9 may have a role in the degradation of IκBα by the proteasome and influence NF-κB activity in human cells. Here we provide evidence that in human embryonic kidney 293 (HEK293) cells, PSMD9 through its PDZ domain interacts with the C-terminus of hnRNPA1 and this tripartite interaction subjects ubiquitinated IκBα to proteasomal degradation enhancing both basal and signal mediated NF-κB activity. By a series of experiments we identify a novel role for hnRNPA1 as a shuttle receptor that recruits IκBα for degradation and

recognizes PSMD9 as a novel subunit receptor on the proteasome. Our results demonstrate an atypical function of hnRNPA1 which seems to integrate into the ubiquitin proteasome pathway through a specific interaction with proteasome bound PSMD9. We speculate about the general role of this interaction and the utility of the PDZ domain interface as a potential drug target.

Results

PSMD9 interacts with the C-terminus of hnRNPA1

Using a bioinformatics approach (*FEBS Open Bio*, submitted) and the knowledge that some PDZ domains interact with C-terminal regions of proteins [5], we predicted putative interacting partners of PSMD9, from the human proteome. This prediction was validated by screening C-terminal peptides for their ability to bind to pure recombinant PSMD9. Using this strategy we identified hnRNPA1 as a novel interacting partner of PSMD9 and further proved that this interaction is mediated by the C-terminal residues of hnRNPA1 (*FEBS Open Bio*, submitted). To test if PSMD9 and hnRNPA1 interact endogenously, as this would be physiologically and functionally relevant, we used PSMD9 antibody to immunoprecipitate PSMD9 from HEK293 cell lysates and probed for the presence of hnRNPA1 using hnRNPA1 antibody. As expected, hnRNPA1 was found in the immunoprecipitation (IP) complex (Fig. 1A). We further validated this endogenous interaction by performing a reverse IP where hnRNPA1 antibody was used for IP and the complex was probed with PSMD9 antibody (Fig. 1B). We reconfirmed our earlier observation that only wild type (wt) hnRNPA1 and not the C-terminal mutant can interact with PSMD9 (Fig. 1C).

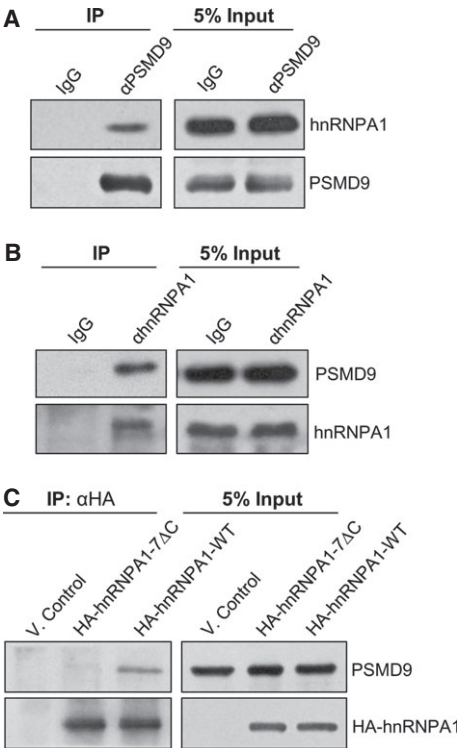

Fig. 1. PSMD9 interacts with wt-hnRNPA1 but not with the 7ΔC mutant of hnRNPA1 *ex vivo*. (A) HEK293 cell lysates were incubated either with PSMD9 antibody-bound Protein-G Sepharose beads or mouse IgG (isotype control) bound Protein-G Sepharose beads. Pull-down complexes were probed with hnRNPA1 and PSMD9 antibodies. (B) HEK293 cell lysates were incubated with either hnRNPA1 antibody-bound Protein-G Sepharose beads or mouse IgG isotype bound Protein-G Sepharose (isotype control). Then pull-down complexes were probed with PSMD9 and hnRNPA1 antibodies and analyzed by WB. (C) HA-wt-hnRNPA1 or 7ΔC mutant HA-hnRNPA1 was transiently overexpressed in HEK293 cells and cell lysates were incubated with HA antibody-bound Protein-G Sepharose beads. Pull-down complexes were probed with PSMD9 antibodies and analyzed by WB.

Overexpression of PSMD9 enhances basal and TNF-α mediated NF-κB activity

In CB3 cells, hnRNPA1 reportedly interacts with IκBα and overexpression of hnRNPA1 in these cells enhances NF-κB transcriptional activity [12]. No such role has been reported for hnRNPA1 in human cells. Since we found that PSMD9 interacts with hnRNPA1 *ex vivo* and hnRNPA1 reportedly influences NF-κB activity, we asked if PSMD9 was involved in this pathway. If so, changes in the levels of PSMD9 must influence NF-κB activity. PSMD9 was overexpressed under doxycycline inducible conditions in three different stable clones (Fig. 2A), and NF-κB transcriptional activity was measured by luciferase reporter assay. In all three inducible clones, NF-κB activity was found to be 3–4-fold higher than that of the uninduced control cells (Fig. 2B). In addition, we regulated the expression of PSMD9 using an inducible system in HEK293 cells (Fig. 2C) and found that doxycycline induced the expression of PSMD9 in a concentration dependent manner, which led to a corresponding increase in NF-κB transcriptional activity monitored using the luciferase reporter assay (Fig. 2D).

The influence of PSMD9 overexpression on NF-κB activity was further validated by demonstrating nuclear translocation of NF-κB (p65) and by electrophoretic mobility shift assay (EMSA). In PSMD9 overexpressing HEK293 cells, there was a significant increase in nuclear p65 in comparison with control cells (Fig. 2E). Upon

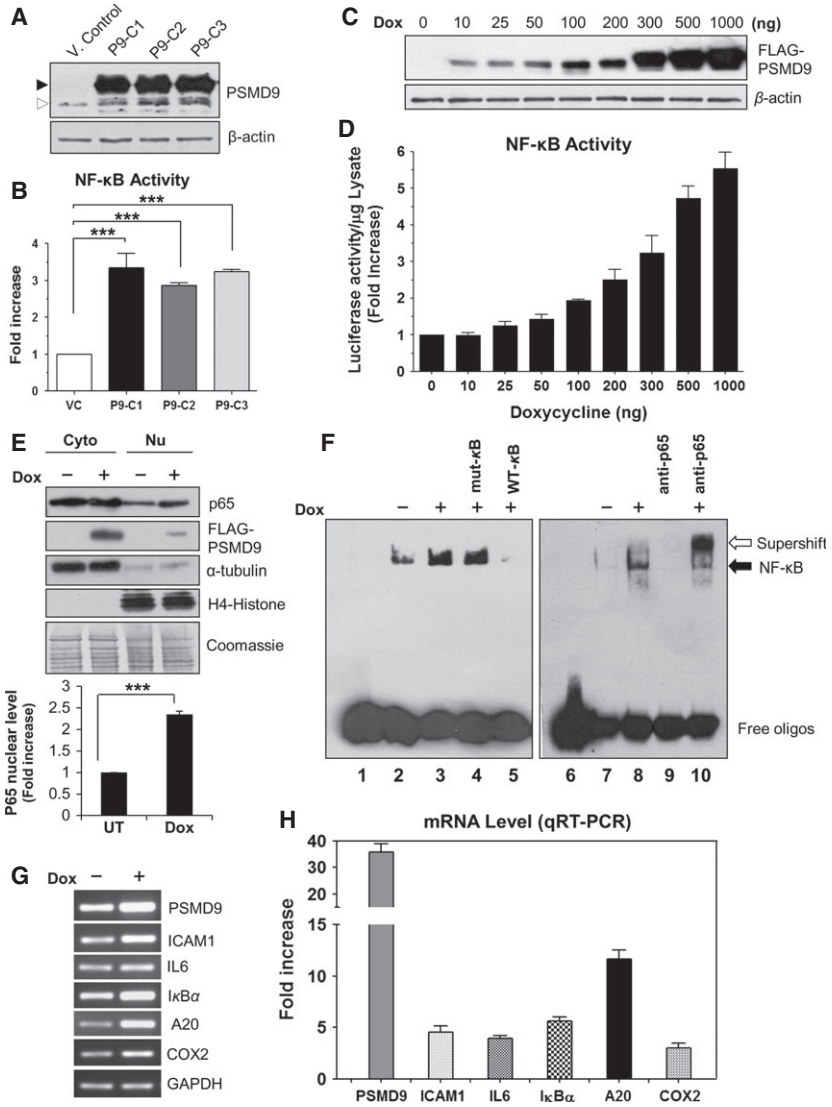

PSMD9 overexpression binding of NF-κB to the κB enhancer element was increased. This binding was competed out by unlabeled wt κB-oligos but not by mutant κB-oligos (Fig. 2F, lanes 4 and 5) [35]. Furthermore when the reaction mixture was incubated with p65 antibody, a supershift band was obtained which confirms the presence of p65 and its DNA binding activity (Fig. 2F, lane 10). In addition, five of the NF-κB target genes, namely intercellular adhesion molecule 1 (ICAM-1), IL-6, IκBα, A20 and cyclooxygenase-2 (COX-2) [36], were several-fold upregulated in PSMD9 overexpression cells compared with vector control cells (Fig. 2G,H). When doxycycline induced or uninduced cells were treated with TNF-α, a potent signal for NF-κB activation [37], both NF-κB DNA binding capacity and its transcriptional activity were increased. This increase was more pronounced in PSMD9 overexpressing cells (Fig. 3A,B, lane 5). These results suggest that PSMD9 is involved in both basal and the signal mediated NF-κB pathway.

PSMD9 overexpression increases NF-κB activity by enhancing degradation of IκBα by proteasome

In the classical NF-κB pathway, upon signal induction, NF-κB bound IκBα is degraded by the 26S proteasome. Since NF-κB activity increased with increase in the levels of PSMD9 in HEK293 cells (current study), we hypothesized that PSMD9 may accelerate the degradation of IκBα by the proteasome. Accordingly when PSMD9 expression was induced by doxycycline there was a visible decrease in IκBα protein after 4–6 h of cycloheximide (CHX) treatment, whereas in uninduced cells reduction in the levels of IκBα was

seen only after 18–24 h of treatment (Fig. 4A). Similarly signal mediated IκBα degradation was considerably enhanced 10 min post TNF-α treatment in cells induced to overexpress PSMD9 (Fig. 4B). These results indicate that PSMD9 is involved in modulating IκBα levels presumably through proteasomal degradation in both basal as well as the signal mediated NF-κB signaling pathway.

To determine the role of proteasome in PSMD9 mediated degradation of IκBα, we treated PSMD9 overexpressing HEK293 cells with proteasome inhibitors. Treatment with MG132 or Velcade significantly inhibited both basal and TNF-α mediated IκBα degradation in cells overexpressing PSMD9 (Fig. 4C,D). In further support of proteasomal degradation, ubiquitinated IκBα was also seen to accumulate when PSMD9 overexpressing cells were treated with the proteasomal inhibitors (Fig. 4C). It is well established that degradation of IκBα by the proteasome, upon signal induction, requires phosphorylation at sites S32 and S36 [13]. To determine whether the processing of IκBα occurs through the same way in the case of PSMD9 mediated degradation, we overexpressed IκBα super-repressor (S32A–S36A) in control cells as well as in PSMD9 overexpressing cells. After 30 min of TNF-α induction, super-repressor IκBα was not degraded even under PSMD9 overexpression conditions whereas endogenous IκBα got degraded significantly (Fig. 4E). In accordance with this, NF-κB activity is decreased significantly in the cells upon overexpression of the super-repressor irrespective of PSMD9 overexpression (Fig. 4F). These results indicate that the phosphorylation at S32 and S36 residues is necessary for the PSMD9 mediated IκBα degradation by the proteasome.

Endogenous PSMD9 is involved in basal and signal mediated activation of NF-κB and IκBα degradation

In order to demonstrate the role of endogenous PSMD9 in NF-κB activation, we knocked down PSMD9 in HEK293 cells using small hairpin RNA (shRNA) under inducible conditions. Upon knockdown of PSMD9, IκBα levels were found to be stable even after 24 h of CHX treatment (Fig. 5A). In the same cells, a reduction in TNF-α induced IκBα degradation was observed whereas in control cells IκBα degradation was already apparent after 20 min of TNF-α treatment (Fig. 5B). Concomitantly a decrease in NF-κB DNA binding activity was observed by EMSA both in TNF-α treated and untreated PSMD9 knockdown cells (Fig. 5C). This was further confirmed by semi-quantitative RT-PCR and real-time PCR of five different NF-κB target genes, namely ICAM-1, IL-6, IκBα, A20 and COX-2, the levels of which decreased in PSMD9 knockdown cells compared with control cells (Fig. 5D,E). These results indicate that endogenous PSMD9 is indeed responsible for the basal and signal induced degradation of IκBα and subsequent increase in NF-κB activity.

Fig. 2. Basal NF-κB activity increases upon PSMD9 overexpression in HEK293 cells. (A) Three clones of HEK293 cells inducibly expressing FLAG-PSMD9 were either treated with doxycycline or left untreated, and the cell lysates were analyzed by WB. (B) The above clones were transfected with 3x κB ConA luc vector or ConA luc control vector and induced with doxycycline (1 $\mu g \cdot mL^{-1}$ of medium). After 48 h of induction NF-κB activity was checked by measuring luciferase activity using dual luciferase substrate. Luciferase activity from firefly luciferase was normalized with renilla luciferase used as a transfection control. Data represent mean luciferase activity per microgram of protein ± SEM of two independent experiments done in triplicate. (C) HEK293 cells inducibly expressing FLAG-PSMD9 were transfected with 3x κB ConA luc vector or ConA luc control vector. Cells were induced with different concentrations (0–1000 $ng \cdot mL^{-1}$ of medium) of doxycycline. After 48 h of induction, levels of FLAG-PSMD9 were analyzed by WB. (D) NF-κB activity was checked by measuring luciferase activity of the above described (in C) cell lysates, using dual luciferase substrate. Luciferase activity from firefly luciferase was normalized with renilla luciferase used as a transfection control. Data represent mean luciferase activity per microgram of protein ± SEM of two independent experiments done in triplicate. (E) HEK293 cells inducibly expressing FLAG-PSMD9 were either treated with doxycycline (1 $\mu g \cdot mL^{-1}$ of medium for 48 h) or left untreated. Nuclear fractions were prepared as described in Materials and methods and analyzed by WB. The graph represents the mean fold increase of p65 nuclear translocation ± SEM of two independent experiments in three different stable clones. (F) HEK293 inducible FLAG-PSMD9 stable clones were either treated with doxycycline (1 $\mu g \cdot mL^{-1}$ of medium for 48 h) or left untreated. The nuclear fractions were subjected to EMSA (following the protocol described in Materials and methods). Lane 1 indicates biotinylated oligos only. The black arrow indicates NF-κB DNA binding activity in doxycycline untreated (lanes 2 and 7) and treated (lanes 3 and 8) cells. NF-κB DNA binding specificity is shown by competing it with 200× unlabeled mutant oligos (lane 4) or wt oligos (lane 5). In lanes 9 and 10 p65 antibody was incubated with the binding reaction mix (with/without lysate) and the white arrow indicates the resulting supershift band. (G) HEK293 inducible FLAG-PSMD9 stable clones either treated with doxycycline for 48 h or left untreated. RNA was isolated and semi-quantitative RT-PCR was performed for five different target genes; the PCR products were run in a 2% agarose gel. (H) Real-time PCR was performed for the same five different target genes. The graph represents glyceraldehyde-3-phosphate dehydrogenase (GAPDH) normalized mean fold increase in mRNA level of the genes ± SEM for three independent experiments done in duplicate.

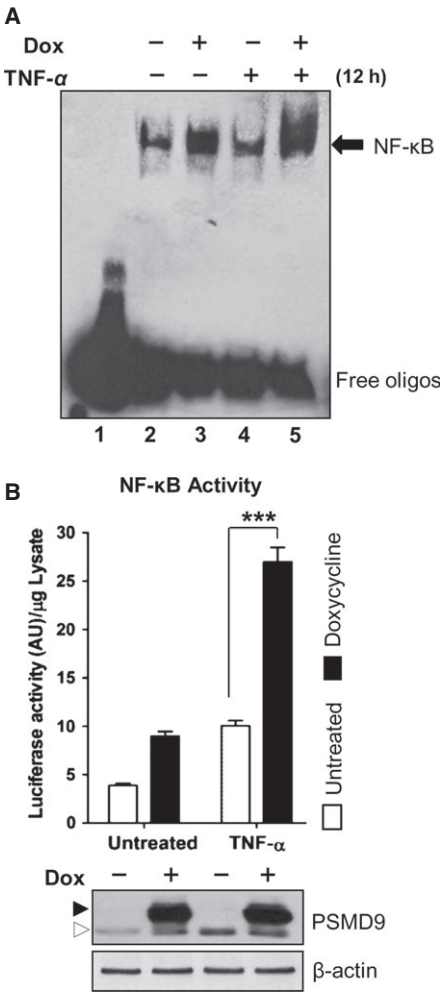

Fig. 3. TNF-α mediated NF-κB activity increases upon PSMD9 overexpression in HEK293 cells. (A) HEK293 inducible FLAG-PSMD9 stable clones were treated with doxycycline (1 $\mu g \cdot mL^{-1}$ of medium for 48 h) and/or with TNF-α (20 $ng \cdot mL^{-1}$ of medium for 12 h) or left untreated. The nuclear fractions were subjected to EMSA (following the protocol described in Materials and methods). Lane 1 indicates biotinylated oligos only. The black arrow indicates NF-κB DNA binding activity in doxycycline untreated (lanes 2 and 4) and treated (lanes 3 and 5) cells. Upon TNF-α treatment NF-κB DNA binding activity increased, shown by the thick gel shift band (in lanes 4 and 5). (B) HEK293 cells inducibly expressing FLAG-PSMD9 were transfected with 3x κB ConA luc vector or ConA luc control vector. Transfected cells were treated with doxycycline (1 $\mu g \cdot mL^{-1}$ of medium for 48 h) and/or with TNF-α for 12 h or left untreated. NF-κB activity was measured as described in Fig. 2B. Data represent mean luciferase activity per microgram of protein ± SEM of two independent experiments done in triplicate. WB shows the level of PSMD9 expression in these cell lysates. Symbol ▶ corresponds to trans-expressed FLAG-PSMD9 and ▷ symbol corresponds to the endogenous PSMD9.

PSMD9 does not affect the IκBα ubiquitination and proteasomal activity

Given its role as an assembly chaperone, PSMD9 expression may influence proteasomal activity which in turn may dictate the overall IκBα levels. We tested the activity of proteasome upon overexpression of PSMD9 and upon silencing the endogenous PSMD9. Proteasomal activity was unaltered in these cells and remained uninfluenced by TNF-α treatment (Fig. 6A). Our observation that PSMD9 does not influence proteasomal activity is in line with a previous report by Shim *et al.* [38]. Here similar to our method the authors used total cell lysates for monitoring proteasomal activity. In another study Keneko *et al.* showed that knocking down PSMD9 results in reduced proteasomal activity [1]. Here, in contrast to our method and those by Shim *et al.*, cell lysates were fractionated by glycerol gradient centrifugation and the fractions were monitored for proteasomal activity. Increase in proteasomal activity is seen in the presence of p27 modulator complex in reconstitution experiments involving subcomplexes of the proteasome [39]. The role of this modulator seems to involve rescue of improperly assembled or damaged 19S particles to ensure correct orientation of the ATPase rings [40].

Due to the importance of ubiquitination in IκBα degradation by the proteasome, we checked the requirement of PSMD9 in this process. We treated both doxycycline induced and uninduced cells with MG132 for 2 h followed by CHX treatment for 6, 12 and 24 h. The initial 2 h of MG132 treatment resulted in a 75% decrease in proteasomal activity. To ensure that after removal of MG132 and during the CHX treatment (used to follow degradation of ubiquitinated IκBα) proteasomes were functional, activity was monitored at every assay point. Then, 12 h following removal of MG132, proteasomal activity was restored almost completely both in PSMD9 knockdown cells and in control cells. Coincident with the time period of CHX treatment and upon PSMD9 gene silencing, levels of ubiquitinated IκBα did not change significantly. Rather an increased accumulation of ubiquitinated IκBα was seen in these PSMD9 knockdown cells. In control cells there was a clear decrease in levels of ubiquitinated IκBα (Fig. 6B). These results indicate that PSMD9 does not affect ubiquitination of IκBα and confirm that cells fail to degrade ubiquitinated IκBα efficiently not because of impaired proteasomal activity but due to the absence of PSMD9.

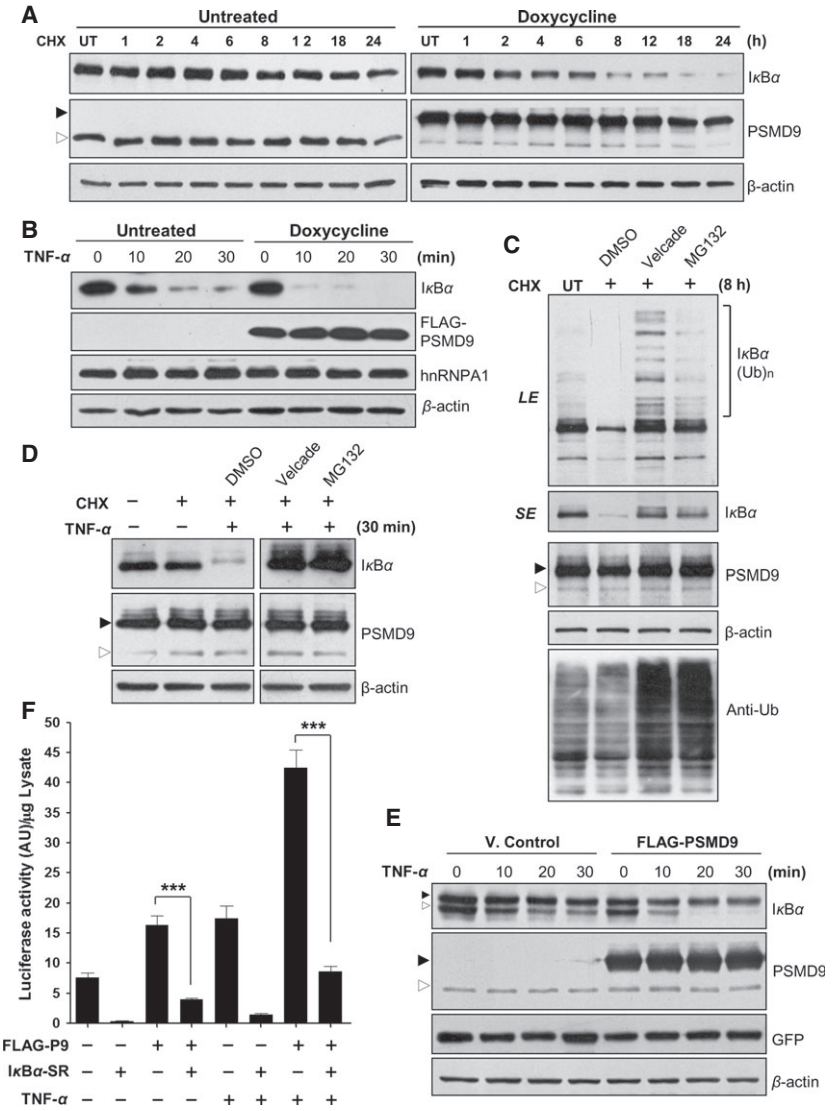

Fig. 4. PSMD9 overexpression accelerates basal and TNF-α mediated IκBα degradation. (A) HEK293 inducible FLAG-PSMD9 stable clones were treated with doxycycline (1 $\mu g \cdot mL^{-1}$ of medium for 48 h) and/or CHX (50 $\mu g \cdot mL^{-1}$ of medium for 1, 2, 4, 6, 8, 12, 18 and 24 h) or left untreated. Cell lysates were prepared and analyzed by WB. (B) Both doxycycline treated or untreated HEK293 inducible FLAG-PSMD9 stable clones were stimulated with TNF-α (20 $ng \cdot mL^{-1}$ of medium) for 0, 10, 20 and 30 min. Cell lysates were subjected to WB. (C) The above doxycycline induced stable clones were treated with CHX (50 $\mu g \cdot mL^{-1}$ of medium for 8 h) (where indicated) and with MG132 (10 μM), Velcade (10 $\mu g \cdot mL^{-1}$ of medium) or 0.1% dimethylsulfoxide for 6 h and analyzed by WB. LE, long exposure; SE, short exposure. At LE accumulation of polyubiquitinated IκBα is observed in the case of Velcade and MG132 treatment. (D) Cells were treated as described in (C) and either stimulated with TNF-α (20 $ng \cdot mL^{-1}$ of medium) for 30 min or left unstimulated and the lysates were analyzed by WB. Cropped image blots for each antibody are of the same exposure and from the same experiment, represented in a convenient manner. Symbol ► corresponds to trans-expressed FLAG-PSMD9 and symbol △ corresponds to the endogenous PSMD9. (E) HEK293 FLAG-PSMD9 stable clones and pCMV-10 empty vector stable clones were transiently co-transfected with pTRIPZ-IκBα-SR and pEGFPN3 vector. Cells were induced with doxycycline (1 $\mu g \cdot mL^{-1}$ of medium) for 48 h and treated with TNF-α (20 $ng \cdot mL^{-1}$ of medium) for 0, 10, 20 and 30 min. Cell lysates were prepared and analyzed by WB. Symbol ► corresponds to trans-expressed FLAG-IκBα-SR or FLAG-PSMD9 and symbol ▷ corresponds to the endogenous IκBα or PSMD9. (F) HEK293 FLAG-PSMD9 stable clones and pCMV-10 empty vector stable clones were co-transfected with pTRIPZ-IκBα-SR and 3x κB ConA luc vector or ConA luc control vector and induced with doxycycline (1 $\mu g \cdot mL^{-1}$ of medium). After 36 h of induction cells were treated with TNF-α (20 $ng \cdot mL^{-1}$ of medium) for 12 h. Cell lysates were prepared and NF-κB activity was measured as described in Fig. 2B. Data represent mean luciferase activity per microgram of protein ± SEM of two independent experiments done in duplicate.

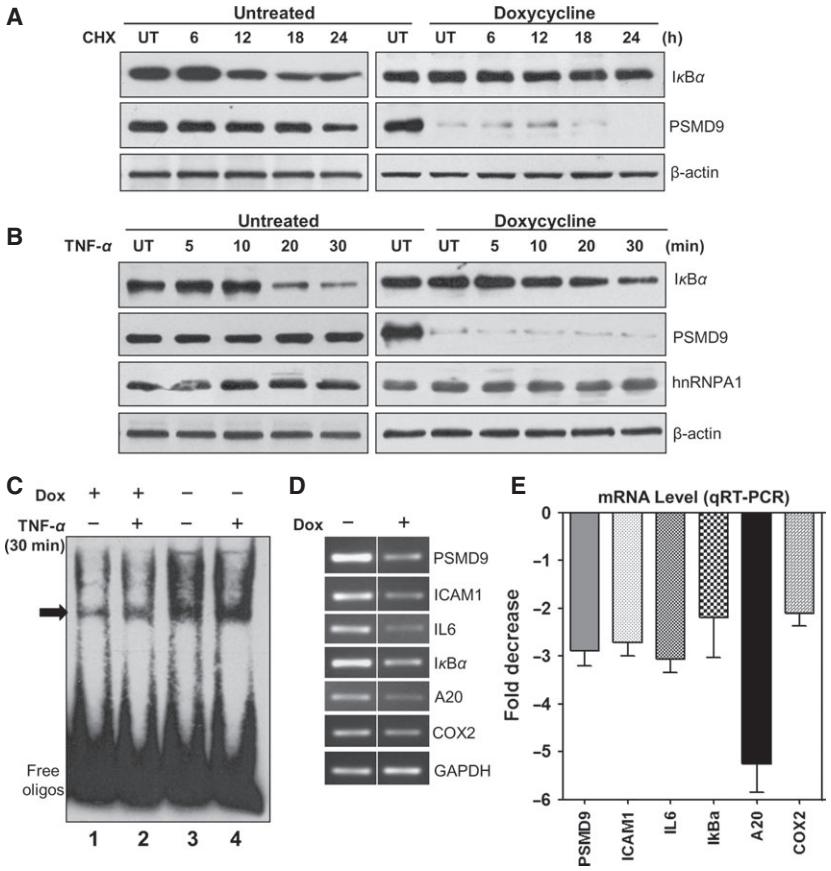

Fig. 5. PSMD9 knockdown reduces basal and TNF-α mediated IκBα degradation and NF-κB activation. (A) HEK293 inducible stable clones expressing PSMD9-shRNA were treated with doxycycline (4 $\mu g \cdot mL^{-1}$ of medium for 48 h) and/or CHX (50 $\mu g \cdot mL^{-1}$ of medium for 1, 2, 4, 6, 8, 12, 18 and 24 h) or left untreated. Cell lysates were prepared and analyzed by WB. (B) Both doxycycline treated or untreated PSMD9 knockdown inducible stable clones were stimulated with TNF-α (20 $ng \cdot mL^{-1}$ of medium) for 0, 5, 10, 20 and 30 min. Cell lysates were subjected to WB. (C) Nuclear fractions of both doxycycline and TNF-α treated or untreated PSMD9 knockdown stable inducible clones were subjected to EMSA. The upper band corresponds to NF-κB DNA binding activity in doxycycline positive (lanes 1 and 2) and doxycycline negative (lanes 3 and 4) cells. (D) PSMD9 knockdown inducible stable clones either treated with doxycycline for 48 h or left untreated. RNA was isolated and semi-quantitative RT-PCR was performed for five different target genes; the PCR products were run in a 2% agarose gel. (E) Real-time PCR was performed for the same five different target genes. The graph represents the glyceraldehyde-3-phosphate dehydrogenase (GAPDH) normalized mean fold decrease in mRNA level of the genes ± SEM for three independent experiments done in duplicate.

The PDZ domain of PSMD9 interacts with hnRNPA1

Point mutations in the PDZ domain of PSMD9 inhibit *in vitro* binding of hnRNPA1 (*FEBS Open Bio*, submitted). Since hnRNPA1 interacts with PSMD9 through its C-terminal residues, this interaction represents a typical PDZ domain–motif interface. We checked if this domain–motif recognition is also a key determinant of interaction inside the cells. We recently showed that Q181G and the β2 L124G/Q126G/E128G triple mutant (all in the PDZ domain) abolished interaction with PSMD9 while L173G (also in the PDZ domain) did not affect binding (*FEBS Open Bio*, submitted). To check the functional relevance of these mutations, we overexpressed FLAG-tagged wt-PSMD9, Q181G-PSMD9, L173G-PSMD9 or the β2 L124G/Q126G/E128G triple mutant in HEK293 cells. Endogenous hnRNPA1 was immunoprecipitated from each cell lysate and probed with FLAG antibody. In accordance with the *in vitro* pull-down assays, wt-PSMD9 and L173G-PSMD9 were detected in the IP complexes. However, neither the Q181G mutant nor the triple mutant of PSMD9 could be detected in these IP complexes (Fig. 7A).

Presence of IκBα was tested in the IP complex from cell lysates of HEK293 cells overexpressing wt-PSMD9, Q181G or the β2 L124G/Q126G/E128G triple mutant. IκBα was detected only in the wt-PSMD9–hnRNPA1

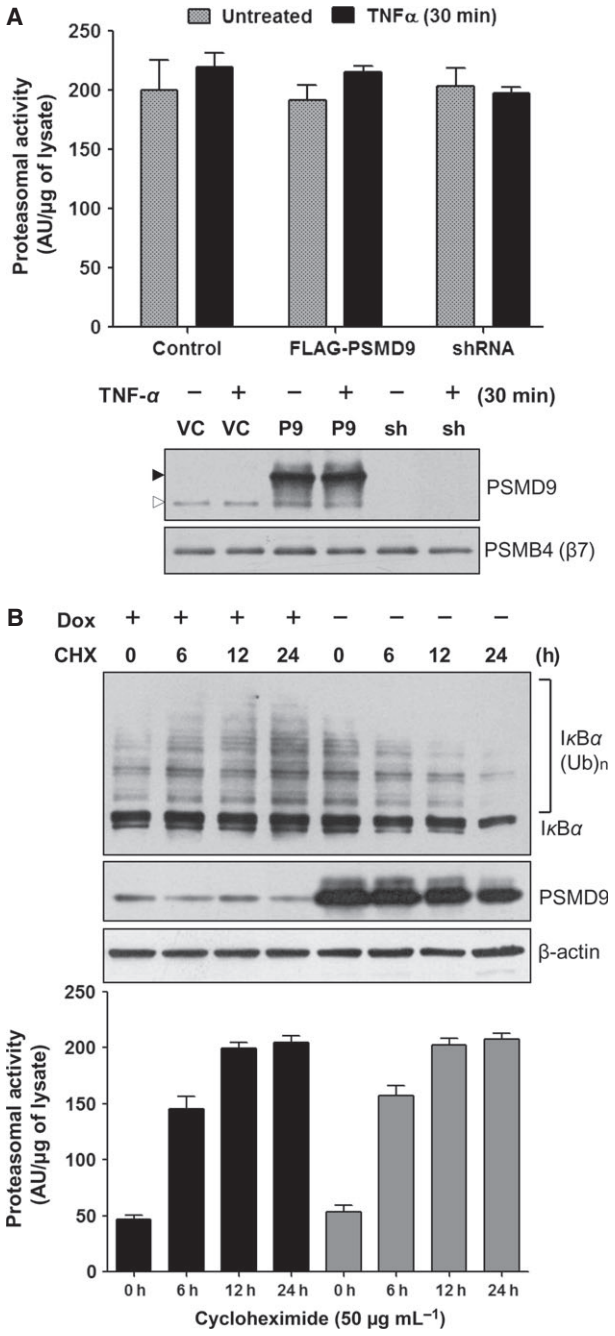

Fig. 6. PSMD9 does not affect proteasomal activity and IκBα ubiquitination. (A) Both the overexpression (FLAG-PSMD9) and knockdown (shRNA) HEK293 inducible stable clones of PSMD9 were treated with doxycycline for 48 h and/or with TNF-α (20 μg·mL^{-1} of medium) for 30 min or left untreated. Cell lysates were prepared with ATP buffer as described in Materials and methods. Proteasomal activity was measured as described in Materials and methods. The Control panel in the graph represents the average value of doxycycline untreated control cells of both the stable clones. Data represent Suc-LLVY-AMC proteasomal activity in arbitrary units (AU·μg^{-1} of lysate) ± SEM of two independent experiments done in duplicate. The WB shows the level expression of PSMD9 in the above cell lysates and PSMB4 is taken as the loading control. Symbol ▶ corresponds to trans-expressed FLAG-PSMD9 and symbol ▷ corresponds to the endogenous PSMD9. (B) HEK293 inducible stable clones expressing PSMD9-shRNA were either treated with doxycycline (4 μg·mL^{-1} of medium for 48 h) or left untreated. In addition cells were treated with MG132 (5 μM) for 2 h followed by treatment with CHX (50 μg·mL^{-1} of medium) for 0, 6, 12 and 24 h. Cell lysates were prepared and analyzed by WB. The graph represents the proteasomal activity, measured as described in Materials and methods, of cells for the above experimental conditions.

complex but not in PDZ Q181G and β2 L124G/Q126G/E128G triple mutant IP complexes (Fig. 7B) suggesting that PSMD9 is probably linked to IκBα through hnRNPA1. Unlike cells overexpressing wt-PSMD9, in cells overexpressing PDZ mutants (Q181G and the β2 triple mutant) IκBα was not efficiently degraded even after TNF-α treatment (Fig. 7C) nor was there a significant change in NF-κB activity (Fig. 7D). In addition, properties of L173G PSMD9 mutant were similar to those of wt-PSMD9 and cells expressing this mutant showed faster IκBα degradation and enhanced NF-κB activation (Fig. 7E,F). These results confirm that specific residues on the PDZ domain of PSMD9 form the interface for binding hnRNPA1 and this domain–motif interaction plays an important role in the NF-κB activation pathway.

PSMD9 is linked to IκBα via hnRNPA1

hnRNPA1 was previously shown to interact with IκBα through its RNA binding domain [12]. We demonstrated that PSMD9 interacted with hnRNPA1 through its C-terminus. And the PDZ mutation analysis indicates that the interaction between PSMD9 and IκBα is probably through hnRNPA1. To determine the structural hierarchy of this tripartite interaction between PSMD9, hnRNPA1 and IκBα, we performed both *ex vivo* and *in vitro* interaction studies. We first verified whether interaction of hnRNPA1 with PSMD9 and IκBα is mutually exclusive or not. When HA-tagged wt-hnRNPA1 and CΔ7hnRNPA1 mutant were pulled down, IκBα was detected in both the pull-down complexes (Fig. 8A) suggesting that C-terminus deletion of hnRNPA1 does not affect its interaction with IκBα. In contrast, PSMD9 was found only in the wt-hnRNPA1–IκBα complex. As inferred from the failure of PDZ mutants to interact with IκBα in the absence of hnRNPA1, these results suggest that wt-PSMD9 and IκBα interaction is indirect and is through hnRNPA1. To further validate these

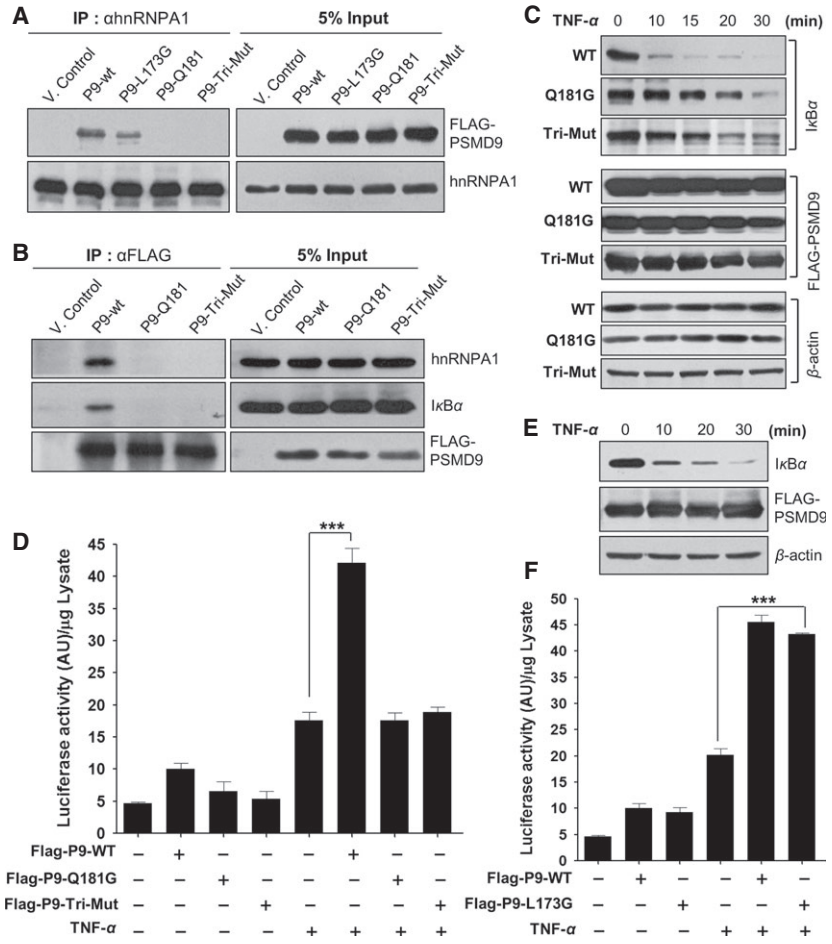

Fig. 7. The PDZ domain of PSMD9 is important for NF-κB activation and IκBα degradation. (A) HEK293 cells were transiently transfected with p3xFLAG-CMV-10-PSMD9, p3xFLAG-CMV-10-PSMD9(L173G), p3xFLAG-CMV-10-PSMD9(triple mutant) or p3xFLAG-CMV-10-PSMD9 (Q181G). Endogenous hnRNPA1 was immunoprecipitated from the cell lysates of the above transfected cells, probed with FLAG antibody and analyzed by WB. (B) HEK293 cells were transiently transfected with p3xFLAG-CMV-10 empty vector/p3xFLAG-CMV-10-wt-PSMD9/ p3xFLAG-CMV-10-PSMD9(Q181G)/p3xFLAG-CMV-10-PSMD9(triple mutant). Cell lysates were incubated with anti-FLAG M2 agarose beads and pull complexes were probed with hnRNPA1, IκBα, FLAG antibodies and analyzed by WB. (C) HEK293 cells were transiently transfected with p3xFLAG-CMV-10-PSMD9/p3xFLAG-CMV-10-PSMD9(Q181G)/p3xFLAG-CMV-10-PSMD9 (triple mutant). After 48 h of transfection cells were treated with TNF-α (20 ng·mL^{-1} of medium) for 10, 15, 20, 30 min or left untreated. Cell lysates were prepared and analyzed by WB. (D) HEK293 cells were co-transfected with p3xFLAG-CMV-10 empty vector or p3xFLAG-CMV-10-PSMD9 (wt, Q181G, triple mutant) and 3x κB ConA luc vector or ConA luc control vector. After 36 h cells were either treated with TNF-α (20 ng·mL^{-1} of medium) for 12 h or left untreated. Cell lysates were prepared and NF-κB activity was measured as described in Fig. 2B. Data represent mean luciferase activity per microgram of protein ± SEM of two independent experiments done in duplicate. (E) HEK293 cells were transiently transfected with p3xFLAG-CMV-10-PSMD9(L173G). After 24 h of transfection cells were treated with TNF-α (20 ng·mL^{-1} of medium) for 12 h or left untreated. Cell lysates were prepared and analyzed by WB. (F) HEK293 cells were co-transfected with p3xFLAG-CMV-10 empty vector or p3xFLAG-CMV-10-PSMD9 (wt or L173G) and 3x κB ConA luc vector or ConA luc control vector. After 36 h cells were either treated with TNF-α (20 ng·mL^{-1} of medium) for 12 h or left untreated. Cell lysates were prepared and NF-κB activity was measured as described in Fig. 2B. Data represent mean luciferase activity per microgram of protein ± SEM of two independent experiments done in duplicate.

observations we overexpressed both the FLAG-tagged wt-IκBα and C-terminal deleted IκBα (amino acids 253–372) in HEK293 cells. As discussed above, C-terminal residues in the ankyrin repeats of murine IκBα are necessary for interaction with hnRNPA1 [12]. When we pulled down the overexpressed FLAG-tagged IκBα, PSMD9 was found in the pull-down complex of wt protein where hnRNPA1 was present and not in the mutant IκBα (which does not interact with hnRNPA1) complex (Fig. 8B). This suggests that

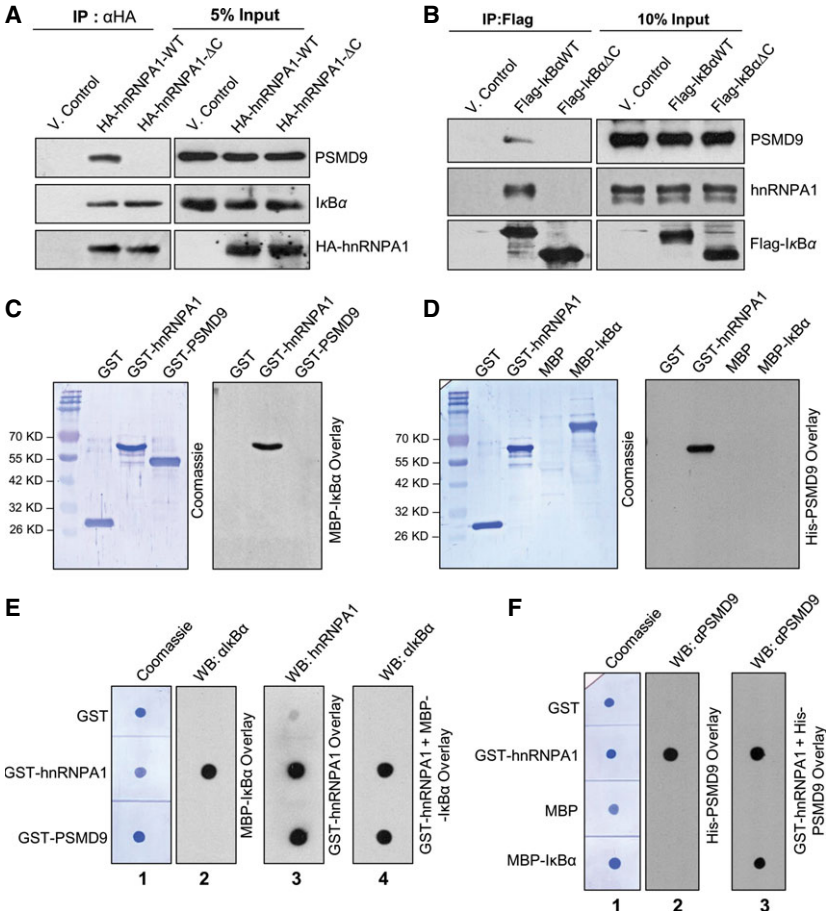

Fig. 8. PSMD9 is linked to IκBα via hnRNPA1. (A) HA-wt-hnRNPA1 and 7ΔC mutant HA-hnRNPA1 were transiently overexpressed in HEK293 cells and cell lysates were incubated with HA antibody-bound Protein-G Sepharose beads. Pull-down complexes were probed with PSMD9 and IκBα antibodies and analyzed by WB. (B) HEK293 cells were transfected with p3xFLAG-CMV-10-wt-IκBα p3xFLAG-CMV-10-ΔCIκBα and cell lysates were incubated with anti-FLAG M2 agarose beads. The pull-down complexes were probed with PSMD9, hnRNPA1 and IκBα antibodies and analyzed by WB. (C) 2 μg of recombinant GST, GST-hnRNPA1 and GST-PSMD9 proteins were run on SDS/PAGE, transferred onto a PVDF membrane and the proteins on the membrane were denatured/renatured using guanidine-HCl AP buffer. Then the membrane was overlaid with recombinant MBP-IκBα (100 nM), probed with IκBα antibody and analyzed by WB. (D) 2 μg of recombinant GST, GST-hnRNPA1 MBP and MBP-IκBα proteins were run on SDS/PAGE, transferred onto a PVDF membrane and the proteins were denatured/renatured on the membrane using guanidine-HCl AP buffer. Then the membrane was overlaid with recombinant His-PSMD9 (100 nM), probed with PSMD9 antibody and analyzed by WB. (E) 1 μg of recombinant GST, GST-hnRNPA1 and GST-PSMD9 proteins were spotted on equilibrated PVDF membrane, blocked with 3% BSA-TBST. The membranes were overlaid with recombinant MBP-IκBα (100 nM) and probed with IκBα antibody (panel 2); overlaid with GST-hnRNPA1 (100 nM) and probed with hnRNPA1 antibody (panel 3); overlaid with both GST-hnRNPA1 (100 nM) and MBP-IκBα (100 nM) and probed with IκBα antibody (panel 4). Panel 1 corresponds to the respective Coomassie stained protein spots on the membrane. (F) 1 μg of recombinant GST, GST-hnRNPA1 MBP and MBP-IκBα proteins were spotted on equilibrated PVDF membrane, blocked with 3% BSA-TBST. The membranes were overlaid with recombinant His-PSMD9 (100 nM) (panel 2) or with both GST-hnRNPA1 (100 nM) and His-PSMD9 (100 nM) (panel 3). Panel 1 corresponds to the respective Coomassie stained protein spots on the membrane.

the interaction between IκBα and PSMD9 is mediated by hnRNPA1.

We performed a series of far western or overlay experiments to substantiate these observations. Recombinant glutathione *S*-transferase (GST) PSMD9 and GST-hnRNPA1 were immobilized on a poly (vinylidene difluoride) (PVDF) membrane followed by overlay of recombinant maltose binding protein (MBP)-IκBα protein and were then probed with IκBα antibody. No IκBα was detected in the GST-PSMD9 lane but it was clearly visible in the GST-hnRNPA1 lane (Fig. 8C). Furthermore, when MBP-IκBα and GST-hnRNPA1 were immobilized on a PVDF membrane, overlaid with His-PSMD9 followed by probing

with PSMD9 antibody, PSMD9 was clearly detected in the GST-hnRNPA1 lane but not in the MBP-IκBα lane (Fig. 8D). In a sandwich dot blot assay, we immobilized GST-PSMD9 on the membrane, followed by overlay with GST or GST-hnRNPA1 and then with MBP-IκBα. When this sandwich was probed with IκBα antibody, MBP-IκBα was found to interact with GST-PSMD9 only when hnRNPA1 was sandwiched in between these two proteins (Fig. 8E). Furthermore, this indirect interaction was validated by reversing the sandwich, i.e. by immobilizing MBP-IκBα and overlay of GST or GST-hnRNPA1 followed by GST-PSMD9 (Fig. 8F). These results altogether confirmed that there is no direct interaction between PSMD9 and IκBα and they can only interact through hnRNPA1, which uses different structural regions for these interactions that are not mutually exclusive.

Interaction between C-terminus of hnRNPA1 and PSMD9 is required for degradation of IκBα as well as NF-κB activity

The involvement of hnRNPA1 in IκBα degradation was shown previously [12]. We have demonstrated here a novel role of PSMD9 and a specific interaction between the PDZ domain of PSMD9 and a SLIM at the C-terminus of hnRNPA1. We asked if hnRNPA1 has any role to play in IκBα degradation/NF-κB activation when interaction with PSMD9 is lost or in the absence of PSMD9. When HA-wt-hnRNPA1 was trans-expressed in HEK293 cells, degradation of IκBα was considerably enhanced after 10 min of TNF-α treatment (Fig. 9A). HA-7ΔChnRNPA1 mutant, on the other hand, had no influence on the degradation of IκBα. Correspondingly, only the HA-wt-hnRNPA1

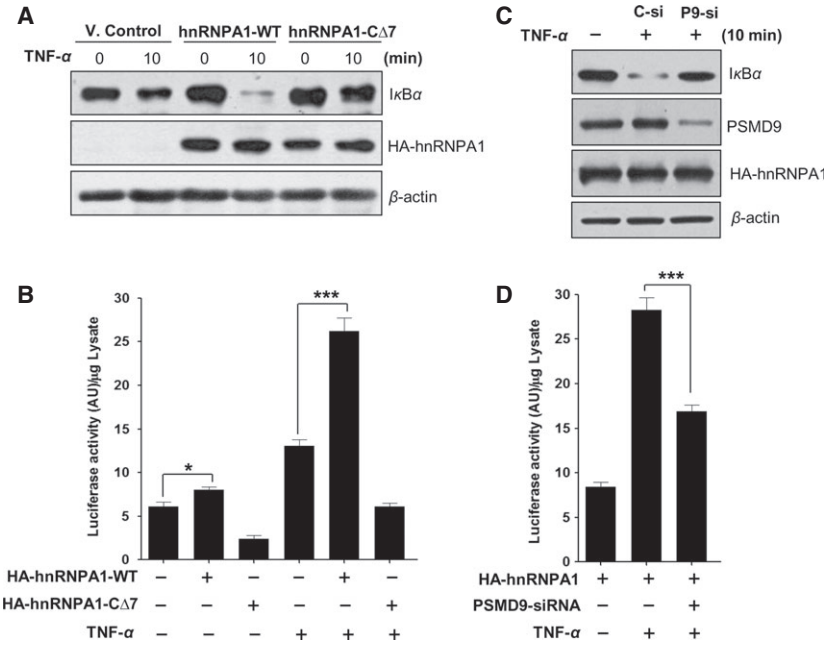

Fig. 9. C-terminus deleted hnRNPA1 mutant fails to enhance TNF-α mediated IκBα degradation and NF-κB activation. (A) HA-wt-hnRNPA1 and 7ΔC mutant HA-hnRNPA1 were transiently overexpressed in HEK293 cells and after 48 h cells were treated with TNF-α (20 ng·mL^{-1} of medium) for 10 min or left untreated. Cell lysates were prepared along with vector control and subjected to WB analysis. (B) HEK293 cells were co-transfected with pCDNA3.1-HA-empty vector or pCDNA3.1-HA-hnRNPA1 (wt or 7ΔC mutant) and 3x κB ConA luc vector or ConA luc control vector. After 36 h cells were either treated with TNF-α (20 ng·mL^{-1} of medium) for 12 h or left untreated. Cell lysates were prepared and NF-κB activity was measured as described in Fig. 2B. Data represent mean luciferase activity per microgram of protein ± SEM of three independent experiments done in duplicate. (C) HEK293 cells were transfected with PSMD9-siRNA/control-siRNA (100 μM) and after 48 h cells were again transfected with pCDNA3.1-HA-wt-hnRNPA1. After 72 h of siRNA transfection cells were either treated with TNF-α (20 ng·mL^{-1} of medium) for 20 min or left untreated. Cell lysates were prepared and analyzed by WB. (D) HEK293 cells were transfected with PSMD9-siRNA/control-siRNA (100 μM) and after 48 h cells were again transfected with pCDNA3.1-HA-wt-hnRNPA1 and 3x κB ConA luc vector or ConA luc control vector. After 60 h of siRNA transfection cells were either treated with TNF-α (20 ng·mL^{-1} of medium) for 12 h or left untreated. Cell lysates were prepared and NF-κB activity was measured as described in Fig. 2B. Data represent mean luciferase activity per microgram of protein ± SEM of two independent experiments done in duplicate.

transfected cells showed a significant increase in NF-κB activity after TNF-α treatment (Fig. 9B). In contrast, cells expressing HA-7ΔChnRNPA1 mutant showed a lower NF-κB activity compared with the control cells. Furthermore, when we silenced PSMD9 and overexpressed HA-wt-hnRNPA1, TNF-α mediated IκBα degradation was significantly reduced (Fig. 9C). In addition, a considerable decrease (up to 40%) in NF-κB activity was also observed in these cells (Fig. 9D). These results suggest that both PSMD9 and hnRNPA1 are in the same pathway and further support the role of PSMD9–hnRNPA1interaction in IκBα degradation and NF-κB activation.

PSMD9 anchors hnRNPA1–IκBα complex on 26S proteasome which facilitates proteasomal degradation of IκBα

PSMD9 is known to be a chaperone of proteasome assembly and is reported to dissociate before the mature complex [1,2,41]. Nas2, the yeast homolog, was not found in any of the cryo EM studies of the proteasome [42–44]. Like other classical chaperones, PSMD9 or its homologs may only be transiently associated with the assembled proteasome. We hypothesized that PSMD9, by virtue of its interaction with the proteasome on one hand and its interaction with hnRNPA1 on the other, would recruit IκBα to the proteasome for degradation. We first asked if endogenous or trans-expressed FLAG-PSMD9 could be located in the proteasome complex. We pulled down the whole 26S proteasomal complex using β7-subunit antibody. When probed for PSMD9 antibody we found both endogenous and FLAG-tagged PSMD9 in the complex. To ensure that PSMD9 is associated with the intact 26S mature complex, we probed the complex for the presence of ATPase subunit (Rpt6), a marker for the base subcomplex, and α5-subunit, a marker of 20S core particle. The results showed that β7-subunit antibody pulls down the intact 26S complex and PSMD9 is indeed associated with the mature proteasome (PSMD9 is not shown to interact with Rpt6). TNF-α treatment did not alter the levels of either endogenous or overexpressed PSMD9 in stable clones. But there was a definite increase in the levels of proteasome bound hnRNPA1 in PSMD9 overexpressing cells which were further enhanced upon TNF-α treatment (Fig. 10A). In contrast, when PSMD9 was silenced, no hnRNPA1 was found in the proteasome pull-down complex even after TNF-α treatment. These results together indicate that recruitment of hnRNPA1 to the proteasome requires the presence of PSMD9.

To enable the degradation of IκBα by the proteasome, PSMD9 not only has to interact with hnRNPA1 but should also interact with the proteasome as demonstrated above. However, based on current evidence PSMD9 seems to harbor only the PDZ-like domain for protein–protein interaction. Therefore it was important to test whether the PDZ mutations affect association of PSMD9 with the proteasome. Affinity pull-down of the 26S proteasome in cells overexpressing PDZ mutant Q181G indicated that this association was unimpaired (Fig. 10B). Proteasomal activity was also unaffected by this mutant (Fig. 10C). Probably there are other regions in PSMD9 that can interact with the proteasome. Although PSMD9 mutants cannot bind to hnRNPA1 because of the endogenous PSMD9, some hnRNPA1 could still be detected in the pull-down complex (Fig. 10B). These results further validate the role of the PDZ domain in proteasomal degradation of IκBα through interaction of PSMD9 with hnRNPA1. In addition these results indicate that PSMD9 functions as an anchor rather than a chaperone and bridges IκBα bound hnRNPA1 to the proteasome. This interaction enables regulated degradation of IκBα and modulates NF-κB activity.

While there is no clear evidence for the presence of PSMD9 on mature proteasomes or for the role of PDZ domains in interaction with ATPase subunits in mammalian cells, the lack of any detectable effect of PDZ domain mutations on the association of PSMD9 with intact 26S proteasomes requires further explanation. To address this we analysed the primary sequence of PSMC6 (Rpt4) and PSMC3 (Rpt5). GRRF was present in PSMC6. Intrigued we co-expressed wt-PSMD9 or PSMD9-Q181G mutant with wt-PSMC6 and performed co-immunoprecipitation studies. The results showed that the Q181G mutation which inhibits binding of PSMD9 to hnRNPA1 does not affect PSMD9 binding to PSMC6 (Fig. 10D). This result in conjunction with the observation that the PDZ mutations do not affect PSMD9 association with proteasome indicates that the interaction with the mature proteasome may not involve Rpt5. Moreover Rpt5 C-terminus is known to play a key role in interaction with the 20S α-subunit necessary for gate opening and activation of the proteasome. Therefore, Rpt5 on mature proteasome is unlikely to interact with PSMD9.

Since we found increased IκBα degradation upon hnRNPA1 overexpression with TNF-α treatment, we wanted to check the recruitment of overexpressed hnRNPA1 on 26S proteasome. HA-hnRNPA1 was overexpressed in HEK293 cells and treated with TNF-α (20 ng for 30 min). Cell lysates were prepared in ATP buffer and 26S proteasome was pulled down

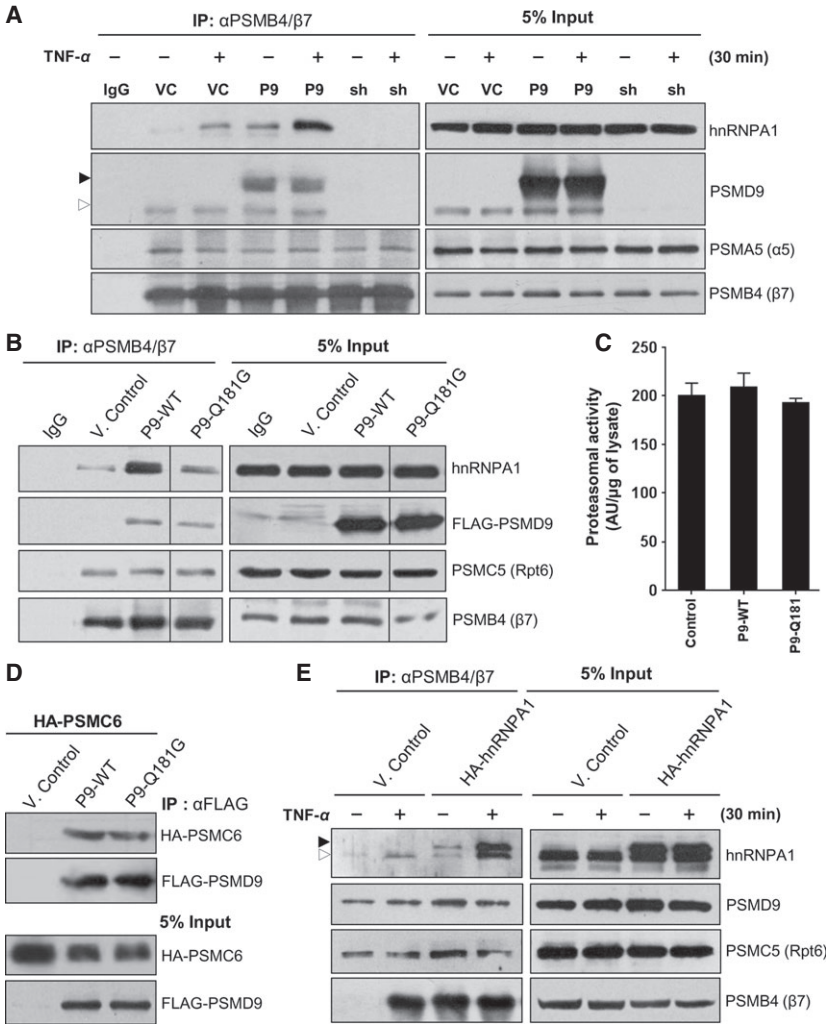

Fig. 10. PSMD9 is crucial for the recruitment of hnRNPA1-IκBα complex on 26S proteasome. (A) Both the overexpression (P9) and knockdown (sh) HEK293 inducible stable clones of PSMD9 were treated with doxycycline for 48 h and/or with TNF-α (20 ng·mL^{-1} of medium) for the next 30 min or left untreated. Cell lysates were prepared with ATP buffer as described in Materials and methods. Whole 26S proteasome was pulled down from the above cell lysates using β7 antibody and probed with different antibodies and analyzed by WB. Symbol ► corresponds to trans-expressed FLAG-PSMD9 and symbol ▷ corresponds to the endogenous PSMD9. (B) HEK293 cells were transiently transfected with pCMV-10 empty vector or pCMV-10-PSMD9 (wt or mutants D157P/Q181G) and cell lysates were prepared in ATP buffer as in Materials and methods. 26S proteasome was pulled down from the above cell lysates using β7 antibody and probed with different antibodies as indicated and analyzed by WB. (C) Proteasomal activity of the above mentioned (in B) cell lysates was measured as described in Materials and methods. Data represent Suc-LLVY-AMC proteasomal activity in arbitrary units (AU·μg^{-1} of lysate) ± SEM of two independent experiments done in duplicate. The WB shows the expression of FLAG-PSMD9 in the above cell lysates and PSMB4 is taken as the loading control. (D) HEK293 cells were co-transfected with pCDNA3.1-PSMC6 and p3X-FLAG-CMV-10, p3X-FLAG-CMV-10-wt-PSMD9 or p3X-FLAG-CMV-10-Q181G-PSMD9. After 48 h of transfection cell lysates were used for pull-down with anti-FLAG-M2 agarose beads and analyzed by WB. (E) HEK293 cells were transfected with pCDNA3.1 empty vector or pCDNA3.1-HA-wt-hnRNPA1 and after 48 h of transfection cells were treated with TNF-α for 30 min. Cell lysates were prepared in ATP buffer (as described in Materials and methods); 26S proteasome was pulled down using β7 antibody and analyzed by WB. Symbol ► corresponds to trans-expressed HA-hnRNPA1 and symbol ▷ corresponds to the endogenous hnRNPA1.

using β7 antibody. When the pull-down complexes were probed with hnRNPA1 antibody, both endogenous and trans-expressed hnRNPA1 levels were found to be increased upon TNF-α treatment, which correlates with the IκBα degradation (Fig. 10E). Furthermore levels of hnRNPA1 remain unaltered upon PSMD9 overexpression (Fig. 4B) or downregulation (Fig. 5B) or after TNF-α treatment. These results are strongly suggestive of a mechanism which involves recruitment of hnRNPA1 to the proteasome complex

during TNF-α signaling that would result in more and more IκBα degradation by the proteasome. Our attempts to substantiate this by capturing IκBα on 26S proteasome with/without TNF-α treatment under hnRNPA1 or PSMD9 overexpressing conditions failed perhaps due to its rapid degradation by the proteasome. Hence all these results suggest that hnRNPA1 either recruits or presents IκBα to the proteasome and this shuttle receptor hnRNPA1 is anchored by PSMD9 on the proteasome. While ubiquitinated IκBα is degraded, hnRNPA1 in all probability is released intact. It is possible that the PSMD9–hnRNPA1 interaction shortens the distance between the substrate and the proteasomal ATPases or ensures that IκBα is not prematurely released from the proteasome.

Discussion

Protein–protein interactions are seminal to signal transduction. They are involved in spatiotemporal regulation of cellular functions. Therefore, identification of novel interactions can help in deciphering unknown functions of a protein. We have established bioinformatics methods for identification of unknown interacting partners of 19S subunits of the proteasome (*FEBS Open Bio*, submitted). Using one such method we identified hnRNPA1, an RNA binding protein involved in RNA metabolism and transport [34], as a novel interacting partner of PSMD9, a PDZ domain containing a subunit of the proteasome. To test whether this interaction is physiologically relevant and to identify functions associated with the interaction, we searched for the reported functions of hnRNPA1. The N-terminal of hnRNPA1 binds to ankyrin repeats in IκBα and this interaction somehow influences the processing of IκBα, the nature or mechanism of which is unclear [12]. Here we demonstrate that PSMD9 through its PDZ domain interacts with hnRNPA1 C-terminus and this domain–motif interaction is necessary for the proteasomal degradation of IκBα. Overexpression of PSMD9 accelerates both basal and TNF-α mediated proteasomal degradation of IκBα. This results in increased NF-κB activation and expression of its target genes. We establish a new role for hnRNPA1 as a shuttle receptor for the degradation of IκBα in HEK293 cells. PSMD9, contrary to its expected role as a chaperone, acts as a part of the 19S recognition module to facilitate delivery of ubiquitinated IκBα to the proteasome via hnRNPA1, as depicted in the model (Fig. 11).

Although the degradation of IκBα by the proteasome has long been established, the mechanism of how it is recruited to the proteasome is not well defined. Here we show how ubiquitinated IκBα is targeted to the proteasome for degradation. This is important because how ubiquitinated substrates in general are recruited to the proteasome is an active area of research. So far two modes of substrate recognition have been well defined. In the direct mode, substrates are recognized by the ubiquitin binding motifs in 19S subunits like Rpn10 containing the UIM domain, or via motifs like pleckstrin in Rpn13 [45,46]. In the indirect mode of recognition, Rad23, Dsk2 and Ddi1 proteins called 'shuttle receptors' bind proteasome

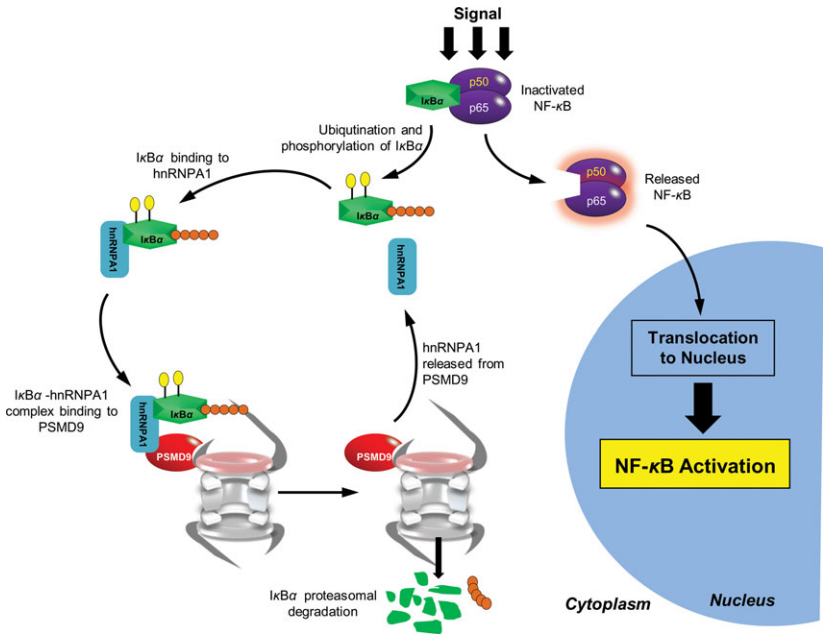

Fig. 11. Model for the mechanism of IκBα presentation and degradation by 26S proteasome. Signal activated and modified IκBα binds to hnRNPA1 and this complex interacts with PSMD9 on 26S proteasome. IκBα gets degraded through proteasomal activity hnRNPA1 shuttles back to bind with free IκBα and the cycle repeats.

through their UBL domains present at the N-terminus while their C-terminal ubiquitin association domain (UBA) binds to ubiquitin chains on the substrates [47,48]. These shuttle receptors bind to the Rpn1 subunit of the proteasome in non-stoichiometric amounts and apparently dissociate with fast kinetics. In an in-depth study, Deshaies group showed that Ddi1 is a proteasomal shuttle receptor that binds to the LRR1 domain of Rpn1 [49] and facilitates the degradation of Ufo1, a Ddi1 substrate. A UBA domain containing protein, p62, interacts with K63 ubiquitin chains of ubiquitinated tau and facilitates its proteasomal degradation by interacting with Rpt1 through its N-terminal PB1 domain [50]. HSP27 may also act as a shuttle receptor that recruits ubiquitinated IκBα to the proteasome for degradation in cancer cells in response to stress signals [51]. In this report HSP27 was shown to bind ubiquitinated IκBα and to the 19S regulatory particle of the proteasome to mediate this degradation. HSP27 recognizes covalently linked ubiquitin on IκBα but how it interacts with the proteasome is unclear. Recently we have demonstrated that non-ubiquitinated proteins can be directly recognized and degraded by 26S proteasome [10].

We describe our findings in the context of these reported mechanisms of substrate recognition and highlight unique features that are an outcome of our study. PSMD9 unlike HSP27 does not directly bind to ubiquitinated IκBα. This interaction is mediated by hnRNPA1 and, therefore, Ub-IκBα is targeted to the proteasome through the indirect pathway. Since the hnRNPA1 level does not change under any conditions tested here, we argue that it acts as a shuttle receptor that brings in Ub-IκBα. Since hnRNPA1 lacks a UBL-like domain, it does not bind to the proteasome in a classical manner like other shuttle receptors. Instead this function is mediated by a C-terminal region of the protein which acts as a recognition signal for the PDZ domain of PSMD9 bound to the proteasome. PDZ domains can recognize native sequences in proteins typically through the C-terminal residues. Such a classical domain–motif interaction for PSMD9–hnRNPA1 is established by our study. Nevertheless, the exact mechanism of hnRNPA1 release, the mode of binding of PSMD9 to the proteasome and the molecular basis of this recognition remain to be investigated.

While our studies show how PSMD9 directly affects the degradation of IκBα by the proteasome which helps in NF-κB activation, there are several upstream steps that process IκBα for degradation. A possible role of PSMD9 in these processes has been somewhat addressed in this study. Since in the absence of any external stimuli PSMD9 overexpression results in increased basal activity of NF-κB, it remains to be seen whether PSMD9 acts as an internal signal for NF-κB activation. This may be dependent or independent of its interaction with hnRNPA1. Previously it was reported that in cells lacking hnRNPA1 (mouse leukemic cells) NF-κB, activity is reduced [12]. Likewise in the current study we show that in cells lacking PSMD9 NF-κB, activity is reduced. Taken together, these studies suggest that PSMD9 and hnRNPA1 are probably not mutually exclusive in the context of the NF-κB signaling pathway which may be explained by their ability to interact with each other.

It will be important to see whether the mechanism of IκBα degradation and NF-κB activity is general to other cell types. While hnRNPA1 is a ubiquitous protein, PSMD9 may be expressed in a cell or tissue specific manner [3]. Although PSMD9 deletion is not lethal in yeast [52], loss of PSMD9 expression may have phenotypic consequences in mammalian cells due to inhibition of NF-κB activity. We have demonstrated that the PDZ domain mutants do not bind to hnRNPA1 and therefore their overexpression does not affect NF-κB activity. Thus small molecules that can target the interaction sites on the PDZ domain of PSMD9 are likely to act as inhibitors of NF-κB activity. Such molecules may be useful in targeting cancer cells that are dependent on a consistently high NF-κB activity for their survival [53,54]. The first step in this direction, however, is to establish the role of the PSMD9–hnRNPA1 interaction in this pathway in such cancer cells.

Based on our findings on the molecular details of the interaction between the PDZ domain of PSMD9 and hnRNPA1, we speculate about a general role for PSMD9 in substrate recognition by the proteasome. For example IκBα may be one of the many examples of how substrates may converge on the proteasome through the PDZ domain of PSMD9. It is possible that other substrates are brought to the proteasome by a similar mechanism through either hnRNPA1 or other shuttle receptors that may carry a similar recognition motif. In addition, by virtue of its binding to ATPase subunits, PSMD9 on the surface of the 19S regulatory particles may be uniquely positioned to ensure rapid unfolding, prevention of premature release of the substrates and translocation of the unfolded protein through the central channel that lines the ATPase ring. Another aspect of our finding is the nature and origin of the components involved in IκBα degradation – a chaperone from the proteasome pathway and an RNA binding protein. Thus it is speculated that there may be other functions mediated by this domain–motif interaction between PSMD9 and

hnRNPA1 relevant to their respective network and/or the crosstalk between different functional modules.

Two important points reported in the literature regarding the association of PSMD9 with proteasomes merit special attention: (a) chaperones such as PSMD9 and PSMD10 have not been found as part of the mature proteasome structure [43,44] and (b) Nas-2, the yeast homolog of PSMD9, has been shown to interact with Rpt5 through C-terminal residues implying a role for the PDZ domain in interaction. We believe PSMD9 or PSMD10 may transiently associate with the mature proteasome. It is likely that only few of the mature 26S proteasomes bind these chaperones at any given moment and they can be washed away under very stringent conditions during IPs or affinity purifications. It is interesting to note that reports on the interaction of shuttle receptors such as Ddi1 in yeast with the proteasome have been controversial. Ddi1 belongs to the UBA-UBL domain containing proteins that bind polyubiquitin chains in substrate proteins. Ddi1 is reported by some to physically interact with the intact proteasome while others question this finding. It is argued by Deshaies group, who find that Ddi1 does indeed interact with the proteasome in a specific and functionally relevant manner, that such discrepancies may be due to the qualitative nature of IP experiments and the rapid dynamics of UBL binding to and dissociation from the proteasome. The same could be true for the proteasomal chaperones such as PSMD9 or PSMD10.

Regarding the involvement of the PDZ domain in the interaction with the ATPase subunits, we find that mutations in the PDZ domain of PSMD9 that affect hnRNPA1 binding do not affect the association with the proteasome. While we do not find any literature evidence for the role of PDZ domains in interaction with the ATPases in mammalian cells, Nas2 in yeast has been shown to interact with Rpt5 or PSMC3 via the C-terminal residues [55]. Although we have not tested the interaction of PSMD9 with PSMC3, interaction of PSMD9 with PSMC6 is unaffected by the PDZ mutations (current study). It is possible that the association of PSMD9 with the mature proteasome is different from its interaction with the ATPase subunits in the modular structure. It is obvious that we are far from a clear understanding of the role of PSMD9 in the functioning of holo 26S proteasome and its interaction with the different subunits. More studies with detailed molecular characterization as reported in this current study will be necessary to clarify the complexity associated with these supramolecular structures.

In summary, we have established that PSMD9 through its PDZ domain interacts with the C-terminus of hnRNPA1, a novel interacting partner, and this interaction regulates degradation of IκBα and, therefore, NF-κB activity in HEK293 cells. hnRNPA1 acts as a shuttle receptor while PSMD9 is the docking site on the 19S regulatory particle. IκBα may be one of the many examples of how ubiquitinated substrates may be recruited on the proteasome through the PDZ domain of PSMD9. It is possible that features of the C-terminal sequence found in hnRNPA1 may be conserved in other shuttle receptors. Our study opens up new areas of investigation on the role of PSMD9 in cellular homeostasis. The generality of this interaction between hnRNPA1 and PSMD9 may propose the interface as a potential drug target in tumor cells relying on high NF-κB activity. Moreover, the interaction between hnRNPA1, a protein well known for mRNA transport and splicing, and PSMD9, a subunit chaperone of the proteasome, is intriguing. Although speculative, whether this interaction influences these well known functions of hnRNPA1 and whether there is crosstalk between the degradation pathway and the RNA metabolism remains to be seen.

Materials and methods

Plasmids

PSMD9 was amplified from PSMD9 cDNA (Origene Technologies) and cloned within *Hin*dIII and *Eco*RI in p3xFLAG-CMV-10 mammalian expression vector (Sigma, USA). For bacterial expression vector pRSETA, *Bam*HI and *Xho*I sites are used for cloning PSMD9. The PSMD9 (L173G), PSMD9(Q181G) and PSMD9(triple mutant L124G-Q126G-E128G) mutants were generated in p3xFLAG-CMV-10-PSMD9 construct by site directed mutagenesis. 3xFLAG-tagged PSMD9 was amplified from p3xFLAG-CMV-10-PSMD9 construct using the primers Fw 5′-ACCGGTCGCCACCATGGACTACAAAGACCATG-3′ and Rv 5′-GAATTCGACAATCATCTTTGCAGAGG-3′ cloned between *Age*I and *Eco*RI into doxycycline inducible vector pTRIPZ (a gift from S. Dalal, Advanced Center for Treatment, Research and Education in Cancer, Navi Mumbai, India). mir30 based shRNA of PSMD9 was PCR amplified using the primers Fw 3′-GGCTCGAGGAAGGTATATTGCTGTTGACAGTGAGCGGCAGATCAAGGCCAACTATGATAGTGAAGCCACAGATGT-3′ and Rv 5′-GCGAATTCCCGAGGCAGTAGGCAGCAGATCAAGGCCAACTATGATACA TCTGTGGCTTCACTATCATAG-3′. The PCR product was digested with *Xho*I and *Eco*RI and inserted into doxycycline inducible vector pTRIPZ. hnRNPA1 was PCR amplified from HEK293 cDNA library generated by RT-PCR of RNA from HEK293 cells and cloned within *Bam*HI and *Xho*I in HA-pCDNA3.1 mammalian expression vector (gift from S. Dalal, Advanced Center for

Treatment, Research and Education in Cancer, Navi Mumbai, India). For bacterial expression vector pGEX-4T-1, *Bam*HI and *Eco*RI sites were used for cloning hnRNPA1. The hnRNPA1(Δ7C) mutant was generated by deleting seven amino acids from the C-terminus. wt IκBα and ΔC mutant (1–252 amino acids) IκBα were amplified from HEK293 cDNA and were cloned into mammalian expression vector p3xFLAG-CMV-10 vector using *Hin*dIII and *Eco*RI sites. wt IκBα was cloned into bacterial expression vector pMALc5X within *Bam*HI and *Eco*RI sites. PSMC6 was PCR amplified from the HEK293 cDNA library generated by RT-PCR of RNA from HEK293 cells and cloned within *Bam*HI and *Xho*I in HA-pCDNA3.1 mammalian expression vector (gift from S. Dalal, Advanced Center for Treatment, Research and Education in Cancer, Navi Mumbai, India). The phospho-mutant pTRIPZ- IκBαSR (S32A–S36A) vector (gift from N. Shirsat, Advanced Center for Treatment, Research and Education in Cancer, Navi Mumbai, India, and D. C. Guttridge, Ohio State University, USA), pEGFPN3 vector and pBSK3 vectors were used for mammalian cell transfection. 3x κB ConA luc vector and ConA luc control vector (gift from N. D. Perkins, Newcastle University, UK) were used for the luciferase reporter assay.

Expression, purification of recombinant proteins

Recombinant His-PSMD9, GST-PSMD9, GST-hnRNPA1 and MBP-IκBα were expressed in *Escherichia coli* BL21 DE(3) using 100 μM isopropyl thio-β-D-galactoside at 18 °C for 18 h. His-PSMD9 and its mutant were purified by Ni-nitrilotriacetic acid column chromatography (Qiagen, Hilden, Germany) using 250 mM imidazole buffer; GST, GST-PSMD9 and GST-hnRNPA1 were purified using glutathione Sepharose beads (GE Healthcare Life Sciences, Amersham, UK) and MBP, MBP-IκBα were purified using amylose beads (NEB, UK) and 10 mM maltose buffer, according to the manufacturer's protocol. His-PSMD9 was FPLC purified using a Superdex-200 column (Amersham, GE Healthcare Life Science).

Far western blot and dot blot

Recombinant GST-PSMD9, GST-hnRNPA1 and MBP-IκBα proteins (2 μg each) were SDS denatured, run on an SDS/PAGE and transferred onto a PVDF membrane. The transferred proteins were denatured/renatured on the membrane using guanidine-HCl AC buffer with the protocol described in Yuliang Wu *et al.* [56]. For dot blot 1 μg of recombinant proteins (GST, GST-hnRNPA1, GST-PSMD9, MBP and MBP-IκBα) were spotted on a methanol equilibrated PVDF membrane. The spotted membranes were blocked in 3% BSA-TBST and overlaid with either His-PSMD9 or MBP-IκBα (100 nM in 1% BSA-TBST) for 1 h. Anti-PSMD9 (mouse monoclonal; Sigma) in 1 : 4000 dilution, anti-hnRNPA1 (mouse monoclonal; Sigma) in 1 : 4000 dilution and anti-IκBα (rabbit polyclonal; Sigma) in 1 : 4000 dilution were used for probing the overlaid proteins.

Cell culture, transfection and reagents

HEK293 cells were cultured in DMEM (Gibco, USA) supplemented with 10% fetal bovine serum (Gibco), 100 IU·mL^{-1} penicillin (Sigma) and 100 μg·mL^{-1} streptomycin (Sigma). For transfection Lipofectamine 2000 (Invitrogen, Carlsbad, CA, USA) or the calcium phosphate method were used according to the manufacturer's protocol. 100 μM of PSMD9 small interfering RNA (siRNA) (Dharmacon; Thermo Scientific, Waltham, MA, USA) or scrambled siRNA (Dharmacon; Thermo Scientific) with Lipofectamine 2000 was used for transfection. Doxycycline (Sigma) 1–4 μg·mL^{-1} of medium, CHX (Sigma) 50 μg·mL^{-1} of medium, TNF-α (Peprotech, Rocky Hill, NJ, USA) 20 ng·mL^{-1} of medium, MG132 (Sigma) 10 μM·mL^{-1} of medium and Velcade (Johnson & Johnson, NJ, USA) 10 μg·mL^{-1} of medium were used for different experiments.

Establishment of stable cell line

HEK293 cells were transfected with p3xFLAG-CMV-10 and p3xFLAG-CMV-10-PSMD9 constructs using Lipofectamine 2000 (Invitrogen) to generate PSMD9 overexpressing stable clones. After 24 h, transfected cells were subcultured and kept under selection in DMEM supplemented with 10% fetal bovine serum and 800 μg·mL^{-1} of G418 (Sigma). After 2–4 weeks G418 resistant single colonies were picked up and grown in DMEM supplemented with 10% fetal bovine serum and 400 μg·mL^{-1} of G418. Three different clones with high FLAG-PSMD9 expression were selected for further studies. For generating doxycycline inducible stable clones, HEK293 cells were transfected with pTRIPZ, pTRIPZ-3xFLAG-PSMD9, pTRIPZ-shRNA-PSMD9 using Lipofectamine 2000. After 24 h transfected cells were subcultured and kept under selection in DMEM supplemented with 10% fetal bovine serum and 800 ng·mL^{-1} puromycin (Sigma). After 5–7 days puromycin resistant single colonies were picked up and grown in DMEM supplemented with 10% fetal bovine serum and 400 ng·mL^{-1} puromycin. Three clones with high FLAG-PSMD9 expression and three clones with maximum PSMD9 knockdown upon doxycycline induction were selected for further studies.

Immunoprecipitation

Cells were pelleted, washed twice with NaCl/P_i and lysed in NP-40 lysis buffer [50 mM Tris pH 7.6, 150 mM NaCl, 0.5% NP-40 detergent, 10 mM NaF, 1 mM Na_2VO_5, 10 mM β-glycerophosphate and 1× protease inhibitor cocktail (Sigma,

P2714)]. For proteasomal pull-down, buffer containing 50 mM Tris (pH 7.6), 5 mM $MgCl_2$, 1 mM ATP, 10% glycerol and 1× protease inhibitor cocktail (Sigma) was used. Briefly, monoclonal antibodies (1 : 1000 vol/vol of antibody : cell lysate) were bound overnight to Protein-G Sepharose beads (GE Amersham) and pre-cleared cell extracts were incubated with antibody-bound Sepharose beads or anti-FLAG M2 agarose (Sigma) for 3 h at 4 °C. After extensive washing with washing buffer [50 mM Tris, pH 7.6, 150–450 mM NaCl, 10 mM NaF, 1 mM Na_2VO_5, 10 mM β-glycerophosphate and 1× protease inhibitor cocktail (Sigma, P2714)], immune complexes were separated by SDS/PAGE and analyzed by western blotting, following standard protocols.

Luciferase reporter assay

Stable clones of HEK293 harboring FLAG-PSMD9 and HEK293 cells transiently transfected with p3xFLAG-CMV-10/p3xFLAG-CMV-10-PSMD9/p3xFLAG-CMV-10-PSMD9 (D157P)/p3xFLAG-CMV-10-PSMD9(Q181G)/pcDNA3.1-HA-hnRNPA1/pcDNA3.1-HA-hnRNPA1(CΔ7) were co-transfected with ConA luc control or 3x κB ConA luc vectors by the calcium phosphate method. After 48 h, cells were lysed and luciferase assays were performed using the Luciferase Assay System (Promega, Fitchburg, WI, USA) in triplicate. In inducible stable clones of control pTRIPZ and pTRIPZ-3xFLAG-PSMD9 after 48 h of doxycycline addition luciferase assays were performed as explained.

Western blotting and antibodies

Cell lysates were prepared with NP-40 lysis buffer and separated on 12–15% SDS/PAGE gels, and western blot (WB) was performed following standard protocols. Antibodies anti-PSMD9 in 1 : 1000 (mouse monoclonal; Sigma, and rabbit polyclonal; Abcam, Cambridge, UK), anti-FLAG in 1 : 8000 (mouse monoclonal; Sigma), anti-hnRNPA1 in 1 : 1000 (mouse monoclonal; Sigma, and rabbit polyclonal; Abcam), anti-HA in 1 : 1000 (rabbit polyclonal; Abcam), anti-IκBα in 1 : 1000 (rabbit polyclonal; Sigma), anti-β-actin in 1 : 2000 (mouse monoclonal; Sigma), anti-α-tubulin in 1 : 2000 (mouse monoclonal; Sigma), anti-acetyl histone H4 K12 in 1 : 1000 (rabbit polyclonal; Cell Signaling, Danvers, MA, USA), anti-β7 in 1000 (mouse monoclonal), anti-α5 in 1 : 1000 (mouse monoclonal), anti-ubiquitin in 1 : 1000 (mouse polyclonal, Sigma) and anti-p65 in 1 : 1000 (rabbit polyclonal, Abcam) were used for western blotting experiments.

RT-PCR and real-time PCR

Total RNA was isolated from HEK293 cells, PSMD9 overexpression and knockdown clone by TRIzol® Reagent (Invitrogen) following the manufacturer's protocol. cDNA was prepared using SuperScript® III Reverse Transcriptase kit (Life Technologies, Invitrogen). Real-time PCR was performed using SYBR Green based Kappa-Biosystems kit (Woburn, MA, USA) and gene specific primers (Table S1).

Electrophoretic mobility shift assay

Nuclear fractions were extracted from HEK293 FLAG-PSMD9 stable clones, HEK293 inducible FLAG-PSMD9 stable clones and HEK293 inducible PSMD9-shRNA stable clones using N-XTRACT kit (Sigma) following the manufacturer's protocol. wt κB-oligo 5′-AGTTGAGGGGACTTTCCCAGGC-3′ and mutant κB-oligo 5′-AGTTGAGCTCACTTTCC CAGGC-3′ [35] were purchased from Sigma and biotin labeled at the 3′ end of the oligos using the Biotin 3′ End DNA Labeling Kit (Thermo Scientific) following the manufacturer's protocol. Both biotinylated complementary oligos were annealed at 65 °C for 10 min followed by incubation at room temperature for 30 min. Then 3–5 μg of nuclear extract was incubated with the biotinylated oligos and poly dI-dC for 20 min at room temperature. This binding reaction was carried out using LightShift® Chemiluminescent EMSA Kit (Thermo Scientific) following the manufacturer's protocol. Reactions were separated on 6% native PAGE, transferred onto positively charged nylon membrane and UV crosslinked for 30 min at 256 nm at 1 cm distance. The membrane was developed onto an X-ray film using Chemiluminescent Nucleic Acid Detection Module (Thermo Scientific) following the manufacturer's protocol.

Proteasomal activity assay

Cells were pelleted, washed twice with $NaCl/P_i$ and resuspended in buffer containing 50 mM Tris (pH 7.6), 5 mM $MgCl_2$, 1 mM ATP, 10% glycerol and 1× protease inhibitor cocktail (Sigma). Cell suspensions were ultrasonicated for four cycles of 20 s each (with 1 s break after each 2 s) at 30 kHz on ice. Proteasomal activity was measured using 25 nM Suc-LLVY-7-amino-4-methyl coumarin substrate and fluorescence readings were taken at excitation 355 nm/emission 460 nm.

Densitometric and statistical analysis

Densitometric quantitation of scanned images was performed using MAC BIOPHOTONICS IMAGEJ. Statistical analysis was performed using GRAPH PAD PRISM 5. To evaluate the significance of the values obtained, an unpaired Student's *t* test was performed. $P < 0.05$ and $P > 0.05$ are considered as significant and non-significant data respectively. In graphs the symbol *** represents P value < 0.001.

Acknowledgements

We thank Dr Neil D. Perkins for providing 3x κB ConA luc vector and ConA luc control vector, Dr Sorab Dalal for providing pTRIPZ and pCDNA3.1 vector, Dr N. Shirsat, Advanced Center for Treatment, Research and Education in Cancer, Navi Mumbai, India, and Dr D. C. Guttridge, Ohio State University, USA, for providing phospho-mutant pTRIPZ-IκBαSR (S32A–S36A) vector and Dr Amit Singh Gautam for discussions. This work was funded by ACTREC-TMH (Grant no. IRG.2657). IS is funded by UGC (University Grants Commission), India; NS is funded by Department of Biotechnology, India.

Author contributions

Indrajit Sahu: planned, performed, analyzed experiments and assisted in manuscript writing. Nikhil Sangith: planned, performed initial NF-κB activity experiments, some *in vitro* interactions and designed PDZ and C-terminal mutations. Manoj Ramteke: initial establishment of stable cell lines and transfection. Rucha Gadre: performed some cloning and *in vitro* interaction experiments. Prasanna Venkatraman: conceived, directed the project and wrote the manuscript.

References

1 Kaneko T, Hamazaki J, Iemura S, Sasaki K, Furuyama K, Natsume T, Tanaka K & Murata S (2009) Assembly pathway of the mammalian proteasome base subcomplex is mediated by multiple specific chaperones. *Cell* **137**, 914–925.

2 da Fonseca PC, He J & Morris EP (2012) Molecular model of the human 26S proteasome. *Mol Cell* **46**, 54–66.

3 Thomas MK, Yao KM, Tenser MS, Wong GG & Habener JF (1999) Bridge-1, a novel PDZ-domain coactivator of E2A-mediated regulation of insulin gene transcription. *Mol Cell Biol* **19**, 8492–8504.

4 Jelen F, Oleksy A, Smietana K & Otlewski J (2003) PDZ domains – common players in the cell signaling. *Acta Biochim Pol* **50**, 985–1017.

5 Lee HJ & Zheng JJ (2010) PDZ domains and their binding partners: structure, specificity, and modification. *Cell Commun Signal* **8**, 8.

6 Lee JH, Volinic JL, Banz C, Yao KM & Thomas MK (2005) Interactions with p300 enhance transcriptional activation by the PDZ-domain coactivator Bridge-1. *J Endocrinol* **187**, 283–292.

7 Banz C, Munchow B & Diedrich K (2010) Bridge-1 is expressed in human granulosa cells and is involved in the activin A signaling cascade. *Fertil Steril* **93**, 1349–1352.

8 Volinic JL, Lee JH, Eto K, Kaur V & Thomas MK (2006) Overexpression of the coactivator bridge-1 results in insulin deficiency and diabetes. *Mol Endocrinol* **20**, 167–182.

9 Ren S, Uversky VN, Chen Z, Dunker AK & Obradovic Z (2008) Short linear motifs recognized by SH2, SH3 and Ser/Thr kinase domains are conserved in disordered protein regions. *BMC Genomics* **9** (Suppl 2), S26.

10 Singh Gautam AK, Balakrishnan S & Venkatraman P (2012) Direct ubiquitin independent recognition and degradation of a folded protein by the eukaryotic proteasomes – origin of intrinsic degradation signals. *PLoS One* **7**, e34864.

11 Nanaware PP, Ramteke MP, Somavarapu AK & Venkatraman P (2013) Discovery of multiple interacting partners of gankyrin, a proteasomal chaperone and an oncoprotein – evidence for a common hot spot site at the interface and its functional relevance. *Proteins*. doi: 10.1002/prot.24494.

12 Hay DC, Kemp GD, Dargemont C & Hay RT (2001) Interaction between hnRNPA1 and IkappaBalpha is required for maximal activation of NF-kappaB-dependent transcription. *Mol Cell Biol* **21**, 3482–3490.

13 Hayden MS & Ghosh S (2008) Shared principles in NF-kappaB signaling. *Cell* **132**, 344–362.

14 Li H & Lin X (2008) Positive and negative signaling components involved in TNFalpha-induced NF-kappaB activation. *Cytokine* **41**, 1–8.

15 Grilli M, Chiu JJ & Lenardo MJ (1993) NF-kappa B and Rel: participants in a multiform transcriptional regulatory system. *Int Rev Cytol* **143**, 1–62.

16 Ghosh S, May MJ & Kopp EB (1998) NF-kappa B and Rel proteins: evolutionarily conserved mediators of immune responses. *Annu Rev Immunol* **16**, 225–260.

17 Baeuerle PA & Baltimore D (1988) I kappa B: a specific inhibitor of the NF-kappa B transcription factor. *Science* **242**, 540–546.

18 Beg AA & Baldwin AS Jr (1993) The I kappa B proteins: multifunctional regulators of Rel/NF-kappa B transcription factors. *Genes Dev* **7**, 2064–2070.

19 Chen Z, Hagler J, Palombella VJ, Melandri F, Scherer D, Ballard D & Maniatis T (1995) Signal-induced site-specific phosphorylation targets I kappa B alpha to the ubiquitin–proteasome pathway. *Genes Dev* **9**, 1586–1597.

20 Li N & Karin M (1998) Ionizing radiation and short wavelength UV activate NF-kappaB through two distinct mechanisms. *Proc Natl Acad Sci USA* **95**, 13012–13017.

21 Mukhopadhyay A, Manna SK & Aggarwal BB (2000) Pervanadate-induced nuclear factor-kappaB activation requires tyrosine phosphorylation and degradation of IkappaBalpha. Comparison with tumor necrosis factor-alpha. *J Biol Chem* **275**, 8549–8555.

22 Hayden MS & Ghosh S (2004) Signaling to NF-kappaB. *Genes Dev* **18**, 2195–2224.
23 Alkalay I, Yaron A, Hatzubai A, Orian A, Ciechanover A & Ben-Neriah Y (1995) Stimulation-dependent I kappa B alpha phosphorylation marks the NF-kappa B inhibitor for degradation via the ubiquitin−proteasome pathway. *Proc Natl Acad Sci USA* **92**, 10599–10603.
24 Tanaka K, Kawakami T, Tateishi K, Yashiroda H & Chiba T (2001) Control of IkappaBalpha proteolysis by the ubiquitin−proteasome pathway. *Biochimie* **83**, 351–356.
25 Miyamoto S, Seufzer BJ & Shumway SD (1998) Novel IkappaB alpha proteolytic pathway in WEHI231 immature B cells. *Mol Cell Biol* **18**, 19–29.
26 Shumway SD, Berchtold CM, Gould MN & Miyamoto S (2002) Evidence for unique calmodulin-dependent nuclear factor-kappaB regulation in WEHI-231 B cells. *Mol Pharmacol* **61**, 177–185.
27 Shumway SD & Miyamoto S (2004) A mechanistic insight into a proteasome-independent constitutive inhibitor kappaBalpha (IkappaBalpha) degradation and nuclear factor kappaB (NF-kappaB) activation pathway in WEHI-231 B-cells. *Biochem J* **380**, 173–180.
28 Ponnappan S, Cullen SJ & Ponnappan U (2005) Constitutive degradation of IkappaBalpha in human T lymphocytes is mediated by calpain. *Immun Ageing* **2**, 15.
29 Palombella VJ, Rando OJ, Goldberg AL & Maniatis T (1994) The ubiquitin−proteasome pathway is required for processing the NF-kappa B1 precursor protein and the activation of NF-kappa B. *Cell* **78**, 773–785.
30 Hoffmann A, Levchenko A, Scott ML & Baltimore D (2002) The IkappaB-NF-kappaB signaling module: temporal control and selective gene activation. *Science* **298**, 1241–1245.
31 Cohen S, Achbert-Weiner H & Ciechanover A (2004) Dual effects of IkappaB kinase beta-mediated phosphorylation on p105 Fate: SCF(beta-TrCP)-dependent degradation and SCF(beta-TrCP)-independent processing. *Mol Cell Biol* **24**, 475–486.
32 Liang C, Zhang M & Sun SC (2006) beta-TrCP binding and processing of NF-kappaB2/p100 involve its phosphorylation at serines 866 and 870. *Cell Signal* **18**, 1309–1317.
33 Moorthy AK, Savinova OV, Ho JQ, Wang VY, Vu D & Ghosh G (2006) The 20S proteasome processes NF-kappaB1 p105 into p50 in a translation-independent manner. *EMBO J* **25**, 1945–1956.
34 Dreyfuss G, Matunis MJ, Pinol-Roma S & Burd CG (1993) hnRNP proteins and the biogenesis of mRNA. *Annu Rev Biochem* **62**, 289–321.
35 Reigstad CS, Lunden GO, Felin J & Backhed F (2009) Regulation of serum amyloid A3 (SAA3) in mouse colonic epithelium and adipose tissue by the intestinal microbiota. *PLoS One* **4**, e5842.
36 Zhou A, Scoggin S, Gaynor RB & Williams NS (2003) Identification of NF-kappa B-regulated genes induced by TNFalpha utilizing expression profiling and RNA interference. *Oncogene* **22**, 2054–2064.
37 Miyamoto S, Maki M, Schmitt MJ, Hatanaka M & Verma IM (1994) Tumor necrosis factor alpha-induced phosphorylation of I kappa B alpha is a signal for its degradation but not dissociation from NF-kappa B. *Proc Natl Acad Sci USA* **91**, 12740–12744.
38 Shim SM, Lee WJ, Kim Y, Chang JW, Song S & Jung YK (2012) Role of S5b/PSMD5 in proteasome inhibition caused by TNF-alpha/NFkappaB in higher eukaryotes. *Cell Rep* **2**, 603–615.
39 DeMartino GN, Proske RJ, Moomaw CR, Strong AA, Song X, Hisamatsu H, Tanaka K & Slaughter CA (1996) Identification, purification, and characterization of a PA700-dependent activator of the proteasome. *J Biol Chem* **271**, 3112–3118.
40 Ferrell K, Wilkinson CR, Dubiel W & Gordon C (2000) Regulatory subunit interactions of the 26S proteasome, a complex problem. *Trends Biochem Sci* **25**, 83–88.
41 Chen C, Huang C, Chen S, Liang J, Lin W, Ke G, Zhang H, Wang B, Huang J, Han Z *et al.* (2008) Subunit−subunit interactions in the human 26S proteasome. *Proteomics* **8**, 508–520.
42 Bohn S, Beck F, Sakata E, Walzthoeni T, Beck M, Aebersold R, Forster F, Baumeister W & Nickell S (2010) Structure of the 26S proteasome from *Schizosaccharomyces pombe* at subnanometer resolution. *Proc Natl Acad Sci USA* **107**, 20992–20997.
43 Lander GC, Estrin E, Matyskiela ME, Bashore C, Nogales E & Martin A (2012) Complete subunit architecture of the proteasome regulatory particle. *Nature* **482**, 186–191.
44 Lasker K, Forster F, Bohn S, Walzthoeni T, Villa E, Unverdorben P, Beck F, Aebersold R, Sali A & Baumeister W (2012) Molecular architecture of the 26S proteasome holocomplex determined by an integrative approach. *Proc Natl Acad Sci USA* **109**, 1380–1387.
45 Deveraux Q, Ustrell V, Pickart C & Rechsteiner M (1994) A 26S protease subunit that binds ubiquitin conjugates. *J Biol Chem* **269**, 7059–7061.
46 Husnjak K, Elsasser S, Zhang N, Chen X, Randles L, Shi Y, Hofmann K, Walters KJ, Finley D & Dikic I (2008) Proteasome subunit Rpn13 is a novel ubiquitin receptor. *Nature* **453**, 481–488.
47 Su V & Lau AF (2009) Ubiquitin-like and ubiquitin-associated domain proteins: significance in proteasomal degradation. *Cell Mol Life Sci* **66**, 2819–2833.
48 Chen L & Madura K (2002) Rad23 promotes the targeting of proteolytic substrates to the proteasome. *Mol Cell Biol* **22**, 4902–4913.

49 Gomez TA, Kolawa N, Gee M, Sweredoski MJ & Deshaies RJ (2011) Identification of a functional docking site in the Rpn1 LRR domain for the UBA-UBL domain protein Ddi1. *BMC Biol* **9**, 33.
50 Babu JR, Geetha T & Wooten MW (2005) Sequestosome 1/p62 shuttles polyubiquitinated tau for proteasomal degradation. *J Neurochem* **94**, 192–203.
51 Parcellier A, Schmitt E, Gurbuxani S, Seigneurin-Berny D, Pance A, Chantome A, Plenchette S, Khochbin S, Solary E & Garrido C (2003) HSP27 is a ubiquitin-binding protein involved in I-kappaBalpha proteasomal degradation. *Mol Cell Biol* **23**, 5790–5802.
52 Watanabe TK, Saito A, Suzuki M, Fujiwara T, Takahashi E, Slaughter CA, DeMartino GN, Hendil KB, Chung CH, Tanahashi N *et al.* (1998) cDNA cloning and characterization of a human proteasomal modulator subunit, p27 (PSMD9). *Genomics* **50**, 241–250.
53 Dolcet X, Llobet D, Pallares J & Matias-Guiu X (2005) NF-kB in development and progression of human cancer. *Virchows Arch* **446**, 475–482.
54 Ravi R & Bedi A (2004) NF-kappaB in cancer – a friend turned foe. *Drug Resist Updat* **7**, 53–67.
55 Lee SY, De la Mota-Peynado A & Roelofs J (2011) Loss of Rpt5 protein interactions with the core particle and Nas2 protein causes the formation of faulty proteasomes that are inhibited by Ecm29 protein. *J Biol Chem* **286**, 36641–36651.
56 Wu Y, Li Q & Chen XZ (2007) Detecting protein–protein interactions by far western blotting. *Nature protocol* **2**, 3278–3284.

Supporting information

Additional supporting information may be found in the online version of this article at the publisher's web site:

Table S1. List of qRT-PCR primers.

Biochem. J. (2012) **447**, 61–70 (Printed in Great Britain) doi:10.1042/BJ20111432

online data

From prediction to experimental validation: desmoglein 2 is a functionally relevant substrate of matriptase in epithelial cells and their reciprocal relationship is important for cell adhesion

Vinita WADHAWAN, Yogesh A. KOLHE, Nikhil SANGITH, Amit Kumar Singh GAUTAM and Prasanna VENKATRAMAN[1]

Advanced Centre for Treatment, Research and Education in Cancer, Tata Memorial Centre, Kharghar, Navi Mumbai 410210, India

Accurate identification of substrates of a protease is critical in defining its physiological functions. We previously predicted that Dsg-2 (desmoglein-2), a desmosomal protein, is a candidate substrate of the transmembrane serine protease matriptase. The present study is an experimental validation of this prediction. As demanded by our published method PNSAS [Prediction of Natural Substrates from Artificial Substrate of Proteases; Venkatraman, Balakrishnan, Rao, Hooda and Pol (2009) PLoS ONE **4**, e5700], this enzyme–substrate pair shares a common subcellular distribution and the predicted cleavage site is accessible to the protease. Matriptase knock-down cells showed enhanced immunoreactive Dsg-2 at the cell surface and formed larger cell clusters. When matriptase was mobilized from intracellular storage deposits to the cell surface there was a decrease in the band intensity of Dsg-2 in the plasma membrane fractions with a concomitant accumulation of a cleaved product in the conditioned medium. The exogenous addition of pure active recombinant matriptase decreased the surface levels of immunoreactive Dsg-2, whereas the levels of CD44 and E-cadherin were unaltered. Dsg-2 with a mutation at the predicted cleavage site is resistant to cleavage by matriptase. Thus Dsg-2 seems to be a functionally relevant physiological substrate of matriptase. Since breakdown of cell–cell contact is the first major event in invasion, this reciprocal relationship is likely to have a profound role in cancers of epithelial origin. Our algorithm has the potential to become an integral tool for discovering new protease–substrate pairs.

Key words: desmoglein-2 (Dsg-2), cellular adhesion, invasion, epithelial cancers, matriptase.

INTRODUCTION

Proteases play a central role in cellular homoeostasis and are responsible for the spatio-temporal regulation of function. Many putative proteases have been identified through genomic approaches leading to a surge in global profiling attempts to characterize their natural substrates [1a]. In order to complement the ongoing efforts to identify physiologically relevant substrates of proteases and assess their cellular functions under normal and pathological conditions, we had proposed a novel prediction strategy [1]. We used sequence information from experimentally proven substrates of endoproteases and incorporated dual filters to identify the most probable candidates. These filters imposed a strong quantitative rule to assess the accessibility of a potential cleavage site and a qualitative co-localization rule which would ensure their likelihood of interaction. By using these criteria we catalogued potential substrates of serine proteases from the PDB and UniProt databases. Identity of the substrates was used for functional annotation to reveal novel functions of the proteases [1]. We have developed a web-based server for users to identify such cleavage sites on their query substrate (http://www.actrec.gov.in/pi-webpages/Prasanna/index.htm).

Matriptase is a type II serine protease found in the membrane of epithelial cells [2]. Under physiological conditions, matriptase plays a crucial role in hair follicle development by processing profilaggrin to filaggrin monomers [3]. The matriptase–prostatin cascade, with matriptase acting upstream of prostatin, has been found to be crucial in epithelial differentiation [4]. Matriptase also plays a crucial role in regulating the survival of developing T-lymphocytes in the thymic microenvironment [5]. Through its action on substrates like pro-HGF (hepatocyte growth factor)/SF-1 (scatter factor 1) and pro-uPA (urokinase-type plasminogen activator) [6–9], matriptase is likely to impart invasive properties to cancer cells. A potential association between matriptase deregulation and Ras-mediated carcinogenesis has been reported [10].

Matriptase is overexpressed in many cancer tissues [11,12], such as primary breast carcinomas [13,14], ovarian tumours of epithelial origin [15–17] and prostate cancer [18]. Clinico-pathological correlation between expression levels of matriptase and different grades of these tumours suggest that matriptase could be a good biomarker for the diagnosis and treatment of malignant breast tumours, a favourable prognostic marker in ovarian cancer and in staging of human prostate adenocarcinoma [14–18]. *In vitro* inhibition of matriptase prevented the growth of prostate and colon carcinoma cell lines with invasive properties [19]. Thus a strong correlation exists between matriptase and cell-invasive properties. In addition matriptase seems to possess strong tumorigenic potential. However, the mechanism by which matriptase mediates invasion remains unclear. Identification of novel substrates would help in correlating changes in expression levels, activity and the observed phenotype. Previously, using our method called PNSAS (Prediction of Natural Substrates from Artificial Substrate of Proteases) [1], we had identified Dsg-2 (desmoglein-2) as a novel putative substrate of matriptase. Dsg-2 is a desmosomal protein which harbours a putative cleavage site for matriptase, LGR∼S (P3P2P1∼P1′), between residues number 565 and 566.

Abbreviations used: DMEM, Dulbecco's modified Eagle's medium; Dsg-2, desmoglein-2, HEK, human embryonic kidney; HRP, horseradish peroxidase; IF, immunofluorescence; IPTG, isopropyl β-D-thiogalactopyranoside; LSM, laser-scanning microscope; Ni-NTA, Ni^{2+}-nitrilotriacetate; PNSAS, Prediction of Natural Substrates from Artificial Substrate of Proteases; rSASA, relative solvent-accessible surface area; SASA, solvent-accessible surface area; siRNA, small interfering RNA; S1P, sphingosine-1-phosphate; TBST, Tris-buffered saline containing 0.05 % Tween 20; wt, wild-type.

[1] To whom correspondence should be addressed (email vprasanna@actrec.gov.in).

Desmosomes are intercellular junctions that confer strong cell–cell adhesion properties. They are found in epithelia and cardiac muscles and are located at the cell membrane, where they act as anchors for intermediate filaments. The core of the desmosomal adhesive complex primarily consists of the desmogleins (Dsg1–4) and desmocollins (Dsc1–3). These glycoproteins belong to the cadherin superfamily of proteins. A decrease in the levels of the desmosomal proteins desmoplakin and plakophilin-1 in oral cancer tissues and a decrease in desmoplakin in breast cancer tissues in relation to normal tissues emphasizes the importance of these cell junction proteins in disease progression and metastasis. This may be also true of other tumour types, like adenocarcinoma and oral squamous cell carcinomas [20–24]. One of the mechanisms by which early stage tumour cells acquire an invasive phenotype is by undergoing EMT (epithelial–mesenchymal transition). This is accompanied by secretion of proteases, which together results in disruption of adherent junctions and desmosomal integrity, enabling cancer cells to dissociate from the primary tumour site and invade the surrounding tissues [21]. Dsg-2 was reported to be a substrate of kallikerin-7, a chymotryptic-like serine protease, in pancreatic cancer cells [25].

Therefore the unique ability of tumour cells to invade and metastasize can be attributed to a fundamental deregulation between its pro-adhesion components and the proteases that degrade the ECM (extracellular matrix) and break cell–cell contact [26]. Since Dsg-2 is responsible for cell–cell adhesion and matriptase is an enzyme implicated in cell invasion, we asked if Dsg-2 would be a relevant physiological substrate of matriptase. In the present study we show that Dsg-2 is indeed a physiologically relevant substrate of matriptase. Reciprocal levels of the enzyme and its cognate substrate at the cell surface results in altering the cell adhesion properties of HCT-116 cells, implying a role for matriptase in cell invasion through its novel substrate Dsg-2.

MATERIALS AND METHODS

Chemicals and reagents

Formaldehyde solution was obtained from Merck (catalogue number 61783705001046). S1P (sphingosine 1-phosphate) (catalogue number S9666) was purchased from Sigma. S1P was prepared at 10 μg/ml in HPLC-grade methanol and final working solution was prepared at 50 ng/ml. BSA (catalogue number A7906), IPTG (isopropyl β-D-thiogalactopyranoside; catalogue number I6758) and mitomycin C (catalogue number M0503) were procured from Sigma. Ampicillin (catalogue number RM 645) was obtained from Himedia.

Cell culture conditions

Experiments were conducted on the human colonic carcinoma cell line HCT-116 wt (wild-type; a gift from Dr Sorab Dalal, ACTREC, Navi Mumbai, India) and HEK (human embryonic kidney)-293 cells. These cells were cultured in DMEM (Dulbecco's modified Eagle's medium) supplemented with 10 % FBS (fetal bovine serum), 1.5 g/l sodium bicarbonate and 1 % antibiotic/antimycotic solution containing streptomycin, amphotericin B and penicillin.

Antibodies

Monoclonal anti-Dsg-2 antibody clone 6D8 and AH12.2 (recognizing the extracellular domain) were purchased from Invitrogen (catalogue number 32-6100) and Santa Cruz Biotechnology (catalogue number sc-80663) respectively. Rabbit anti-(human matriptase) antibody, which recognizes the extracellular protease domain (residues 800–855), was obtained from Bethyl laboratories (catalogue number A300-221A). Secondary HRP (horseradish peroxidase)-labelled anti-mouse (NA931) and anti-rabbit (NA934) antibodies were procured from GE Healthcare. Primary rat monoclonal anti-CD44 antibody, Alexa Fluor™ 488-conjugated sheep anti-(rat IgG) antibody and anti-rat HRP-labelled secondary antibodies were gifts from Dr Rajiv Kalraiya (ACTREC, Navi Mumbai, India) and primary monoclonal anti-E-cadherin antibody was a gift from Dr Sorab Dalal.

Total cell lysate preparation and subcellular fractionation

Cells from 95 % confluent dishes of HCT-116 wt cells were trypsinized and washed twice with 1× PBS. Pellets were suspended in lysis buffer [50 mM Tris (pH 7.5), 125 mM NaCl and 0.5 % Nonidet P40 with 1× cocktail of protease inhibitors], briefly vortex-mixed and incubated on ice for 30 min. Cell suspension was then centrifuged at 15 000 rev./min (Plastocraft Rota 4R rotor) for 15 min at 4 °C. The supernatant was collected and stored at − 20 °C. A Subcellular Protein Fractionation kit (78840) by Pierce and Thermo Scientific were used for preparing membrane and cytosolic fractions. The amount of protein in the cell lysates was estimated by the Bradford method using BSA as standard.

SDS/PAGE and Western blotting

Cell lysates were mixed with 1× Lammelli's sample buffer under non-boiling conditions and proteins were separated by SDS/PAGE (10 % gel). To detect Dsg-2, samples were boiled for 5 min followed by SDS/PAGE (7.5 % gel). The proteins were transferred on to PVDF membranes overnight at 4 °C (Bradford wet-transfer blotting apparatus set at 70 V and 200 mA). Unbound sites were blocked using 3 % BSA in TBST [Tris-buffered saline containing 0.05 % Tween 20 (pH 7.4)] for 2 h. Incubation with primary antibody for matriptase (1:250 dilution) and Dsg-2 AH12.2 clone (1:250 dilution) was performed for 2 h at room temperature (25°C). Secondary antibodies against matriptase (1:5000 dilution) and Dsg-2 (1:2500 dilution) were incubated for 1 h at room temperature. Each incubation step was followed by six washes, each for 10 min, with TBST. The blots were developed using the ECL (enhanced chemiluminescence) Plus kit (GE Healthcare RPN2132) on Kodak X-ray films.

Detection of shed ectodomain of Dsg-2 in the conditioned medium of HCT-116 wt cells

One million HCT-116 cells were seeded in six 90-mm dishes and allowed to grow until they reached 98 % confluence. The growth medium from confluent monolayers was removed and cells were subjected to overnight serum starvation. Cells were washed twice with 1× PBS and incubated in a serum-free medium containing 50 ng/ml S1P for 2 h at 37 °C. Post-incubation, the conditioned media were collected, pooled and centrifuged at 400 ***g*** for 5 min at 4 °C and then concentrated using Amicon Ultra-4 centrifugal filter units, 10 kDa nominal molecular mass limit (Millipore), according to the manufacturer's instructions.

To detect shed Dsg-2, equal concentrations of control and S1P-treated conditioned medium were mixed with Lammelli's buffer and immunoblotted as described above. Primary Dsg-2 AH12.2 clone (1:250 dilution) was incubated for 2 h at room temperature followed by anti-mouse-HRP (1:2500 dilution) for 1 h at room temperature.

Immunofluorescence microscopy

Cells were seeded on to autoclaved coverslips and grown to confluence. For the S1P-based experiments, cells were subjected to overnight serum starvation followed by incubation with 50 ng/ml S1P for 2 h. For the siRNA (small interfering RNA)-mediated matriptase down-regulation, cells were treated with 50 nM of siRNA against matriptase with 2.5 μl/ml of transfection reagent. Cells were incubated for 24 h and then the siRNA-containing medium was replaced by normal complete medium. The cells were allowed to proliferate for another 24 h and fixed (see below). To study the effect of exogenously added purified recombinant matriptase, HCT-116 wt cells were incubated with 5 or 10 μg/ml of proteolytically active matriptase (constituted in incomplete DMEM adjusted to pH 8.8) for 2 h at 37 °C.

For immunostaining, cells were fixed and permeabilized (3.7 % formaldehyde for 20 min at room temperature and 0.05 % Triton X-100 for 10 min at room temperature respectively). BSA (3 %) was used to block non-specific sites (37 °C for 30 min). For co-localization studies of matriptase with Dsg-2, CD44 or E-cadherin, fixed cells were stained with rabbit polyclonal anti-matriptase antibody (1:50 dilution in 1× PBS with 3 % BSA) and anti-Dsg-2 antibody [both the 6D8 and AH12.2 clones (1:50 dilution)], rat anti-CD44 (1:50 dilution) or mouse anti-E-cadherin (1:50 dilution) for 2 h at 37 °C. Secondary antibodies were diluted to 1:100 in 3 % BSA in 1× PBS and incubation was carried out for 1 h at room temperature. Matriptase Alexa Fluor™ 488- (catalogue number A11008, Invitrogen) or Alexa Fluor™ 568- (catalogue number A11011, Invitrogen) conjugated goat anti-(rabbit IgG) antibody, Dsg-2 Alexa Fluor™ 568- and E-cadherin Alexa Fluor™ 568-conjugated goat anti-(mouse IgG) antibody (catalogue number A11004, Invitrogen) and CD44 Alexa Fluor™ 488-conjugated sheep anti-(rat IgG) antibody were used as secondary antibody conjugates. Individual controls for each primary antibody or the secondary antibodies were used. Each incubation step was followed by two washes with 1× PBS.

To visualize the nuclei and DNA, cells were stained with 1 μg/ml DAPI (4′,6-diamidino-2-phenylindole) for 30 s at 37 °C followed by 1× PBS wash. All of the coverslips were mounted in PBS containing 50 % glycerol and 5 mM DABCO (1,4-diazadicyclo[2.2.2]octane).

Confocal images were obtained using the LSM (laser-scanning microscope) 510 Meta Carl Zeiss confocal system with Argon 488 nm and Helium/Neon 543 nm lasers. Images were acquired using Observer Z.1 microscope using a plan-apochromat ×63 oil objective lens with ×2 optical zoom. Processing of the acquired images, mean fluorescence intensity and overlap coefficient measurements were done using LSM software.

Hanging-drop assay

Cell counts were adjusted to 20 000 cells/μl in complete DMEM. They were suspended as 35-μl-sized drops from the lid of a well (24-well plates) and incubated for 16 h at 37 °C in 5 % CO_2. PBS (1×) was used to maintain humidity. Post-incubation, each drop was mixed five times, fixed with 10 μl of 3 % glutaraldehyde and the aliquots (40 μl) were spread on autoclaved coverslips to be air dried [27]. Finally, the coverslips were mounted on to slides as described above. Images of five random fields for each sample were taken with a plan-Neofluar lens (numerical aperture = 0.3) at ×10 on an upright AxioImager Z1 microscope (Carl Zeiss). The area of cell clusters was determined using Axiovision rel 4.5 software (Zeiss).

Specific knockdown of matriptase using siRNA

ON-TARGETplus smart pool siRNA for matriptase (catalogue number L-003712-00), SiGLO Green transfection indicator (catalogue number D-001630-01-05) siRNA and transfecting reagent (catalogue number T2001-63) and 5× siRNA buffer (catalogue number B-002000UB100) were purchased from Dharmacon Scientific. Freeze-dried siRNAs were reconstituted and diluted in the requisite buffers in DEPC (diethyl pyrocarbonate; catalogue number D-5758, Sigma)-treated autoclaved eppendorfs. siRNAs were reconstituted in 1× siRNA buffer and their integrity was confirmed by nanodrop spectrophotometer following the manufacturer's instructions. Further dilutions were carried out with 1× siRNA buffer to obtain 20 μM and 100 μM stocks which were further diluted to 50 nM for the reactions. Transfection efficiency of 77 % was observed by FACS in SiGLO-transfected HCT-116 wt cells. For optimal knockdown of matriptase, 30 000 HCT-116 wt cells/ml were seeded on to autoclaved coverslips or sterile 35-mm dishes. They were treated with 50 nM of matriptase siRNA in 2.5 μl/ml of transfection reagent. FITC-labelled siRNA served as the negative control. After a 24 h incubation, the medium was replaced by normal complete medium. Cells were allowed to proliferate for another 24 h and harvested for Western blotting, IF (immunofluorescence) or cell-adhesion assays.

Constructs, expression and purification of the active protease domain of matriptase

Matriptase cDNA in a pcDNA 3.1 vector was a gift from Dr Chen-Yong Lin (University of Maryland, Baltimore, MD, U.S.A.). The nucleotides corresponding to amino acids 596–855 (the autocatalytic and proteolytic domains of matriptase) were cloned using BamH1 and KpnI restriction enzymes with the forward (5′-GGATCCGGCTCAGATGAGAAGGACTGC-3′) and reverse (5′-GGTACCTACCCCAGTGTTCTCTTTGAT-3′) primers from Sigma. The PCR product was ligated to the pRSETA vector and transformed in *Escherichia coli* Rosetta strain cells. Expression was induced with 100 μM IPTG for 16 h at 24 °C. Bacterial cells were harvested, suspended in lysis buffer [50 mM Tris (pH 8.0), 500 mM NaCl, 10 % glycerol and 1 mM BME (2-mercaptoethanol)], sonicated (10 cycles of 1 cycle per min) and centrifuged at 20 000 rev./min (Sorval RC 5 rotor plus SS 34) for 30 min, the supernatant was collected and the pH was adjusted to 8. The catalytic domain of matriptase was purified using a Ni-NTA (Ni^{2+}-nitrilotriacetate) affinity chelating column (catalogue number 30210, Qiagen) followed by size-exclusion chromatography (Superdex75, 16/60 column). Protein fractions were collected from 60 to 80 ml and samples were run on an SDS/PAGE gel (12 %). Fractions containing a single band at 27 kDa, corresponding to the molecular mass of matriptase, were pooled. Enzyme activity was monitored by incubating 120 μg β-casein with 0.25 μg/μl of purified recombinant matriptase in 200 μl of reaction mixture [100 mM Tris (pH 8.8) containing 0.5 μg/ml BSA]. β-Casein alone served as the control. Samples were incubated for 5 h and subjected to SDS/PAGE (15 % gel) analysis.

Cloning of Dsg-2 and creation of the R565A mutant

During processing and trafficking of Dsg-2 en route to the cell surface, signal and propeptide sequences (residues 1–50) will be cleaved. Therefore any tag at the N-terminus will have to be fused after the 50th amino acid. How this will affect folding, processing, transport and yield of Dsg-2 at the membrane surface

is hard to predict. A tag at the C-terminus will not be reflective of proteolysis since it would protrude into the cytoplasm and may remain even after cleavage at the extracellular domain. Therefore we chose to overexpress the wt (cDNA of human Dsg-2 was a gift from Dr Werner Franke, German Cancer Research Center, Heidelberg, Germany) and mutant Dsg-2 in their native forms. We used the pCMV 3× FLAG vector for cloning (Invitrogen) for the following reasons: (i) we routinely use this vector in our laboratory for all mammalian protein expression; (ii) all of the proteins so far have exhibited excellent expression without alteration in localization or function; and (iii) no toxicity has been observed so far. wt Dsg-2 was cloned between NotI and BamHI restriction sites with the forward primer (5′-AATGTGCGGCCG-CGATGGCGCGGACGCGGGAC-3′) and the reverse primer (5′-ATCGTCGGATCCTTAGGAGTAAGAATGCTGTA-3′). When Dsg-2 is translated and processed, the FLAG tag will be removed and is unlikely to cause any problems associated with folding and trafficking. Site-directed mutagenesis (R565A within LGRS) was performed using PCR-based amplification with the forward primer (5′-GAAAAAGCTTGGGGCGAGTGAAATTCAGTT-3′) and the reverse primer (5′-AACTGAATTTCACTCGCCCCA-AGCTTTTTCT-3′).

Over-expression of wt and mutant Dsg-2 in HEK-293 cells

HEK-293 cells were seeded on to autoclaved coverslips and grown to 80 % confluence. They were transfected with any of the following: pCMV10 3× FLAG construct containing no gene, Dsg-2 wt or mutant Dsg-2 (R565A) using the calcium phosphate method. The cells were incubated for 48 h and treated with purified recombinant proteolytically active matriptase at 10 μg/ml and processed for IF as described above.

Statistical analysis

For each assay (where applicable) three independent experiments were performed. The *P* value for the intensity measurements was statistically analysed using an unpaired Student's *t* test and ANOVA (SPSS version 15 and Graphpad Prism). All of the statistical data were calculated from three independent experiments.

RESULTS

Predicted cleavage site KLGR∼SEIQ in the ectodomain of Dsg-2 is accessible to matriptase

Using our prediction program PNSAS we had identified Dsg-2 (from the proteome database) as one of the putative substrates of matriptase [1]. Both Dsg-2 and matriptase are cell-surface proteins. Dsg-2 is very important for cell adhesiveness and breaching of cell–cell contact is one of the early events in invasion and metastasis. Matriptase is an enzyme implicated in metastasis. Therefore we were curious to find if matriptase regulated the cell surface expression of Dsg-2 by cleaving it. If so, changes in the expression levels of active matriptase would reciprocally influence the surface levels of Dsg-2. Information from the UniProt-derived sequence of Dsg-2 (entry Q14126) is schematically represented to indicate the topological distribution and glycosylation sites of different regions of the protein (Figure 1a). The matriptase cleavage site is indicated by the asterisk symbol. The P3P2P1∼P1′ positions of the putative matriptase cleavage site in Dsg-2 are occupied by LGR∼S, with the scissile bond located between Arg^{565} and Ser^{566}. The molecular sizes of the expected cleavage fragments are also indicated (Figure 1a).

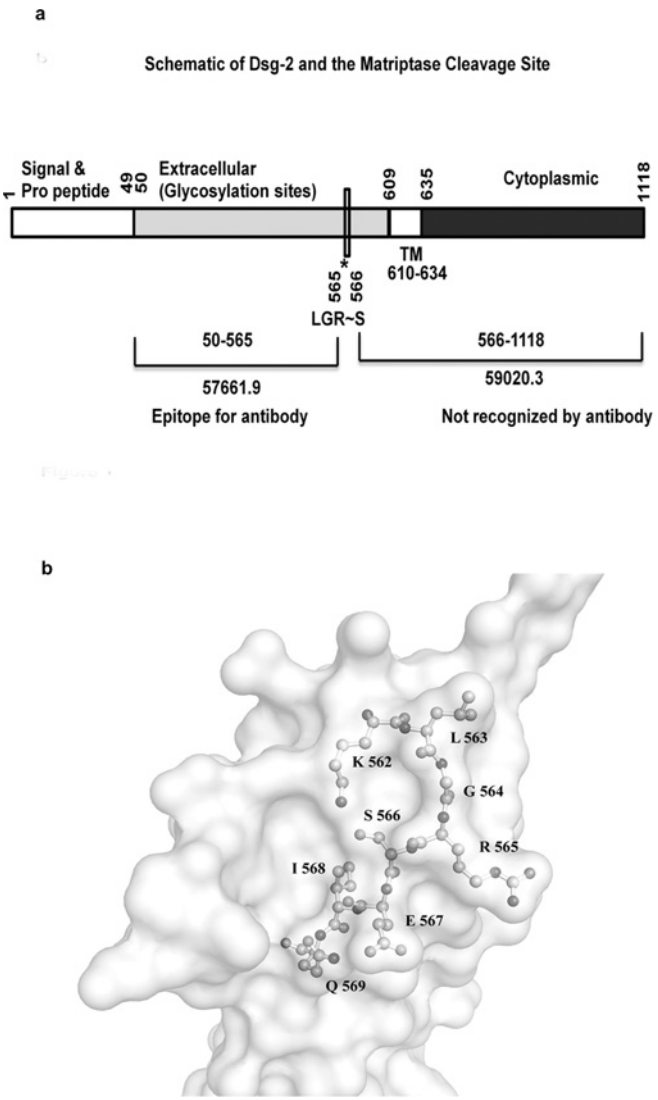

Figure 1 Presence of a predicted matriptase-specific cleavage site on Dsg-2 and its accessibility

(**a**) The topology of Dsg-2 and the expected size of the matriptase-generated products. (**b**) The structure of Dsg-2 was modelled based on its homology to cadherin. Residues 562–569 harbouring the predicted cleavage site between Arg^{565}–Ser^{566} (P1-P1′) are represented as sticks.

Since such a short sequence may be shared both by substrates and non-substrates of a protease, our program imposes filters to narrow down on the most probable physiologically relevant candidate substrates. One of the filters uses surface accessibility, which is computed from the high-resolution three-dimensional structure of the protein. There is no structure for Dsg-2 in the PDB. However, this protein belongs to the cadherin family (member 5) of proteins. The protein fold consists of four cadherin and six desmoglein repeats. The FASTA sequence of Dsg-2 was submitted to Modbase [28]. The most probable structure was built using the X-ray structure of c-cadherin ectodomain (PDB code 1L3W). The target sequence of amino acids 50–599 of Dsg-2 exhibited 34 % sequence identity with amino acids 2–540 of c-cadherin. The cleavage site LGR∼S (scissile bond between 565 and 566) is neither part of the desmoglein repeat or the cadherin domain. However, the region is nevertheless clearly modelled and could be overlaid with the corresponding region from c-cadherin (results not shown). We also independently modelled the structure of

Table 1 Co-localization of matriptase and Dsg-2 in HCT-116 wt cells

Double immunostaining for matriptase and Dsg-2 was carried out to ascertain their co-localization on the cell surface. The extent of their co-localization was measured as an overlap coefficient of their individual intensities using LSM software. An overlap coefficient of 0.9 is indicative of 90 % co-localization between matriptase and Dsg-2.

Co-localization coefficient CH3-T1	Co-localization coefficient CH3-T3	Weighted co-localization coefficient CH3-T1	Weighted co-localization coefficient CH3-T3	Overlap coefficient
0.186	0.191	0.182	0.198	0.9

Dsg-2 using homology modelling against known structures in the PDB. Mouse N-cadherin ectodomain (PDB code 3Q2W) with 34 % identity in the region of amino acids 51–601 and a low DOPE (discrete optimized protein energy) score was modelled using Modeller [29] and the structure was verified using a Ramachandran plot. It is clear from Figure 1(b) that the LGR∼S region is in a solvent-exposed part of the modelled protein and the putative cleavage site is likely to be well accessible to the protease. The SASA (solvent-accessible surface area) value of the octapeptide KLGR∼SEIQ (amino acids 562–569) harbouring the putative cleavage site between amino acids 565 and 566 was calculated using Surface Racer 5 [30]. This value can be compared with a known and easily accessible protease cleavage site in α-antitrypsin (AAGA∼MFLE; PDB code 1QLP; SASA value = 811.6) which is cleaved by matrix metallopeptidase 7 to obtain the rSASA (relative SASA) value, a quantitative index of accessibility. We had used this protein earlier as the reference point for calculating rSASA values of substrates [1]. Using this reference, the rSASA value for the Dsg-2 cleavage site will be 0.78, indicating that the site must be readily accessible to matriptase.

Co-localization of matriptase and Dsg-2 in HCT-116 wt cells

In order for an enzyme to act on its substrate, both should be found in the same subcellular compartment. Therefore the second filter that is imposed by PNSAS is subcellular distribution. Both matriptase and its candidate substrate Dsg-2 are transmembrane proteins. To ascertain the presence of these two proteins at the membrane surface and to analyse the extent to which they co-localize in HCT-116 wt cells, a double immunostaining was performed. The anti-matriptase antibody that we chose exclusively recognizes an epitope in the extracellular domain spanning amino acids 615–822. The monoclonal anti-Dsg-2 (clone 6D8) antibody recognizes an epitope in the extracellular domain of Dsg-2 harbouring the predicted cleavage site. Using these antibodies for immunostaining we found that matriptase and Dsg-2 are present on the surface of HCT cells with an overlap coefficient of 0.9, indicating that 90 % of matriptase and Dsg-2 are close to each other (Figures 2a and 2b, and Table 1). Western blotting of the subcellular fractions of HCT-116 wt cells with the same matriptase-specific antibody and AH12.2 clone for Dsg-2 revealed two immunoreactive bands, in the membrane fractions of the cells. They correspond to ∼80 kDa for matriptase and ∼130 kDa in the case of Dsg2 (Figure 2c).

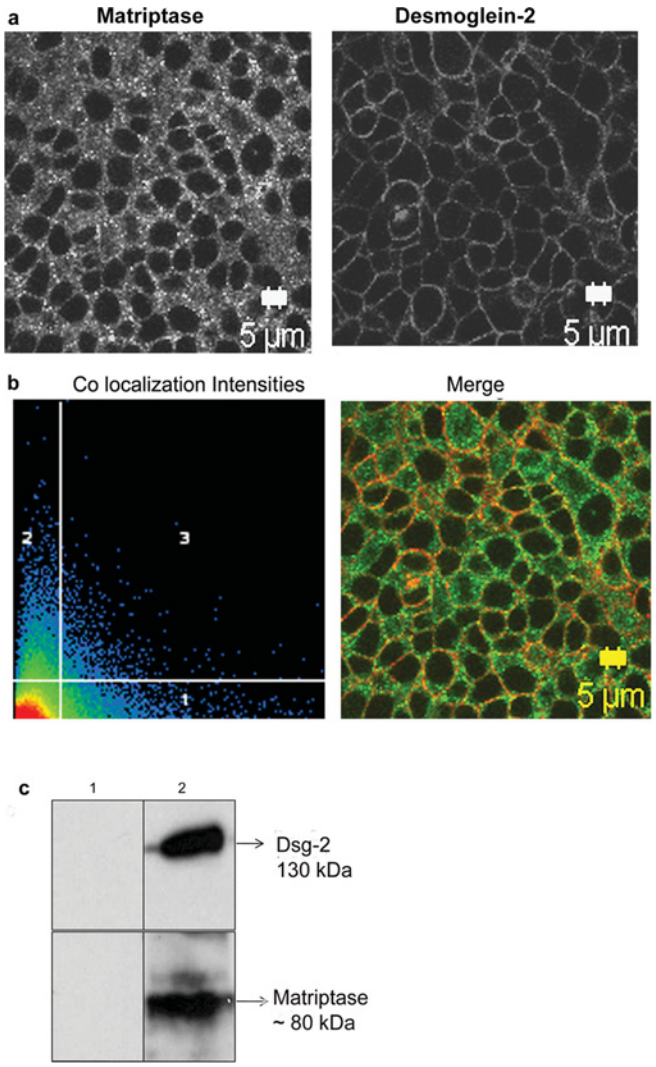

Figure 2 Detection and co-localization of matriptase and Dsg-2 on the surface of HCT-116 wt cells

(**a**) Double immunolabelling was performed using respective antibodies specific against the extracellular domain of matriptase and Dsg-2. (**b**) The merged confocal micrograph shows an overlap coefficient of 0.9. The results are representative of three independent experiments. (**c**) Western blotting of the subcellular fractions of HCT-116 wt cells showing the presence of Dsg-2 (AH 12.2 clone, ∼130 kDa) and matriptase (∼80 kDa) in the membrane fractions. Lane 1 is cytosolic fraction and lane 2 is membrane fraction.

siRNA-mediated down-regulation of matriptase in HCT-116 wt cells results in more immunoreactive Dsg-2 at the cell surface

In order to demonstrate that Dsg-2 is a candidate substrate for matriptase in the cellular context, we used siRNA to down-regulate the enzyme in HCT-116 wt cells. If Dsg-2 was a substrate for matriptase then upon depletion of the enzyme the levels of immunoreactive Dsg-2 should increase. The antibody we chose is established to interact with the extracellular domain harbouring the cleavage site. After 48 h of siRNA treatment, Western blotting showed a 95 % decrease in the band intensity of matriptase confirming knock-down (Figure 3a). Parallel IF studies showed that the intensity of matriptase signal in siRNA-treated cells was diminished by 61 % ($P = 0.023$) with a concomitant 55 % increase in the intensity of Dsg-2 ($P = 0.022$) (Figure 3b and Supplementary Figure S1 at http://www.BiochemJ.org/bj/447/bj4470061add.htm). To

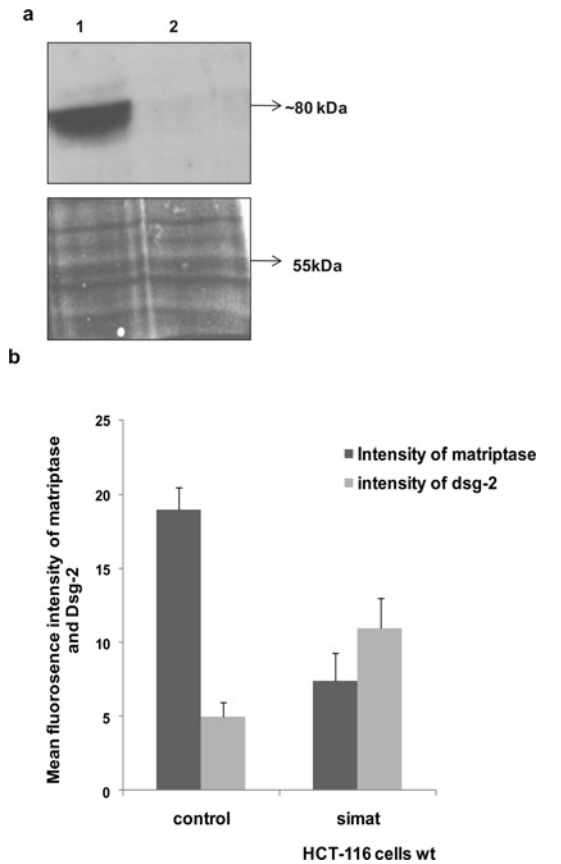

Figure 3 Effect of down-regulation of matriptase on immunoreactivity of cell surface Dsg-2 in HCT-116 wt cells

(**a**) Upper panel, Western blotting of control and matriptase-siRNA-treated cell lysates. The cell lysates from the control (lane 1) and matriptase-siRNA-treated HCT-116 wt cells (lane 2) were probed for matriptase (~80 kDa) expression. Lower panel, a Coomassie Blue-stained PVDF membrane demonstrating equal loading of the samples. (**b**) Graphical representation of the mean fluorescence intensities of Dsg-2 and matriptase in control and matriptase siRNA-treated cells (simat). Mean fluorescence intensities were measured using LSM software of 50 cells chosen at random. Error bars represent S.D.

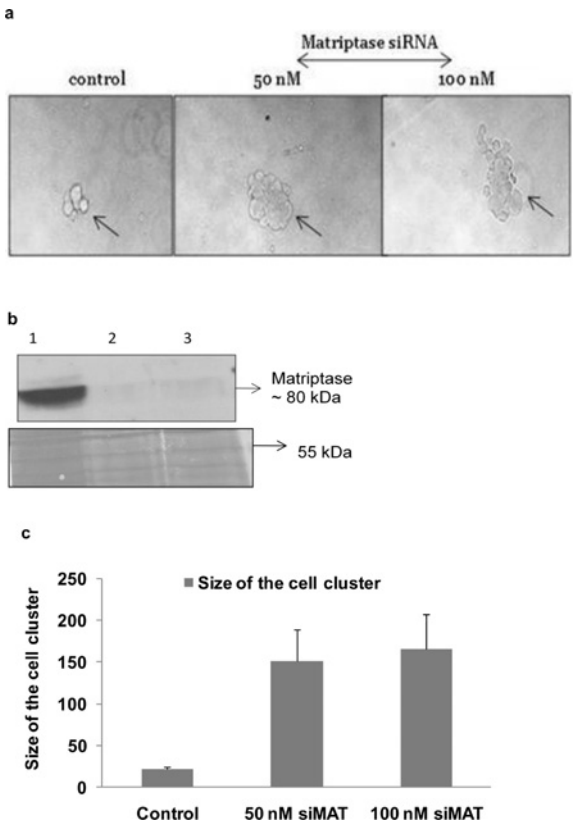

Figure 4 Effect of down-regulation of matriptase on cell–cell adhesion

(**a**) Differential interference contrast image of cells in both the control and matriptase-knockdown cells at ×20 magnification. (**b**) Upper panel, Western blotting of control and matriptase-siRNA-treated cell lysates. The cell lysates from the control (lane 1), 50 nM matriptase-siRNA-treated (lane 2) and 100 nM matriptase-siRNA-treated (lane 3) HCT-116 wt cells were probed for matriptase (~80 kDa) expression. Lower panel, Coomassie Blue-stained PVDF membrane demonstrating equal loading of samples. (**c**) Graphical representation of the cluster size in control and HCT-116 cells treated with 50 and 100nM of siRNA against matriptase (siMAT). More than five fields were chosen at random. Error bars represent S.D.

verify that the up-regulation of Dsg-2 on the cell surface was a specific response to matriptase down-regulation, we checked levels of two other surface proteins, CD44 and E-cadherin, in the knock-down cells. Among these two proteins, CD44 carries a potential cleavage site, QART, whereas E-cadherin lacks any known cleavage site for matriptase. We observed no measurable differences in the levels of CD44 (Supplementary Figure S2 at http://www.BiochemJ.org/bj/447/bj4470061add.htm) and E-cadherin (Supplementary Figure S3 at http://www.BiochemJ.org/bj/447/bj4470061add.htm) between control and siRNA-treated HCT-116 wt cells. The lack of cleavage of CD44 harbouring a putative cleavage site for matriptase is probably due to its inaccessibility or requirement for additional levels of regulation. We could not model the structure of CD44 due to a lack of appropriate templates. It seems that cleavage of Dsg-2 by matriptase is a specific and well-regulated process in the context of a cell.

Matriptase down-regulated cells form bigger cell clusters owing to increased levels of Dsg-2

Dsg-2 is a key desmosomal protein involved in maintaining cell–cell contact via homophilic and heterophilic interactions with other desmosomal proteins of adjacent cells. Increase in the levels of Dsg-2 at the cell surface is expected to increase cell adhesiveness. If cleavage of Dsg-2 by matriptase was functionally relevant then one may expect increase in cell–cell contact in matriptase knock-down cells mediated by Dsg-2. To test this possibility a hanging-drop assay was performed [27]. As expected, the cells treated with siRNA for matriptase formed bigger clusters ($152.1 \pm 38.3\ \mu$m) when compared with the control cells ($21.7 \pm 3.0\ \mu$m) (Figure 4). This indicates that activity of matriptase is an important regulator of cell–cell adhesion via Dsg-2 and this reciprocal relationship between the levels of matriptase and Dsg-2 could be one of the parameters that determine cell invasiveness.

Exogenously added pure active recombinant matriptase decreases the levels of immunoreactive Dsg-2 on the cell surface of HCT-116 wt cells

To prove further that matriptase alters levels of Dsg-2 at the cell surface by cleaving it, a recombinant matriptase corresponding to amino acids 596–855 was expressed, isolated and purified. A single band at 27 kDa corresponding to the molecular mass of recombinant matriptase was observed (Figure 5a). This was confirmed to be matriptase by Western blotting (results not

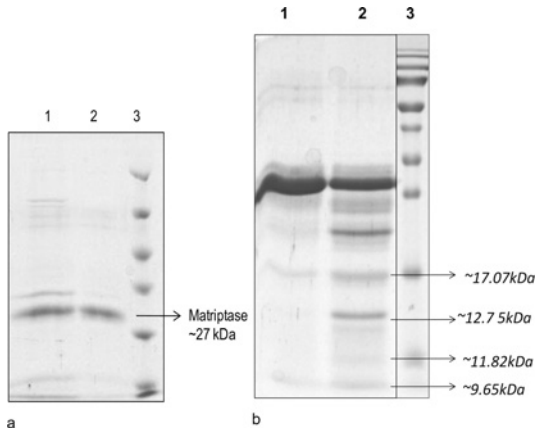

Figure 5 Purification of recombinant matriptase and its effect on β-casein degradation

(**a**) SDS/PAGE (12 % gel) showing protein profile of matriptase during purification. Samples from Ni-NTA (lane 1), Sephadex S200 fraction (lane 2) and prestained marker (lane 3) were loaded. (**b**) Degradation of β-casein by purified recombinant matriptase. The samples from β-casein incubated with matriptase for 0 h (lane 1), for 5 h (lane 2) and prestained marker (lane 3) were run on SDS/PAGE (15 % gel). The image is a composite presentation of samples run in different wells of the same gel, as shown by the lines dividing the lanes.

shown). Purified matriptase was able to hydrolyse β-casein, an unstructured protein used routinely to monitor the *in vitro* activity of endoproteases. Following a 5 h incubation with matriptase, distinct fragments of β-casein corresponding to $\sim$17 kDa, 12 kDa, 11 kDa and 9 kDa were observed only in the presence of recombinant matriptase (Figure 5b).

HCT-116 wt cells were then incubated with this proteolyticaly active pure recombinant matriptase at 5 and 10 μg/ml concentrations for 2 h and were processed for immunostaining. There was a marked reduction in the immunostaining of Dsg-2 in the matriptase-treated cells. The mean fluorescence intensity of Dsg-2 in the cells treated with 5 and 10 μg/ml of matriptase was 55.7 % ($P = 0.006$) and 34.1 % ($P = 0.032$) respectively as compared with their untreated counterparts (Figure 6). Unlike Dsg-2, no effect was seen in the intensity of CD44 and E-cadherin (Supplementary Figure S4 at http://www.BiochemJ.org/bj/447/bj4470061add.htm) levels. The cells without any matriptase at pH 7.5 and at 8.8 (optimum pH for matriptase activity) had comparable intensity values for Dsg-2 (Figure 6a), thereby confirming that pH itself did not induce any change in Dsg-2 expression. In both the control and the treated samples the cells displayed fillopodial projections, which may be due to serum starvation.

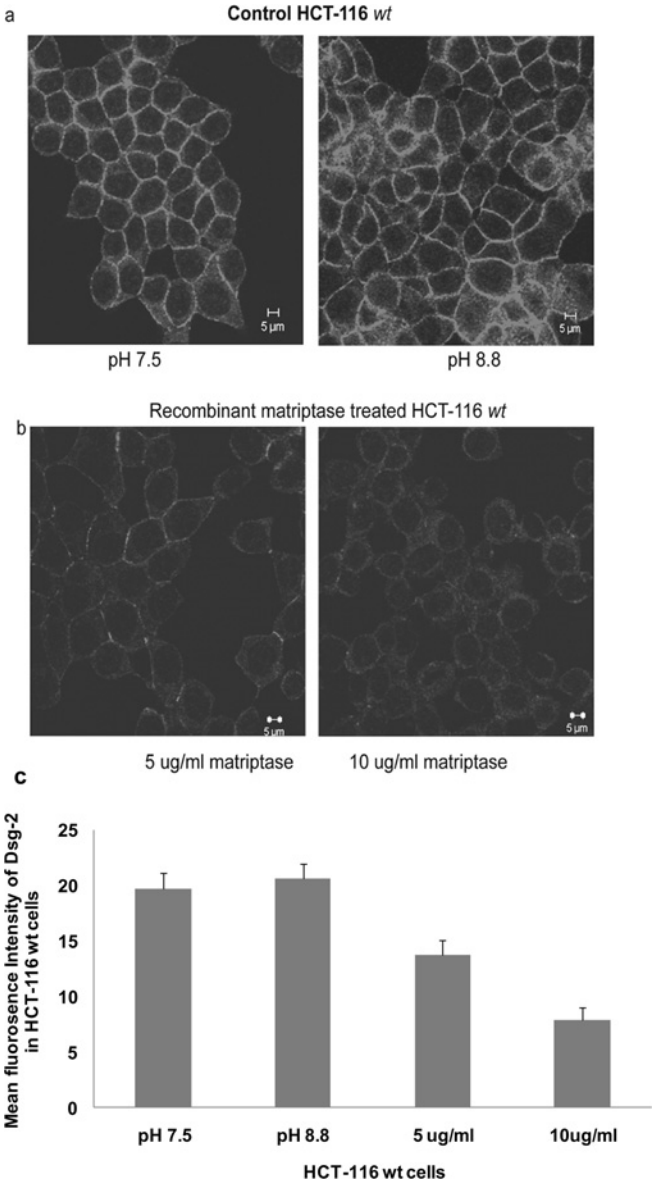

Figure 6 Effect of recombinant matriptase on the immunoreactivity of Dsg-2 at the surface of HCT-116 wt cells

The difference in immunoreactive levels of Dsg-2 in control and cells treated with pure matriptase was monitored using IF. (**a**) Dsg-2 in control HCT-116 wt cells incubated in serum-free DMEM at pH 7.5 and 8.8. (**b**) HCT-116 wt cells treated with 5 μg/ml and 10 μg/ml of pure matriptase. (**c**) Graphical representation of mean fluorescence intensity of Dsg-2 in control and matriptase-treated HCT-116 cells. Error bars represent S.D.

Mobilization of intracellular pools of matriptase to cell surface by S1P decreased surface levels of Dsg-2

Previous studies have reported that S1P caused accumulation and activation of matriptase at mammary epithelial cell–cell contacts [2–4]. In order to further establish specific cleavage of Dsg-2 by endogenous matriptase, we stimulated HCT-116 wt cells with S1P. Subsequent to treatment with S1P, there was a time-dependent progressive increase in the levels of matriptase [48.7 % increase after a 2 h incubation ($P = 0.01$)]. There was a corresponding decrease in immunoreactive Dsg-2 amounting to a 40.3 % ($P = 0.017$) loss in intensity (Figures 7a and 7b, and Supplementary Figure S5 at http://www.BiochemJ.org/bj/447/bj4470061add.htm). Under the same conditions, the intensity values of Dsg-2 and matriptase in untreated cells remained essentially unaltered. These results confirm the reciprocal relationship between endogenous matriptase and Dsg-2, which reiterates that Dsg-2 is a physiologically relevant substrate of matriptase.

To facilitate the identification of the cleaved products, the cell lysates and concentrated conditioned media of the control and S1P-treated HCT-116 cells were immunoblotted. A distinct decrease in the band intensity of Dsg-2 in the whole-cell lysates was accompanied by concomitant appearance of a $\sim$80 kDa fragment in the conditioned medium of both the samples (Figure 7c). In correlation with the presence of more active matriptase at the cell surface, the 80 kDa band in the S1P-treated cells exceeded that of the control cells. On the basis of

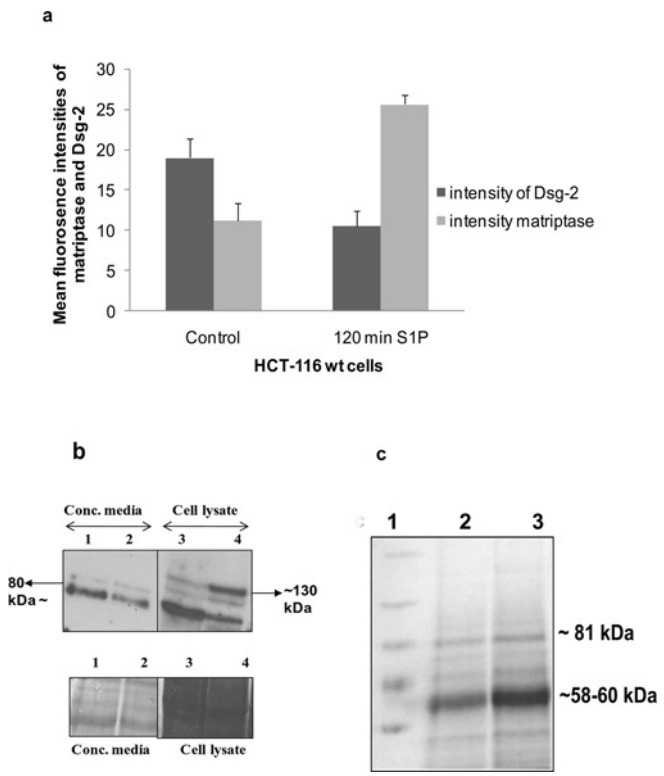

Figure 7 Effect of S1P on the relative levels of cell surface matriptase and Dsg-2 in HCT-116 wt cells

(**a**) Graphical representation of the mean fluorescence intensities of Dsg-2 and matriptase in control and 50 ng/ml S1P-treated cells. Mean fluorescence intensities were measured as before. Error bars represent S.D. (**b**) Upper panel, Western blot of conditioned medium and lysates of control and cells treated with S1P. Conditioned medium from S1P-treated cells (lane 1) and control cells (lane 2), lysates from S1P-treated cells (lane 3) and control cells (lane 4) were probed for Dsg-2 expression. Lower panel, a Coomassie Blue-stained PVDF membrane demonstrating equal loading of the samples. (**c**) Coomassie Blue staining of pooled conditioned media of control and 50 ng/ml S1P-treated HCT-116 wt cells. The fragments corresponding to cleaved products at ∼80 kDa and the ∼58–60 kDa regions can be seen. Prestained protein marker (lane 1), conditioned medium of control cells (lane 2) and conditioned medium of S1P-treated HCT-116 cells (lane 3).

previous reports, we envisaged that this fragment could be the shed ectodomain of Dsg-2 [25]. Appearance of the 80 kDa fragment in the control cells is probably due to the normal ongoing cleavage of Dsg-2 at the cell surface by matriptase which is further augmented by S1P treatment. Some amount of this product could be due to ongoing apoptosis-like mechanisms, which might contribute to anikoisis or detachment of cells from the surface via cleavage of adhesion-promoting proteins like Dsg-2.

In order to verify the identity of the cleaved products, the UniProt sequence of Dsg-2 was submitted to Expasy Protparam (http://www.expasy.org/tools/protparam.html) [31] and the theoretical molecular masses of the expected fragments were calculated. After removing both the pro and signal peptide sequences, the molecular mass of Dsg2 was calculated to be 116 kDa. However, an immune reactive product at 130 kDa was consistently detected upon Western blotting of the membrane fraction, indicating that this is probably the glycosylated form of Dsg-2. If matriptase cleaved at the predicted site within Dsg–2 (LGR∼S) it would generate two fragments: a 50–565 amino acid fragment of ∼57 kDa (57661.9), which would harbour the epitope for the AH12.2 antibody [32], and a 566–1119 amino acid fragment of ∼59 kDa (59020.3) (Figure 1a). Consistent with this estimate, Coomassie Blue staining of the S1P-treated conditioned media revealed a product at ∼58–60 kDa (Figure 7d) which was not immune reactive and an immune reactive band at a higher molecular mass of ∼80 kDa. This fragment with an aberrant molecular mass may originate from the epitope harbouring amino acids 50–565 and is probably glycosylated like the parent protein.

Matriptase cleaves Dsg-2 at the scissile bond within LGR∼S

So far all of the results show that matriptase cleaves endogenous Dsg-2 and the cleavage most likely occurs within LGR (P1)∼S (P1′). In order to unequivocally establish the specific cleavage site, it will be important to show that mutation at the predicted site in Dsg-2 prevents cleavage by matriptase. We decided to overexpress the wt and mutant Dsg-2 carrying a point mutation at Arg^{565} (R565A) and incubate them with purified matriptase.

HEK-293 cells were transfected with the wt and mutant Dsg-2 (R565A) under the constitutive promoter CMV (cytomegalovirus). To confirm overexpression, at 48 h post-transfection the cells were harvested for Western blotting (Figure 8a) or were immunostained. Both Western blotting- and IF-based mean fluorescence intensity measurement confirmed >1.8-fold overexpression of Dsg-2 in the wt and mutant populations. Transfected cells were incubated with 10 μg/ml of proteolytically active recombinant matriptase, as described above. There was a marked reduction in the immunostaining of Dsg-2 in the cells treated with matriptase. The mean fluorescence intensity of Dsg-2 in matriptase-treated untransfected cells was 44.9 % ($P < 0.0001$), in cells overexpressing wt Dsg-2 28.5 % ($P < 0.0001$) and in cells overexpressing mutant Dsg-2 it was 75.6 % ($P < 0.0001$) as compared with their respective untreated counterparts (Figure 8b).

The 25 % loss in Dsg-2 intensity in the mutant cells is probably due to matriptase-mediated degradation of the endogenous Dsg-2 rather than proteolysis of mutant Dsg-2. Hence we can safely conclude that the inability of matriptase to cleave mutant Dsg-2 could be due to the absence of Arg^{565} at the P1 position of the scissile bond in the LGR∼S sequence that is recognized and cleaved by matriptase. To eliminate observer bias, wider fields (152 μm×152 μm) accommodating a greater number of cells were randomly chosen and acquired as 'tile images' using Zen software. Similar differences in Dsg-2 immunostaining between matriptase-treated and untreated wt or mutant overexpressing cells were observed (results not shown). This corroborates our above results that the mutation affected the ability of matriptase to cleave Dsg-2 at the predicted site.

Our repeated attempts to recapitulate the IF results by Western blotting were unsuccessful. We assume that, in light of excessive expression of wt and mutant Dsg-2 by the cells, 10 μg/ml of matriptase may be insufficient to bring about the significant proteolysis that could be detected in cell lysates. Cells treated with matriptase exceeding 10 μg/ml underwent rapid and progressive detachment from the coverslips. To avoid compromising the cells' viability, we decided to use 10 μg/ml matriptase and employ IF to simultaneously visualize and reliably quantify the subtle changes in the Dsg-2 expression levels in response to matriptase.

DISCUSSION

We had previously proposed a method, called PNSAS, to predict putative substrates of endoproteases with the hope that it will be a useful complementary approach in the current day attempts towards global profiling of proteases and their substrates [1]. The power of this method lies in the use of short peptide motifs which

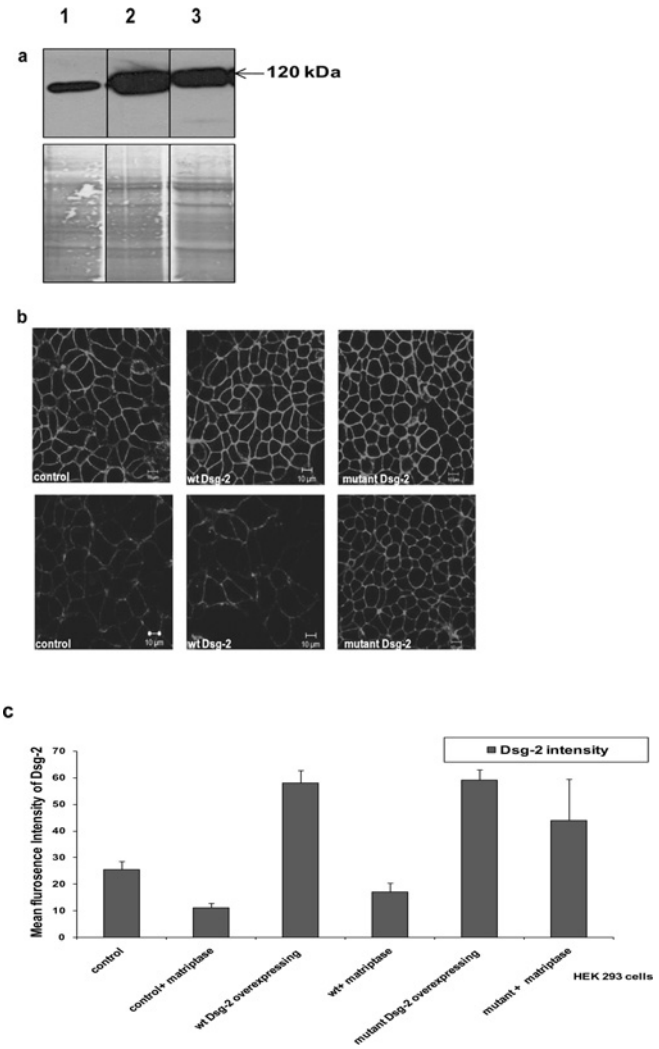

Figure 8 Effect of recombinant matriptase on the immunoreactivity of Dsg-2 in HEK-293 cells overexpressing wt or mutant (R565A) Dsg-2

(**a**) Upper panel, Western blotting of lysates of HEK-293 control, wt and mutant (R565A) Dsg-2 overexpressing cells. Lysates from untransfected control cells (lane 1), wt Dsg-2 overexpressing cells (lane 2) and mutant Dsg-2 overexpressing cells (lane 3) were probed for Dsg-2 expression. Lower panel, a Coomassie-Blue stained PVDF membrane demonstrating equal loading of the samples. The image is a composite presentation of samples run in different wells of the same gel, as shown by the lines dividing the lanes. (**b**) Difference in immunoreactive levels of Dsg-2 in control and cells treated with pure matriptase was monitored by IF. Upper panel, untreated control, wt and mutant Dsg-2 overexpressing HEK-293 cells. Lower panel, the corresponding cells treated with 10 μg/ml of pure matriptase. (**c**) Graphical representation of mean fluorescence intensity of Dsg-2 in untreated and matriptase-treated control, wt and mutant Dsg-2 overexpressing HEK-293 cells. Error bars represent S.D.

on one hand are big enough to provide specificity and on the other are small enough to cover a broad spectrum of proteins. In addition our method uses physiologically relevant filters, namely accessibility in terms of the folded structure of a protein and subcellular localization. We chose to test the ability of matriptase to cleave Dsg-2, a surface membrane protein important for cell adhesion. Breaching of cell–cell contact is an important event in the process of invasion and metastasis.

By a systematic study we have clearly demonstrated that matriptase regulates steady state levels of Dsg-2. To do so we have used: (i) pure active recombinant matriptase added exogenously to cleave Dsg-2 at cell surface and (ii) altered the endogenous surface levels of active matriptase by either down-regulating its expression or by mobilizing it from subcellular deposits. By combining IF and Western blot analysis to monitor the levels of Dsg-2 under these different conditions, we show that a decrease in levels of Dsg-2 is accompanied by what seems to be a cleaved product in the conditioned medium of treated cells. We were able to demonstrate the specificity of this cleavage process using CD44 and E-cadherin, levels of which were unaffected. In addition we overexpressed a mutant Dsg-2 (R565A) in which the predicted cleavage site at P1, Arg^{565}, was mutated to an alanine residue. Upon the addition of exogenous purified matriptase, HEK-293 cells expressing mutant Dsg-2 retained significantly higher levels of the immunopositive Dsg-2 as compared with the cells expressing wt Dsg-2 or the untransfected cells. These experiments taken together provide strong evidence that Dsg-2 is cleaved by matriptase at the predicted site. Our modelled structure shows that this is a distinct possibility since the predicted site is in a well-accessible region. The presence of Dsg-2 with an intact extracellular domain at the cell surface when matriptase was down-regulated resulted in increased cell–cell contact and adhesiveness.

Matriptase, as described in the Introduction section, is overexpressed in many solid tumours of epithelial origin and is implicated in cell invasion and metastasis. However, the mechanism by which matriptase can achieve these remains unclear. By demonstrating the ability of matriptase to regulate the levels of Dsg-2, we provide a plausible rationale for the role of matriptase in cell invasion and metastasis. Similar to our cell-based studies, when the levels of matriptase increase then Dsg-2 is likely to be cleaved more in tumour tissues by matriptase. This would provide a gain of function phenotype by which cells would increase their motility by breaking cell–cell contact, creating an environment conducible for invasion and metastasis. Whether a similar inverse correlation in the levels of Dsg-2 and matriptase exits in cells of solid tumours and whether they are responsible for invasive properties remains to be seen. Since cell invasive properties are controlled by many factors, it will be difficult to establish a direct correlation between the two phenomena. Nevertheless our results suggest that such a strong possibility exists and provides proof of principle that our prediction program is likely to get integrated in global profiling studies of *in vivo* substrates of endoproteases.

AUTHOR CONTRIBUTION

Vinita Wadhawan planned the study, conducted experiments, analysed data and wrote the paper; Yogesh Kolhe and Amit Kumar Singh purified and characterized matriptase; Nikhil Sangith cloned Dsg-2 and performed the mutation; and Prasanna Venkatraman designed and directed the project and wrote the paper.

ACKNOWLEDGEMENTS

The authors would like to acknowledge Vaishali V. Kailaje, Tanuja O. Durve and Jairaj J. Kasale of Digital Imaging Centre, ACTREC (Advanced Centre for Treatment, Research and Education in Cancer) for their assistance in acquisition of LSM confocal images, Sadhana Kannan for help with the statistical analysis and Arun Kumar for help with the modelling.

FUNDING

This work was supported by ACTREC [grant number 2383]. V.W. was supported by a fellowship from Lady Tata Memorial Trust.

REFERENCES

1a Lopez-Otin, C. and Overall, M. C. (2002) Protease degradomics: a new challenge for proteomics. Nat. Rev. Mol. Cell Biol. **3**, 509–519

1 Venkatraman, P., Balakrishnan, S., Rao, S., Hooda, Y. and Pol, S. (2009) A sequence and structure based method to predict putative substrates, functions and regulatory networks of endo proteases. PLoS ONE **4**, e5700
2 Oberst, M. D., Singh, B., Ozdemirli, M., Dickson, R. B., Johnson, M. D. and Lin, C. Y. (2003) Characterization of matriptase expression in normal human tissues. J. Histochem. Cytochem. **51**, 1017–1025
3 Pearton, D., Dale, B. A. and Presland, R. B. (2002) Functional analysis of the profilaggrin N-terminal peptide: identification of domains that regulate nuclear and cytoplasmic distribution. J. Invest. Dermatol. **119**, 661–69
4 Netzel-Arnett, S., Currie, B. M., Szabo, R., Lin, C. Y., Chen, C., Chai, K. X., Antalis, T. M., Bugge, T. H. and List, K. (2006) Evidence for a matriptase–prostasin proteolytic cascade regulating terminal epidermal differentiation. J. Biol. Chem. **281**, 32941–32945
5 List, K., Haudebschild, C. C., Szabo, R., Chen, W. J., Wahl, S. M., Swaim, W., Engleholm, L. H., Behrendt, N. and Bugge, T. H. (2002) Matriptase/MT–SP1 is required for postnatal survival, epidermal barrier function, hair follicle development, and thymic homeostasis. Oncogene **21**, 3765–3779
6 Takeuchi, T., Harris, J. L., Huang, W., Yan, K. W., Coughlin, S. R. and Craik, C. S. (2000) Cellular localization of membrane-type serine protease 1 and identification of protease activated receptor-2 and single-chain urokinase-type plasminogen activator as substrates. J. Biol. Chem. **275**, 26333–26342
7 Lee, S. L., Dickson, R. B. and Lin, C. Y. (2000) Activation of hepatocyte growth factor and urokinase/plasminogen activator by matriptase, an epithelial membrane serine protease. J. Biol. Chem. **275**, 36720–36725
8 Uhland, K. (2006) Matriptase and its putative role in cancer. Cell. Mol. Life Sci. **63**, 2968–2978
9 List, K. (2009) Matriptase: a culprit in cancer. Future Oncol. **5**, 97–104
10 List, K., Szabo, R., Molinolo, A., Sriuranpong, V., Redeye, V., Murdock, T., Burke, B., Neilson, B. S., Gutkind, S. and Bugge, T. H. (2005) Deregulated matriptase causes *ras*-independent multistage carcinogenesis and promotes *ras*-mediated malignant transformation. Genes Dev. **19**, 1934–1950
11 Oberst, M. D., Anders, J., Xie, B., Singh, B., Ossandon, M., Johnson, M. D., Dickson, R. B. and Lin, C. Y. (2001) Matriptase and HAI-1 are expressed by normal and malignant epithelial cells *in vitro* and *in vivo*. Am. J. Pathol. **4**, 1301–1311
12 Jin, X., Hirosaki, T., Lin, C. Y., Dickson, R. B., Shouichi, H., Kitamura, H. and Miyazaki, K. (2005) Production of soluble matriptase by human cancer cell lines and cell surface activation of its zymogen by trypsin. J. Cell Biochem. **95**, 632–647
13 Benaud, C. M., Oberst, M., Dickson, R. B. and Lin, C. Y. (2002) Deregulated activation of matriptase in breast cancer cells. Clin. Exp. Metastasis **19**, 639–649
14 Jin, J. S., Cheng, T. F., Tsai, W. C., Sheu, L. F., Chiang, H. and Yu, C. P. (2007) Expression of the serine protease, matriptase, in breast ductal carcinoma of Chinese women: correlation with clinicopathological parameters. Histol. Histopathol. **22**, 305–309
15 Oberst, M. D., Johnson, M. D., Dickson, R. B., Lin, C. Y, Singh, B., Stewart, M., Williams, A., Naufussi-al, A., Smyth, J. F., Gabra, H. and Sellar, G. C. (2002) Expression of the serine protease matriptase and its inhibitor HAI-1 in epithelial ovarian cancer: correlation with clinical outcome and tumor clinicopathological parameters. Clin. Cancer Res. **8**, 1101–1107
16 Tanimoto, H., Shingemasa, K., Tian, X., Gu, L., Beard, J. B., Sawasaki, T. and O' Brien, T. J. (2005) Transmembrane serine protease TADG-15 (ST14/Matriptase/MT-SP1): expression and prognostic value in ovarian cancer. Br. J. Cancer **92**, 278–283
17 Johnson, M. D., Oberst, M. D., Lin, C. Y. and Dickson, R. B. (2003) Possible role of matriptase in the diagnosis of ovarian cancer. Expert. Rev. Mol. Diagn. **3**, 331–338
18 Saleem, M., Adhami, V. M., Zhong, W., Longley, B. J., Lin, C. Y., Dickson, R. B., Reagan-Shaw, S., Jarrard, D. F. and Mukhtar, H. (2006) A novel biomarker for staging human prostate adenocarcinoma: overexpression of matriptase with concomitant loss of its inhibitor, hepatocyte growth factor activator inhibitor-1. Cancer Epidemiol. Biomarkers Prev. **15**, 217–227
19 Forbs, D., Thiel, S., Stella, M. C., Sturzebecher, A., Schweinitz, A., Steinmeter, T, Sturzebecher, J. and Uhland, K. (2005) *In vitro* inhibition of matriptase prevents invasive growth of cell lines of prostate and colon carcinoma. Int. J. Oncol. **27**, 1061–1070
20 Chidgey, M. and Dawson, C. (2007) Desmosomes: a role in cancer? Br. J. Cancer **96**, 1783–1787
21 Davies, E. L., Cochrane, R. A., Hiscox, S., Jiang, W. G., Sweetland, H. M. and Mansel, R. E. (1997) The role of desmoglein 2 and E-cadherin in the invasion and motility of human breast cancer cells. Int. J. Oncol. **11**, 415–419
22 Narayana, N., Gist, J., Smith, T., Tylka, D., Trogdon, G. and Wahl, J. K. (2010) Desmosomal component expression in normal, dysplastic, and oral squamous cell carcinoma. Dermatol. Res. Pract. **2010**, 649731
23 Hiraki, A. T., Shinohara, M., Ikebe, T., Nakamura, S., Kurahara, S. and Garrod, D. R. (1996) Immunohistochemical staining of desmosomal components in oral squamous cell carcinomas and its association with tumour behaviour. Br. J. Cancer **73**, 1491–1497
24 Krunic, A. L., Garrod, D. R., Madani, S., Buchanan, M. D. and Clark, R. E. (1998) Immunohistochemical staining for desmogleins 1 and 2 in keratinocytic neoplasms with squamous phenotype: actinic keratosis, keratoacanthoma and squamous cell carcinoma of the skin. Br. J. Cancer **77**, 1275–1279
25 Ramani, V. C., Hennings, L. and Haun, R. S. (2008) Desmoglein 2 is a substrate of kallikrein 7 in pancreatic cancer. BMC Cancer **8**, 373
26 Roycik, M. D., Fang, X. and Sang, Q.-X. (2009) A fresh prospect of extracellular matrix hydrolytic enzymes and their substrates. Curr. Pharm. Des. **15**, 1295–1308
27 Kundu, S. T., Gosavi, P., Khapare, N., Patel, R., Hosing, A. S., Maru, G. B., Ingle, A., Decaprio, J. A. and Dalal, S. N. (2008) Plakophilin3 downregulation leads to a decrease in cell adhesion and promotes metastasis. Int. J. Cancer **123**, 2303–2314
28 Pieper, U., Webb, B. M., Barkan, D. T., Schneidman-Duhovny, D., Schlessinger, A., Braberg, H., Yang, Z., Meng, E. C., Pettersen, E. F., Huang, C. C. et al. (2011) MODBASE, a database of annotated comparative protein structure models and associated resources. Nucleic Acids Res. **39**, 465–474
29 Eswar, N., Madhusudhan, M. A., Webb, B., Madhusudhan, M. S., Eramianm, D., Shen, M., Pieper, U. and Sali, A. (2006) Comparative protein structure modeling with MODELLER. Curr. Protoc. Bioinf. **5**, 5.6
30 Tsodikov, O. V., Record, Jr, M. T. and Sergeev, Y. V. (2002) Novel computer program for fast exact calculation of accessible and molecular surface areas and average surface curvature. J. Comput. Chem. **23**, 600–609
31 Gasteiger, E., Hoogland, C., Gattiker, A., Duvaud, S., Wilkins, M. R., Appel, R. D. and Bairoch, A. (2005) Protein identification and analysis tools on the ExPASy server. In The Proteomics Protocols Handbook (Walker, J. M., ed.), pp. 571–607, Humana Press, Totowa
32 Nava, P., Laukoetter, M. G., Hopkins, A. M., Laur, O., Gerner-Smidt, K., Green, K. J., Parkos, C. A. and Nusrat, A. (2007) Desmoglein-2: a novel regulator of apoptosis in the intestinal epithelium. Mol. Biol. Cell **18**, 4565–4578

Received 26 August 2011/9 July 2012; accepted 11 July 2012
Published as BJ Immediate Publication 11 July 2012, doi:10.1042/BJ20111432

Biochem. J. (2012) **447**, 61–70 (Printed in Great Britain) doi:10.1042/BJ20111432

SUPPLEMENTARY ONLINE DATA

From prediction to experimental validation: desmoglein 2 is a functionally relevant substrate of matriptase in epithelial cells and their reciprocal relationship is important for cell adhesion

Vinita WADHAWAN, Yogesh A. KOLHE, Nikhil SANGITH, Amit Kumar Singh GAUTAM and Prasanna VENKATRAMAN[1]

Advanced Centre for Treatment, Research and Education in Cancer, Tata Memorial Centre, Kharghar, Navi Mumbai 410210, India

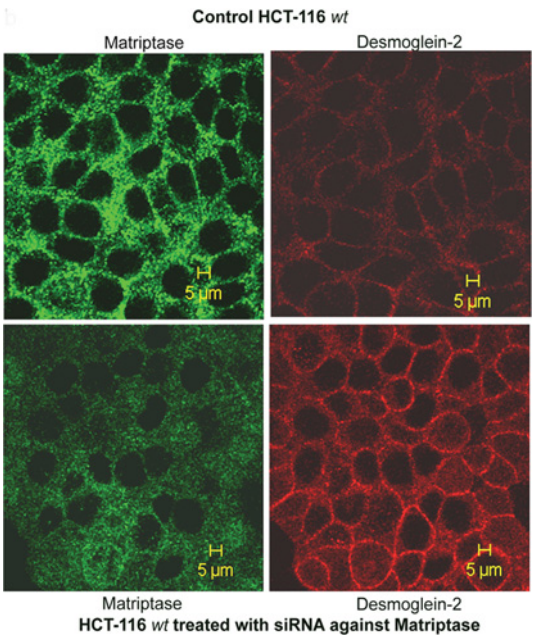

Figure S1 Effect of down-regulation of matriptase on immune reactivity of cell surface Dsg-2 in HCT-116 wt cells

Differences in immunoreactive levels of matriptase (green) and Dsg-2 (red) upon matriptase down-regulation was monitored by IF. The upper panels show control HCT-116 cells, whereas the lower panels show cells transfected with 50 nM of matriptase siRNA. The results are representative of three independent experiments.

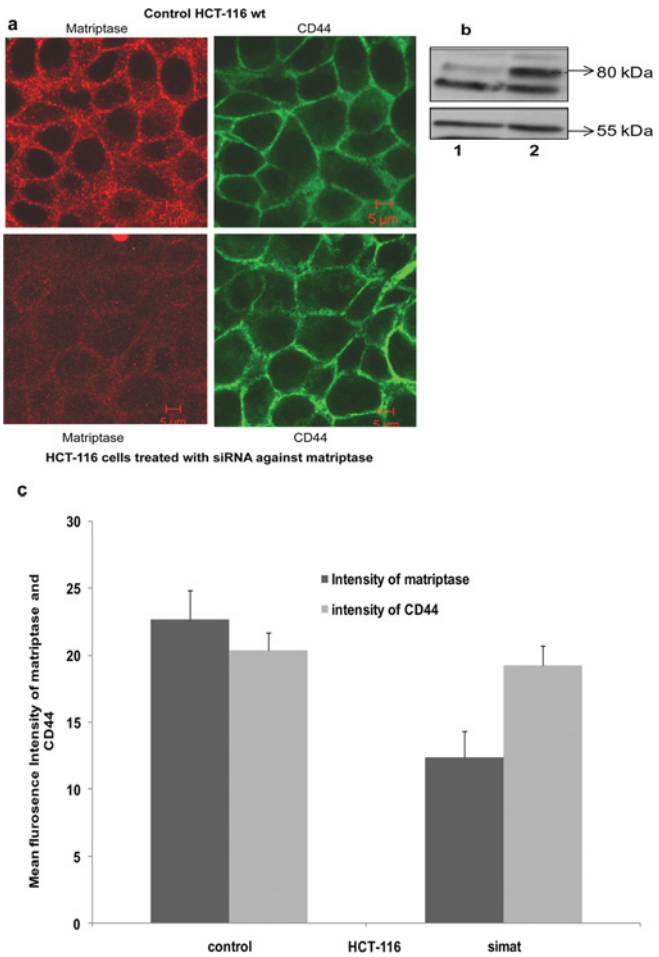

Figure S2 Effect of down-regulation of matriptase on immune reactivity of cell surface CD44 in HCT-116 wt cells

(**a**) The difference in immunoreactive levels of matriptase (red) and CD44 (green) upon matriptase down-regulation was monitored by IF. The upper panels show control HCT-116 cells, whereas the lower panels show cells transfected with 50 nM of matriptase siRNA. (**b**) Western blotting of cell lysates from matriptase siRNA- (lane 1) or control siRNA- (lane 2) treated cells was probed for matriptase. Lower panel, the 55 kDa band that serves as the loading control. (**c**) Graphical representation of the mean fluorescence intensities of CD44 and matriptase. Mean fluorescence intensities were measured as described in the Materials and methods section of the main text. The results are representative of two independent experiments. Error bars represent S.D.

[1] To whom correspondence should be addressed (email vprasanna@actrec.gov.in).

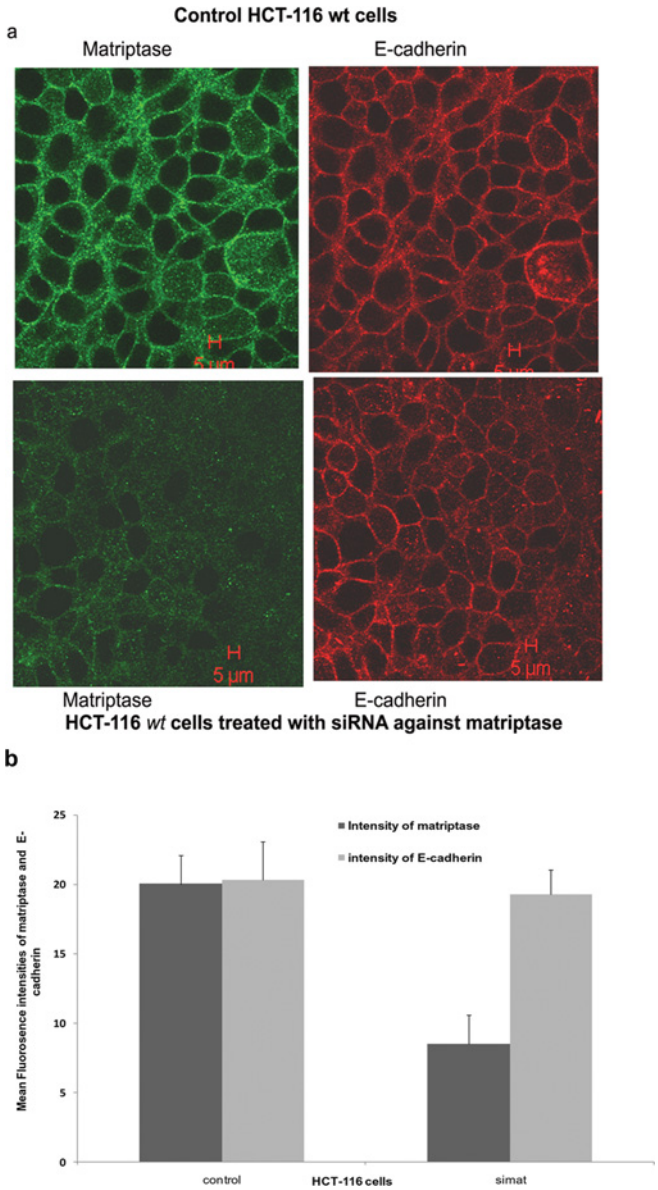

Figure S3 Effect of down-regulation of matriptase on immune reactivity of cell surface E-cadherin in HCT-116 wt cells

(**a**) The difference in immunoreactive levels of matriptase (green) and E-cadherin (red) upon matriptase down-regulation was monitored by IF. The upper panels show control HCT-116 cells, whereas the lower panels show cells transfected with 50 nM of matriptase siRNA. (**b**) Graphical representation of the mean fluorescence intensities of E-cadherin and matriptase. Mean fluorescence intensities were measured as described in the Materials and methods section of the main text. The results are representative of two independent experiments. Error bars represent S.D.

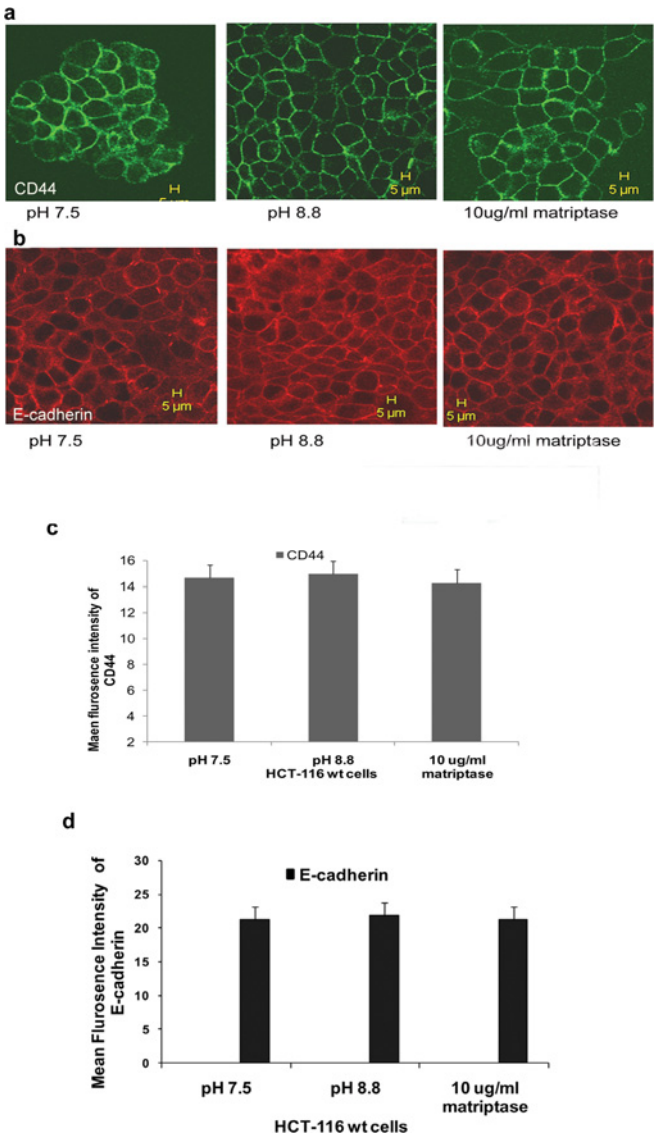

Figure S4 Effect of recombinant matriptase on immune reactivity of CD44 and E-cadherin at the cell surface

The difference in immunoreactive levels of CD44 (green) and E-cadherin (red) upon exogenous addition of matriptase. CD44 (**a**) and E-cadherin (**b**) were probed in control (serum-free DMEM at pH 7.5 and 8.8) cells and cells treated with 10 μg/ml of pure recombinant matriptase. Graphical representation of mean fluorescence intensities of CD44 (**c**) and E-cadherin (**d**) in control and matriptase-treated HCT-116 cells. The mean fluorescence intensity of CD44 and E-cadherin was measured as described in the Materials and methods section of the main text. The results are representative of two independent experiments. Error bars represent S.D.

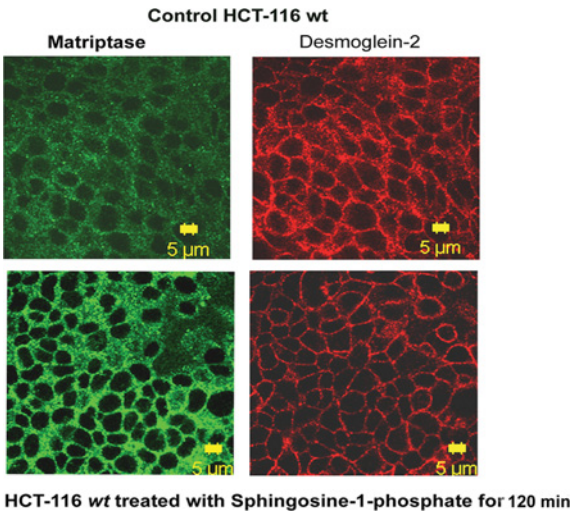

Figure S5 Effect of S1P on relative levels of matriptase and Dsg-2 on the surface of HCT-116 wt cells

Double immunolabelling was done to monitor the difference in immunoreactive levels of Dsg-2 (red) and matriptase (green) in control and cells treated with S1P. The upper panels show HCT-116 wt cells, whereas the lower panels show cells treated with 50 ng/ml S1P for 120 min. The results are representative of three independent experiments.

Received 26 August 2011/9 July 2012; accepted 11 July 2012
Published as BJ Immediate Publication 11 July 2012, doi:10.1042/BJ20111432